PATHOGENESIS OF ESSENTIAL TREMOR: CHARACTERIZATION OF POTENTIALLY INVOLVED ENDOGENOUS ALKALOIDS OF DIETARY ORIGIN AND EVALUATION OF THEIR ACTIVITY ON AN ORIGINAL 3D NEUROSPHERE MODEL

A thesis submitted for obtaining the degree of Doctor in Biomedical and Pharmaceutical sciences

By Rania ARO

Promotor : Prof. Pierre DUEZ, Therapeutic Chemistry and Pharmacognosy Unit, UMons

Co-promotor : Prof. Mario MANTO, Department of Neurology, CHU-Charleroi

Jury members : Prof. Bertrand Blankert, Laboratory of Pharmaceutical Analysis, UMONS

Prof. Jean-Marie Colet, Human Biology and Toxicology Unit, UMONS

Dr Alexandra Tassin, Laboratory of Respiratory Physiology, Pathophysiology and Rehabilitation, UMONS

Dr Anne-Cécile Le Lamer, UMR 152 PharmaDev, University of Paul Sabatier – Toulouse 3, France

Dr Laurent Nguyen, GIGA-Stem Cells - Molecular Regulation of Neurogenesis, ULiège

Academic year 2020-2021

"In the midst of difficulty lies opportunity."

"Albert Einstein"

Acknowledgements

Summary

Objectives

Our work aimed to (*i*) study, thanks to an original analytical approach, the formation of β-carbolines alkaloids and isoquinolines, from volatile and non-volatile carbonyl compounds generated by the Maillard reaction; and (*ii*) identify their possible implication in the pathogenesis of essential tremor.

Methods

The literature suggesting a link between meat overcooking, β-carbolines and essential tremor etiology, we began by exploring the levels of β-carbolines alkaloids in overcooked meats to assess whether the actual levels are as low as described (3,8 - 8.5 ng/g). In view of the difficulties and the dubious interest in measuring β-carbolines in meat, at levels hardly accessible to the analytical equipment available in our laboratory, we decided to focus our attention on cooking compounds that could be involved in the generation of biologically active endogenous alkaloid artefacts. Thus, we developed a methodology to search for precursor carbonyl compounds produced during the Maillard reaction in overcooked meats to (*i*) extract and identify volatile and non-volatile carbonyls; (*ii*) study their reactivity with endogenous amines (spontaneous reactions at 37°C) and identify the reaction products; (*iii*) study *in silico* their predicted pharmacokinetic and toxicological properties towards the central nervous system; (*iv*) study *in vitro* their possible toxicity on a 3D neurosphere model; (*v*) test their possible tremorgenic involvement in an *in vivo* model.

Results and conclusion

This approach allowed us to identify the spontaneous synthesis of the alkaloid 1-benzyl-6,7-dihydroxy-1,2,3,4 tetrahydroisoquinoline (1-benz-THIQ-diol), likely to be endogenously formed, that *in silico* predicted possible CNS toxicant effect to propose a pharmacological study to reveal a possible relation with ET. To assess the neurotoxicity of harmane and 1-benz-6,7-diol THIQ, we have developed a 3D neurosphere culture (implemented for the first time at UMONS). This culture has shown its ability to yield a reproducible 3D model in terms of diameter, morphology and proportions of cells present (neurons / astrocytes); this is moreover an interesting model for toxicity studies.
The role of harmane as a neurotoxic agent was supported in this study, but at a high concentration hardly compatible with its content in overcooked meat. So far, our *in vitro* data do not support an eventual neurotoxic effect for 1-benz-6,7-diol THIQ. We applied this last compound, which has not been studied in the literature, to an animal model of essential tremor for a preliminary study that remains to be pursued (tests carried out at the University of Bristol, in collaboration with Dr Kathryn Bennett).

Abbreviation :

1-Benz-THIQ-diol: 1-benzyl-1,2,3,4-tetrahydroisoquinoline-6,7-diol

1-Isobutyl-DHβCa: 1- isobutyl dihydrobetacarboline

1-Pentyl-DHβCa: 1-pentyl-dihydrobetacarboline

1-Pentyl-THIQ-diol: 1-pentyl-1,2,3,4-tetrahydroisoquinoline-6,7-diol

1-Pentyl-THβCa-ol: 1-pentyl-1,2,3,4-tetrahydrobetacarboline-6 ol

1-Phenyl-DHβCa: 1-pheny-dihydrobetacarboline

2D, 3D: two dimension, three dimension

ACTH: Adrenocorticotropic hormone

ADL: Activities of daily living

AMPA: α-amino-3-hydroxy-5-methyl-4-isoxazole propionic acid

BBB: brain blood barrier

Bn : Benzyl

cAMP: cyclic Adenosine monophosphate

cf. : from Latin: confer/conferatur, meaning "compare"

CNS: Central nervous system

Cr: creatine

CYP: Cytochromes P450

DAT: Dopamine transporter

DBS: Deep brain stimulation

DCFH: dichlorodihydrofluorescein

DCFH-DA: dichlorodihydrofluorescein diacetate

DCN: Deep cerebellar nuclei

DNA: Deoxyribonucleic acid

DNT: Developmental neurotoxicity

EAAT: Excitatory amino acid transporter

ECM: extracellular matrix

EGTA: Ethylene glycol-bis(β-aminoethyl ether)-N,N,N′,N′-tetraacetic acid

ET: Essential tremor

EtOAc: Ethyl acetate

fMRI: Functional magnetic resonance imaging

GABA: Gamma aminobutyric acid

GABAA α-1: Gamma-aminobutyric acid receptor subunit alpha-1

GABAA: Gamma aminobutyric acid A

GABAB: Gamma aminobutyric acid B

GABRA1: Gamma-aminobutyric acid type A receptor alpha1 subunit

GAD: Glutamic acid decarboxylase

GAT: GABA transporter

GK: Gamma knife surgery

GLN: Glutamine

GLNT: Glutamine transporter

GLT: Glutamate transporter

GLU: Glutamate

GSH: Glutathione

H_2SO_4: Sulfuric acid

HC: Healthy control

HCA: Heterocyclic amine

HCl: Hydrochloric acid

HDP: Hanging drop microplates

hESCs: human embryonic stem cells

hiPSCs: human induced pluripotent stem cells

HS-SDME: Headspace single-drop microextraction

HTMOB: 4-hydrazinyl-N, N, N-trimethyl-4-oxobutan-1-aminium iodide

i.e. : that is

ION: Inferior olivary nucleus

IQ: isoquinoline

KGDH: α-ketoglutarate dehydrogenase complex

KO : Knockout

MAOA: Monoamine oxidase A

MAOB: Monoamine oxidase B

MDMA: 3,4-Methylenedioxy-methamphetamine

Me : Methyl

MEG: Magneto encephalography

MPP+: 1-methyl-4-phenyl-pyridinium

MPTP: 1-methyl-4-phenyl-1,2,3,6-tetrahydropyridine

MRI: Magnetic resonance imaging

mRNA: Messenger ribonucleic acid

MRPs: Maillard reaction products

Na2WO4: Sodium tungstate

Na3PO4: Sodium phosphate

NAA: N-acetyl aspartate

NAD: Nicotinamide adenine dinucleotide

NADPH: Nicotinamide adenine dinucleotide phosphate (reduce form)

NaOH: Sodium hydroxide

NMDA: N-methyl-D-aspartate channel

N-MeTH-βC: N-methyltetrahydrobetacarboline

NMT: N-methyltransferases

NO: Nitric oxide

NSCs: Neural stem cells

OA: Octanoic acid

OCT: organic cation transporter

PC: Purkinje cells

PC12: pheochromocytoma cells

PEG: Poly ethylene glycol

PEMA: Phenylethylmalonamide

PET: Positron emission tomography

PFBHA: O-2,3,4,5,6-(pentafluorobenzyl)hydroxylamine

P-gp: P-glycoproteins

RN: Red nuclei

ROS: Reactive oxygen species

RT: Room temperature

rTMS: Repetitive transcranial magnetic stimulation

SAFE: Solvent Assisted Flavor Evaporation

SH-SY5Y: immortalised human derived cell line of dopaminergic neuroblastoma

SIN-1: 3-morpholinosydnonimine

tACS: Transcranial alternating current stimulation

TAL: Thalamus

tCR: total creatine

tDCS: Transcranial direct current stimulation

TH: Tyrosine hydroxylase

THIQ: Tetrahydroisoquinoline

ULP: ultra-low attachment microplates

VDCC: Voltage-dependent calcium channel

vGAT: Vesicular GABA transporter

vGLUT: Vesicular glutamate transporter

VIM: Ventral intermediate nucleus

Wdr81: Gene (WD repeat-containing protein 81)

βCA: Beta carboline alkaloid

Table of Contents

1. Introduction

1.1 Essential tremor

1.1.1 Definition

Essential tremor (ET) is a progressive neurodegenerative and movement disorder that causes involuntary and rhythmic shaking, it is characterized by a slowly progressive postural and/or kinetic involuntary tremor, a bilateral action tremor affecting predominantly the arms, the head and/or the voice [1]. ET is primarily a kinetic tremor; the main clinical features of ET consist in kinetic tremor of the arms (tremor occurring during guided voluntary movements) with frequencies of 4 to 12 Hz, followed by postural and/or kinetic tremor of cranial structures (*i.e.,* neck, jaw, voice) [2]. Patients usually first become aware of the tremor when they are holding newspaper or utensils or when reaching for objects. When ET affects the neck muscles, patients exhibit either yes-yes or no-no oscillations of the head. Furthermore, ET can affect the vocal cords, causing a tremulous voice while singing or talking [3]. As time evolves, ET tends to impair balance and gait, and may even cause falls.

Apart from this first group of motor features, recent research points out a variety of cognitive and psychiatric signs. One of the most common non-motor symptoms in ET is the presence of mild cognitive deficits [4], notably for verbal fluency, naming, mental set-shifting, verbal memory, and working memory; deficits in olfaction and hearing loss have also been observed in ET but the published studies remain inconclusive [5]. Significant relationships are reported between ET and depression [5], poor nocturnal sleep quality and sleep disturbances [6]. Non-motor symptoms could be a part of the disease in the early stages; indeed depression and anxiety are more common in young patients with ET [6]. In fact, depressive symptoms appear to be stronger predictors of tremor-lowered quality of life than the motor aspects of tremor itself [7].

Obviously, and even if some patients will never come to medical attention, both motor and non-motor ET symptoms result in significant psychosocial and physical disabilities, interfering with activities of daily living (ADL) such as eating, drinking, writing [3]. The classical view of ET as a monosymptomatic condition is now replaced by the concept of a heterogeneous disorder with multiple motor and non-motor features of varying degrees.

1.1.2 Incidence and prevalence

ET is among the most prevalent disabling and poorly understood neurological movement disorders, especially affecting elderly people, but also appearing in young adults and even during childhood [8]. The disease has been reported not only by neurologists, but also by internists, geriatricians, and general practitioners [9]. The adjusted incidence is about 619 per 100.000 person-years among persons aged 65 and older [10]. However, the prevalence estimates have varied enormously amongst studies, and it is therefore difficult to establish the prevalence at a world level.

A meta-analysis by Louis and Ferreira [11] identified 28 studies over 19 countries, with prevalence ranging from 0.01 % (Nigeria, China; all ages) to 20.5 % (USA; over 65 years) (Table 1.1).

By pooling prevalence in all age classes, the worldwide prevalence was then estimated at 0.9 %. The prevalence markedly increased with age (overall, 4.6 % for ages $\geq$ 65 years), and especially with advanced age [11]. Although data are quite incomplete in numerous cases and the prevalence of ET may show regional and possibly ethnic differences.

A majority of studies do not show a gender difference in ET prevalence (ratio men to women of 1.08:1.00); 6 studies indicate a gender imbalance (5 studies; ratio men: women 1.65:1.00) whereas one study indicates higher prevalence in women (ratio men: women 0.39:1.00) [11].

The very high incidence and prevalence raise the question of a predisposition to the disease [8]. Age is clearly a risk factor for ET, most studies indicate a marked age-associated rise so that prevalence may be higher than 20 % in the oldest patients [11].

Table 1.1: Prevalence of ET in population-based studies. The studies are ordered from lowest to highest prevalence (expressed in %). There are differences between studies regarding the screening process and epidemiological methods, in addition of variability in terms of age of examined subjects (notably, Canadian and US studies gather mainly elderly patients) (source [11]).

Year	Country	Prevalence%	Ages	Were all patients examined in the study? (by whom?)
1987	Nigeria	0.01	All	Unclear from study description
1985	China	0.01	All	No
2008	Tanzania	0.04	All	No
1990	Ethiopia	0.04	All	No
1993	Saudi Arabia	0.1	All	No
1993	Tunisia	0.2	All	No
1994	Uruguay	0.2	All	No
2005	Singapore	0.3	≥ 50	No
1976	New Guinea	0.4	All	Yes (Field officer)
1994	Italy	0.4	All	Yes (Neurologist)
1982	USA	0.4	≥ 4	No
1989	Spain	0.6	All	Yes (Nurses, general practitioners)
2008	Israel	0.8	≥ 65	Yes (Neurologist)
2007	Italy	0.8	≥ 41	Yes (General practitioners)
2008	India	1.4	≥ 60	No
1960	Sweden	1.4	All	No
1988	India	1.6	All	No
1995	USA	2.2	≥ 65	No but information provided on sensitivity of screening instrument
2008	Turkey	3.1	≥ 18	Yes
1997	China	3.2	≥ 50	Yes (Neurologist)
2005	Austria	3.4	50-89	Yes (Neurologists, geriatricians, other medical specialists)
2003	Turkey	4	≥ 40	Yes (Neurologist)
2001	Spain	4.8	≥ 65	No but information provided on sensitivity of screening instrument
2003	Spain	4.8	≥ 65	No but information provided on sensitivity of screening instrument
2009	USA	5.5	≥ 65	Yes (handwriting samples reviewed by movement disorder specialist)
1982	Finland	5.6	≥ 40	No but information provided on sensitivity of screening instrument
1994	Canada	14.3	≥ 65	Yes
1996	USA	20.5	≥ 65	Yes (Not specified)

1.1.3 Pathogenesis

ET is a complex disorder, poorly understood both in terms of etiology and pathophysiology. Epidemiological data suggest that a combination of genetic abnormalities with putative non-genetic (e.g., environmental) factors lead to a slowly progressive neurodegeneration that causes shaking and other disturbances of neurologic function. Neuroimaging studies have provided arguments for a disorder of the CNS. Reported outcomes from fMRI (functional Magnetic Resonance Imaging) (Figure 1.1) and cortico-muscular MEG (Magneto Encephalography) analyses indicate that ET is mainly a disease of central origin, involving in particular 3 key-nodes within the numerous brain networks: the cerebellum, the thalamus and the primary motor cortex [12, 13] (Figure 1.2).
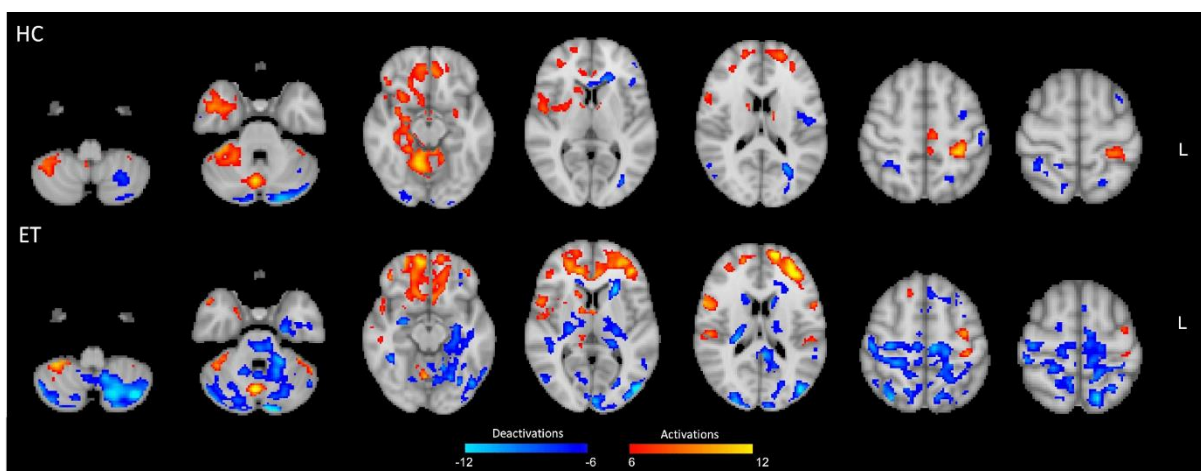
Figure 1.1: fMRI Activation and deactivation maps. Fixed-effects group analysis results for task outstretching of the right arm (patients with essential tremor [ET] and healthy controls [HC]). Statistical maps are thresholded by using clusters determined by $Z > 6$ (activations) and $Z < -6$ (deactivations) with a (corrected) cluster significance threshold of $p < 0.05$. ET patients displayed statistically different activation and deactivation mapping when tremor triggered by maintaining a posture with their right arm (source [14]).

Many hypotheses relate to the pathophysiology of ET, with two dominant central models: a conventional physiological model, also called *"olivary model"*, and the more recent "*degenerative cerebellar model*", underpinned by molecular mechanism, cell biology and anatomo-pathology. Other hypotheses include "*the central oscillator model*" and "*the gamma-aminobutyric acid (GABA) moldel*".
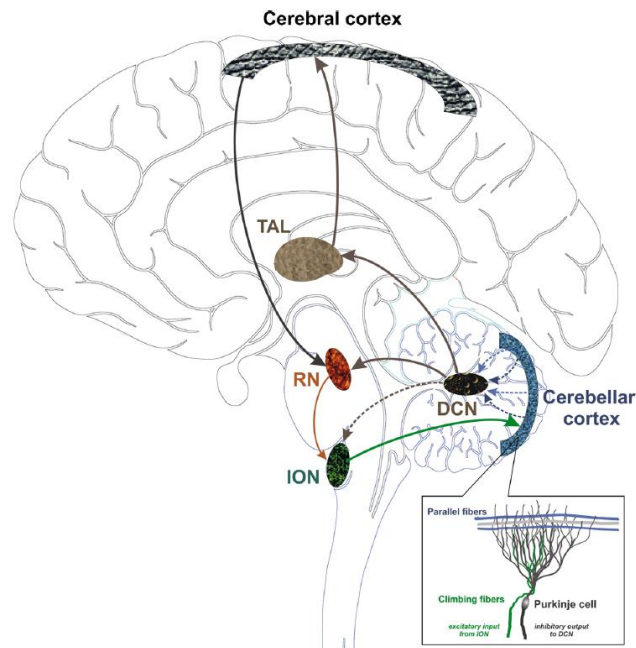
Figure 1.2: Schematic drawing of cerebellar connections. Excitatory connections in full line and inhibitory connections in dashed line.The cerebellum, the thalamus (TAL) and the primary motor cortex are the three key-nodes in tremor generating within the numerous brain networks. The abnormal activity transmitted through cerebello-thalamocortical pathways, that includes red nuclei (RN) and deep cerebellar nuclei (DCN), implicated in ET; an abnormality appear cerebellar-related: Purkinje cell loss, abnormal rhythmic activity generated by the inferior olivary nucleus (ION) (source [14, 15]).

1.1.3.1 The Inferior olive hypothesis "*olivary model*"

In this model ET would be a primary electrical/electrophysiological disorder, resulting from the overactivity of pacemaking neurons located in the inferior olivary nucleus. These neurons, which are coupled by gap junctions, fire in a rhythmic manner and target both the Purkinje neurons in the cerebellar cortex and cerebellar nuclei. The over-activity of the inferior olive would lead to a rhythmical burst firing in the cerebellar cortex and cerebellar nuclei (the sole output of the cerebellar circuitry), therefore producing tremor through an abnormal olivo-cerebellar activity and via the cerebello-thalamo-cortical output channels [16, 17].

This model (Figure 1.3), that puts forward the inferior olive as the pacemaker of ET based on reciprocal connections with the cerebellum and the intrinsic ability to generate rhythmic bursting activity, supported by evidence from harmaline-induced tremor animal model, studies indicate that injection of harmaline triggers rhythmic burst activity in the inferior olivary nucleus (ION) which was lost after damaging the ION [17, 18]. In addition, several

evidence from positron emission tomography (PET) and resonance imaging (fMRI) studies that suggest a higher intrinsic activity in the ION in ET patients [19, 20]. However this model and its evidence was less supported over time while more evidence doubt its validity [21].
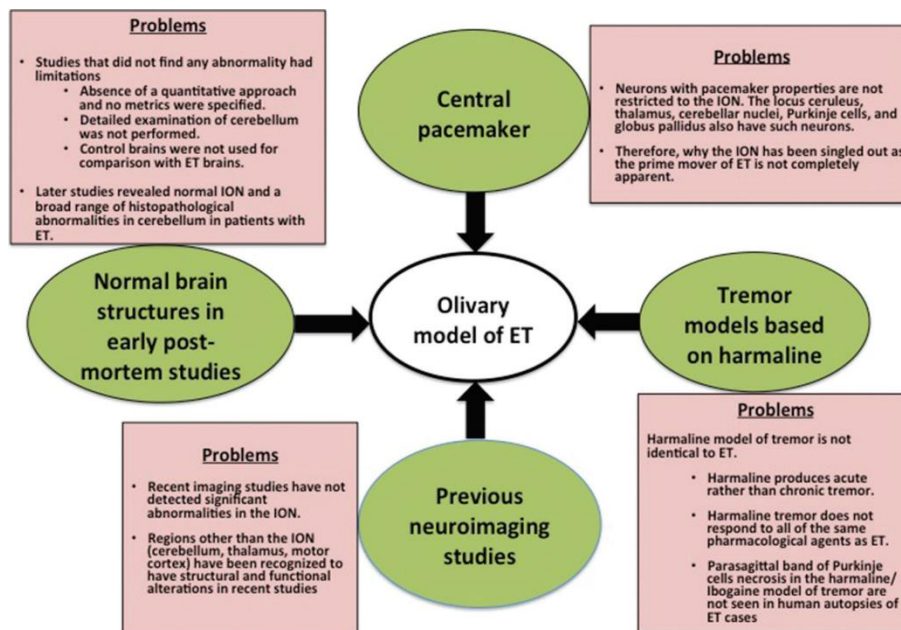
Figure 1.3: Summary of the observations which augured the existence of an olivary model of ET and their respective problems (Louis 2017) (source [21]).

1.1.3.2 The Degenerative cerebellar hypothesis

This model based on intensive tissue studies that identified structural changes within the cerebellar cortex circuitry itself surpasses the olivary model. Indeed, a loss of Purkinje cells was demonstrated by post-mortem investigations in ET cases using cells count, as well as linear density measurements [22]. The population of Purkinje cells would in fact represent the site of initial molecular/cellular events (hence the terminology of *"purkinjopathy"*) [23], generating a secondary remodeling/rewiring within the cerebellar cortex, with subsequent changes in adjacent neuronal populations (mainly the interneurons surrounding the Purkinje neurons). The formation of this aberrant cerebellar circuitry is probably central to the pathogenesis of ET, with notably thickened axons and remodeled basket cells [24, 25].

ET, as a progressive, age-related, disease, appears indeed truly *neurodegenerative* in nature [26]. This theory is further supported by evidence of brain iron accumulation [27]; such iron

deposits have been observed in other neurodegenerative disorders, such as Alzheimer's, Parkinson's and Huntington's diseases, which are also progressive disorders associated with ageing. In all these devastating disorders, cell loss occurs in combination with other cerebral changes or deposits (such as Lewy bodies for instance) [28]. It is noteworthy that the phenotype of these diseases includes a constellation of motor/non-motor dysfunctions [29].

However, the neurodegenerative hypothesis does not explain the early onset cases and the clinically very slow and heterogeneous progression of ET in other cases. Some patients show combinations of tremor and minor cerebellar symptoms with no evidence of other brain structures involvement. Furthermore, although there are clinical and electrophysiological arguments of cerebellar manifestations in ET patients, the reversibility of these symptoms and signs by ethanol intake (or thalamic deep brain stimulation: DBS; this is a matter of debate see section 1.1.6.2) challenges the neurodegenerative hypothesis [30, 31]. Some, however, may claim that DBS is very active in Parkinson's disease whose pathogenesis is clearly neurodegenerative. Moreover, it can be argued that the Purkinje cells loss could be the result of long-standing tremor and not its cause (given that the cerebellum receives numerous afferences via the spinocerebellar pathways and the pontocerebellar tracts), although one would expect a progressive cerebellar degeneration in all steady tremor conditions if this were true [5].

1.1.3.3   The central oscillator hypothesis

In this hypothesis, ET genesis is based on inherent neural instability that leads to the generation of rhythmic bursts in central oscillating pacemakers such as thalamic nuclei (neurons of the inferior olivary complex also fall in this category). Through their tight interconnections within motor system networks, these oscillators become entrained, coupling their firing patterns to result in visible and pathologic tremors. This view can account at least partially for the heterogeneity of ET manifestations and therapeutic responses. Although structural alterations are not a pre-requisite for a neural instability, a pre-existing structural damage in the brain is a likely ground [5, 32]. Nevertheless, reports highlight those key structures involved in tremor genesis such as thalamic nuclei and the inferior olivary complex are normal. Furthermore, the fact that degeneration of inferior olive does not lessen tremor

reinforces the concept that the inferior olivary nucleus does not play a critical role in the generation of tremor in these patients [33].

1.1.3.4 The gamma-aminobutyric acid (GABA) hypothesis

Gamma-aminobutyric acid (GABA) is an inhibitory neurotransmitter involved in widespread functions in CNS, it is locally synthesized from the amino acid glutamate in the presence of the enzyme L-glutamic acid decarboxylase (GAD), GABA has to bind to the heteromultimeric receptors $GABA_A$ and $GABA_B$ to be effective. PET (Positron Emission Tomography) studies suggest a gamma-aminobutyric acid GABAergic dysfunction in tremor generation. A correlation has been identified between flumazenil[1] uptake, and tremor rating scales, pointing towards abnormalities in GABA receptor binding. This defect would lead to a lack of inhibition within the cerebellar microcircuits, especially at level of the cortico-nuclear synapses between Purkinje and cerebellar nuclei neurons; the resulting glutamatergic overactivity (disinhibition of cerebellar nuclei) would generate tremor along the cerebello-thalamo-cortical pathways [34, 35]. This mechanism is supported by the observation that ET is highly responsive to ethanol, benzodiazepines and barbiturates, which all facilitate inhibitory neurotransmission by binding to the $GABA_A$ receptor in the brain [36]. A pharmacological correction of GABA dysfunction then seems to present a potential therapeutic effect in ET.

1.1.4 Etiology

ET might be triggered by a combination of both intrinsic and extrinsic mechanisms. Regarding the latter, environmental risk factors probably contribute to the etiology in a considerable proportion of cases. Yet, there has been relatively little discussion in the tremor literature about a clear identification of these factors. Exposure to beta-carbolines, mercury, lead, organochlorine pesticides have all been incriminated [37]. The effects on ET of different life styles have been investigated, *i.e.* Mediterranean diet indicates a possible positive effect of ET risk lowering, while elevated meat consumption has a negative effect on

---

[1] flumazenil is a selective benzodiazepine receptor antagonist bind to benzodiazepine receptor site of the $GABA_A$ receptor

ET cases related only to men [38]. On the other hand, some intrinsic mechanisms, more specifically genetic factors related to familial ET, are recognized and the susceptible hereditary gene components have been identified[2] [38].

Harmane, a lipophilic heterocyclic amine (HCA) in the β-carboline alkaloid (βCA) group, is a potent tremor-producing neurotoxin. It is often found in the human diet and therefore a lifelong exposure is plausible. Blood concentrations are elevated in patients with ET as compared with controls and increased blood harmane concentration could be associated with cerebellar neuronal damage (Table 1.2) [39].

Table 1.2: Blood harmane concentration in Et patient vs control in different studies.

Concentration of harmane in blood	Familial ET	Sporadic ET	Controls
Log harmane (n=268) [40]	0.50 ± 0.54 g^{-10}/m		0.35 ± 0.62 g^{-10}/ml
Median of Harmane (n=268) [41]	2.90 g^{-10}/ml	2.41 g^{-10}/ml	2.09 g^{-10}/ml
Harmane/Harmine (n= 541) [42]	46.7 ± 140.4	28.3 ± 108.1	13.5 ± 50.3

Louis et al. have demonstrated a strong inverse correlation between cerebellar N-acetyl aspartate (NAA) to creatine (Cr) ratio [3] (NAA/Cr) and blood harmane concentrations in 12 ET cases, where every 1 g^{-10}/mL unit increase in log blood harmane concentration was associated with a 0.41 unit decrease in cerebellar NAA/tCr. The correlation was absent in other brain regions such as thalamus and basal ganglia, or with other neurotoxins such as lead or manganese [39]. In addition, animal studies have demonstrated that harmane and other βCAs produce cerebral damage. However, further confirmations on human post-mortem tissues, including accurate measurements of βCAs levels, are needed [37]. In order to avoid artifactual βCAs formation, tissues from autopsies should be preserved without formol/formaline solutions.

---

[2] Linkage studies have mapped susceptibility loci at gene regions on chromosome 3q13 (ETM1) in Icelandic families, chromosome 2p22-25 (ETM2) in American families, and chromosome 6p23 in North American families (ETM3).

[3] NAA/Cr; a marker of neuronal damage where NAA is a derivative of aspartic acid. It is synthesized and stored primarily in the neurons and hence it is called a marker of neuronal density and viability, Creatine (Cr) is synthesized from amino acids primarily in the kidneys and liver and transported to the peripheral organs by blood and is called as energy metabolism marker. A decrease in the Cr level is due to increased metabolic demands of the tumorous tissue in the brain

1.1.5 Experimental animal models of ET

Animal models of tremor have been developed in experimental neurology because they remain a cornerstone, not only for understanding the pathophysiology of human tremor disorders, but also for the development of novel therapeutic agents. At least two approaches have been used to trigger in animals' tremor reminiscent of ET:

1. Administration of tremorgenic drugs such as harmaline.
2. Use of various inbred strains.

1.1.5.1 Harmaline-induced tremor in rodent model

It has been proposed as a possible model of essential tremor [43]. There are similarities between this model and ET, in particular the attenuation induced by ethanol [44]. Harmaline induces an action tremor with both kinetic and postural components. Anatomically, neurons of the inferior olivary nucleus (ION) have excitatory projections to the Purkinje cells of the cerebellar cortex (climbing fibers). As mentioned earlier, the ION neurons are electrically coupled and generate synchronous oscillations of membrane potentials. Harmaline acts directly on ION neurons, modulating their rhythm-generating ionic currents and facilitating rhythmic discharges. In rodents, it is presumed that harmaline-induced bursting is transmitted from the cerebellum to motor neurons in the spinal cord via the brainstem, thus resulting in generalized tremor (Figure 1.4).

However, three points have questioned the relevance of this model for the pathophysiology of ET, *(i)* the primary target of harmaline: the role of the ION neurons remains controversial in ET and harmaline also directly interferes with several brain neurotransmitters; *(ii)* the transmission pathways: in ET, the cerebello-thalamo-cortical pathways are considered as the main route of electrical bursts spreading from the cerebellar circuitry towards the motor cortex and, subsequently, from the motor cortex to the motor neurons of the spinal cord; and *(iii)* species-specific differences have been observed in the response of the olivocerebellar system to harmaline and in the vulnerability of the Purkinje cell layer [45].
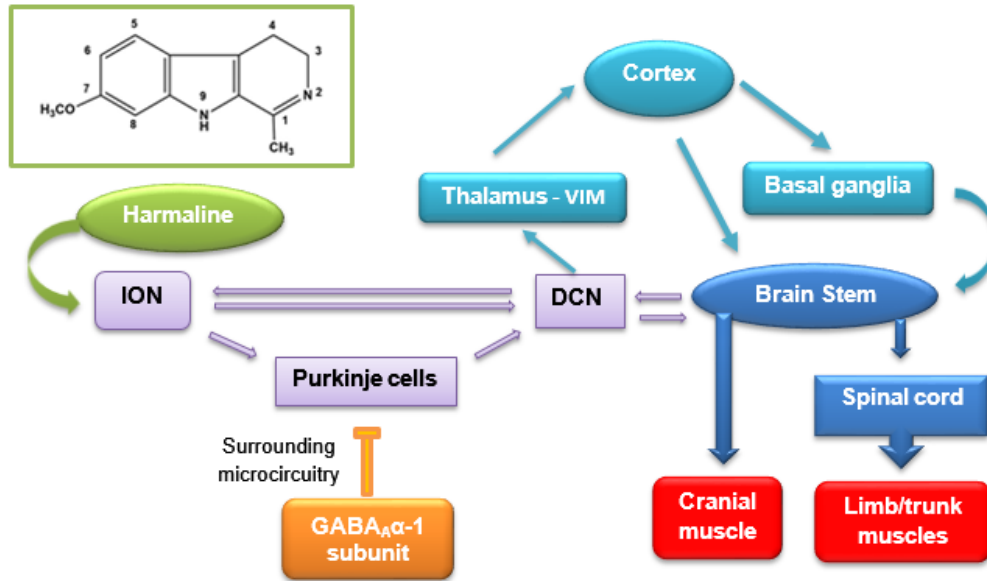
Figure 1.4: Tremor-generating mechanisms and related structures in the CNS. Harmaline directly acts upon coupled neurons of the inferior olive (ION) that are electrically coupled by cytosolic pores formed by the neuron-specific connexin 36 (Cx36) for transmission of electrical. Harmaline enhances neuronal synchrony and rhythmicity in the whole olivocerebellar system via the climbing fiber system. Deep cerebellar nuclei (DCN) project themselves back to the inferior olive via the inhibitory nucleo-olivary pathway. In GABA$_A$ receptor α-1 subunit knockout mice, neuronal response to synaptic GABA is lost in cerebellar Purkinje cells, resulting in rhythmical activities.(VIM: Ventral intermediate nucleus) (original)

1.1.5.2 Degenerative animal Models

A survey of animal models with chronic partial Purkinje cells loss has been reviewed [46] since clinical studies suggest relation between Purkinje cells loss and ET [22]. However, there is a limitation in those reviewed studies as tremor was not their primary interest, In addition, there are no constant results, some models with chronic severe loss of Purkinje cells show no tremor *i.e.* Purkinje cell degeneration mouse where the lost Purkinje cells axon terminals on DCN neurons are replaced by astrocytic glial leaflets [47]; while other models with acute severe loss or chronic partial loss of Purkinje cells may display tremor, *i.e.* Weaver mouse, scrambler mouse, sticky mouse, toppler mouse, WDR81 mouse, shaker rat, PC degeneration in cats [46]. For all those models, further studies are needed to determine the similarity of induced tremors with those observed in ET patients. Still, this suggests that if tremor is associated with PC loss, some other aspect related to degeneration is required for tremor to occur.

1.1.5.3   The GABA$_A$ receptor α-1 subunit knockout mouse model

This model GABAA receptor alpha-1 subunit (GABRA1) knockout line (KO) [48] represents another rodent model of tremor, providing additional insight into the GABAergic mechanism involved in tremor genesis. Deletion of the GABA$_A$ receptor α-1 subunit produces a tremor with postural and kinetic components similar to essential tremor. In these mice, the response to synaptic and exogenous GABA is lost in cerebellar Purkinje cells, but the brain remains morphologically intact. As in the harmaline model, the tremor can be inhibited by ethanol consumption. This tremor is genetic and persistent, an advantage as compared to short-lived chemical-induced tremors. Moreover, the efficacy of the few drugs used in the treatment of human ET is also observed in α-1 knockout mice, lending further support to the model, and possibly providing insight on ET-associated GABAergic dysfunction.

However, this model should not be regarded as a genuine model of ET [49]. First, it has been shown that genetic mutations in the GABA$_A$ receptor α-1 gene have likely no significance in ET. Indeed, the frequencies of the GABRA1 genotypes and allelic variants do not differ between ET patients and control subjects [50, 51]. Secondly, the onset of ET generally appears in elderly population and just occasionally during childhood, while tremor occurs early in development in these knockout mice. Finally, there are noticeable differences regarding the tremor frequency (knockout mouse: 16–22 Hz; ET: 4–12 Hz) [49]. However, tremor frequency is known to be related in particular to the biomechanical features of limbs, such as inertia which is much higher in human.

As none of the animal models completely mimics the phenotype of human ET or recapitulates its histopathology, this clearly limits the prospects of discovering effective therapeutic agents. Also, to better understand the roles of the environment, new models are definitely needed. For instance, simple *in vitro* models, notably neurospheres, 3D lab-grown bundles of human brain cells that mimic the architecture of the cerebral cortex [52], could be adequate to assess neurotoxic agents and potential mechanisms leading to ET. This novel knowledge might help in devising new therapeutic options to identify neuroprotective measures for early-stage patients.

1.1.6 The Treatment of ET

There is still no cure for ET and no therapy has shown an effect on the reduction of the natural progression of the disease. Current symptomatic treatments aim to reduce the involuntary movements as much as possible, providing relief and improving the quality of life (Table 1.3). Current therapies are based on drugs and surgical procedures. The therapeutically option is selected according to the severity of tremor and side effects.

1.1.6.1 Pharmacotherapy

All medications used to reduce tremor have initially been developed and approved for other indications (Table 1.3) [53]. The treatment can be used intermittent, as needed or scheduled basis in minimal functional or social disability, or suppressive therapy in patient with moderate to severe functional or social disability. Unfortunately, the benefit declines with time.

Beta blockers

Beta blockers such as propranolol is one of the drug of choice [54]. Although propranolol is a well-known nonselective β-adrenergic receptor antagonist, the specific mechanism of its antitremor action has not been fully uncovered. The beneficial effect appears to be mainly due to blockade of peripheral beta-2 receptors on extrafusal muscle fibers and muscle spindles [55], even if there may also be a synergistic CNS effect [56]. The daily dose varies from 40 to 800 mg/day with an average dose of 182.5 mg/day [57, 58]. There is no convincing evidence that doses higher than 320 mg/day may provide any additional benefit [58]. The proportion of responders varies from 50 to 70 %, and the average tremor reduction is about 50% when compared with placebo [59]. Efficacy of both conventional and long acting propranolol is established only for tremor affecting the upper extremities, while the head tremor response is quite limited [57, 60]. Side effects include worsening of a pre-existing asthma, sinus bradycardia and fatigue. The β adrenergic antagonists atenolol (β-1 selective) and sotalol (nonselective) are also used for tremor control; atenolol is proposed for patients with an increased risk of bronchospasms [61].

Anti-seizure medications

In the first line therapy also the anti-tremorgenic action of primidone, an anticonvulsant of the barbiturate class which is metabolized into the active metabolites phenobarbital and phenylethylmalonamide (PEMA), is not fully understood. Primidone reduces high-frequency repetitive firing of neurons and modifies transmembrane sodium and calcium channels ion movements, a possible mechanism for both its anticonvulsant and antitremor activities [62]. The daily doses range from 50 to 1000 mg/day and the average dose is around 500 mg/day. Average tremor improvement is up to 75 % reduction from the baseline, even though most studies reported approximately 50 % improvement when compared with placebo [57, 63]. Primidone presents a high incidence of adverse effects, such as nausea, ataxia and confusion, ranging from 22 to 72 % of patients, resulting in a dropout rate from therapeutic studies ranging from 20 to 30 % [64, 65].

Primidone and propranolol may be used in combination to treat limb tremor when monotherapy does not sufficiently reduce tremor [54].

Gabapentin, an anticonvulsant with a structure similar to GABA, probably interacts with auxiliary subunits of voltage-gated calcium channels [66]. According to some studies, gabapentin reduces tremor intensity by 77 % when used as monotherapy in doses of 1,200 mg/day [67].

Topiramate presents complex mechanisms of anticonvulsant action, but it remains unknown which mechanism plays a role in tremor control. Its use is limited by the high incidence of adverse effects [68]

Tranquilizers

The benzodiazepine drugs such as alprazolam and clonazepam [54]. The benzodiazepine alprazolam is an allosteric modulator of the GABAergic neurotransmission, potentiating the influx of chloride ions. The resulting hyperpolarization of the cell membrane inhibits action potential firing [69]. Alprazolam at 0.125 to 3 mg/day reduces limb tremor intensity by 25 to 34 %. Side effects are mild, with sedation and fatigue most common, reported in 50 % of patients [70]. Clonazepam at 0.5-6 mg/day may be particularly useful for treatment of orthostatic tremor, a rare variant of ET, also can be considered in patients with worsening of

tremor due to anxiety or emotional stress. The risk of drug abuse or possible withdrawal symptoms should not be underestimated for benzodiazepines.

Clozapine, an atypical neuroleptic, is recommended only for refractory cases of limb tremor in ET due to the rare but serious risk of agranulocytosis [54, 71], further studies to approve efficacy is needed.

Others

Ethanol decreases tremor severity in up to 50 % of ET patient by unknown mechanism, animal data suggest that ethanol decreased synchronization of inferior olive oscillations by blocking low-threshold calcium channels [72], but the side effects of sedation and intoxication clearly limit its use. However, this has led to new trials for the treatment of ET, especially with long-chain alcohols such as 1-octanol and its metabolite octanoic acid (OA). 1-octanol was demonstrated to be safe and effective with excellent tolerability [73, 74]. Preclinical and early-stage clinical trial data indicate a promising efficacy and acceptable safety for OA, the 1-octanol active metabolite, with more favorable pharmacological properties for drug delivery. However, further studies on long-term safety and efficacy of OA are still needed [75, 76].

A future therapeutic option could be based on the administration of vanillin, a commonly used food additive and flavoring agent. Experimentally, vanillin reduces harmaline-induce tremors in rats. However, the mechanism of action remains again unclear. A potent inhibitory effect on serotonin pathways in the brain has been suggested [77]. Trials in human are missing.

Table 1.3: the recommendation treatment for ET

Line of therapy	Medications	Pharmaceutical class	Dose (mg/day)	Efficacy (%)
1st line	Propranolol	Beta blocker	40-320	50-60
	Primidone	Anti-seizure	50-1000	50
2nd line	Topiramate	Anti-seizure		22-37
	Atenolol	Beta blocker	50-100	25-37
	Sotalol	Beta blocker	80-240	/
	Alprazolam	Tranquilizers	0.125-3	25-34
	Gabapentine	Anti-seizure	1200-1800	33-77
3rd line	Clonazepam	Tranquilizers	0.5-6	/
	Clozapine	Tranquilizers	6.25-75	/

1.1.6.2 Surgical treatment

Thalamotomy

Thalamotomy causes a lesion in the ventral intermediate nucleus (VIM) of the thalamus. The target area is stereotactically localized. Micro-electrodes recordings are used to identify the typical pattern of discharges, confirming the location of the target. Neurostimulation with a macroelectrode can be applied in the awake patient during surgery to estimate tremor reduction and side effects. Unilateral thalamotomy reduces contralateral limb tremor in 80 to 90 % of patients with ET [78, 79]. Bilateral thalamotomy is rarely performed nowadays because of common and often severe side effects [80, 81].

Deep brain stimulation

Deep brain stimulation of the thalamus (DBS) uses high frequency electrical stimulation exerted via an implanted electrode in order to modify the activity of the target area. The exact mechanisms by which DBS suppresses tremor are unknown, and postmortem examinations have not shown any permanent anatomic changes other than the electrode tract [82]. In most cases, four electrodes are placed in VIM at a distance of 1.5 mm from each other, are connected to a pulse generator implanted in the chest wall. Electrode montage, voltage, pulse frequency and pulse width can be adjusted to optimize tremor control [83]. This flexibility in placing and adjusting the "functional lesion" is the main advantage of DBS as compared to thalamotomy that causes an irreversible lesion. Potential disadvantages of DBS include the higher cost and effort in programming and maintaining the device, in addition to dysfunction of the device related to cables. Following unilateral and bilateral DBS, mean tremor improvement reaches up to 60 to 90 % on clinical rating scales as compared to baseline [84, 85].

A long-term study of DBS indicates that, although the benefits continue in most patients, a 35 % of patients reported tremor recurrence [86]. The tremor recurrence can sometimes be effectively treated by changing the parameters of stimulation.

A comparative study on 68 patients concludes that thalamic stimulation and thalamotomy are equally effective for the suppression of drug-resistant tremor, but thalamic stimulation has fewer adverse effects and results in a greater improvement of ET symptoms [78].

Gamma knife surgery (GK)

Gamma knife surgery (GK) is a non-invasive treatment based on radiation beams, from multiple angles to an intracranial target based on anatomical imaging. In the case of ET, the target is the VIM. Alone, each beam is too weak to damage the healthy tissue through which it travels. However, the combined radiation is strong enough at the crossings of the beams to generate a local lesion. Several studies have found favorable results with gamma knife thalamotomy, but the clinical improvement can take weeks to months. In follow-up studies, 92.1% of patients were entirely or nearly tremor-free postoperatively, and 88.2% remained tremor-free four years after the GK [87, 88]. Unfortunately delayed complications, such as complex movement disorders, have been reported [89].

Repetitive transcranial magnetic stimulation (rTMS)

Repetitive transcranial magnetic stimulation (rTMS) utilizes an electromagnet placed on the scalp to generate magnetic field pulses possessing roughly the strength of an MRI scan. The magnetic pulses stimulate an area of about 2.5 cm diameter on the surface of the brain. At low frequency (1 Hz), TMS induces small, sustained reductions in activity in the stimulated part of the brain. Low-frequency rTMS of the cerebellum can effectively modulate the cerebellar output, significantly improving total and specific (tremor, drawing, functional disability) scores, and reducing tremor amplitude [90]. However, a large clinical trial is still missing.

Transcranial direct current stimulation (tDCS)

Another evolving technique of brain neurostimulation is transcranial direct current stimulation (tDCS) [91], a powerful tool for the modulation of the cerebral and cerebellar cortex excitability. The current (usually between 1 and 2.5 mAmp) is delivered at various sites, including the cerebellum and the frontal lobe [92]. Results obtained with the technique of transcranial alternating current stimulation (tACS) suggest that a single neural oscillator insures the temporal stability of ET tremor versus parkinsonian tremor frequency. There is a genuine hope that these techniques will be refined in the next years to reduce ET [93].

1.2 Beta-carbolines and their putative mechanisms of action

Alkaloids are a huge group of organic compound of natural origin (most often of vegetal origin), nitrogenous, more or less basic, of restricted distribution and endowed, at low doses, with marked pharmacological properties [94]. Alkaloids, among many other biological activities, can stimulate or inhibit various receptors, have a role in cell growth and regulation mechanisms, alter DNA, interfere in immune system, present analgesic, narcotic or stimulant activities, sometimes leading to problems such as morphinism, respiratory depression or addictions [95, 96]; their medicinal role has long been a key for developing important drugs and they are actively investigated for new therapies, e.g. for cancer, metabolic or microbial diseases. For man, their source is generally exogenous, through herbal medicines or drugs, but they can be endogenous, formed by spontaneous or enzymatic reactions between carbonyl compounds, often aldehydes, and amines, playing a role in cell activity and in organism's adaptation and regulation mechanisms [95].

The βCAs are a group of indole alkaloids that notably includes harmane, harmine and harmaline (Figure 1.5). βCAs exhibit potent biological, psychopharmacological, and toxicological activities. They occur naturally in plants, foods, and can be formed endogenously in mammals and humans [97].

1-methyl-9*H*-pyrido[3,4-*b*]indole
(harmane) (1)

7-methoxy-1-methyl-9*H*-pyrido[3,4-*b*]indole
harmine (2)
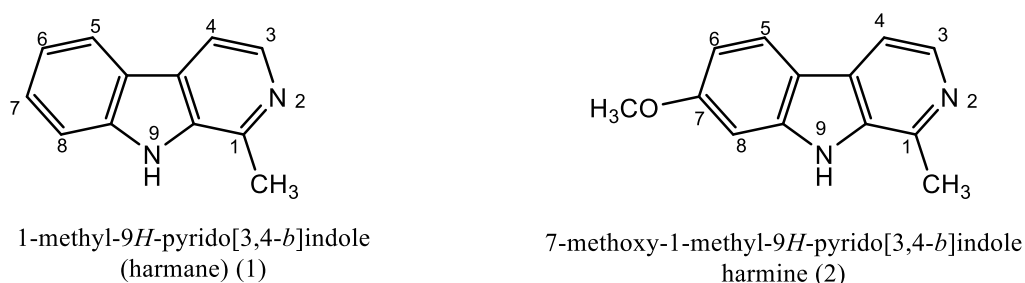
Figure 1.5: Chemical structures of major β-carboline alkaloids (βCAs), 1- harmanse , 2- harmine

Structurally, βCAs are heterocyclic amines, consisting of a combination of five- and six-ringed cycles, containing 2 amine groups. There is some structural similarity with 1-methyl-4-phenyl-1,2,3,6-tetrahydropyridine (MPTP) (Figure 1.7), which is commonly used to produce a major toxin-induced animal models for Parkinson's disease [98]. Like MPTP, the βCAs are highly neurotoxic.

Harmane crosses the blood-brain barrier passive diffusion, thanks to its lipid solubility, and also concentrates in the brain through an active uptake mechanism specific for indole compounds [99, 100]. Laboratory animals exposed to harmane and other heterocyclic amines develop an intense and generalized action tremor a few minutes after administration. Tremor resembles ET [101] and is accompanied by destruction of cerebellar tissues [102, 103]. The increased blood harmane concentrations in ET patients have clearly generated an interest in this pathogenesis hypothesis. However, the mechanisms behind this observation are not clear; increased chronic dietary intake and/or genetic-metabolic factors could be concomitantly involved [41, 102, 104]. Indeed, harmane is particularly abundant in meats, and its concentration is increased by certain cooking practices (e.g., long cooking times, over-cooking) [97, 105], notably through the Maillard reaction, [106, 107].

This alkaloid can also be endogenously generated in human tissues and brain through a Pictet-Spengler reaction arising from aldehydes condensation with tryptamine derivatives (Figure 1.6) [108].
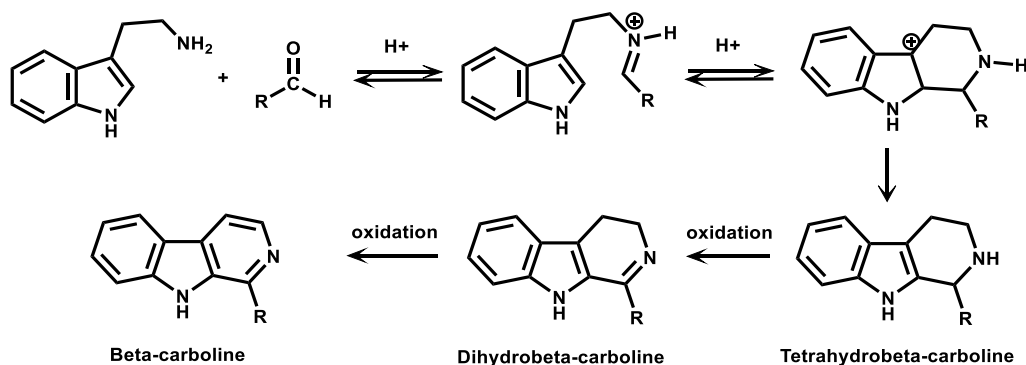
Figure 1.6: Pathway for endogenous synthesis of βCAs by condensation of endogenous tryptamine with aldehydes or keto-acids. Similar reaction could occur with tryptamine derivatives, such as serotonin.

1.2.1 Bioactivation and metabolization of beta-carbolines

The 1-methyl-4-phenyl-1,2,3,6-tetrahydropyridine MPTP (Figure 1.7) is well known to be neurotoxic. Its bioactivation to 1-methyl-4-phenylpyridinium MPP$^+$ is carried out by the MAO$_B$ and MPP$^+$ is selectively absorbed into the nigrostriatal dopaminergic neurons via a dopamine transporter (DAT). Given some structural analogy with MPTP, the potential neurotoxic effects of βCAs were investigated [109]. βCAs are usually less toxic than

MPTP/MPP+. As pointed out in section 1.2, βCAs occur naturally and have been detected in human brain and therefore might contribute to the degeneration of dopaminergic neurons upon chronic exposure [110]. βCA's are also transported by DAT, but with lower efficiency than dopamine. They present enhanced cytotoxicity in DAT-expressing cells. Nevertheless, the low affinities of βCAs to DAT suggest other absorption pathways of potentially neurotoxic βCA$^+$s, independent of DAT [111].

The eventual neurotoxicity of endogenous and exogenous βCAs is probably affected by several factors, including their bioavailability, their toxic potential, their bioactivation/metabolism, their pKa and their affinity for DAT.

The bioactivation of βCAs by N-methyltransferases (NMT) into the cationic neurotoxicants 2-Me-βCA$^+$s and 2,9-diMe-βCA$^+$s is important for their relocalization to the brain and neurotoxicity [112] . Although the N-methylation may occur on both nitrogens, the methylation of the indole nitrogen appears to be the rate limiting step in the development of toxicity [113]. Toxicity increases for βCAs methoxylated on the indole ring [110, 112].

Oxidative metabolism is another route for beta-carboline bioactivation [108, 114], through a reaction catalyzed by heme peroxidases, including myeloperoxidase and lactoperoxidase; these could be key catalysts for the bioactivation of endogenous and naturally occurring N-Me-βCAs [108, 114].

Metabolization of βCAs in the liver and peripheral tissues by P450 enzymes (CYP1A, CYP1A2, CYP2C9, CYP2C19 and/or CYP2D6, depending on the βCA) may serve as detoxification routes, leading to hydroxylated βCAs, suggesting a possible role for cytochromes in protecting from these neurotoxins [115].

1-methyl-4-phenyl-1,2,3,6-tetrahydropyridine (MPTP) (3)   1-methyl-4-phenylpyridinium (MPP+) (4)
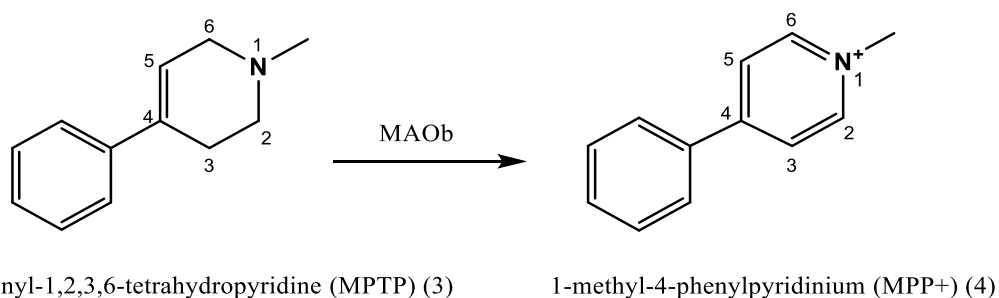
Figure 1.7: Chemical structures of (1) 1-methyl-4-phenyl-1,2,3,6-tetrahydropyridine MPTP (2) 1-methyl-4-phenylpyridinium MPP$^+$

1.2.2 Beta-Carbolines: neurotoxin or neuroprotective?

The neurotoxicity of βCAs depends on the dose. High or chronic doses trigger neurotoxicity [113]. By contrast, low doses may increase dopamine levels and perhaps even present protective properties [116].

Neuroprotective effect

To achieve neuroprotection, both enzymes MAO_A and MAO_B should be inhibited to a certain level. This inhibition decreases the production of detrimental reactive oxygen species (ROS), a primary factor in neurodegeneration. Interestingly, βCAs (norharman and harman) have been identified in cigarette smoke can inhibit MAO enzymes [117]. This inhibition may explain the reduced risk of Parkinson's disease observed in smokers [118]. Nevertheless, it should be emphasized that, although neurodegenerative diseases share many pathological features like oxidative stress, iron accumulation, excitotoxicity and elevated ROS production [119], the neuroprotective action of tobacco smoke cannot be generalized to other neurodegenerative diseases, for example Alzheimer's disease [120].

An example of protective effects is the administration of harmine to a rat model of global cerebral ischemia. Harmine attenuates cerebral infarct volumes and decreases neuronal death. It also causes a significant elevation of the glutamate transporter-1 (GLT-1) mRNA/protein and a remarkable attenuation of astrocyte activation [121]. This translate into a neuroprotective effect in a rat model of amyotrophic lateral sclerosis disease [122]. GLT-1 dysfunction has been shown in the pathogenesis of multiple neurological disorders, including stroke and Alzheimer's disease. These findings certainly warrant further studies.

Neurotoxic effect

Calcium has been incriminated in the pathogenesis of neurodegeneration, the calcium homeostasis deregulation implicates several mechanisms, such as alterations of calcium buffering capacities, deregulation of calcium channel activities, or excitotoxicity that could indirectly cause neurodegeneration. Since GABA pathways are involved in the control of calcium influx, directly via GABAergic receptors and indirectly via astrocytes and glial networks [123], the modulation of GABA transmission is potentially interesting when a neuroprotection is envisioned. It would be worth studying the putative relationship with

22

βCAs, since the hypothesis of an intra-cellular calcium imbalance may apply to all human degenerative processes [124]. Also, the relationships between βCAs and L-glutamic acid decarboxylases isoforms GAD67 and GAD65 (molecular weights of 67 and 65 kDa, respectively) should be further investigated, since these isoforms are responsible for regulating the biosynthesis of GABA and its packaging into synaptic vesicles [125]. Very interestingly, GAD inhibition triggers a N-methyl-D-aspartate NMDA-mediated neuronal degeneration [126]. Recent reports highlight that MDMA (3,4-methylenedioxy-methamphetamine) reduces GAD67 in the hippocampus, with an increase in seizure susceptibility involving glutamate receptor activation [127]. This confirms the importance of GAD67 in the homeostasis of the balance GABA/glutamate. Harmaline increases the extra-cellular concentrations of glutamate in cerebellar nuclei and impairs the NMDA-mediated regulation of glutamate (Figure 1.8) [128]. As discussed here over, ET is highly responsive to alcohol, benzodiazepines and barbiturates, which all facilitate inhibitory neurotransmission by binding to the GABA$_A$ receptor in the brain [36]; a pharmacological correction of GABA dysfunction thus has a potential for ET therapy.
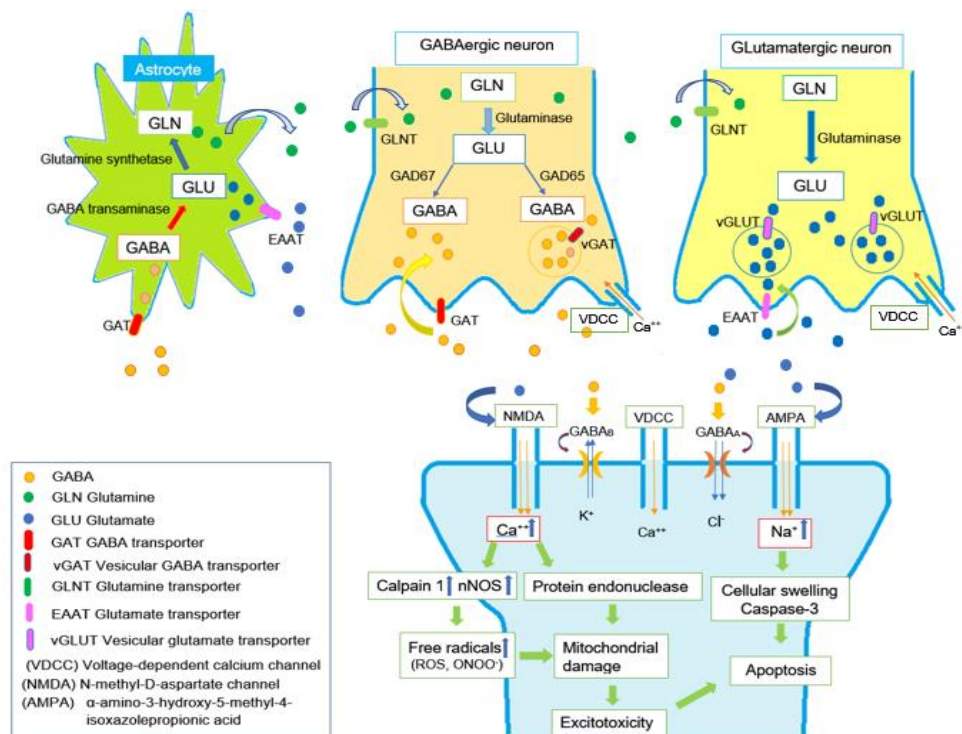
Figure 1.8: Illustration of an astrocyte (green), a pre-synaptic Gabaergic (brown) neuron, a pre-synaptic Glutamatergic neuron (yellow) and a post-synaptic neuron (blue). Overstimulation of glutamatergic receptors results in an excitotoxic cascade triggered by an excess of calcium entry at the post-synaptic site (original).

1.2.3 Beta-Carbolines alkaloids and medicinal plants

The β-carboline alkaloids are natural indole alkaloids with different degrees of aromaticity, they are widely distributed in nature, including various plants and foodstuffs. These compounds are first detected in *Peganum harmala* (Zygophyllaceae, Syrian Rue) a plant that is known for inducing hallucinations and used in traditional medicine for its antimicrobial, analgesic, antinociceptive and abortion effects [129-131]. This plant has different molecules, but the most important are the β-carboline alkaloids harmalol, harmaline, and harmine. Moreover, they are also present in many other plants such as *Banisteriopsis caapi* (also known as ayahuasca) or *Tribulus terrestris* and in *Nicotiana tabaTribulus terrestris* and in *nicotiana tabacum* leaves and cigarette smoke. The neuroactive effects of these molecules may be in part explained by their inhibition of monoamine oxidases (MAO), the enzymes responsible for catalyzing the oxidation of biogenic amines, such as tryptamine, noradrenaline, serotonin and tyrosine, which may affect the development of disorders, such as depression, Parkinson's disease, and Alzheimer's disease [132]. Another study suggests a positive effect on memory due to their affinity with the N-methyl-D-aspartate (NMDA) receptor that controlls synaptic plasticity and memory function [133].

Another β-carboline indole alkaloid, dehydroevodiamine, derived from *Tetradium ruticarpum*, has neuroprotective effects that have been explained by the inhibition of glutamate uptake and release; other studies support the notion that NO is somewhat involved, or suggest an inhibition of NADPH oxidase [134].

All the above demonstrate the different biochemical activities and multiple pharmacological effects of β-carboline indole alkaloids; therefore, there is an interest to study more these compounds for a reduction of their potential risks but also to develop novel pharmacological target.

1.3 Tetrahydroisoquinoline alkaloids and their putative mechanisms of action

The isoquinoline alkaloids are natural substances and one of the largest alkaloid groups; the isoquinoline IQ or tetrahydroisoquinoline THIQ ring is their basic structure (Figure 1.9), they are heterocycles amines consisting of a combination of a benzene ring with a pyridine or piperidine ring.

Isoquinoline ring (5)   Tetrahydroisoquinoline ring (6)
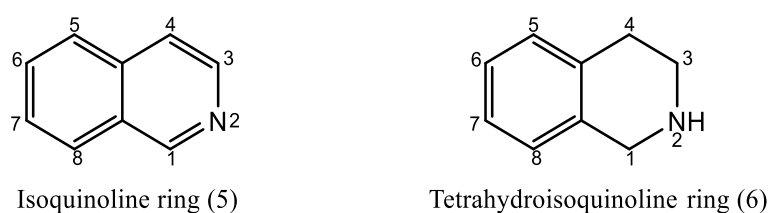
Figure 1.9: Basic elements of the isoquinoline alkaloid skeleton (5) isoquinoline IQ ring (6) tetrahydroisoquinoline THIQ ring.

Tetrahydroisoquinolines (THIQs) are widely distributed among plants, foods and in the environment; some of them are present in the mammalian brain and, since 1980, they are considered as endogenous compounds. The exogenous compounds have the ability to cross the blood–brain barrier (BBB) [135, 136]. The THIQ family contains different subgroups, based on the eventual additional rings connected to the basic structure, the presence of catechol and the N-methylation (Figure 1.10).

1-Me-THIQs (7)   N-Me-1-Me-THIQs (8)   Salsolinol (9)   N-Me-1-Bn-THIQs (10)   1-(3'-4' DH)Bn-THIQs (11)
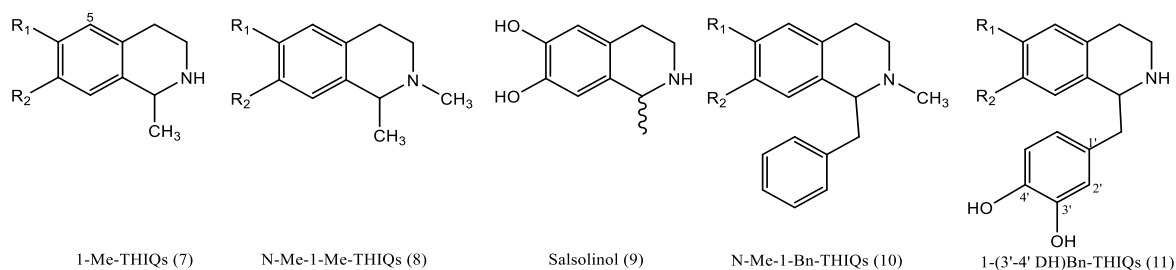
Figure 1.10: Some THIQs derivatives (7) 1-methyl-1, 2, 3, 4-tetrahydroisoquinolines, (8) 1- methyl-2-methyl-1,2,3,4-tetrahydroisoquinolines, (9) salsolinol (1-methyl-6,7-dihydroxy-1,2,3,4-tetrahydroisoquinoline), (10) 1-benzyl-1, 2, 3, 4-tetrahydroisoquinolines, (11) 1-(3'-4' dihydroxy)-benzyl-1,2,3,4-tetrahydroisoquinolines.

The administration of THIQs to a wide range of animal models (primates and mice) was found to reduce the tyrosine hydroxylase (TH)[4] activity and dopamine levels in the brain[5] [137, 138]. Structurally, THIQs/IQs are also somewhat similar to MPTP, the exogenous neurotoxin discussed in section 1.2.1.

The THIQs form endogenously in the brain under physiological conditions by Pictet-Spengler-type reactions through condensation of a biogenic amine (phenylethylamine or catecholamine) with aldehydes, ketone or ketoacids and the conversion to a cationic toxic forms is realized via N-methylation by N-methyl transferases followed by oxidation through MAOs (Figure 1.11) [135].
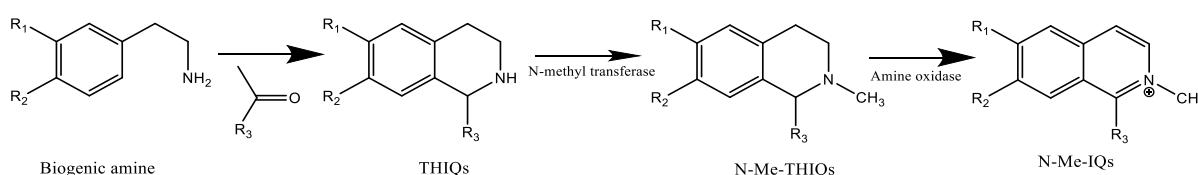
Figure 1.11: Production of THIQs through Pictet-Spengler type reaction between an aldehyde and a biogenic amine, followed by enzymatic conversions to N-Me-TIQs and N-Me-IQs$^+$.

Nonetheless, the formation of THIQs may also be realized through enzymatic pathway. For example, the biosynthesis pathways for (R)-N-Me- salsolinol can be derived via Pictet-Spengler type reactions or via an enzymatic reaction (the condensation of dopamine with pyruvic acid) (Figure 1.12) [139].

It was proposed that THIQs might inhibit the mitochondria electron transport chain complex I so the toxicity could be similar to the one induced by MPTP/MPP+ (Figure 1.13), i.e. a failure of the mitochondrial energy metabolism and the production of ROS [140]. A study of 22 molecules of IQs, including 15 THIQs shows the role of DAT-mediated cellular uptake in their dopaminergic toxicity [141].

Further, some THIQs might cause oxidative stress through the production of isoquinolinium cations by the non-enzymatic auto-oxidation of N-Me-THIQs, yielding the highly reactive

---

[4] Tyrosine hydroxylase (TH) is s the enzyme responsible for converting tyrosine to dopamine
[5] The reduction of dopamine level in the brain implicated in different nervous system diseases: Parkinson's disease; symptoms include tremors, slowed movement, and sometimes psychosis.

hydroxyl radicals. This results in DNA damage and apoptotic cell death; the presence of Fe^{2+} boosts this mechanism while the antioxidants inhibit it. This has notably been shown for N-methylsalsolinol on dopaminergic neuroblastoma SH-SY5Y cells [142].
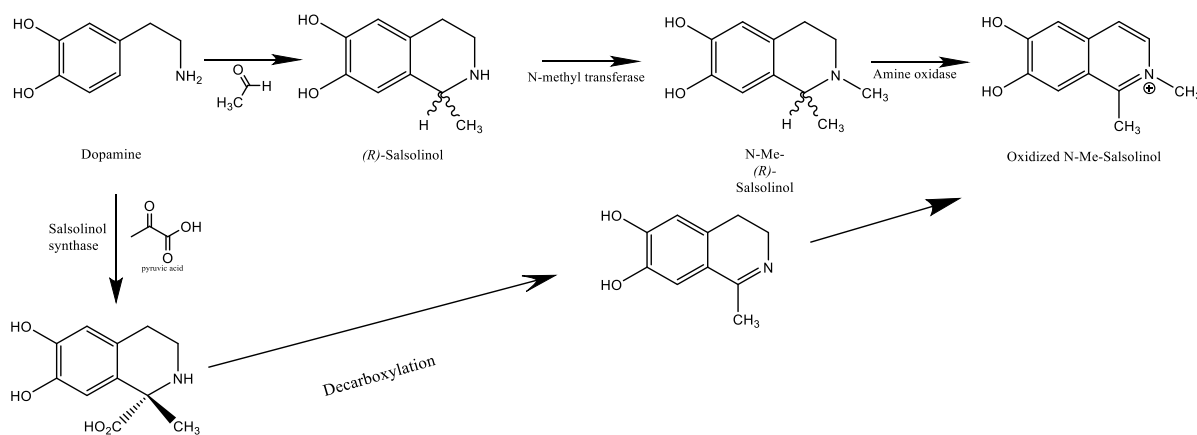
Figure 1.12: Stereo-specific enzymatic production of salsolinol from dopamine via (R)-salsolinol and pyruvic acid, followed by decarboxylation, and its non-enzymatic formation by the Pictet-Spengler reaction of dopamine with formaldehyde.
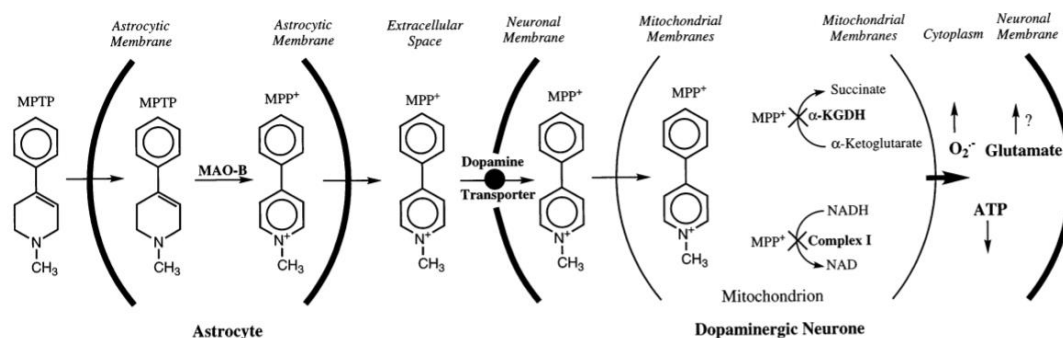
Figure 1.13: Illustration of the mechanism of action of MPTP as suggested by McNaught et al.1998 [135]. After crossing the BBB through simple diffusion, MPTP is oxidized by MAO_B in astrocytes to produce its active metabolite MPP+. MPP is released to the extraneuronal space; then, via the dopamine re-uptake system, it is accumulated into dopaminergic neurons. In neurons, MPP+ is concentrated in the mitochondria, via an energy dependent mechanism, where it inhibits the complex 1 of the respiratory chain and the α-KGDH of the tricarboxclic acid (TCA) cycle. Consequently, there is ATP depletion, elevation of ROS and possibly an increase in the glutamate levels that precede neuronal death.(source [135])

1.3.1 Bioactivation and metabolization of THIQs

The activation of THIQs might be through N-methylation via N-methyltransferase and oxidation via MAO. On one hand, the N-methylation is an important step in the *in vivo* activation of THIQ as N-Me THIQs derivatives appear more neurotoxic. For example, upon perfusion of (R)-salsolinol in rat brain, its N-methylated derivative (NM(R)Sal = (R)-1-methyl-6,7-dihydroxy-1,2,3,4-tetrahydroisoquinoline) appears more concentrated in the vicinity of dopaminergic neurons, inducing behavioral changes very similar to those observed in Parkinson's disease: hypokinesia, stiff tail, limb twitching at rest and postural abnormality [143, 144].

On the other hand, the oxidation of THIQs is indispensable for the selectivity and intensity of neurotoxic effects on dopaminergic neurons; the comparison of necrotic effects of NM(R)-Sal and its isoquinolinium ion indicates a more potent toxicity of the ion that notably results in ATP depletion [143, 145].

The metabolization of THIQs in the liver and peripheral tissues by P450 CYP2D isoenzymes is a main detoxification and elimination pathway, through the formation of 4-hydroxyl-ions; there is a suggestion that the inhibition of liver metabolization does increase the THIQs concentration in the brain and the possibility of neurotoxic effects [146]. The concentration of exogenous THIQs in the brain also appears related to their brain entry through the organic cation transporter (OCT) system, known also as the extra-neuronal monoamine transporter, more specifically OCT3, and their brain elimination through P-glycoproteins (P-gp); any modulation of these transporters will then affect the brain concentrations [147].

1.3.2 THIQs: neurotoxins or neuroprotectors?

As discussed in the previous sections, the pharmacokinetic and cytotoxic (induction of ROS) characteristics of some isoquinoline derivatives resemble those of MPTP. These THIQs properties, their endogenous formation and wide presence in the environment make it reasonable to assume that an acute or chronic exposure to some THIQs might lead to neurodegenerative diseases.

The THIQs and their derivatives seem to present a broad range of actions in the brain and a potential neuroprotective role cannot be neglected. By contrast with MPTP, some THIQs in fact increase the levels of glutathione (GSH), nitric oxide (NO), and S -nitrosothiols, with a positive impact on the redox capacities, consequently affording a protection against oxidative stress [148]. Notably, an endogenous metabolite found in brain, is reported to be neuroprotective and has the ability to antagonize the effects of MPTP and other neurotoxins; as 1-Me-THIQ has no affinity to dopamine receptors and does not interfere with the inhibition of the mitochondrial respiratory complex I, this neuroprotective effect has been proposed to result from direct antioxidant effects and/or induction of antioxidative enzymes [149]. Some *in vivo* and *in vitro* evidence also indicate the ability of 1-Me-THIQ to reversibly inhibit MAO_A and MAO_B, to antagonize glutamatergic systems [150], and to confer neuronal tolerance to excitotoxicity [151]. Such neuroprotective effects are not exclusive to 1-Me-THIQ and were reported for other molecules like salsolinol; while the oxidated form of N-methyl(R)salsolinol is a neurotoxicant that induces apoptotic cell death, (R)salsolinol has the ability to scavenge hydroxyl radical produced by oxidation of dopamine.

It seems then that the neurotoxicity and neuroprotection presented by catechol isoquinolines may be ascribed either to their oxidation or their scavenging of ROS [152].

Despite their structure somewhat similar to MPTP, we can assume that not all THIQs have toxic effects; their biological actions are critically dependent on their catechol moieties and metabolism, so while some THIQs are potent neurotoxins, like tetrahydropapaveroline THP (1-[(3,4-dihydroxyphenyl)methyl]-1,2,3,4-tetrahydroisoquinoline-6,7-diol) and 1-benzyl-1,2,3,4-tetrahydroisoquinoline (1BnTHIQ), others, such as higenamine (1-[(4-hydroxyphenyl)methyl]-1,2,3,4-tetrahydroisoquinoline-6,7-diol) and 1-methyl-1,2,3,4-tetrahydroisoquinoline (1-MeTHIQ), are neuroprotectants and have neurorestorative actions [153].

1.3.3 Isoquinolines and medicinal plants

Isoquinoline and tetrahydroisoquinoline alkaloids, widespread among the plant kingdom, are also active compounds of widely used traditional herbal medicines, for example opium (*Papaver somniferum* L.), ipeca (*Carapichea ipecacuanha* (Brot.) L.Andersson, synonym of *Cephaelis ipecacuanha* (Brot.) Willd.[154], peyotl (*Lophophora williamsii* (Lem.) J.M.Coult.), curare (*Strychnos icaja* Baill.),… Some of them are very well known for neuroprotective effects.

Berberine (Figure 1.14), an isoquinoline alkaloid found in medicinal herbs like Coptidis Rhizoma (*Coptis chinensis* Franch.) and Phellodendri Cortex (*Phellodendron amurense* Rupr.) is used to treat metabolic disorders, microbial infections, and inflammation but is also known as anxiolytic, antidepressant, antinociceptive and neuroprotective. Recent studies on berberine neuroprotective efficacy indicate multiple mechanisms, notably anti-inflammatory effects on microglia, the main immune system of the brain, antioxidant effects, cholinesterase inhibition and anti-amyloid effects [155, 156].

(R/S)-Salsolinol (Figure 1.10), a THIQ famous for its dopaminergic activity, is present in *Theobroma cacao* L.; in cacao and chocolate, salsolinol seems to play a role in chocoholism (chocolate addiction) through multiple effects on the pituitary gland, leading to inhibition of cAMP formation and β-endorphin and adrenocorticotropic hormone (ACTH) release; salsolinol also has the ability to bind to D_3 dopamine receptors, a family close to D2 receptors which gives it an importance in drug design for dopamine-related disorders [157, 158].
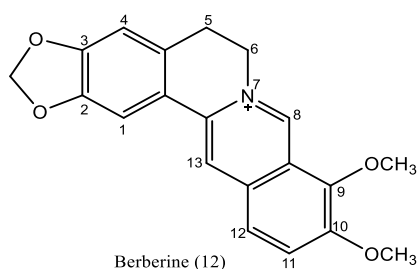
Figure 1.14: Structure of berberine (12).

1.4 Maillard reaction

The Maillard reaction [159], named according to its first describer Louis-Camille Maillard in 1912, known also as the major "cooking reaction", is a succession of non-enzymatic glycation thermal reactions that provide the basis for the browning colors and aromas characteristic of cooked foods, e.g. grilled meat, roasted coffee, fried onions or toasted bread.

The Maillard reaction (Figure 1.16) is a complex network of reactions subdivided by Hodge into [159]:

1- An initial stage begins by electrophilic condensation of a carbonyl group (Figure 1.16 reaction A), usually on an aldose[6] or sometimes a ketose, and an amino group, commonly on a protein, peptide or amino acid, followed by elimination of water to yield a Schiff base (an acyclic imine sugar adducts, i.e. a N-substituted glycosylamine). All these reactions are completely reversible and usually in equilibrium. This amine-sugar condensation is followed by an irreversible Amadori[7]/Heyns[8] rearrangement (reaction B) [160].

2- An intermediate stage includes 3 different types of reactions: *(i)* the sugar dehydration (Figure 1.16 reaction C), that could occur in different ways, depending on the pH (loss of 2 and 3 water molecules in alkaline or neutral and acid conditions, respectively); *(ii)* the sugar fragmentation (Figure 1.16 reaction D), suggested to occur by retroaldolisation or oxidative fission; and *(iii)* the Strecker degradation (Figure 1.16 reaction E) that involves the deamination of an external amino acid in the corresponding aldehyde.

3- A final stage that includes *(i)* the aldol condensation (Figure 1.16 reaction F) of the aldehydes produced by reactions C, D and E, these reactions are catalyzed by amines to give aldols and N-free polymers ; and (ii) complex aldehyde-amine polycondensations (Figure 1.16 reaction G) to produce high-molecular weight heterocyclic nitrogen compounds, the highly colored melanoidins. The condensation

---

[6] Reducing sugar

[7] The Amadori rearrangement is an isomerization of an aldosylamine in the corresponding α-amino ketose (ketosamine)

[8] The Heyns rearrangement is an isomerization of a ketosylamine in the corresponding α-amino aldose (aldosamine)

might be with amines like tryptamine or dopamine, followed by an eventual Pictet-Spengler -type reaction, leading to the formation of various βCAs and THIQs heterocycles (Figure 1.15).

This reaction needs a high temperature (140-165°C) and largely depends on the heating conditions, pH, water content and amino acids/peptides/proteins profile of the cooked food; so different amounts of different compounds, still largely uncharacterized, can be formed to give a variety of potential flavors. There is a major interest in this reaction for food processing, pharmacology, toxicology and life sciences [161, 162].
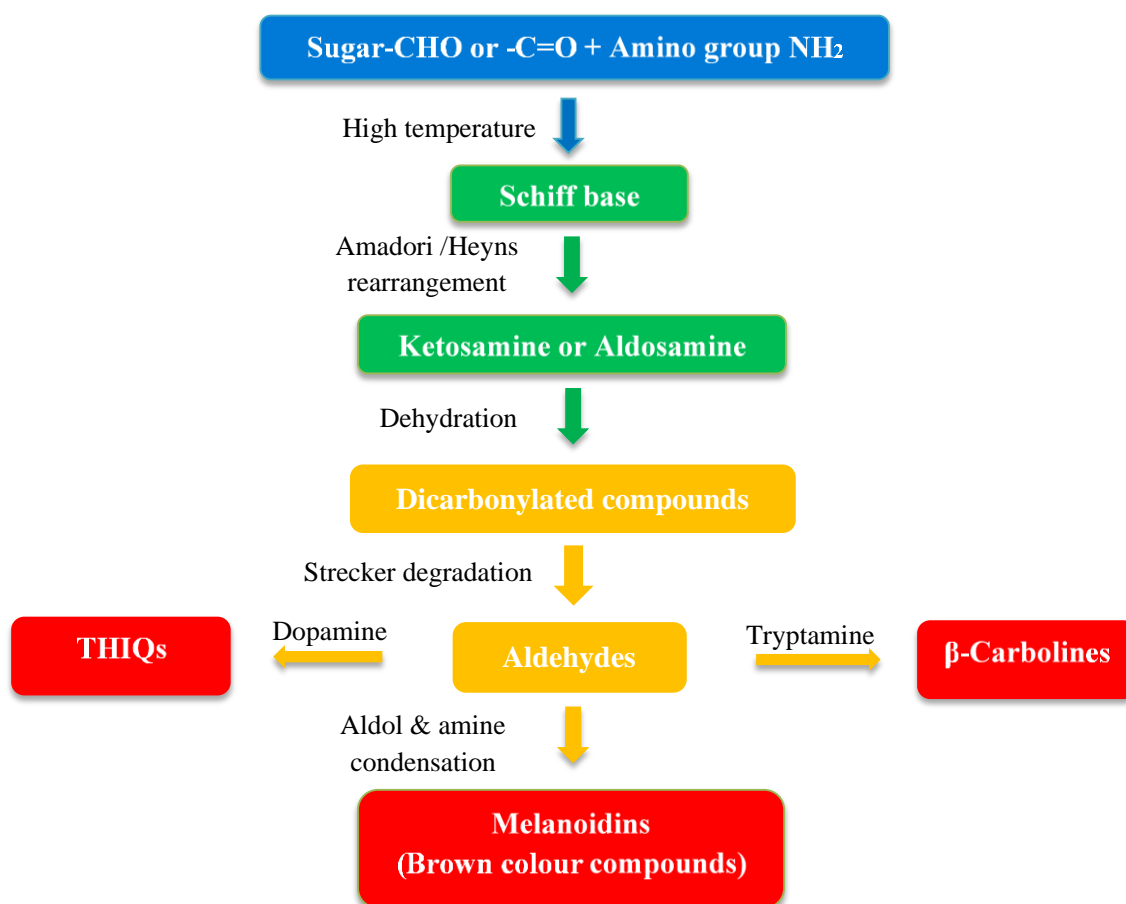
Figure 1.15: Suggested pathway for the formation of β-carbolines and tetrahydroisoquinolines through the products of Maillard reaction, as a result of condensation of aldehydes product of Strecker degradation with dopamine or tryptamine (original).
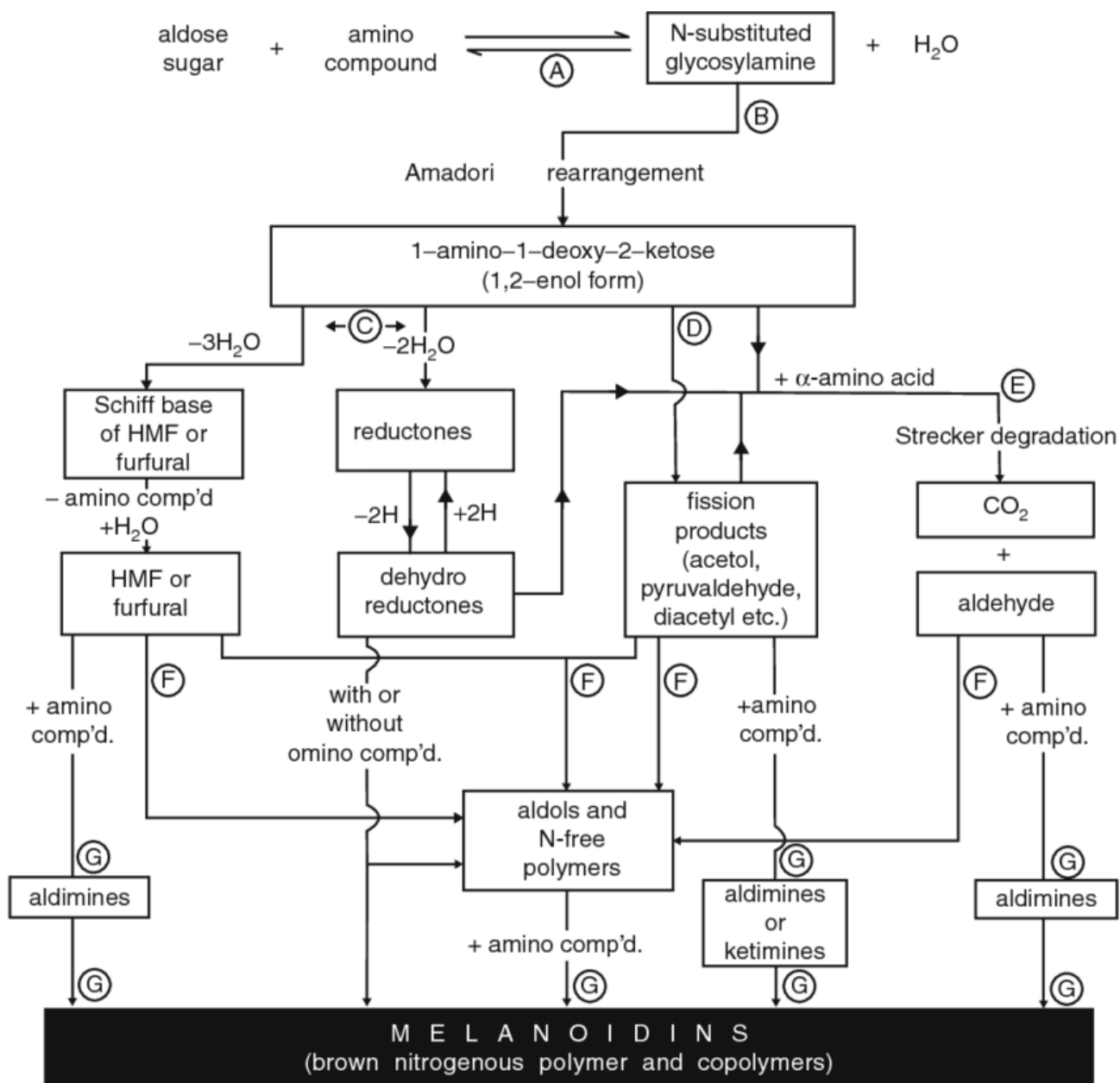
Figure 1.16: Modified Scheme of the Maillard reaction (Hodge) (source [163]). The carbonyl group of the sugar reacts with the amino group of the amino acid (A), producing N-substituted glycosylamine and water. The unstable glycosylamine undergoes Amadori rearrangement, forming ketosamines (B). There are several ways for the ketosamines to react further: i) Produce 2 waters and reductones or 3 waters and schiffbase (C) ii) short-chain hydrolytic fission products can be formed (D). c) Strecker degradation to aldehydes and CO_2 (E). Finally, aldol condensations to produce aldols and N free polymers (F), and complex aldehyde-amine polycondensations to produce brown nitrogenous polymers and melanoidins (G).

1.5 Mammalian endogenous alkaloids

Mammalian endogenous alkaloids occur, naturally or accidentally, through non-enzymatic or enzymatic reactions, and include a range of derivatives, such as isoquinolines, β-carbolines and thiazolidines. Their production is depending on the concentration of biogenic amines and/or carbonyl compounds and might change during certain pathological conditions or metabolic disorders [164, 165].

The principal mammalian alkaloids are condensation products of aldehydes or α ketoacids with *(i)* catecholamines (e.g. dopamine, norepinephrine), or their precursor amino acids, to yield 6,7 dihydroxy-1,2,3,4 tetrahydro-isoquinolines; and *(ii)* with indolamines (e.g. serotonine or tryptamine), to yield 1,2,3,4 tetrahydro-β carbolines. Those endogenous metabolites of neurotransmitters are normally present in small amounts, but their concentrations may increase during certain diseases or pathological conditions such as CNS complications of chronic alcoholism or Parkinson's disease [96]. For example, the production of TIQs is likely in alcoholism, through the first ethanol metabolite, acetaldehyde that *(i)* has been shown to condense with dopamine to yield (R/S) salsolinol (see section 1.3); and *(ii)* competitively inhibits nicotinamide-adenine dinucleotide-linked aldehyde dehydrogenases, preventing the further degradation of 3,4-dihydroxyphenylacetaldehyde, the MAO metabolite of dopamine; this arylacetaldehyde has been hypothesized to condense with dopamine to yield tetrahydropapaveroline, a neuroactive compound possibly related to opioids (Figure 1.17) [164, 166]. Such TIQs probably participate in the pathogeny of alcoholism. The limited capacity of brain to oxidize aldehydes may be of pharmacological importance in the presence of drugs such as chloral hydrate and paraldehyde which inhibit this enzyme [167].

This intriguing possible formation of endogenous highly active metabolites raises many questions. More investigations are clearly needed to determine whether reported increases in β-carbolines and/or THIQs levels are related to dietary sources through *(i)* direct uptakes of food-borne alkaloids; or *(ii)* uptakes and/or *in vivo* formation of carbonyl metabolites that increase the alkaloids endogenous synthesis. In addition, it would be important to study the possible function and role of these alkaloids to determine whether such increases are a cause or a consequence of disease/disorder.
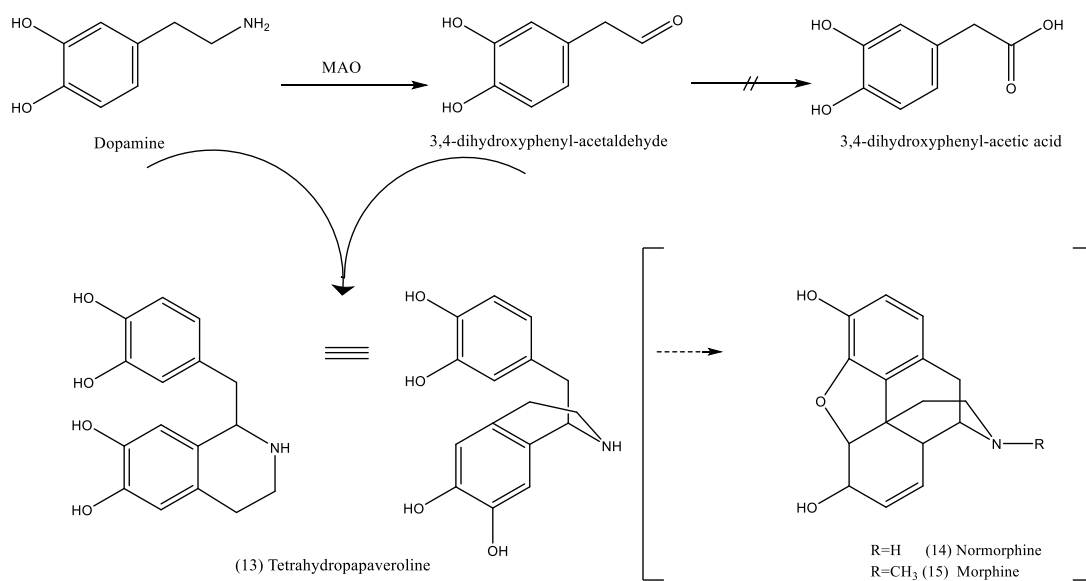
Figure 1.17: Representation of the hypothesis of dopamine condensation with his MAO metabolite to yield (13) tetrahydropapaveroline (THP), an alkaloid with a clear structural proximity to (14) R=H normorphine, (15) R=CH$_3$ morphine, as possible basis for biological activities.

1.6 *In vitro* models applied in the study of drugs and toxicants

Cell culture systems are indispensable tools widely used for *in vitro* research studies, in which cells or tissues are maintained alive outside the living organism or their biological surroundings by culturing in adequate supported artificial media. The aim of such models is to simplify the study of complicated *in vivo* phenomena or biological properties by creating a well-controlled environment with defined conditions that facilitate the evaluation of cell response in quantitative and repeatable conditions. The applications of *in vitro* models are long established in different science fields like tissue engineering, drug discovery or toxicity studies (Figure 1.18).
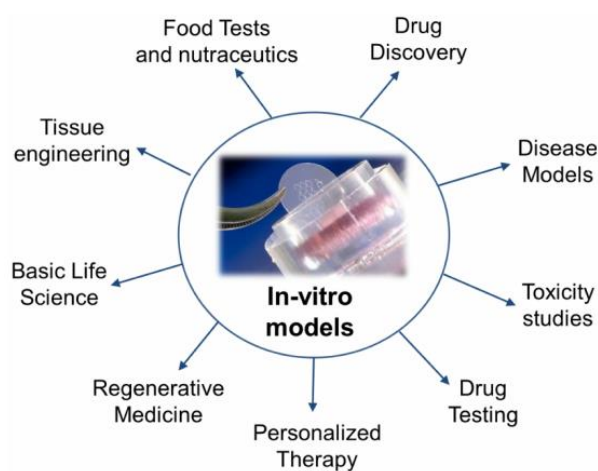
Figure 1.18: Application of in vitro models (source [168]).

1.6.1   2D cell cultures in the study of drugs and toxicants

The widest used *in vitro* models are classical 2D models based on two-dimensional cell monolayers adherent on flat surfaces. This methodology is well-established, simple, convenient, cost effective and highly reproducible with a certain ease of handling, imaging and quantifying. Also, in a suitably installed model, the nutrients, growth factors and oxygen are equally distributed among cells. Even though 2D cell cultures have proven their capability in cell-based studies, they are unable to faithfully represent a complex *in vivo* environment which has a direct reflect on the result of tests applied on it.

In drug discovery (Figure 1.19), the first step is basic research, in which *in vitro* pharmacology has an important role, followed by *in vitro* and *in vivo* preclinical

developments (study of pharmacology, metabolism, toxicity), then clinical trials (definition of dosage, metabolism, efficacy and safety). Part of failures in clinical trials relates to the often partial information gathered from *in vitro* assays; the dominant 2D cell culture tests may mask or exaggerate the response to drugs tested in such unnatural microenvironments; for example, cytotoxicity assays based on 2D cell cultures present important limitations that may partially account for the high reported rates of clinical trial failures in anticancer therapy [169]. It is now admitted that the closer to *in vivo* environment in which the cultured cells grow, the better they mimic the future *in vivo* response to drugs; this certainly allows to reduce the number of animals used in research, reduce the costs and increase the chances to develop an effective drug.
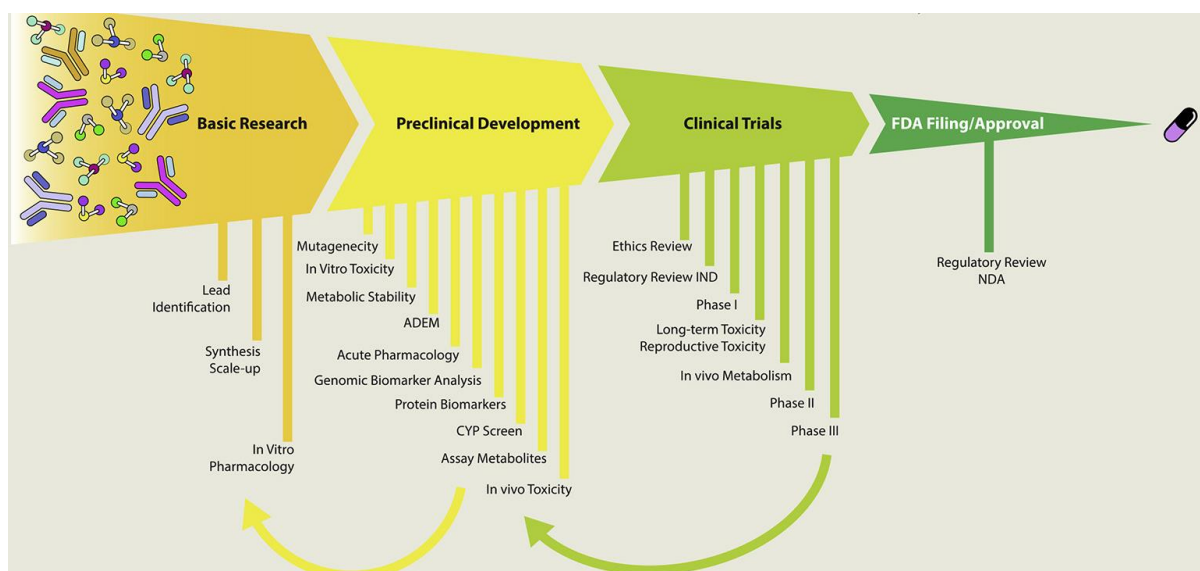
Figure 1.19: A schematic of the activities involved in the drug discovery and development process. At the left the basic research on small molecules and biological molecules being considered for development based on in vitro pharmacology. Specific activities in the stages of preclinical development; they include studies of absorption, distribution, excretion and metabolism (ADEM), screening for activity at cytochrome P450 (CYP) liver enzymes, then the clinical trials with ethics review and regulatory filings for Investigational New Drug (IND).Finally, the approval based on regulatory review to arrive a New Drug Application (NDA) (source [170]).

In the CNS drugs field, particularly, the development times and failure rates appear extremely high, compared to most other drugs [170]; the failure rates of CNS drug candidates at the pre-clinical stage reaches almost 99 % and surpasses the 90 % in phase 1, especially for neurodegenerative diseases [171, 172]. For this reason, it is indispensable to develop more relevant *in vitro* models that can effectively bridge the gap between traditional 2D cultures

and animal models, more faithfully representing the *in vivo* cells behaviors, more predictive in their response and cost-effective.

1.6.2   3D cell culture in the study of drugs and toxicants

In vivo cells grow within a complex three-dimensional (3D) microenvironment which limits the relevance of 2D culture systems to an *in vivo* situation, and makes them the less biologically relevant models, missing complex cell-to-cell interactions [173-176]. *In vivo* microenvironments and their dynamics are poorly understood and remain a major challenge in developing a representative *in vitro* model. Huang et al [177], classified the key elements of a cellular microenvironment in four groups (Figure 1.20): *(i)* the neighboring cells; adjacent cells directly interact through direct cell-cell physical contacts and indirectly by soluble factors and mechanical communication through the fibrous extracellular matrix (ECM); *(ii)* the factors soluble in the aqueous microenvironment include basic nutrients, signaling molecules like hormones and growth factors; *(iii)* the ECM itself, a complex network of non-cellular components that provide a biological scaffold and regulate the cell growth, viability, motility and differentiation; and *(iv)* the physical fields that include the stress-strain, heat, magnetic or electrical stimuli that *in vivo* cells respond to [177].
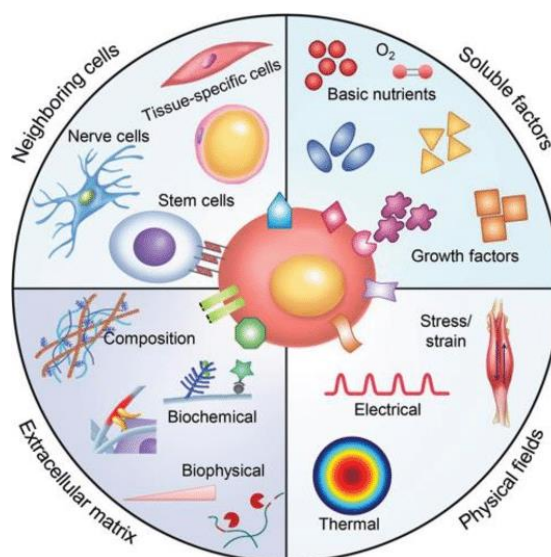
Figure 1.20: Schematic representation of the essential components of the cellular microenvironment that provides structural support and regulates cell behavior. (Adapted from (Huang et al., 2017). Copyright © 2017American Chemical Society; source [178].

The adjunct of a third dimension to the culture system allows to introduce these important aspects of extracellular matrix, cell-to-cell exchanges, spatial organization, nutrient access, cell geometry and cell mechanics; those affect various receptors engaged in interactions, modulating cell response and gene/protein expression, closely mimicking the cellular microenvironment [179, 180]. And thus, a 3D model is expected to better mimic the *in vivo* behavior of cells than 2D cultures (Table 1.4) [177, 181].

This reasoning led to the development of various models that simulate organs such as retina, intestine, pituitary, heart, brain or liver [182-188]. The ability of spheroidal models to predict toxicity has notably been shown and such cultures are expected to improve toxicology screening tests [189-191].

Table 1.4: Key differences in cellular characteristics and processes between two-dimensional and three-dimensional Culture Systems [192]

Key Characteristics	2D-Cell Culture	3D-Cell Culture	References
Cell Shape	Flat and stretched	Natural shape (ellipsoid/polarized) is retained	[193]
Cell interface to medium	All cells are equally exposed to media components	As in physiological conditions, there is a gradient availability of media components. Upper layers of cells are highly exposed over the lower layers *(Heterogeneous exposure)*	[194, 195]
Cell junction	Cell junctions are less prevalent and do not mimic physiological conditions	Cell junctions are prevalent and enable cell-to-cell communication.	[196]
Cell differentiation	Moderate and poor differentiation	Improved differentiation	[197]
Drug metabolism	Drug metabolism not well observed	Enhanced drug metabolism with increased expression of CYP enzymes	[198, 199]
Drug Sensitivity	Cells are sensitive and drugs show high efficacy	Cells often show higher resistance and drugs lower potency	[200]
Cell Proliferation	Higher proliferation rate than in natural environment	Proliferation rate may be high or low, it is based on cell type and 3D-cell culture technique	[201, 202]
Response to stimuli	Poor response to mechanical stimuli of cells	Well-established responses to mechanical stimuli of cells	[203]
Viability	Sensitivity to cytotoxins	Higher viability and lower susceptibility to external factors	[200]
Apoptosis	Higher susceptibility to drug-induced apoptosis	Enhanced resistance to drug-induced apoptotic stimuli	[204]

1.6.2.1 Organotypic cultures

Organotypic cultures correspond to the culture of organ or tissues, collected from an organism, that conserve the structural and connection organization of the original tissue. They are usually derived from early post-natal animals to ensure modelling the *in vivo* maturity, differentiation, and organization of cells (Figure 1.21). This model allows to maintain the architecture of organ or tissue, permitting the study of different populations of cells or individual cells in a state very close to *in vivo* conditions [205]. The model was applied on lung [206], small intestine [207], colon [208], brain [209] and aorta [210]. The challenges with this model are maintaining tissue viability, and the complexity of interpretation an experimental manipulation even though the optical access was facilitated in the experimental interventions within native stromal tissues [205].
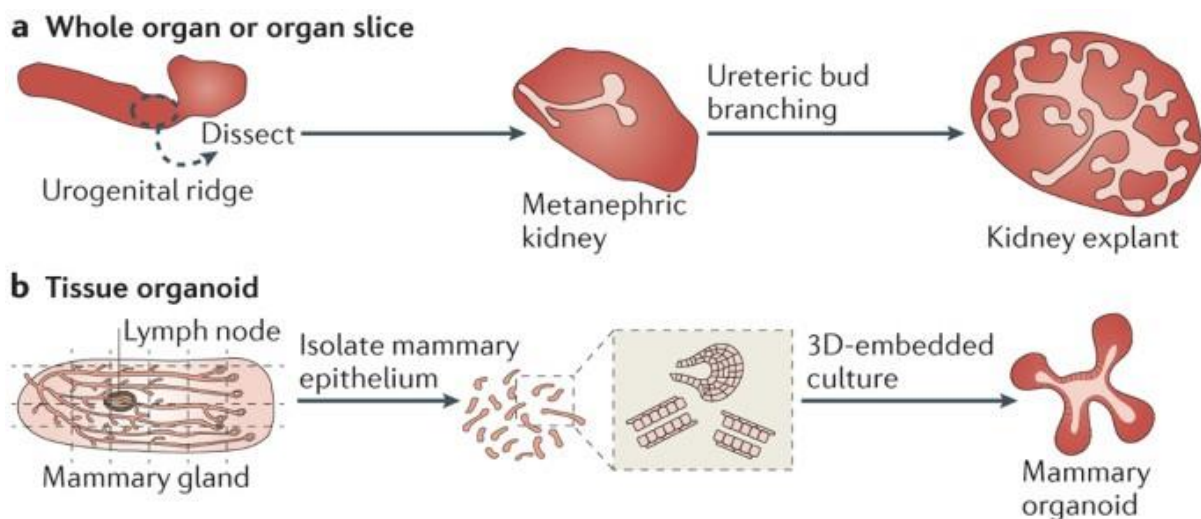
Figure 1.21: Represent cellular inputs to organotypic cultures. A) Whole-organ and organ-slice cultures. Explants of metanephric kidney that have been isolated from the embryonic urogenital ridge will undergo vigorous branching morphogenesis in three-dimensional (3D) culture. B) Tissue organoid cultures. Isolated mammary epithelial from mammary gland processed by mechanical disruption and enzymatic digestion into epithelial tissue fragments, that have been cultured after removing the native stromal cells and extracellular matrix, resulting organoids contain diverse epithelial cell types organized in their normal spatial (source [205]).

1.6.2.2 3D models

The 3D models are obtained through different techniques (Table 1.5) that can be classified in two groups (Figure 1.22), i.e. non-scaffold models (self-aggregation of spheroids in "hanging drops" and micro-wells) and scaffold models (biological, i.e. hydrogels, and solid scaffolds).
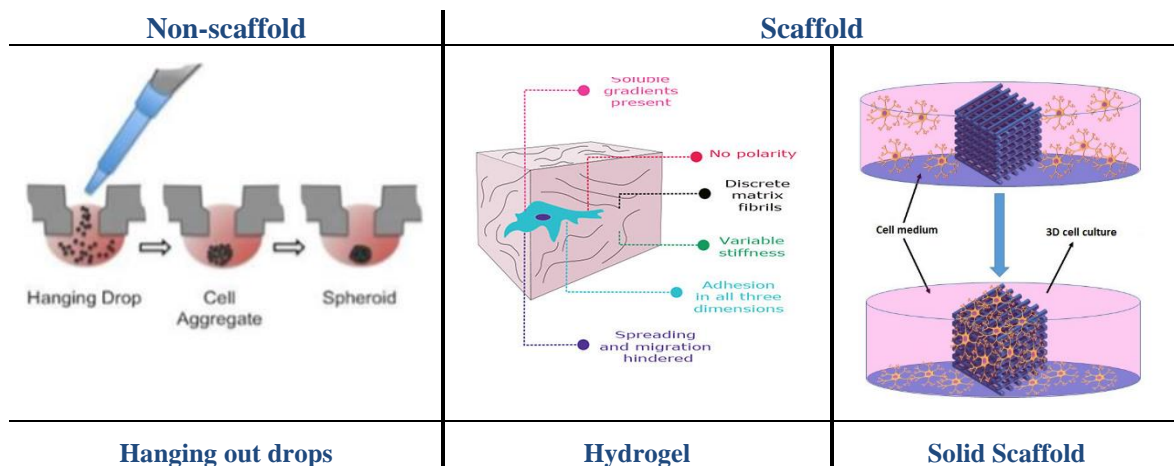
Figure 1.22: Simple illustration for the3D cultures techniques with two major groups non-scaffolds represented by hanging out drops techniques and scaffold groups with two major subgroup with hydrogel scaffold that might be from different resource and solid scaffold that could takes different shapes (source [211-213]).

1.6.2.2.1 The non-scaffold models

Those models are based on the self-assembly and aggregation of cells in 3D spheroid structures over time in the absence of attachment scaffold/surface; the size of spheroids can be controlled by the number of dispensed cells. This group comprises 4 subgroups or methods:

I. ***Hanging drop plates***

This method can be applied in special *"hanging drop"* plates (HDP) (Figure 1.23); these *"hanging drop"* plates present unattached bottoms that allow the formation of discrete droplets small enough to avoid spheroid displacement when manipulating, the simple spheroid formation by gravity is easily accessible. Spheroids formed in HDP plates have evolved into a common 3D cell culture technology in cancer research [214], hepatotoxicity [215] neurotoxicity [216] and others. However, the lack of cell-ECM interaction and the difficulties of media exchange, spheroid

handling and transfer step, in addition to the need of transferring the spheroids to another plate for prolonged culture or experimental procedures, limit this method.
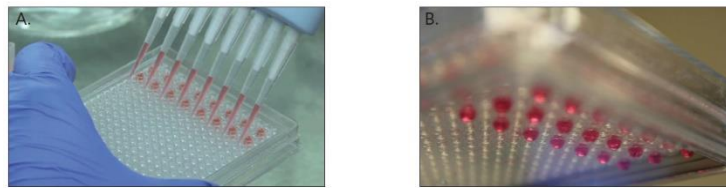
Figure 1.23: Visualization of hanging drop microplate in 96- and 384-well configurations top and bottom openings (source images courtesy of 3D Biomatrix [217]).

II. ***Hanging drop in ultra-low attachment microplates (ULP)***

In these plates (Figure 1.24), round- or V-shaped wells ensure the formation of isolated spheroids in the center position and, unlike HDP, the well shape and depth provide larger media volume capacity to allow various experiments in the same plate, still the media exchange is a critical step. The ULP is incorporated into current research for the development of cell culture system models and improved assay for drug screening where the propagation and cell viability after exposure to cytotoxic agents was examined [218-220] as well as drug delivery assessments [221].
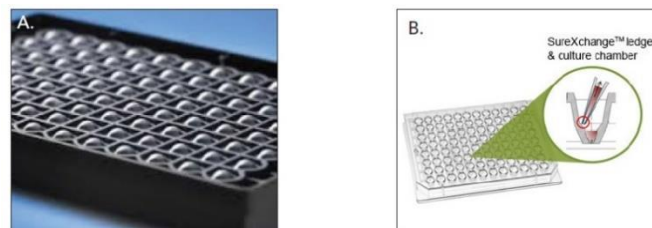
Figure 1.24: Image of (A) Corning ultra-low attachment (ULA) spheroid microplates round and (B) tapered well bottom configurations (source [217]).

III. ***Spheroids auto-assembled in lab-molded agarose microwells***

The complexity of hanging drop spheroid culture microplate and the inconvenience of ultra-low attachment microplates (loss of spheroids when pipetting the medium) create the need to develop efficient, convenient and low-cost tools for spheroid culture [222]. An engineering solution, created by different 3D agarose shape printing for scaffold-free small diameter wells, proves biocompatibility as cells do

not adhere to agarose, favoring cell-to-cell adhesion. Different models were developed [223-225] and a commercial molds (3D Petri Dish) are available for different application (Figure 1.25); for example, researchers applied this mold to study complex therapeutic effects in 3D tumor microenvironments [226, 227]
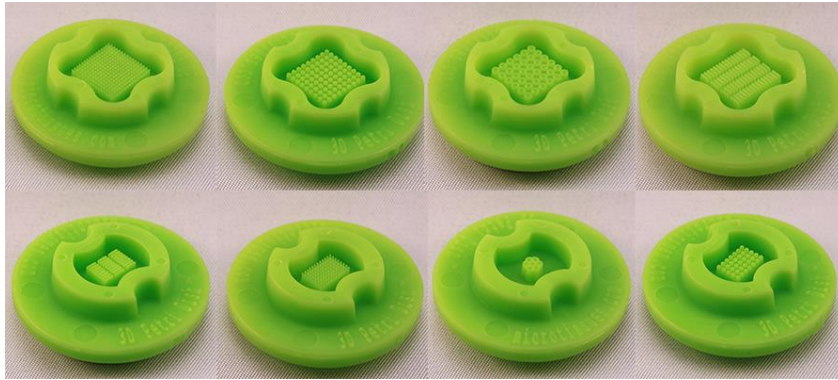
Figure 1.25: Image of eight micro-molds designed for casting 3D Petri Dishes® (source [228]).

IV.   *Microfluidic systems.*

In this more complex model (Figure 1.26), the cells are seeded in compartments separated by micropillars and continuously perfused with nutriments and oxygen along with removal of cell waste [229]. This model can be combined with scaffold or supporting matrix [230]. Various microfluidic systems have been used in different cell-based and tissue-based applications [231]. Most applications are centered on cell biology [232], drug discovery [226, 233], toxicological studies [234, 235], and tissue engineering [236].
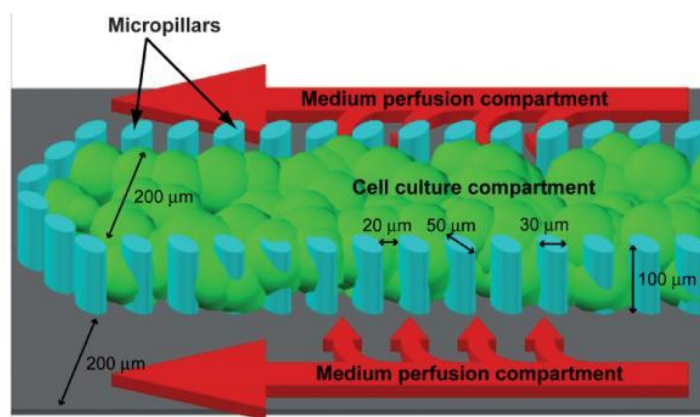
Figure 1.26: A microfluidic perfusion 3D cell culture system using micropillars to separate cells from perfusion medium. Cells are perfused with cell culture medium through gaps between micropillars (source [237]).

1.6.2.2.2 The scaffold-based models

I. _Biological scaffolds (hydrogels)_

Hydrogel provide microenvironments supposed to closely mimics _in vivo_ conditions. The matrix, usually based on ECM components of biological origin or natural sources (collagen, laminin, gelatin,…) (Figure 1.27), provides cellular functions and increases cells viability. The hydrogel ensures a matrix that allows _(i)_ cells attachment and organization in 3D structures; and _(ii)_ permeation by soluble nutriments, hormones and growth factors. In this method the cells are mixed with the hydrogel (formed by a dispersion of proteins in buffer) and then molded in microplate wells; tissue-like structures can be formed by layering separate hydrogel suspensions with different types of cells. The studies demonstrate the ability of 3D synthetic microenvironments design to support cell viability and direct cell adhesion [238], differentiation [239] proliferation [240], and migration [241].
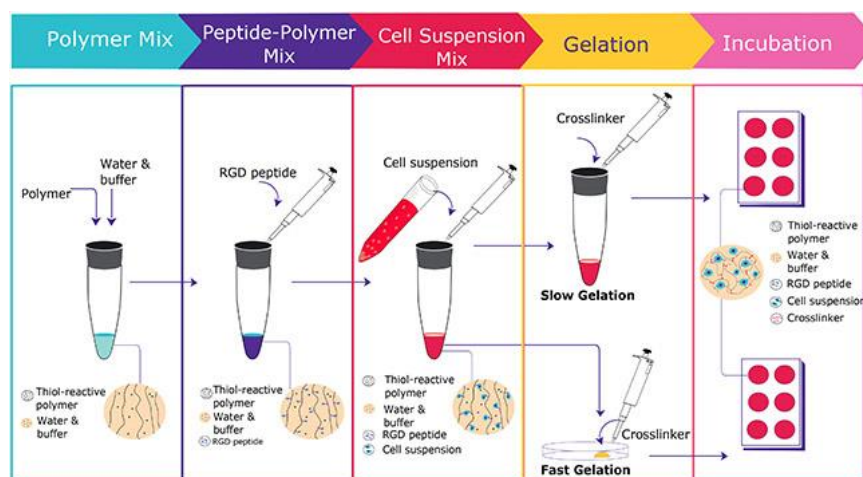
Figure 1.27: Illustration for TrueGel3D™ protocol flowchart (Merck), the protocol start with preparation of polymer mix usually is a basic hydrogel scaffold that does not interfere with cells, followed with addition of arginine-glycine-aspartate (RGD) peptide that support cell adhesion, then cell suspension will be added and mix gently, finally a cross linker like poly ethylene glycol (PEG) will be added and the mixture plated in a culture dish. (source [242]).

II. _Solid scaffolds_

This model seem particularly practical because they are customizable, widely available and do not require a specific cell treatment nor components different from 2D cultures; this means that routine protocols can be easily transposed [243-245].

The cells are seeded in matrices pre-designed to mimic an *in vivo* ECM architecture; they fill the space in the scaffold, attach and migrate to construct a 3D culture. The polymers used as solid scaffolds are polystyrenes and polycaprolactones built in different shapes, including porous disc, electrospun fibers and orthogonal layers (Figure 1.28). A micro or nano-patterned plates, also available, contains endless array of imprinted micropatterns on the surface of plates coated for low adhesion (Figure 1.29).

The different solid scaffold types are used for a variety of applications especially in tissue engineering. For example, Porous scaffold was useful to modelling skin structure [246] and formation of contractile 3D heart muscle [247], moreover the formation of osteon-like structures through a combination of electro-spinning and other manufacturing techniques [248] and tumor like structure [249]
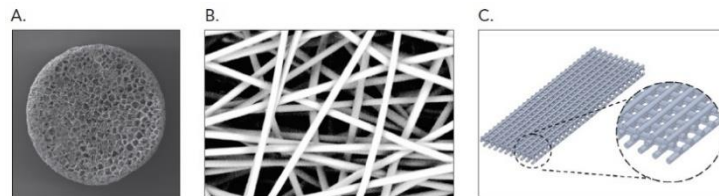
Figure 1.28: Illustration of solid scaffold (A) Porous disc; (B) Electrospun fibers; and (C) Orthogonal layering geometric configurations of polymeric 3D scaffolds (source [217]).

Figure 1.29: Nanopatterned cell culture plate features a biomimetic nanopatterned surface to enhance the structural development of cells and tissues and improve the physiological relevance of cell-based assays. (source [250]).

Table 1.5: Examples of 3D cell culture models in the study of drugs and toxicants

Type of model	Source and type of cells	Tested compounds	Endpoints measured	Ref.
Hanging drops in microplates	Human (A2780 and OVCAR3 ovarian cancer cell lines)	cisplatin	Viability	[251]
	Monkey (COS7) Murine (ES-D3) Human (A431.H9)	5-fluorouracil tirapazamine	Osmolality measurement Viability	[252]
Hanging drop in ultra-low attachment microplates	Human (UW228-3) NSC (Foetal human brain tissue)	Etopside	Viability (cytotoxic effect)	[219]
	Human (40 tumor cell line)	17-AAG (HSP90 chaperone inhibitor), PI-103 (PI3 kinase/mTOR inhibitor) or CCT130234 (PLCγ inhibitor)	Comparison of cell culture techniques, growth kinetic assay, functional assay, inhibition, invasion and viability	[253]
HDP in agarose microwells	HeLa, C2C12, HepG2 and MCF-7	50 % ethanol	Respiratory activity, viability	[254]
	Human DPSCs, HUVECs	Microtissue approach for dental pulp tissue engineering	Angiogenesis and pulp-like tissue regeneration in vivo	[255]
Combination of microfluidic technology with 3D cell culture	Adult rat hippocampal stem/progenitor cells (AHPCs)	Microfluidic technique within alginate-based fibrous hydrogels	Cell proliferation and differentiation	[256]
	Murine (NIH/3T3 cell)	Cell laden microfluidic hydrogels	Viability	[257]
HDP + biological scaffolds	MCF7, LNCaP, NCI-H1437	Fulvestrant and docetaxel	Growth curve, treatment response	[258]
	Human (MDA-MB-231 breast cancer cells)	Collagen I and BME in either a liquid-like or gelled as extracellular matrix	The role of fibrillar environments in controlling breast cancer cell, invasion efficiency	[259]
Solid scaffolds models	Human, MCF-7	Tamoxifen	Cytotoxicity, cell growth and carbohydrate metabolism	[260]

However, the implantation of 3D cultures remains a challenge. On one hand, many tools have been developed to efficiently produce 3D cultures including solid scaffold, natural or synthetic hydrogels, different plate types (HDP, ULP), microfluidic devices... which makes it difficult to select the most relevant 3D system; it is likely that, depending on the organ to pattern, the optimal system can be/should be different but, to our best knowledge, there are no rules so far to guide the choice of a culture model. On an other hand, the 3D models *(i)* are grown in limited flows, resulting in non-homogeneous supply of nutrients and evacuation of metabolic waste, with the formation of necrotic hearts; *(ii)* afford few protection against shear-stress related to manipulations; and *(iii)* present a risk of agglomeration between spheroids [261].

1.7 *In vitro* models for the evaluation of neurotoxicity and neuroprotection.

The nervous system has many cell types with multiple functions, complex anatomy and unique structural and functional characteristics; this complex organization makes the evaluation of neurotoxicity and neuroprotection following an exposure to chemical, biological, or physical influences, a real concern in neurosciences.

Neurotoxicity is conceivable as a consequence of direct effects on neural structure, glia-neuron interactions, or the organization and plasticity of the nervous system; it may target one or more neurons, resulting either in a loss of neurons by apoptosis or necrosis, in a dysfunction of the axons or in a disturbance of neurotransmission. It could be a permanent or a reversible damage, directly after exposure to a toxicant or delayed, sometimes for years, and it can involve the complete nervous system or part of it [262]. Vice versa, a neuroprotection preserves the neural structure and function or slows down the progression of neurodegeneration or malfunction by interfering with a cascade of cell death or damage, by helping the nervous system to recover and/or by providing a protective effect; such neuroprotection can be conceived before or during the progression of nervous system damage [263].

In vitro models are widely used in neurotoxicity screening; compared to *in vivo* studies, they provide fast, cost-effective and reliable methods with an ability to control the neurotoxicant

concentration, the duration of exposure, the cell type and environment, in addition to a certain ease of manipulation, high reproducibility and the ability to yield information about the mechanisms of neurotoxicity with less ethical issues. Still there are limitations in mimicking the real cell environment and homeostatic mechanisms and in estimating the behavioral endpoints; furthermore, *in vitro* models will not give information about the role of route of administration, distribution in the body, passage of BBB and metabolism [264].

For evaluation of neurotoxicity, *in vitro* mammalian cells are the largest used model, with complexities varying from the simplest to the most complicated, notably including subcellular systems, cell lines, primary cells, reaggregate cultures, brain slices and organotypic explants. The choice of model depends on the functional, biochemical, or morphological features of neurotoxicant target(s).

1.7.1 Subcellular system models

These models have been used in neurotoxicology to evaluate pathways of signal transduction or a specific point related to the safety, for example:

- Isolated mitochondria are used to evaluate the effect of neurotoxicants on this organelle bioenergetics since mitochondria are involved in Ca^{++} homeostasis, production of ATP and ROS and are a most important crossroad for cell death pathways [265].

- Synaptosomes[9] [266] are used to study metabolic pathways, energy production, ion movements, neurotransmitters synthesis, storage and release or oxidative injury. This model can represent the mitochondria deficient in some neurodegenerative diseases like Parkinson's disease [267].

---

[9] Synaptosomes are artificial, membranous sacs that contain synaptic components and are generated by subcellular fractionation of homogenized or ground-up nerve tissue. They are often referred to as "pinched-off nerve endings," because the lipid bilayers naturally reseal together after the axon terminals are torn off by the physical shearing force of homogenization [266].Bai F, Witzmann FA. Synaptosome proteomics. Subcellular Biochemistry. 2007;43:77-98.

1.7.2 Cell lines and immortalized cell lines

These models, derived from tumors of mouse, rat and human harbor a genetic change that modifies their growth potential and their proliferation becomes unlimited. The cell lines produce homogenous cell populations in massive quantities and reproducible mode, they can be cryopreserved indefinitely, and they are commercially available (e.g., several neuroblastoma or glioma cell lines or PC12 cells). They give the possibility to gather information from a single cell and their biochemical, physiological, and electrophysiological correlations important for neurobiological studies. These models drastically reduce the numbers of animals used but the cells are transformed, lacking some of quite important *in vivo* characteristics (e.g. DNA damage or apoptotic signaling pathways, growth regulation, …), and their response to neurotoxicants may be changed; these considerations can be overlooked by some researchers, leading to irrelevant observations… Besides the homogeneity of cells limits the cell-cell interactions [268], except in a few co-culture studies (cf Section 1.7.4).

1.7.3 Dissociated primary cultures

These models are obtained from brain tissues dissociated into individual cells and grown in culture plates, the culture conditions playing an important role in defining the types of cells growing in culture; specific media conditions can favor one cell type *i.e (i)* the incorporation of DNA synthesis inhibitors to kill dividing cells decreases the proliferation of glia and fibroblasts; or *(ii)* an increase in serum concentration favors the growth of glia over the neurons; while *(iii)* a mix of neurons and glia is obtained with balanced media [269]. The viability and differentiation of cells depend on the seeding density, the presence of serum, trophic factors, oxygen tension and the composition of substratum. In favorable conditions, the cells develop axons and dendrites, ion channels and synapses. The one cell type models are more used for neurobiology than neurotoxicity studies because no single type of cells can mimic the complex nervous system [270].

1.7.3.1   Glial cells primary cultures

These cells are extracted from postnatal brain of rat or mouse harbor three types of glial cells, astrocytes, oligodendrocytes (Schwann cells) and microglial cells. There is a suggestion that glial cells may have neuroprotectant effect through metabolism and detoxification of xenobiotics [271]; however those same enzymes could also transform a pro-toxicant into a neurotoxin [272]. This important interplay between glial cells and xenobiotics makes this model important to predict the neurotoxicity of molecules.

1.7.3.2   Neural cells primary cultures

These cultures are derived from dissociated fetal brain tissue of mouse, rat, chicken or human. Using a fetal brain tissue presents the advantages that different regions of brain or of peripheral nervous system are included in the cultures, that are then more representative of the *in vivo* structures; moreover, the soma is small and the limited dendritic and axonal growth preserves the cell during the dissociation step. However, the choice of brain regions determines the neuronal population; for example primary cultures of *(i)* cortical neurons mainly combine GABAergic and cholinergic neurons, so they express the functional $GABA_A$ and NMDA receptors [274]; this model is widely used to determine the neurotoxic potential of compounds [275, 276]; *(ii)* hippocampal express GABA receptors, a model also important in neurotoxicology [277, 278]; *(iii)* cerebellar granule neurons are mainly constituted of glutamatergic excitatory cells and express the NMDA receptors; the over activation of NMDA produces an excitotoxic neuronal death, making this culture a good neurotoxicology model [279]; *(iv)* primary cultures of sensory neurons, established from dorsal ganglia of spinal cord, express ion channels receptor and respond to acute depolarization, to chemical, thermal and mechanical stimuli; those properties expand the use of this model in the assessment of neurotoxicity, although the cell isolation is a complex procedure [280, 281].

1.7.3.3   Neuronal cells primary cultures

These cells are dissociated from a tissue of central nervous system (CNS) or peripheral nervous system (PNS). These cultures better preserve the morphological, physiological, electrophysiological and neurochemical properties of *in situ* neurons compared to cultures of

cell lines and immortalized cell lines [273]. This model is important in neurobiological studies, enabling the investigation of distinct axons or dendrites or specific mechanism through neuronal circuity; also cultures from PNS have been proposed for use in neurotoxicological studies [100, 273].

1.7.4   Neuron-Glia co-cultures

These models consist in a mixed culture between neurons and glial cells, aiming to reproduce *in vitro* the *in vivo* cell-to- cell interactions that notably depend on the release of soluble factors [274]. The cells are physically separated in such a way that the proinflammatory and oxidative factors released by glial cells can be exchanged with neurons.

In sandwich co-culture models, one type of cells is seeded in a petri-dish, a second one on coverslips that are inverted to face the first culture; the two surfaces are separated by a paraffin dot on the coverslip edge (Figure 1.30). The two types of cells face each other without direct connection but they do share the medium and thus excreted/diffused soluble substances. This model provides the possibility to study the effects of molecules on neuronal viability and activity in the presence or absence of glial cells [275].
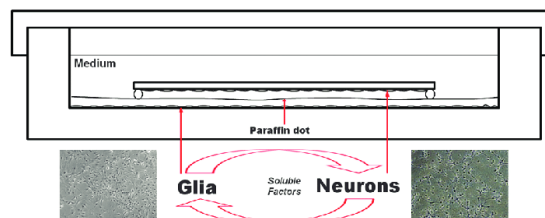
Figure 1.30: Neuron glia sandwich co culture. Glial cells are seeded at the bottom of Petri dishes while neurons on the top of glass cover slips. Coverslips are inverted so that neurons face the glia monolayer. Paraffin dots create a narrow gap to separate neurons from glial cells. The two cell populations can be exposed together to the tested com pounds and then separated at the end of the treatment to perform different studies (source [276]).

Another model for co-culture is based on seeding the neurons in a petri-dish, the glial cells in another petri-dish (Figure 1.31); these are then collected and inserted in the neurons petri-dish on a mesh insert. This system is used in stem cells biology to investigate the role of different microenvironment factors on proliferation and differentiation but also in neurotoxicity studies [269, 273].
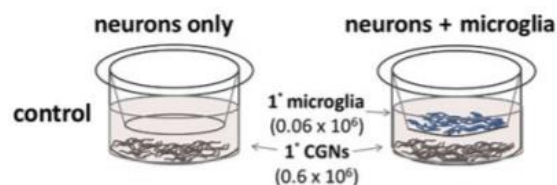
Figure 1.31: Co-culture neuron-glial: primary cerebellar granule neurons CGN grown in culture for 10 days were combined with 3.0 µm mesh inserts, or inserts containing microglia sub-cultured for two days (6.0×10^4 cells/insert) (source [273]).

1.7.5   Organotypic cultures

Organotypic cultures notably offer the opportunity to study the synaptic transmission between different brain regions, as deduced by functional synaptic connections between two different slice cultures [277]. There are two subtypes of brain organotypic cultures: *(i)* the slice cultures from different brain regions, like hippocampal, cerebellar or spinal cords, yielding different models to study xenobiotic-induced effects [278, 279]; *(ii)* the organ/explant cultures, in which all or part of organ is maintained in culture; the tissue architecture and cell-cell interactions are better preserved in this model, as well as the ratio neurons/astrocytes, better simulating the in vivo situation; there is also the possibility for co-cultures with other dissociated cells, yielding a model appropriate for neurotoxicology [280].

1.7.6   Neural stem cells (NSCs)

Human brain specific features and complexity do not fully compare to animal brain. Therefore, there is a need for modeling human brain; for that, human embryonic stem cells (hESCs) were proposed in view of their ability to differentiate into any cell type of the human body, depending on particular growth factors, in addition to their ability of self-renewal. However, due to ethical problems, the scientists resorted to generating human induced pluripotent stem cells (hiPSCs) from human somatic cells, by reprogramming them to pluripotency by overexpression of specific transcription factors; hiPSCs have the same properties as hESCs, with an advantage of a possible variety when selecting genetic backgrounds [281]. As summarized in Table 1.6. and Figure 1.32 , different methods were developed for the generation of neuronal tissue from humans. This type of cells may be relevant for the study of developmental neurotoxicity (DNT), allowing to investigate the

effects of large numbers of chemical compounds on neurodevelopmental processes, e.g. cell division or neuronal and glial differentiation; this results in reliable, relevant and fast model, not to mention the respect of animal welfare and the 3Rs (Replacement, Reduction, and Refinement) [282]. Such models of neural stem cells, especially in three dimensions (section 1.6.2), have been proposed as closest to *in vivo* conditions, especially for neurotoxicology [283-285]; however the culture costs, the length of differentiation protocols and the variability from line to line, due to genetic variability of the donors, still limit their applications [285].
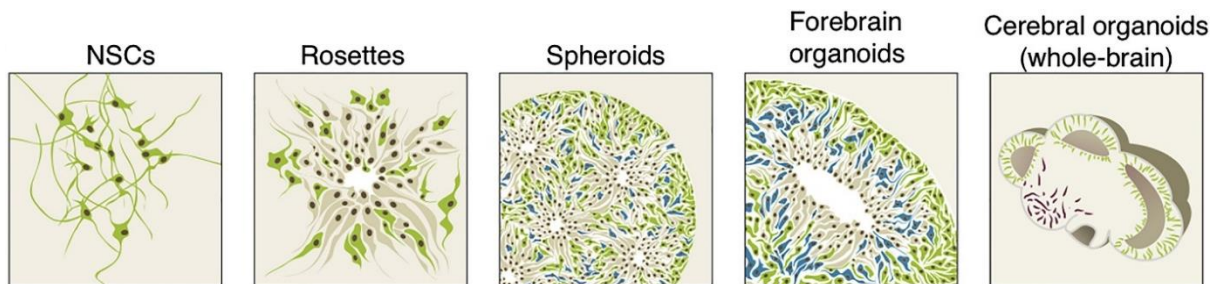
Figure 1.32: A review of Kelava and Lancaster 2016 on stem cell models [286], describes the different in vitro techniques applied to model the brain tissues: (*i*) neural stem cells (NSCs) in 2D cultures, developed from embryonic stem cell (ESC) or induced pluripotent stem cells (iPSCs); (*ii*) rosettes, that present an apical lumen close to embryonic neural tube, generated from differentiated aggregates of PSCs, called "embryoid bodies" (EBs); a derivation of the an EB-derived rosette approach to yield SFEB (serum free culture of embryoid bodies) in which the differentiation of ESCs to neural precursors induces in the absence of serum; the long period of development indicates that the SFEB do not completely flatten upon plating so and they are sometimes called SFEBq. (*iii*) the spheroids, a 3D self-organization of cells embedded in a supportive extracellular matrix gel; (*iv*) the forebrain organoid, a derivation of the SFEB approach (absence of serum or growth factors) with embedding in a supportive extracellular matrix gel; and (*v*) the so-called "cerebral organoids" that present a variety of brain regional identities (source [286]).

1.7.7 Three dimensional systems

Three dimensional systems, as discussed in Section 1.6.2, maintain the neuronal cells properties and more closely represent *in vivo* conditions, considering the importance of the extracellular matrix in regulating neuronal development, adhesion, proliferation, differentiation, migration and even regeneration after injuries [287]. Given that normal connections of neuronal cells expand in all directions, various 3D *in vitro* models have been developed, starting from simple aggregates [288] to advanced tools and to highly organized 3D environments [289].

These 3D models are generally derived from dissociated fetal cells [290] or immortalized cell lines [291] but also from hESCs and hiPSCs [286]. The field of stem cells has been vastly developed in the last decade; different methodologies, different growth factors and inhibitors (that notably regulate intracellular signaling and biological responses) were applied to achieve the differentiation and development of cultures. A summary of *in vitro* methods for the generation of neuronal tissue from human and mouse PSCs is presented in Table 1.6.

For neurotoxicology research, 3D models undeniably surpass 2D models and animal studies as they offer reproducibility, cells organization, rearrangement and maturity, availability of high number of aggregates, increased viability, balanced neuron/astrocyte ratio, the possibility to maintain cultures for weeks and to introduce modified cells [292, 293]; therefore 3D models are more and more investigated for both neuropharmacology and neurotoxicity testing [294, 295].

Table 1.6: Overview of recently developed in vitro methods for the generation of neuronal tissue from human and mouse PSCs, methods are listed chronologically. (The following abbreviations used: EB., embryoid bodies; Inh., inhibition; Act, Activin; AA, ascorbic acid, ESC embryonic stem cell; NE Neurenteric. The abbreviations of growth factors are repertoried in the original source [286]).

Method	EB Step?	Growth Factors or Inhibitors	Entirely 3D?	Protocol Overview[a]	Technical Requirements [b]	Timing[c]	Ref.
Neural rosettes	yes	FGF2	no	ESC→EBs→plating→rosettes	manual isolation	7 days	[296]
Neural progenitors (NPs)	no	none	no	ESC→NPs	none	4 days[§]	[297]
Forebrain NPs	yes	Wnt inh., Nodal/Act/TGFβ inh.	no	ESC→EBs→plating→ forebrain NPs	none	10 days[§]	[298]
Propagating rosettes	yes	FGF2, SHH, FGF8, AA, BDNF	no	ESC→EBs→plating→ rosettes→propagation	manual isolation	12–16 days	[299]
Cortical NPs	no	cyclopamine	no	ESC→ cortical NPs	none	10–14 days	[300]
Large forebrain rosettes	yes	Wnt inh., Nodal/Act/TGFβ inh., BMP inh.	no	ESC→EBs→plating→ forebrain rosettes	none	10 days[§], 46 days	[301]
Neural rosettes	no	Nodal/Act/TGFβ inh., BMP inh.	no	ESC→neural rosettes	none	11 days	[302]
Propagating rosettes	yes	FGF2, EGF	no	ESC→EBs→plating→ rosettes→propagation	manual isolation	8–15 days	[303]
Retinal organoids	yes	none	yes	ESC→EBs→optic cup →retinal organoids	manual dissection, 40% O_2	24 days[§]	[304]
Adenohyphysis organoids	yes	Hh agonist, additional depending on endocrine types	yes	ESC→EBs→Rathke's pouch pituitary progenitors	40% O_2	21–33 days[§]	[186]
Neural rosettes	no	Nodal/Act/TGFβ inh., BMP inh., retinoids	no	ESC→neural rosettes	none	15 days	[305]
Large forebrain rosettes	yes	FGF2, Wnt inh., Nodal/Act/TGFβ inh., BMP inh.	no	iPSC→EBs→plating→ forebrain rosettes	none	45–50 days	[306]
Neuroepithelial cysts	no	none	yes	ESCs→NE cysts→retinal pigment epithelium; or spinal chord	none	5 days	[307, 308]
Whole-brain organoids	yes	none	yes	ESC/iPSC→EBs→Matrigel embed→agitation→ brain organoids	manual embedding, agitation	30–40 days	[309]
Forebrain organoids	yes	Nodal/Act/TGFβ inh., Wnt inh.	yes	ESC→EBs→forebrain organoids	40% O_2	42 days	[310]
Cerebellar organoids	yes	Nodal/Act/TGFβ inh., FGF2, FGF19, SDF1	yes	ESC→EBs→cerebellar organoids	none	35 days	[311]
Cortical spheroids	yes	Nodal/Act/TGFβ inh., BMP inh., FGF2, EGF, BDNF, NT3	yes	iPSC→EBs→cortical spheroids	none	43 days	[312]
Aggregates of large forebrain rosettes	yes	BMP inh., Wnt inh., FGF2, EGF	no	iPSC→EBs→plating→ forebrain rosettes→ floating aggregates	manual isolation	42–44 days	[313]
Hippocampal-Choroid plexus organoids	yes	Wnt inh., Nodal/Act/TGFβ inh., Wnt(CHIR), BMP4	yes	ESC→EBs→Hippocampal-Choroid plexus organoids	40% O_2	35–42 days	[314]
Forebrain, midbrain, or hypothalamic organoids	yes	Nodal/Act/TGFβ inh., BMP inh., additional depending on region	yes	iPSC→EBs→Matrigel embed→scaled-up agitation→ regional organoids	manual embedding, 3D printed agitation in multi-well	28 days	[315]

a Factors in neural induction or regional specification are listed.
b Technical requirements beyond standard sterile TC culture facilities
c Timing from human PSCs (except §, which indicates timing from mouse PSC) to achieve the result listed in the table.

2. Objectives

2.1 Study context

Essential tremor (ET) is a neurological condition that causes a rhythmic trembling of the hands, head, voice, legs, and trunk, and makes normal tasks like eating or writing difficult. It is one of the most prevalent neurological diseases that affects elderly people, although it can also appear in young adults [316]. Despite the high prevalence of this disorder, its mechanisms and etiology remain poorly understood and the treatments are relatively limited, they do not slow or stop the progression of the disease. Two main hypotheses are put forward on the pathogenesis of essential tremor, a disorder of the olivocerebellar pathway (olivary model) and a primary alteration of the cerebellar cortex (degenerative cerebellar). There is converging evidence that both genetic and environmental factors are fundamental in triggering and worsening ET pathogenesis. Hence, the identification of environmental factors is a critical step to propose prevention strategies or interventional studies aiming at risk reduction.

Notably, in ET patients, the blood levels of harmane, a β-carboline alkaloid, have been found to be abnormally increased and harmane has been detected in post-mortem brain samples [98]. Accordingly, the β-carboline alkaloids have yielded major interest; the measured elevated levels in ET patients were tentatively explained as a result of increased dietary intake, impaired ability of metabolization (genetic cause) or increased endogenous production (genetic and sporadic causes). β-Carboline alkaloids (βCAs) are indole alkaloids notably including harmane, harmine or harmaline; these fat-soluble compounds, rapidly distributed to the brain, naturally occur in plants and food, and are also endogenously produced in mammals and humans. Whereas some of these alkaloids are known as potent tremor inductors, exhibiting neurotoxicological properties, other βCAs have been shown to be neuroprotective, antioxidant, and anti-inflammatory [317].

Environmental factors like dietary components, cigarette smoke or beverage, imply daily exposures to β-carboline alkaloids but their endogenous production in human tissues and brain should not be neglected. Food cooking, through Maillard reaction, notably generates β-CAs but also aldehydes that can condense with endogenous amines to form β-CAs and isoquinolines. As some nutriments are known to influence neurological movement disorders, notably in Parkinson's disease with e.g. negative effects of milk and meat and

chemopreventive effects of micronutrients (vitamins B, the antioxidant vitamins C and E, vitamin D, flavonoids) and macronutrients (fish, polyunsatured omega-3 fatty acids) [318], the investigation of ET dietary epidemiology appears important to assess both diet and diet-induced compounds as risk or protection factors in its aetiology.

Neurotoxicity or neuroprotection studies are ideally based on animals; but such *in vivo* research is becoming less and less resorted to, due to 3Rs regulations (replacing, reducing and refining) implemented to reduce the number and suffering of research animals. *In vitro* models are then now widely used to replicate certain aspects of neurotoxicity; these essentially consist in 2D models based on cultures of cancer cell lines, primary cells, cells derived from stem cells and mixed cells. However, pharmaco-toxicological assays based on such 2D cell cultures show important limitations that may partially account for the high rate of clinical trial failures observed in neurosciences; this is most probably linked to the limited ability of these models to mimic the *in vivo* cell environment [190]. More recently, new models based on organotypic sections from different regions of the brain and 3D cultures were introduced to improve the simulation of the living organ; their ability to predict toxicity has already been demonstrated and these models are expected to improve the biological activity screening tests [191]. Although the implementation of 3D culture remains a challenge, many tools have been developed to efficiently produce 3D cultures, including solid scaffolds, natural or synthetic hydrogels, hanging drop in micropatterned or non-adherent surface plates, microfluidic devices [244]. Non-scaffold methods seem particularly practical, as they are customizable, widely available and do not require specific cell treatments or assay components different from 2D cultures, which means that routine protocols can be easily transposed.

2.2 Starting Hypothesis

Dietary factors have been examined as possible disease contributors in Parkinson's disease and many other neurological disorders. The dietary epidemiology of ET, however, has not been rigorously studied; there have been few studies, and, therefore, little is known about a possible association between ET and dietary factors. From the few published data, factors derived from diet drew our attention, precisely overcooked meats, and the identification of Maillard reaction-derived compounds possibly implicated in ET.

Even though the Maillard reaction has been widely studied, many of its products are not fully characterized and their biological effects need more investigation. As reported, Maillard reaction is responsible for reducing the nutritional value of foods through the degradation of some amino acids and vitamins, and the generation of indigestible compounds. Reports have linked the high concentration of Maillard reaction products (MRPs) in diet to health conditions and diseases, mainly through the glucose and lipid metabolisms, and inflammatory mediators [319].

The presence of proteins, carbohydrates and water facilitate the occurrence of Maillard reaction while cooking; these conditions apply to the main edible part of animal, the muscle, that is composed of 72-75 % water, 21 % nitrogenous compounds (protein, nucleotides, peptides, creatine, and creatinine), 2.5 - 5 % lipids, ~1 % carbohydrates, vitamins and minerals (potassium, phosphorus, sodium, chlorine, magnesium, calcium, and iron); as the reaction strongly depends on temperature and duration of cooking, the resulting MRPs differ with cooking practices [320].

β-carboline alkaloids, including harmane the molecule possibly incriminated according to ET literature, is reported as a MRP resulting of the condensation of indole-alkylamines with aldehydes. Such a condensation may occur exogenously and endogenously but is not limited to β-carboline alkaloids and could also generate other tremor-producing chemicals, such as THIQs.

We hypothesize that the elevated blood concentrations of harmane associated with essential tremor (ET) [40, 42, 104] might due not only to increased exogenous exposure to βCAs, but also, to their precursor aldehydes.

2.3 Definition of the objectives

Considering that current in vitro and animal models of ET do not completely mimic the human presentation of the disease and that there is a growing demand to develop alternative models to better understand a possible link between dietary factors and ET, we propose to:

- Extract and identify the alkaloids and the volatile and non-volatile carbonyl compounds produced during Maillard reaction in overcooked meats, thanks to an original analytical approach.
- Study the possible implications of extracted carbonyl compounds to react with biogenic amines to form βCAs or isoquinolines.
- Identify products of the reactions.
- Study identified molecules based on *in silico* prediction of pharmacokinetic and toxicological properties on the central nervous system.
- Develop and validate an original *in vitro* 3D neural model (neurosphere culture) for the assessment of neurotoxic and neuroprotective effects of the meat extracts and identified compounds. Determine their possible implication in the pathogenesis of essential tremor and examine a possibly emerging link between MRPs and ET.

3. Material and Methods

3.1 Material

3.1.1 Reference standards

The standards used during the experimental work are presented in Table 3.1:

Table 3.1: β-carbolines, aldehydes, amino acids and biogenic amines reference standards

	Name	Supplier	Purity
	β-carbolines		
1	Harmaline	Aldrich	≥ 95 %
2	Harmalol hydrochloride dihydrate	Aldrich	80 %
3	Harmane	Aldrich	98 %
4	Harmine	Aldrich	98 %
	Isoquinolines		
1	1-benzyl-1,2,3,4-tetrahydroisoquinoline-6,7-diol	Azepine LTD	95 %
	Aldehydes		
1	2-Methylbutyraldehyde	VWR 'Alfa Aesar'	≥ 95 %
2	3-(Methylthio)propionaldehyde	Sigma-Aldrich	≥ 97 %
3	4-(Dimethylamino)butyric acid hydrochloride	Sigma-Aldrich	98 %
4	5-(Hydroxymethyl)furfural	Sigma-Aldrich	≥ 98 %
5	Acetaldehyde	Sigma-Aldrich	≥ 99 %
6	Acrolein	Sigma-Aldrich	90 %
7	Aldehydes mixture (556) 15 components 1000 µg/ml each of formaldehyde, acetaldehyde, propionaldehyde, butyraldehyde, valeraldehyde, hexanal, 1-heptanal, octanal, nonanal, decanal, cyclohexanone, crotonaldehyde, benzaldehyde, glyoxal, methylglyoxal in acetonitrile	CPA chem	≥ 95.4 %
8	Benzaldehyde (Analytical standard)	Sigma-Aldrich	PHR
9	Formaldehyde	VWR	39 % w/v
10	Furfural	Sigma-Aldrich	99 %
11	DL-Glyceraldehyde	Sigma-Aldrich	≥ 90 %
12	Glycolaldehyde dimer	Sigma-Aldrich	
13	Hexanal (Analytical standard)	Sigma-Aldrich	≥ 95 %
14	Isobutyraldehyde	VWR	98 %
15	Isobutyraldehyde (Analytical standard)	Sigma-Aldrich	≥ 97 %
16	Isovaleraldehyde	Fluka AG Blush SG	> 97 %
17	Phenylacetaldehyde	Sigma-Aldrich	≥ 90 %
18	Propionaldehyde (Analytical standard)	Sigma-Aldrich	≥ 98 %

	Name	Supplier	Purity
	Amino acids and biogenic amines		
1	γ-Aminobutyric acid	Sigma	> 99 %
2	Dopamine hydrochloride	Sigma	≥ 97,5 %
3	Epinephrine hydrochloride	Sigma	≥ 98 %
4	Serotonin Hydrochloride	Sigma	≥ 98 %
5	Tryptamine	Acros	98 %
6	L-Tryptophan	Roth	> 98.5 %

3.1.2   Reagents and chemical substances

The reagent and chemical substances used during experimental work are presented in Table 3.2:

Table 3.2: Reagent and chemical substances references.

	Name	Supplier	Purity
1	Alkane standard solution C8-C20 (Analytical standard)	Supelco	≥ 99.9 %
2	1,2-Dibromoethane (Analytical standard)	Sigma Aldrich	≥ 99.6 %
3	2,4-Dinitrophenylhydrazine hydrochloride solution	Sigma-Aldrich	For TLC derivatization
4	Acetyl chloride	Alfa Aesar	98 %
5	Dimethyl aminobutyric acid hydrochloride	Alfa Aesar	≥ 98 %
6	EGTA	Sigma-Aldrich	Molecular biology
7	Hydrazine hydrate	Sigma-Aldrich	50-60 %
8	Iodomethane stabilized	Acros organics	99 %
9	Methyl ethyl ketone	VWR	100 %
10	Ninhydrin	Sigma Aldrich	ACS reagent
11	Nitrate de bismuth (III)	Honeywell Fluka	≥ 98 %
12	O-(2,3,4,5,6-Pentafluorobenzyl) hydroxylamine Hydrochloride	BeanTown Chemical	≥ 99 %
13	Oxalic acid dihydrate	VWR	99 %
14	Potassium hydrogen phthalate	Acros organics	≥ 99.9 %
15	Potassium Iodide	VWR	≥ 98 %
16	Sand	VWR	≥ 99 %
17	Semicarbazide hydrochloride	Sigma-Aldrich	≥ 99 %
18	Silica gel (fraction 80-200 mesh)	Avantor	Grade 60
19	Sodium chloride	VWR	99 %

	Name	Supplier	Purity
20	Sodium dodecyl sulfate (SDS)	Sigma-Aldrich	Molecular biology
21	Sodium hydroxide	Chem Lab	$\geq 99\%$
22	Sodium sulfate, anhydrous $\geq 99.0\%$	VWR	$\geq 99\%$
23	Sulfuric acid ACS	VWR	97 %
24	Tetrabutylammonium iodide	Alfa Aesar	98 %
25	Triton X-100	Sigma-Aldrich	Laboratory grade
26	Trizma base	Sigma-Aldrich	$\geq 99.9\%$

3.1.3 Solvent

The solvent used during experimental work are presented in Table 3.3:

Table 3.3: Solvents.

	Name	Supplier	Purity
1	Acetic acid glacial	VWR Chemicals	99%
2	Acetonitrile HPLC grade	VWR Chemicals	$\geq 99.9\%$
3	Ammonia > 28 %	VWR Chemicals	31 %
4	Deionized water	UMONS	
5	Deuterated methanol	Sigma-Aldrich	$\geq 99.8\%$
6	Dichloromethane	Sigma-Aldrich	$\geq 99.8\%$
7	Dichloromethane	VWR Chemicals	99 %
8	Diethyl ether	VWR Chemicals	$\geq 98\%$
9	Ethanol	Carl Roth	96 %
10	Ethyl acetate	VWR Chemicals	99 %
11	Formic acid HPLC grade	Chem Lab	$\geq 99\%$
12	Hydrochloric acid 37 %	VWR Chemicals	34-37 %
13	Methanol	VWR Chemicals	> 99.5 %
14	Methanol	VWR Chemicals	$\geq 99.8\%$
15	Methanol HPLC grade	VWR Chemicals	$\geq 99.8\%$
16	Methanol HPLC grade	Sigma-Aldrich	$\geq 99.8\%$
17	n-Heptane HPLC grade	VWR Chemicals	$\geq 99\%$
18	tert-Butyl methyl ether	Sigma-Aldrich	99.8 %
19	Toluene	VWR Chemicals	> 99,5 %

3.1.4 Devices and apparatus

The following devices were used during the experimental work:

- *For the extractions and reactions*:

  Mixer mill MM400 (Retsch, Germany), horizontal rotator (Labo-Modern, Germany), centrifuge (Herolab uniCen MR, Germany), rotary evaporator R-210 coupled with vacuum controller V-850, recirculating chiller F-305 and heater bath B-49 (BUCHI, Switzerland), Thermo cell Heating & Cooling Block CHB-201 (BIOER, Chine) and MR Hei-Tec Package Hot Plate Stirrer (Heidolph, Germany), Thermometer VWR TD11.

- *For the chromatographic identifications*:
- A qualified HPTLC system from CAMAG consists of an automatic TLC sampler 4, automatic developing chamber ADC2, TLC visualizer 2, derivatizer and TLC plate heater III, driven by the VisionCATS Ultimate software (CAMAG, Switzerland).
- 1260 Infinity II LC system, consisting of a quaternary pump G7111A, vial sampler G7129A, multicolumn thermostat (MCT), diode array detector (DAD) G7115A and fluorescence detector (FLD) G7121A, driven by the LC Open Lab software (Agilent technologies, United States).
- Merck-Hitachi 7000 HPLC System, consisting of L-7100 pump, L-7200 auto sampler, L-7400 UV detector, software Hitachi System Manager HSM (Merck-Hitachi, United States).
- Expression L compact mass spectrometer (CMS) equiped with electrospray ionization (ESI), in both the positive and negative ionization modes, driven by the Advion software (Advion, United States).
- TLC-MS interface (CAMAG, Switzerland) connected with 515 HPLC pump (Waters, United States). This device incorporates an extraction head that forms a leak-tight seal on the surface of the TLC plate, which allows an extraction solvent to be delivered onto the TLC spot followed by a direct coupling to the inlet of the Expression L compact mass spectrometer.
- Gas Chromatograph (GC) System 8860 coupled to a single quadrupole mass spectrometer GC/MSD 5977B (Agilent technologies, United States).

- A LC-coupled mass spectrometer Micromass Quattro Premier (Waters, United States) equipped with atmospheric pressure ionization source AP. This tandem quadrupole LC-MS/MS is driven by the MassLynx 4.0 Software.
- Autospec 6 F mass spectrometer (Waters, United States) equipped with electronic (EI) and chemical (CI) ionizations / direct introduction of solid and liquid samples / accurate mass measurements (HRMS) / collision-induced dissociation experiments.
- NMR spectra were obtained on a Bruker AVANCEII 500 spectrometer with a 11.75 T standard bore magnet equipped with a 5 mm wide helium-cooled probe and an automatic 24-sample convert, also on a Bruker NEO 600 spectrometer with a 14 T standard bore magnet operated by Dr C. Henoumont in department of general and organic chemistry and biomedical in the university of MONS.

The following apparatus was used for the extraction:
- Soxhlet extractor (DURAN®) that allows extraction from solids with relatively small amounts of solvents. The solvent is continuously recirculated and distilled from the extracted sample before contacting the solid again. The extract is concentrated in the distillation flask. The apparatus comprises a percolator to circulate the solvent, a cellulose thimble that retains the solid to be extracted (Whatman™), and a siphon mechanism, that periodically empties the thimble and is connected with a condenser (Figure 3.1)
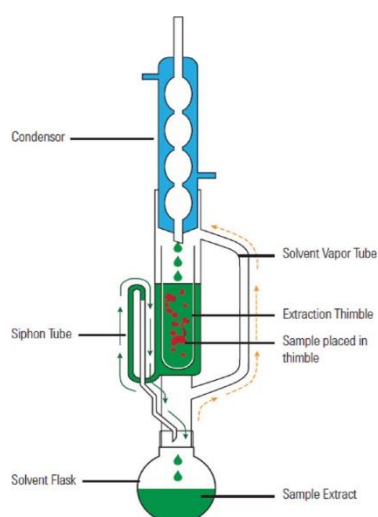
Figure 3.1: Soxhlet extractor apparatus, the solid sample is placed in the thimble extraction filter and the solvent in the solvent flask, that contains a stirrer bar. A condenser ensures an effective vapor cooling, and drips back down into the chamber housing the solid material, then the siphon side arm periodically empties the thimble (source [321]).

- The Solvent Assisted Flavor Evaporation (SAFE) apparatus allows a special high-vacuum distillation technique for the isolation of thermolabile flavors under gentle conditions. A sample is extracted with solvent and transferred via a dropping funnel into a distillation vessel (left) maintained under high vacuum and at 40-50°C; the vapor spray will form immediately and drifts to the head where two propeller-shaped barriers are mounted to retain non-volatile material whereas the volatile substances and solvent vapors are transferred to a flask cooled by liquid nitrogen (right). The concept of the SAFE extraction apparatus is similar the principle of diffusion pump[10]; in the SAFE the vacuum moves the vapor to the cooled trap. The particular equipment design allows very efficient and low-loss processing (Glasbläseri Bahr, Germany) (Figure 3.2)
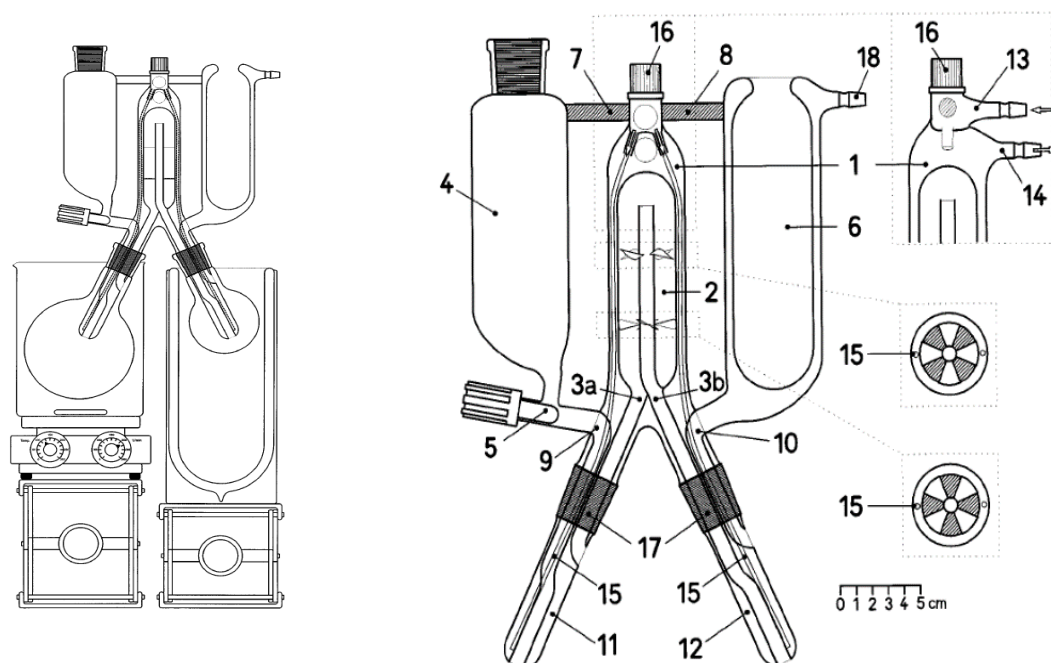
Figure 3.2: Description of distillation equipment for performing solvent assisted flavor evaporation (SAFE). 1-The head; 2- The distillation head equipped with 2 propeller-shaped barriers to remove non-volatile material from the vapors; 3a- The vapor inlets to the head; 3b- The distilled inlet to the trap; 4- Dropping funnel that contains the raw solvent extract; 5- Vacuum stopcock; 6- Cooling trap, filled with liquid nitrogen; 7 and 8- Supports; 9- Outlet of the dropping funnel; 10- Outlet of cooling trap (vacuum outlet); 11- and 12- Legs; 13- Water inlet; 14- Water outlet; 15- Two flexible polyethylene tubes guide the water flow to the bottom of both legs to afford effective temperature regulation by avoiding the formation of air bubbles;16- Screw cap (air extractor); 17- Ground joints NS 29 to fix distillation vessels; 18- Vacuum inlet (source [322]).

---

[10] Which uses the vapor of a boiling fluid to capture air molecules; the gravity and the downward direction of the vapors move the air molecules towards the bottom of the pump

3.1.5 Animals

- BL6 mice were provided by Charles River (Saint-Germain sur l'Arbresle, France). The animals were housed in a controlled environment (t°, 20°C; humidity, 55%; night/day, 12h/12h) . All animal procedures and experiments were performed in accordance with the guidelines established by the European Communities Council (Directive 2010/63/EU of March 4, 2014) and approved by of UMONS veterinary ethics committee of the Faculty of Medicine and Pharmacy (Approval N°: LA2500635T protocol approval GO/04/02).

- Adult male Hood Lister rats were provided by Charles River (Saint-Germain sur l'Arbresle, France). All animal procedures were performed in accordance with the United Kingdom Animals (Scientific Procedures) Act 1986 and local ethical guidelines.

3.1.6 Culture

The following material and reagents were used for the preparation and maintaining of cultures and for testing (Table 3.4):

Table 3.4: Material and reagents used for the preparation, maintaining and testing of the in-vitro model:

	Name	Supplier	Code
1	MicroTissues® 3D Petri Dish® 24-96	Sigma	Z764043-6EA
2	MicroTissues® 3D Petri Dish® 24-35	Sigma	Z764051-6EA
3	Invitrogen™ UltraPure™ Agarose	Fisher	11553277
4	Hank's Balance Salt Solution (HBSS)	Gibco	12549069
5	Gibco™ B-27™ Electrophysiology Kit	Fisher	11632149
6	Penicillin-Streptomycin	Fisher	11548876
7	Gibco Glutamax 100X	Fisher	11574466
8	Gibco Fetal bovine serum (FBS)	Fisher	11573397
9	Cell strainer 40 µm pore size	Merck	CLS431750-50EA
10	Invitrogen CellEvent caspase 3/7 green	Fisher	11390952
11	Propidium iodide 1.0 mg	Fisher	11599296
12	Resazurin sodium salt	Sigma	R7017-5G
13	Dichlorodihydrofluorescein diacetate	Sigma	D6883-50MG
14	4′,6-Diamidino-2-phenylindole (DAPI)	Sigma	A4099.0005
15	Polyethylene glycol (PEG) 8000	Sigma	4344336
16	Formamide 'grade biologie	Sigma	444475W

	Name	Supplier	Code
17	Casein high purity grade	VWR	E666-500G
18	Staurosporine 100 µg	Fisher	10042804
19	Glass bottom dish (Confocal dishes for microscopy)	VWR	734-2905
20	12-well removable chambers	Ibidi	81201
21	MAP2	Thermofisher	PA5-85755
22	GFAP Antibody (rabbit)	Thermofisher	PA1-10019
23	Anti-Tau antibody	abcam	ab80579
24	GFAP Antibody (mouse)	Thermofisher	A-21282
25	Anti-Iba-1	Wako Chemicals	019-19741
26	Anti-β-tubulin	Sigma	T5293
27	Goat anti-Rabbit IgG (H+L) Cross-Adsorbed Secondary Antibody, Alexa Fluor 594	Thermofisher	A-11012
28	Goat anti-Rat IgG (H+L) Cross-Adsorbed Secondary Antibody, Alexa Fluor 594	Thermofisher	A-11007
29	Goat anti-Rabbit IgG (H+L) Cross-Adsorbed Secondary Antibody, Alexa Fluor 488	Thermofisher	A-11008
30	Goat anti-Rat IgG (H+L) Cross-Adsorbed Secondary Antibody, Alexa Fluor 489	Thermofisher	A-11029

3.1.7 Microscopy

The following systems were applied for imaging the cultures:

- Zeiss axiovert 25 inverted transmitted light phase contrast tissue culture microscope with HAL 6V, objective 5X /0.12, 10X/0.25 camera DP200

- Field emission scanning electron microscope (JEOL, JSM-7200F), operating at 2 kV with secondary electron detection; metallization with a JFC 1100E ion sputtering device.

- Olympus IX 70 fluorescence microscope, equipped with a Hamamatsu digital camera C11440, a LED illuminator pE-340 fura, two filter cube U-MWIG3, U-MWIBA3, driven by the Cell dimension software.

- Laser Scanning confocal Microscope LSM 710 of ZEISS equipped with Airyscan detector, spectral (32-channels) PMT detector, 7 laser lines, driven by the ZEN blue software.

3.2 Methodology

3.2.1 Preparation of overcooked meat samples

The choice of meat and the cooking methods were selected for a maximal generation of b-carbolines; a review by Pfau. et al. 2004 indicates that the contents of norharmane and harmane were the highest in broiled chicken (622 and 133 ng/g, respectively) and in flame broiled meat (795 and 169 ng/g) [97].

➢ Pieces of beef and chicken muscles were purchased from local supermarket and were cut to very thin slices.

➢ The beef was broiled in lab oven (Nabetherm, Germany).

➢ The chicken was broiled in a domestic oven, the slices were turned to have a homogenous brown color on the two faces.

➢ The temperature was monitored, and cooking times were according to the observation of surface browning (Table 3.5).

Table 3.5: Meet cooking procedure for beef and chicken

Meat sample	Equipment/ Method	Temperature ($^{\bullet}C$)	Time (min)
Beef	Lab oven	270	24
Chicken	Domestic oven	200	40

➢ The meat was grinded by a powerful ball mills (RETSCH MM400), the vibration frequency was 300 min^{-1} for 30 second.

➢ The meat fond (browned meat juices) was collected with distilled water and filtered with filter paper.

3.2.2 Extraction of overcooked samples

3.2.2.1 Extraction of β-carbolines by an alkaline detergent solution

The method of extraction was originally described by Louis ED et al. 2007, for the quantification of harmane in meat samples; the detection limit corresponds to 1 ng harmane per gram of meat tissue [323, 324]. We applied the method with slight modifications[11]; briefly:

The meat samples (10 g) were homogenized in 40 mL of a buffer (1:4, g/ml) composed of 20 mM Tris (pH 7.5), 5 mM EGTA, 1% Triton X-100 and 0.1% sodium dodecyl sulfate. The homogenization was followed by digestion with 25 mL NaOH 1 M (RT, 2 h); the samples were centrifuged at 2400 g and the top-layer of fats was removed by using a filter paper. The samples were then extracted with an equivalent volume of ethyl acetate - diethyl ether (98:2); the two phases were shaken by hand for 1-2 min, incubated on a horizontal rotator (Labo-Modern, Germany) at room temperature for 45 min and centrifuged at 800 g for 10 min. The upper organic solvent was collected with glass Pasteur pipette, and the aqueous phase was reextracted twice with ethyl acetate - diethyl ether. The collected organic phases were combined and evaporated to dryness and the residue was dissolved in 1 ml of methanol. (Schema 3.1).

To evaluate the protocol, the extraction procedure was applied with β-CAs standards:

1- Harmane (100 ng) in methanol was mixed with 2 ml buffer and followed the same steps of extraction.

2- A mixture of harmane, harmine, harmalol and harmaline (1.2 mg each) was added to 10 g of chicken sample and followed the same step of extraction.

---

[11] (*i*) Deletion of protease inhibitor cocktail; (*ii*) centrifugation at 2400 g; (*iii*) replacement of t-butyl ether by diethyl ether

```
┌─────────────────────────────────────┐
│ Homogenization the 10.0 g of meat     │
│ samples with detergent buffer pH 7.5  │
└─────────────────────────────────────┘
                    │
                    ▼
        ┌─────────────────────┐
        │ Digestion with NaOH 1M │
        └─────────────────────┘
                                Centrifuge at 800 g for 10 min
```

┌──────────────┐   ┌──────────────────┐   ┌──────────────┐
│ Top fat layer │   │ The liquid phase │   │ The solid phase │
└──────────────┘   └──────────────────┘   └──────────────┘
        │   │   │
        ▼   ▼   ▼
┌──────────────┐   ┌──────────────────────┐   ┌──────────────┐
│ Removed with │   │ Extraction with ethyl │   │ Discarded   │
│ filter paper │   │ acetate and diethyl ether │   └──────────────┘
└──────────────┘   └──────────────────────┘
                                Centrifuge at 800 g for 10 min

┌────────────────────┐   ┌────────────────────┐
│ The organic phase   │   │ The aqueous phase   │
└────────────────────┘   └────────────────────┘
                                               │
                                               ▼
                              ┌────────────────────────────┐
                              │ Re-extracted 2 times with ethyl │
                              │ acetate and diethyl ether   │
                              └────────────────────────────┘

Collected

                    ┌────────────────────┐   ┌────────────────────┐
                    │ The organic phase   │   │ The aqueous phase   │
                    └────────────────────┘   └────────────────────┘
                              │
                              ▼   Evaporate to dryness
                    ┌────────────────────────────┐
                    │ Dissolved in 1 mL of methanol │
                    └────────────────────────────┘

Schema 3.1: The modified extraction method of β-carbolines from overcooked meat and poultry by an alkaline detergent solution.

3.2.2.2 Extraction of β-carbolines by a general alkaloid method

The base of this method was described by Tsuchiya et al., 1995 to determine tetrahydro-β-carbolines in brain [325]; the method was applied with slight modifications[12].
Briefly:

150 g of poultry samples were treated with aqueous sodium hydroxide (1 M NaOH) until alkaline reaction detected with pH paper, then the samples were transferred in a Soxhlet apparatus, covered with a thin layer of sand and extracted with 350 mL of ethyl acetate, overnight (18 h, i.e. 63 cycles) (Figure 3.3).

Afterwards, the extract was concentrated to 200 mL and extracted 3 times by an equivalent volume of 0.1 M HCl.

The combined aqueous phases were washed 2 times by 50 ml of ethyl acetate, alkalinized with sodium hydroxide (1 M NaOH) to reach pH 12 and extracted 3 times with 200 mL of ethyl acetate.

Finally, the ethyl acetate extracts were combined, dried over anhydrous sodium sulfate Na_2SO_4, transferred in a weighed balloon, evaporated to dryness, and weighed (Schema 3.2).
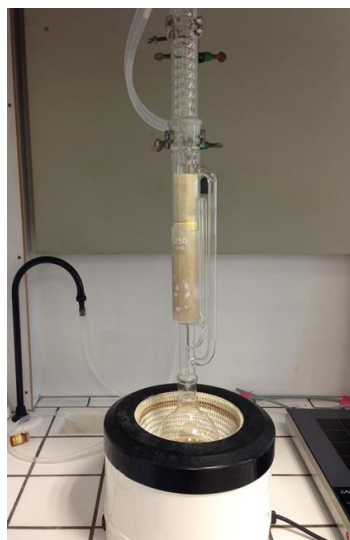
Figure 3.3: The Soxhlet extraction applied to a poultry sample in our lab.

---

[12] We omitted the treatment of the brain before extraction with H_2SO_4, Na_2WO_4 in potassium phosphate buffer (pH 8.5); we applied a Soxhlet organic extraction, the percentage of EtOAc/HCl mixture was modified from 5 :1 v/v to 1/1; we did not add sodium phosphate to the aqueous phase before the extraction.

```
                    ┌─────────────────────────────┐
                    │  Alkalization the poultry samples │
                    │     with NaOH 1M to pH 12    │
                    └─────────────────────────────┘
                                 │  Transferred to Soxhlet apparatus
                                 ▼
                    ┌─────────────────────────────┐
                    │   Extracted with ethyl acetate │
                    └─────────────────────────────┘
                                 │  Transferred to separatory funnel
                                 ▼
                    ┌─────────────────────────────┐
                    │     Extracted with HCl 0.1 M  │
                    └─────────────────────────────┘
```

Alkalization the poultry samples with NaOH 1M to pH 12

— Transferred to Soxhlet apparatus →

Extracted with ethyl acetate

— Transferred to separatory funnel →

Extracted with HCl 0.1 M

The aqueous phase | The organic phase

Re-extracted 2 times with HCl 0.1 M

Collected

The aqueous phase | The organic phase

Alkalinized with NaOH to pH 12

Extracted with ethyl acetate 3 times

The organic phase | The aqueous phase

Dried over anhydrous Na2SO4

Evaporated to dryness | Discarded

Schema 3.2: The modified extraction method of poultry meat by a general alkaloid meethod, The first step consisted in ethyl acetate extraction of the alkalinized meat samples by Soxhlet apparatus to ensure complete extraction with small quantity of solvent, followed by partitioning HCl/EtOAc.

3.2.2.3 Extraction of volatile carbonyl compounds by Solvent Assisted Flavor Evaporation (SAFE)

In order to extract volatile compounds, we applied a method designed for the isolation of volatile molecules from non-volatiles in solvent extracts, relying on an innovative distillation unit (a SAFE unit); the principle is based on high-vacuum transfer, which ensures a fast and careful isolation of volatiles from complex matrices [322] (Figure 3.4).

Figure 3.4: View of the assembled equipment for SAFE, the temperature of the water in the left leg and the head is 30°C, ensured by water inlet. The left vessel is incubated in a water bath at 40°C; on the other side, the trap and right vessel are cooled by liquid nitrogen at -196°C. The arrow indicates the vessel in which the sample is introduced (original image).

For this method 22 mL of each of the samples described hereunder were extracted in triplicate, the SAFE apparatus being cleaned by a distillation of 10 mL of water between the samples:

1- Aqueous sample: overcooked poultry meat was extracted with deionized water in a 1: 5 ratio (w/v), in a closed vessel placed in an ultrasonic bath (30° C for 6 h), then centrifuged (10 min, 2000 g) to collect the supernatant.

2- The meat fond (browned meat juices) that was collected from the oil-less overcooking of 1000 g of chicken with 250 mL distilled water.

3- Deionized water (procedural blank).

4- The "Aldehydes mixtures-556", containing 15 components and diluted at 40 ng/mL each in deionized water

The SAFE apparatus must be prepared before starting the distillation; for that, the water bath of the left was heated at 40°C, the water entered by inlet (Figure 3.2, N°13) was thermostat at 30°C, then a high vacuum (0.4 Pa) was applied; finally, the liquid nitrogen was added to the right bath and trap.

When the installation of SAFE apparatus was terminated, 22 mL of the sample was added to the dropping funnel and the distillation procedure was started by dropping the sample into the left vessel (drop by drop). A vapor from volatiles and solvent is transferred to the head where there are barriers to remove the non-volatile materials from the vapor, the latter entering the right vessel to condense.

3.2.2.4 Extraction and isolation of volatile carbonyl compounds by headspace single-drop microextraction (HS-SDME) with droplet derivatization

In line with the previous method (3.2.2.3), a second technique was applied to identify volatile aldehydes, based on headspace single-drop microextraction (HS-SDME) with droplet derivatization.

The microextraction, an analytical technique first described by Jeannot, M.A. (1996) [326], ensures solvent extraction in a simple inexpensive apparatus involving very little solvent consumption, followed by gas chromatographic (GC) analysis. In the original technique, a small drop of a water-immiscible organic solvent, containing an internal standard, is formed at the end of a Teflon rod that is immersed in a stirred aqueous sample solution for a given time; the probe is then withdrawn from the aqueous solution, and the organic phase is sampled with a micro-syringe and injected into the GC for identification and quantification (Figure 3.5).
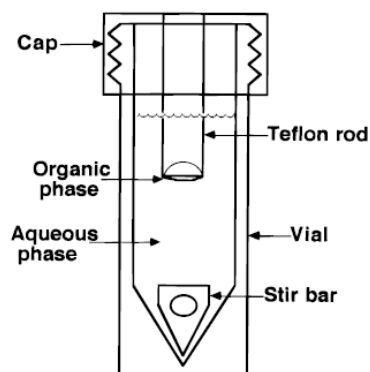
Figure 3.5: The solvent microextraction system as described by Jeannot, M.A. (1996).The solvent apparatus consists of a 1-mL vial that contains the aqueous sample and a rod-shaped Teflon probe hollowed out, filled with 8 µL of organic solvent, immersed in the aqueous sample, and held in place by a cap. A magnetic stirrer is used to stir the aqueous phase (source [326]).

This method was modified to head-space for droplet derivatization with O-(2,3,4,5,6-pentafluorobenzyl) hydroxylamine Hydrochloride (PFBHA) by Li et al. (2005) and applied on volatiles aldehydes in blood [327]. The head-space extraction is a dynamic gas phase extraction to quantify volatiles in solid or complex liquid samples, and derivatization of aldehydes with PFBHA to form the corresponding oximes is very well known, rapid and complete reaction (Figure 3.6).
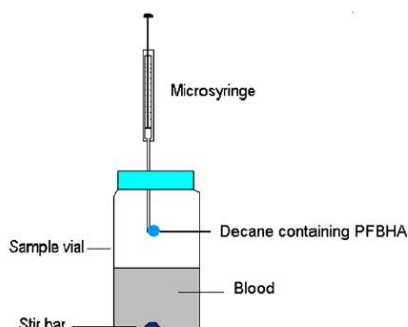
Figure 3.6: HS-SDME with droplet derivatization of aldehydes as described by Li et al. (2005): a microsyringe exposes a small drop of a water-immiscible organic solvent (that contains the derivatizing reagent and internal standard) to the headspace of a stirred aqueous sample solution for a given time at fixed temperature (source [327])

Several parameters can affect HS-SDME with droplet derivatization, *(i)* the choice of the extraction solvent that depends on its low volatility, its ability to extract the analytes, and its peaks that should be well separated from the analyte peaks in the chromatogram; *(ii)* the temperature of extraction which should be high enough to ensure the vaporization of analytes and their absorption in the microdroplet without evaporating the microdroplet solvent (loss of extraction solvent); *(iii)* the stirring rate that is particularly important to enhance the mass

transfer in the aqueous phase, and decrease the time needed to reach the thermodynamic equilibrium between aqueous phase and headspace without affecting the stability of droplet; and *(iv)* the volume of organic solvent; while using a large organic drop results in an increased analytical response, larger drops are difficult to manipulate and are not reliable.

Based on the above, the heptane was selected for our extraction, the temperature was fixed at 60°C, the stirring at 450 rpm, the volume of organic solvent at 3 µL and the time of extraction at 6 min.

We applied this method on the solutions below:

1- Aqueous sample: overcooked poultry meat was extracted with deionized water in a 1: 5 ratio (w/v) in a closed vessel placed in an ultrasonic bath (30 ° C for 6 h), then centrifuged (10 min, 2000 g) to collect the supernatant.

2- The chicken fond (browned chicken juices) that was collected with distilled water (250 mL for 1000g of raw chicken).

3- Deionized water (procedural blank).

4- The "Aldehydes mixtures-556", containing 15 components and diluted at 50 ng each in 1 mL of deionized water

The solution of PFBHA in heptane was prepared by dissolving 20 mg of PFBHA into 1 mL deionized water; the 1 mL of PFBHA aqueous solution was extracted with 1.0 mL of heptane ; the expected final concentration of PFBHA is about 16 mg/mL [327].

For each extract, 1 mL of sample and 10 µL of 0.6 mM methyl ethyl ketone in water (internal standard) were transferred to a closed 4-mL vial (amber screw vial 45x14.7mm, BGB) containing a small magnetic rod. The vial was placed in a water bath at 60°C under stirring and a drop of 3 µL of PFBHA in heptane was suspended from the micro-syringe (Figure 3.7) [322].

Figure 3.7: HS-SDME application, the vial containing the sample and magnetic rod is placed in a water bath at 40°C; stirring speed, 450 rpm; volume of suspended PFBHA in heptane from the micro syringe, 3 µL (original images).

3.2.2.5 Extraction and isolation of carbonyl compounds by condensation with a silica-gel supported reagent

The extraction is based on the reactivity of the carbonyl group towards a semicarbazide reagent to form a semicarbazone (Figure 3.8).

This condensation ensures the separation of carbonyl compounds from other solutes in an organic solvent (hexane or toluene) extract, in which the semicarbazones are invariably insoluble.

Singh et al (1979) [328] further developed the concept by proposing a solid phase reagent that we applied to profile aldehydes in our meat samples.
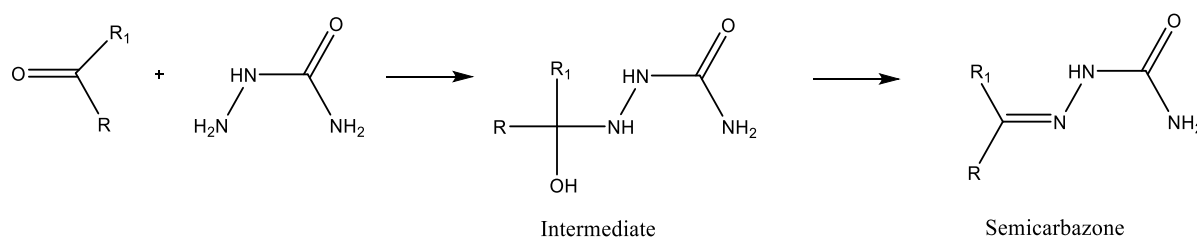
Figure 3.8: The condensation of a carbonyl group with a semicarbazide group to form a semicarbazone.

Preparation of the silica-gel supported reagents

Semicarbazide hydrochloride (5.0 g; 0.045 mole) was added to a solution of NaOH (2.0 g; 0.05 mole) in water-MeOH (1 : 1; 60 ml).

To the resulting clear solution, silica gel (fraction 80-200 mesh, bulk density, 0.71 g/ml; 45 g) was introduced with stirring.

Subsequently, the whole mixture was mechanically shaken (1 h) at 30- 35° C and water-MeOH was removed on a rotary evaporator (90°C; 80-90 mm Hg; 30-45 min) to yield a white free-flowing powder. The final reagent was stored in a brown bottle at room temperature.

Extraction and condensation of ketonic/aldehydic material

A meat sample (165 g) was transferred in a Soxhlet apparatus and extracted with toluene (350 mL) for 18 h.

After concentration to about 100 mL, the toluene extract was added with 30 g of the semicarbazide-silica reagent (1.0 g of reagent corresponds to 54.2 mg of semicarbazide that could condense 2.5 mmoles of carbonyl compounds).

The mixture was heated ($70 \pm 2°C$) and stirred for 12-18 h, the absence of the carbonyl compound in the solution was determined at the end of this step, through the absence of yellow to orange spots in a TLC test when spraying a 0.005 M 2,4-dinitrophenylhydrazine (DNPH) solution in ethanol.

Next, the mixture was cooled, filtered and the solid washed with the same solvent (4 x 50 ml, room t°); the absence of aldehydes/ketones was similarly verified in the wash solvent.

The filtrate and wash solutions were discarded while the solid phase was treated to regenerate the ketones/aldehydes.

Regeneration of the ketone/aldehydes from semi-carbazones

The solid phase containing the semi-carbazones was added to a solution of oxalic acid (9 g) in water (160 ml); after addition of toluene (100 ml), the mixture was stirred and refluxed for 4-5 h.

After cooling, the liquid phase was transferred to a separatory funnel and the silica gel washed with toluene (50 ml x 2), also transferred to the funnel.

After the separation of phases, the aqueous phase was extracted with toluene (100 ml x 2) and the extracts combined with the main toluene extract.

The combined toluene extracts were washed with water (100 ml x 2) and with a saturated NaCl solution (~26 %; 50 ml), then dried with anhydrous sodium sulfate (Na_2SO_4).

Finally, the solvent was transferred in a weighed balloon, evaporated to dryness, and the regenerated carbonyl compounds were weighed (Schema 3.3).

This extraction ends up by a distillation of toluene to yield the final extract; despite the use of a fractionated distillation (vacuum distillation with a Vigreux column), we could not recover a fraction with a boiling point lower than toluene. This indicates a loss of all volatile carbonyl compounds; therefore, this method was intending the non-volatile compounds.
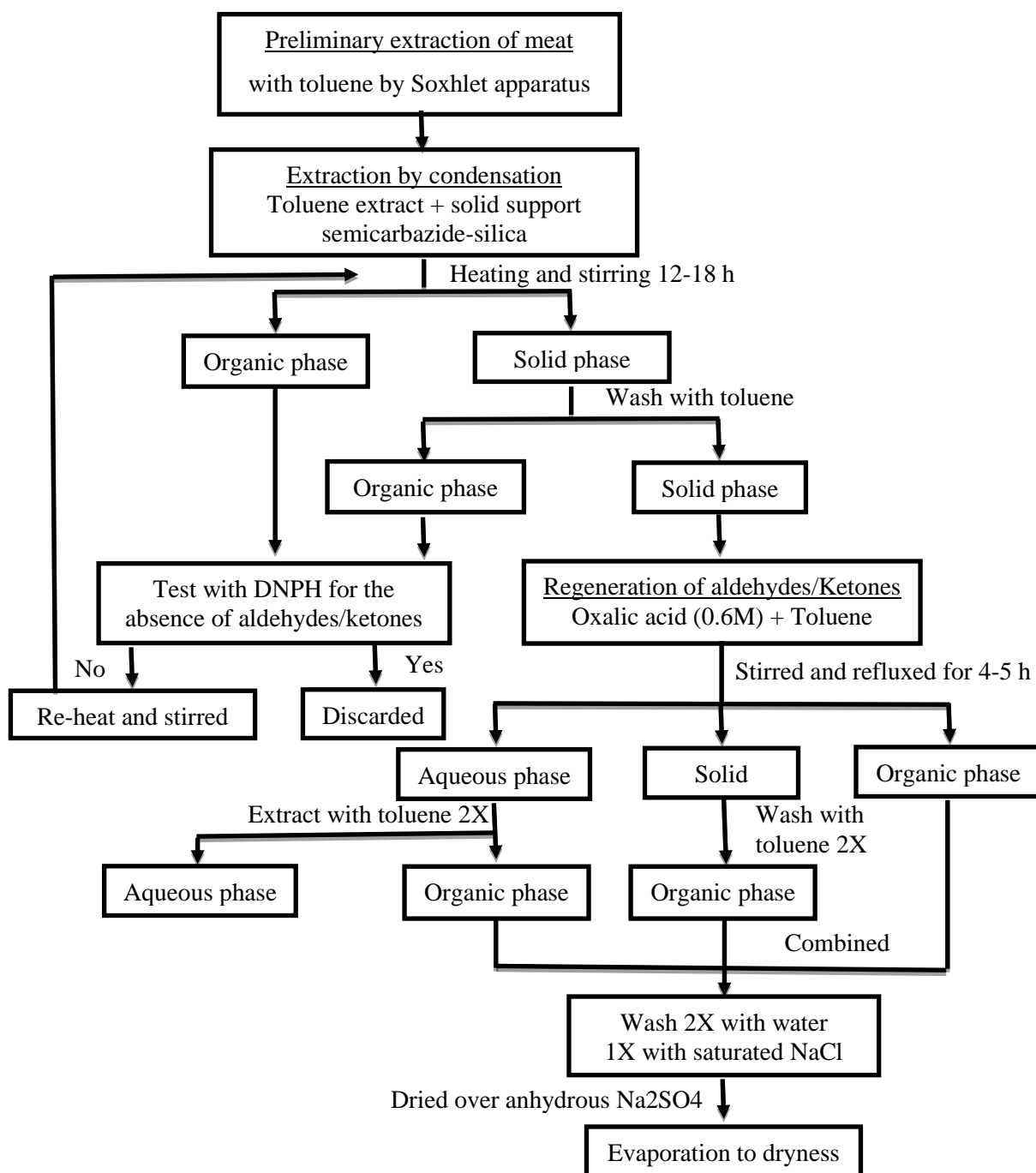
Schema 3.3: The extraction of meat sample by Soxhlet apparatus followed by isolation of aldehydes by condensation with silica-gel supported reagents samples, then regeneration from silica by oxalic acid and portioning with toluene.

3.2.3 Characterization of extracts

3.2.3.1 Identification of β-carbolines

3.2.3.1.1 Thin-layer chromatography analysis (TLC)

Thin-layer Chromatography (TLC) is a solid-liquid chromatography technique, simple, precise and inexpensive for a preliminary analysis of mixtures; the separation of the compounds depends on their different solubilities and adsorption to the two phases between which they are partitioned. TLC is a useful and rapid method to evaluate the number of components in a mixture, their identity and purity, through three steps - spotting, development, and visualization.

The TLC was applied here for qualitative analysis, to determine the number of components in the extract, and their identity by comparing with the reference standard. The comparison was based on UV-Vis detection, on the color or fluorescence after derivatization with specific reagents and on the retention factor (Rf), that is defined as the distance traveled by the compound divided by the distance traveled by the solvent. If two substances have the same Rf value, they are likely (but not necessarily) the same compound. If they have different Rf values, they are different compounds.

The application was made with these conditions:

- Stationary phase: TLC Silica gel 60 F254, 10x20 cm, Merck, Germany.
- Mobile phase: dichloromethane - methanol - 10 % ammonia in proportions of (80:20:1.5, v/v/v)
- Standards: methanolic solutions at concentrations of 10 mM (harmane 1.82 mg/mL, harmine 1.4 mg/mL, harmaline 1.4 mg/mL, harmalol 2.7 mg/mL)
- Sample: Each sample (~150 mg) was dissolved in 3 mL of methanol.
- Preconditioning: The chromatography tank (flat bottom chamber, 20x20 cm; Camag), was saturated with 30 mL of mobile phase for 20-30 min. Filter paper was lined inside of the tank to equilibrate the chamber with solvent vapors.
- Sample application: 5 µL of standards and samples were applied as 8-mm bands, either manually or automatically by using CAMAG® Automatic TLC Sampler 4, at laboratory temperature.

- Development: The TLC plate was placed in vertical position, and the chromatography was allowed to proceed over 8.5 cm. The development lasts approximately 15 min.

- Drying step: was performed in vertical position for 10-15 min under the hood.

- Detection: the chromatogram was evaluated by two methods:

  UV Detection at wavelengths 366 nm (fluorescence) and 254 nm (quenching).

  Chemical Detection with Dragendorff's reagent, a specific reagent for alkaloids and heterocycle nitrogen compounds, that was sprayed on the plate.

This method was also applied using the automated CAMAG TLC system.

3.2.3.1.2 High Performance Liquid Chromatography (HPLC) of β-carbolines

High Performance Liquid Chromatography (HPLC) is a form of column chromatography widely used to separate, identify, and quantify components dissolved in a liquid solvent with a high analytical resolution. The solvent (known as the mobile phase) is pumped at high pressure through a column packed with a chromatographic solid support (stationary phase). The dissolved components are injected in the system and detected. Their retention times will vary depending on the interactions between the stationary phase, the molecules being analyzed and the solvent. Analytes that have the higher affinity to the stationary phase or the lower solubility in the mobile phase will exit the column slower.

The HPLC separation of alkaloids was performed on the Agilent HPLC system for the alkaline detergent extract (3.2.2.1 p.72), and on the Merck-Hitachi HPLC for the general alkaloid extract (3.2.2.2 p.74). The compounds were eluted on a Luna 5µm phenyl hexyl column (250 x 4.60 mm) (Phenomenex, Utrecht, Netherlands), equipped with a guard column; before injection, extract samples were centrifuged or filtered on 0.45 µm PTFE filter. The mobile phase consisted of a gradient between 0.1 % formic acid in deionized water (phase A) and a mixture acetonitrile - methanol (1:1; v/v) (phase B).
The gradient was inspired from Bensalem et al. (2014) [329] : equilibration time 15 min at 0 % B; 0 min, 1 % B; 5 min, 10 % B; 10 min, 2 5% B; 15 min, 50 % B; 17 min 100 % B; the flow rate was set at 1.5 mL/min, the column temperature at 40°C and the UV-detector at 254 nm.; 5 µl of methanolic samples were injected..

3.2.3.2 Chromatographic analysis of carbonyl compounds (HPLC-MS/MS and GC-MS)

Environmental aldehydes are in general small polar and volatile molecules that are biochemically unstable; for this reason, derivatization with different reagents is widely used in their identification and quantification. Derivatization can also improve volatility, chromatographic separation and peak symmetry, MS ionization, MS/MS fragmentation and the analytical sensitivity. The best-known reagents applied to the analysis of aldehydes are 2,4-dinitrophenylhydrazine (2,4-DNPH), 2,4,6-trichloro-phenylhydrazine (TCPH) and O-(2,3,4,5,6-pentafluorobenzyl) hydroxylamine (PFBHA) [330]. The analytical methods usually used are gas chromatography (GC) and high-performance liquid chromatography (HPLC), generally coupled with mass spectrometry (GC-MS, HPLC-MS, GC-MS/MS, HPLC-MS/MS), that allow identification by analyzing characteristic fragmentations. Direct infusion in a mass spectrometer can also be applied, through an electrospray interface (ESI-MS/MS).

3.2.3.2.1 Derivatization with 4-hydrazinyl-N, N, N-trimethyl-4-oxobutan-1-aminium iodide (HTMOB) and analysis by mass spectrometry

For the separation of total carbonyl compounds obtained by solid-phase reagent extraction (3.2.2.5 p.80), a modified Girard T derivatizing reagent was selected, i.e., the 4-hydrazinyl-*N, N, N*-trimethyl-4-oxobutan-1-aminium iodide (HTMOB). Girard T derivatives are generally known to provide analytical sensitivity with electrospray ionization tandem mass spectrometry ESI-MS/MS for a range of carbonyl compounds; however, the high-mass product ions are always a minor proportion of the total ions in product ions spectra. To improve the sensitivity of aldehydes and ketones analysis, a new Girard T reagent was proposed by Johnson (2007) who modified the connecting methylene chain to facilitate fragmentation to a single product ion; with its three methylene chain, 4-hydrazino-*N,N,N*-trimethyl-4-oxobutan-1-aminium iodide (HTMOB) yields carbonyl derivatives with superior ESI-MS/MS fragmentation characteristics (Figure 3.9) [331]. However, this reagent is not commercially available and so, we decided to synthesize HTMOB.
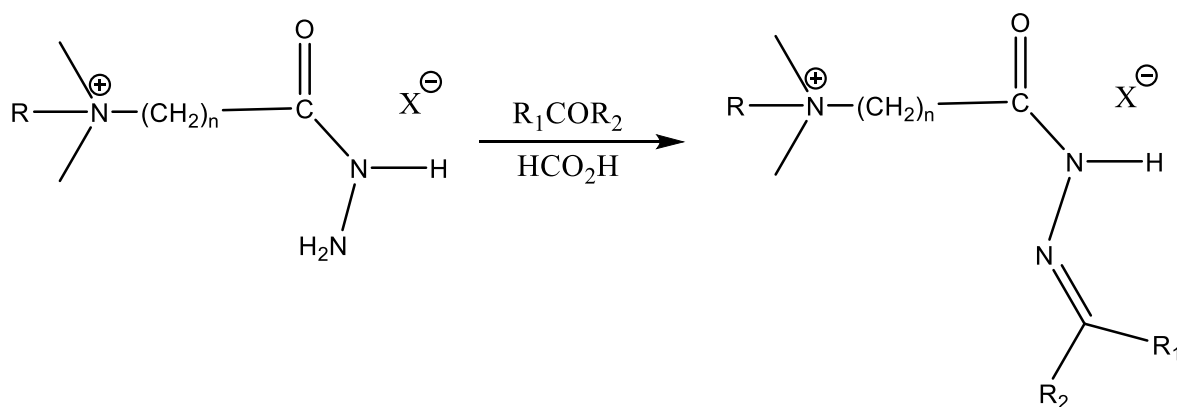
Hydrazine	R	n	X
Girard T	CH_3	1	Cl
HTMOB	CH_3	3	I

Figure 3.9: Chemical structures of Girard T and modified Girard reagents and their hydrazone derivatives of aldehydes (R1 or R2 = H) and ketones.

Synthesis of HTMOB

HTMOB was synthesized from the method of Johnson DW (2007), with the help of M. Simons, R. Lienard and P. Gerbaux [331].

Step 1: Esterification of butyric acid

A solution of hydrogen chloride in ethanol was prepared by slowly adding acetyl chloride (12.5 mL) to absolute ethanol (50 mL) with cooling on ice bath. Then, dimethylaminobutyric acid hydrochloride (2.0 g) was added and the solution was heated at 80°C for 2 h. After the evaporation of solvent in a rotary evaporator, a concentrated ammonia solution (10 mL) was slowly added with cooling on ice bath. Finally, the solution was extracted with ethyl acetate (10 mL) three times and the collected ethyl acetate solution was evaporated to yield ethyl dimethyl aminobutyrate as a colorless liquid. For the verification, mass spectrum must apply.

Step 2: Methylation - formation of a quaternary ammonium salt

The ethyl dimethylaminobutanoate collected in the first step was dissolved in dichloromethane (1 mL), and iodomethane (312 mg, 2.2 mmol) was slowly added to form a white solid precipitate of 4-ethoxy-*N,N,N*-trimethyl-4-oxobutan-1-aminium iodide. The solid was filtered off on a Büchner, washed two times with dichloromethane (1 mL) and dried The methylation was verified with ESI mass spectrum: *m*/z 174 (M$^+$).

Step 3: Ester hydrazinolysis - formation of HTMOB

Hydrazine hydrate (500 mg) was added to the solid product of step 2 and heated at 80°C for 2 h with stirring and condenser. The mix was dried to remove the excess hydrazine by prolonged flushing with air at 80°C. Finally, the residue was recrystallized from methanol/diethyl ether (1/1) by adding the solid to the hot mix solvent, followed by cooling to obtain HTMOB as white crystals. The methylation was verified with ESI mass spectrum: m/z 160 (M$^+$), and NMR.

Derivatization of Aldehydes with HTMOB

In a preliminary trial, the derivatization was applied on benzaldehyde as reference and the aldehyde extract 3.2.2.5 p.80.

The reaction was started by adding, in Eppendorf tubes, 100 µL of benzaldehyde (10 mM in MeOH) or the aldehyde extract (2 mg/ml in MeOH) to 100 µL of a 10 mM HTMOB methanolic solution containing 4 µL glacial acetic acid; the mixture was vortex-mixed, heated at 75° C for 3 h and evaporated to dryness. The residue was dissolved in acetonitrile - water - formic acid (50 : 50 : 0.025, v/v/v) (0.5 mL) and analyzed with ESI-MS/MS with monitoring of a neutral loss of m/z 59 (ESI-QToF system).

The following experiments were performed with M. Simons for his Master thesis, in collaboration with the Laboratory of Organic Synthesis and Mass Spectrometry of UMONS (S²MOS). In view of identifying the aldehydes in our extracts, we first developed a database of mass spectra, based on standard aldehydes we derivatized with HTMOB. A series of aldehyde standards was chosen, based on bibliographic works reporting the presence of aldehydes in food [332, 333].

A slight modification was applied to the analysis method, regarding the injection solvent that was replaced by HPLC methanol to increase the sensitivity of mass spectrometry.

Preparation of the samples, standards and HTMOB

✓ The stock solution of HTMOB 50 mM was prepared by dissolving 28.7 mg in 2 mL MeOH containing 1% formic acid

✓ The reference aldehydes were individually dissolved in MeOH to yield 50 mM solutions

✓ The brown chicken juice (3.2.1) was collected with deionized water, then filtered through a syringe with a filter of 0.45 µm. To purify the extract, 10 µL were partitioned with 1 mL

tert-n-butyl methyl ether; the mix was stirred for 1 min with vortex, then the ether was carefully removed using a Pasteur pipette.

✓ 3 mg of the extract isolated by condensation with the silica-gel supported reagent (3.2.2.5, p.80) were dissolved in 500 µL of methanol (HPLC grade), stirring for 1 min. For the working solution, a dilution of 100 times was made with the same solvent.

Derivatization with HTMOB

In Eppendorf tubes, 100 µL of the solution of 1 % formic acid in HTMOB 50 mM were added to 100 µL of each standard aldehyde, incubated 10 min at room temperature, brought to 1 mL with methanol and infused in the mass spectrometer.

For extracts and cooking juices, 20 µL of 1 % formic acid in HTMOB 1 mM were added to 10 µL of samples; the reaction mix was filtered on a 0.45 µm Teflon filter before injection.

Mass spectrometry

The Micromass Quattro Premier (Waters), driven by the MassLynx 4.0 software, was used in direct injection with the following settings: capillary voltage, 3.1 kV, 80°C; cone voltage, 20V, 120°C; extractor voltage, 4V; analysis flow, 10µL/min. ESI spectrum were recorded in positive mode, applying full scan, daughter scan and neutral loss.

3.2.3.2.2 Derivatization with PFBHA and analysis by Gas Chromatography-Mass Spectrometry (GC-MS)

In this work the derivatization reagent *O*-2,3,4,5,6-(pentafluorobenzyl)hydroxylamine (PFBHA) was applied to detect the aldehydes, the reaction of PFBHA with carbonyl compounds being described as instantaneous. Analyses were performed by gas chromatography coupled with mass spectrometry (GC/MS) in Total Ion Chromatogram (TIC) and Extracted Ion Chromatogram (EIC) modes. The aldehyde-PFBHA oxime derivatives are clearly identified by the presence of the *m/z* 181 fragment (C_6F_5-CH_2). Usually, for most asymmetrical carbonyl compounds derivatized with PFBHA, the two isomers (E) and (Z) are formed (Figure 3.10).
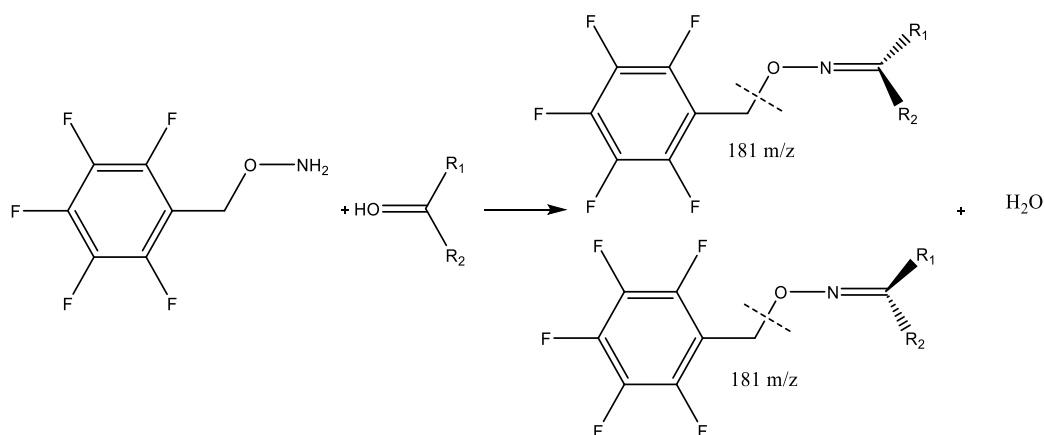
Figure 3.10: Reaction mechanism of O-PFBHA derivatization with carbonyl group, with the loss of *m/z* 181 by ionization.

The SAFE extraction was followed by derivatization with PFBHA, based on the United States Environmental Protection Agency EPA method of June 1998.

Accordingly, to adjust the pH to 4, 200 mg of potassium hydrogen phthalate were added to 20 mL of each SAFE extract, to the Aldehydes mixture (556) (15 components) or to the blank (deionized water).

Then, 1 mL of a fresh preparation of PFBHA (15 mg/mL H_2O) was added, the mix was gently homogenized by shaking, placed in a water bath (35°C for 2 h), cooled at room temperature for 10 min and added with 50 µL (2 to 4 drops) of concentrated sulfuric acid to destroy the excess reagent and avoid its extraction as much as possible. Subsequently, 4 mL of hexane containing the internal standard (1,2-dibromoethane, 0.4 µg/mL) ("fortified solvent") were added, the mix was shaken manually for 3 min and let to stand for 5 min to allow the phases to separate.

The upper layer of hexane was drawn off, using a Pasteur pipet, into a smaller 8-mL vial containing 3 mL of 0.1 M sulfuric acid. Again, the mix was shaken for 30 sec and was left for 5 min for phases separation; this step of acid wash reduces the reagent and other interferants from the final extract. Finally, the top hexane layer was drawn off for injection into the gas chromatograph (Schema 3.4).

The extract was analyzed on a gas chromatograph equipped with a split/splitless injector, and a mass spectrometry detector. The Column was a DB5-MS 30 m x 0.25 mm i.d., 0.25 µm film thickness and the following settings were applied: carrier gas, helium; head pressure, 15 psi; injection volume, 1 µL; injector temperature, 220°C; spitless injection, 1 min split

delay; detector transfer line, 300°C; source, 70 keV. Temperature program: 50°C for 1 min, program at 4°C/min to 220°C, program at 20°C /min to 250°C and hold at 250°C for 10 min.

The same method was applied for the HS-SDME reaction mix. This method was applied in triplicate for all extracts.

```
┌─────────────────────────────────────────────┐
│   20 mL of sample + 20 mg K-H-Phthalate KHP  │
└─────────────────────────────────────────────┘
                    │  Check the pH at 4
                    ▼
          ┌──────────────────────┐
          │  Addition of 1mL of PFBHA │
          │       (15mg/mL)       │
          └──────────────────────┘
                    │  Incubation at 35 °C for 2 h
                    ▼
      ┌────────────────────────────────────┐
      │  50 µL of H₂SO₄ + 4mL hexane with IS │
      └────────────────────────────────────┘
                 Mix for 3 min and rest 5 min
          ┌───────────────────┴───────────────────┐
          ▼                                         ▼
  ┌────────────────┐                     ┌────────────────┐
  │  Aqueous phase │                     │  Organic phase │
  └────────────────┘                     └────────────────┘
                                                  │
                                                  ▼
                                      ┌────────────────────────┐
                                      │  3 mL of H₂SO₄ 0.1 M    │
                                      └────────────────────────┘
                                          Mix for 30 sec and rest 5 min
                           ┌──────────────────┴──────────────────┐
                           ▼                                       ▼
                   ┌────────────────┐                  ┌────────────────┐
                   │  Aqueous phase │                  │  Organic phase │
                   └────────────────┘                  └────────────────┘
                                                                │
                                                                ▼
                                                        ┌────────────────┐
                                                        │     To GC      │
                                                        └────────────────┘
```
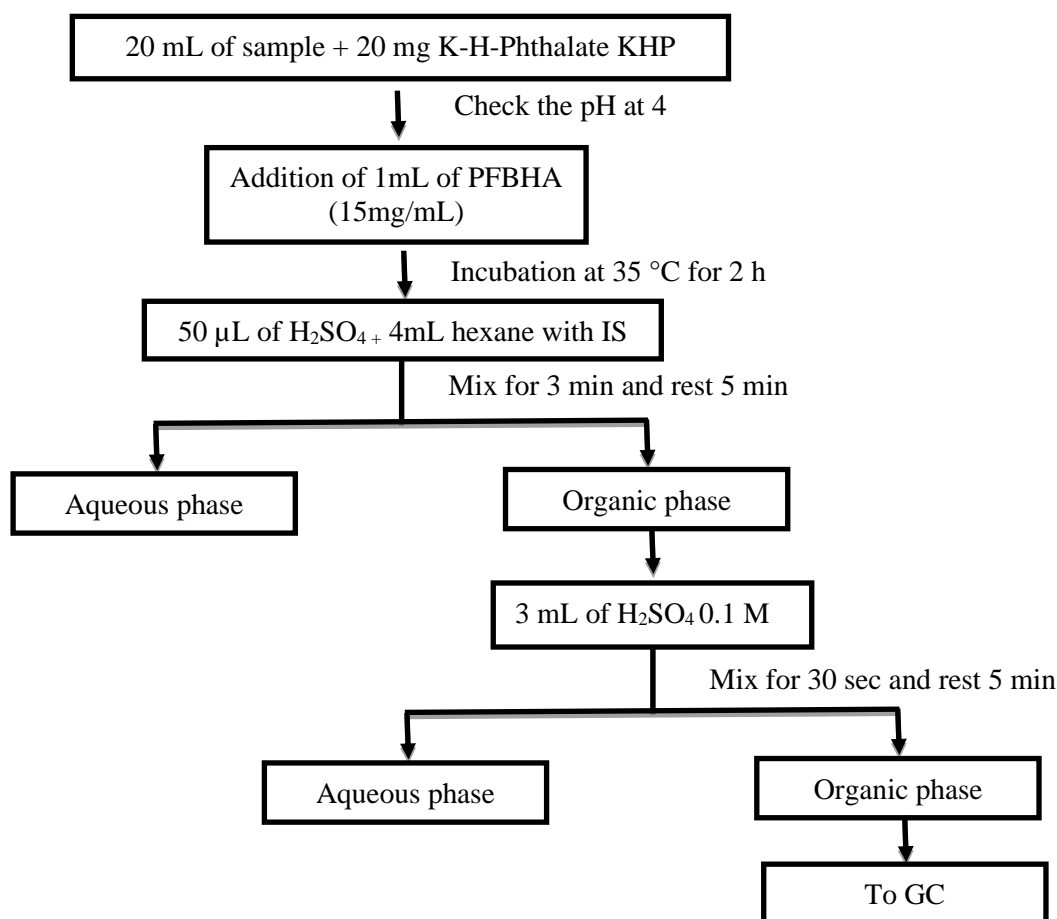
Schema 3.4: Schema of PFBHA derivatization of SAFE extract.

3.2.4 Identification of artefactual compounds likely to form by reaction with endogenous amines

Human exposure to aldehydes is implicated in multiple diseases, including diabetes, cardiovascular diseases, neurodegenerative disorders (i.e., Alzheimer's and Parkinson's Diseases), and cancer. Because these compounds are strong electrophiles, they can react with nucleophilic sites in DNA, proteins and biogenic amines to form reversible and irreversible

modifications. These modifications, if not eliminated or repaired, can lead to alteration in cellular homeostasis, cell death and ultimately contribute to the pathogenesis of diseases. Biogenic amines are important nitrogenous compounds that may also react with aldehydes to form isoquinoline or β-carboline compounds (so-called "endogenous alkaloids"), some of these substances being reported to have pharmacological activities.

The cooking of meats is known to generate carbonyl compounds, notably through the Maillard reaction; therefore, the possibility of generating endogenous β-carboline or isoquinoline alkaloids through an endogenous condensation with neurotransmitters such as epinephrine, norepinephrine, dopamine, serotonin, γ-aminobutyric acid (GABA) or tryptamine was investigated for a bioactivity potential or alleged activity.

3.2.4.1 Detection of alkaloid artifacts by TLC

The method to identify such an "artifactual" formation of β-carboline alkaloids was deduced from Bunel, et al. [334]. It is based on direct contact in equimolar concentrations between the aldehydes identified in the meat extracts and neurotransmitter for 16 h at 37°C, in aqueous medium; when the aldehyde or neurotransmitter was not soluble in water, methanol was our second choice, whereas, to solubilize tryptophan, an alkaline medium was used. To maintain the incubation conditions, a digital laboratory block heater thermo cell by Bioer technology was used.

TLC analysis was performed after reaction according to these conditions:
- ✓ Stationary phase: TLC Silica gel 60 F254, 10x20 cm, Merck, Germany.
- ✓ Mobile phase: ethyl acetate - acetic acid - methanol (6 : 2 : 2, v/v)
- ✓ Sample application: 5 μL of standards and samples were applied as 8-mm bands, by using the Camag® Automatic TLC Sampler 4, at laboratory temperature.
- ✓ Detection: the chromatogram was evaluated by two methods:
  - UV Detection at wavelengths 366 nm (fluorescence) and 254 nm (quenching).
  - Chemical Detection by spraying a ninhydrin reagent, quite specific for primary and secondary amines; the plate was then heated at 105°C for 5 min.

A reaction was confirmed by the presence of at least one spot that did not match any spot in both reactant molecules.

3.2.4.2 Identification of alkaloid artifacts by HPTLC/MS

This method is ideal for analytical uses, coupling the easiness and speed of thin-layer chromatography (TLC) with the power of mass spectrometry (MS) identification. Using a silica-gel matrix of HPTLC-MS grade reduces the background impurities to improve the detection limit down to the nanogram range.

After the separation was completed and the plate dried, MS was performed with a desorption-based technique (spot dialysis from the silica layer, Figure 3.11). The TLC-MS apparatus by Camag was used for elution with 0.5% formic acid in LC-MS grade methanol and transfer to the mass spectrometer inlet.
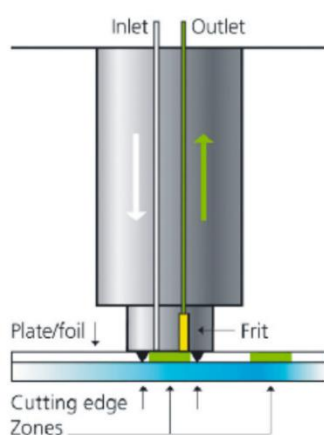
Figure 3.11: The working principle of elution-based TLC/MS that enables the dissolution of the analyte from the silica plate by a solvent and transfer to the mass spectrometer in the liquid phase (the TLC directly coupled with mass spectrometry). (source [335]).

For the samples for which a reaction between aldehyde and neurotransmitter was confirmed by TLC (section 3.2.4.1 p.91), HPTLC was performed, according to these conditions:

✓ Stationary phase: Silica gel 60 F_{254} MS grade,10x20 cm HPTLC plates (Merck, Germany)

✓ Mobile phase: ethyl acetate - acetic acid - methanol (6 : 2 : 2, v/v); development up to 1 cm from the top of the plate

✓ Sample application: 5 μL of standards and samples were applied as 8-mm bands, by using the Camag® Automatic TLC Sampler 4, at laboratory temperature.

✓ Detection: the spots of interest were defined under UV light 254 nm and outlined with a graphite pencil; the plate was transferred to the TLC/MS surface to elute the spots to the mass spectrometer. Mass spectra were acquired in positive mode with full-scan mass spectral acquisition.

3.2.5   *In-silico* prediction evaluation of neurotoxicity and neuroprotection

Traditional toxicity tests based on animal models are expensive and low-throughput, in addition to; ethical considerations demand decreasing the numbers of animals used in science. A major challenge resides in the increasing number of chemicals to which humans, plants or the environment are exposed, with possible harmful effects, which underlines the importance to study their eventual toxicity. Therefore, original methods are being devised as *"in silico toxicology"*, applying statistics and computer science for toxicity assessment or prediction.

From the various methods generating models to predict toxicity endpoints, we could access e-MolTOx and pkCSM for the seven identified compounds and crossed the obtained results with PubChem information for the same molecule or a nearby molecule.

3.2.5.1   *In silico* prediction with eMolTox

e-MolTOx is a publicly accessible web system, based on machine learning, for the prediction of different types of toxic parameters associated with a given molecule. The construction of the model is based on collecting different types of *in vitro / in vivo* data, in addition to toxic substructure analysis; a total of 174 datasets collected and Mondrian conformal prediction were used to estimate the confidence of the resulting predictions [336].

The eMolTox results page consists of two main sections: *(i)* a table of all the potential active endpoints with the confidence that the query compound might have. In addition to the structure of the most similar active compounds in the database to justify predictions; and *(ii)* a table with all the matched toxic or reactive substructures highlighted on the molecule, with the corresponding potential toxicity.

The database was searched by *(i)* transforming the molecule to SMILE format by using an Optical Structure Recognition (OSRA) software https://cactus.nci.nih.gov/cgi-bin/osra/index.cgi; *(ii)* providing the SMILES format to eMolTox web server http://xundrug.cn/moltox; *(iii)* selecting the desired types of toxicity prediction.

3.2.5.2 *In silico* prediction of pharmacokinetic properties with pkCSM

The pharmacokinetic properties (ADMET, i.e. absorption, distribution, metabolism, excretion and toxicity) of the seven compounds were predicted *in silico*, using the pkCSM web server.

pkCSM is based on an algorithm that predicts pharmacokinetic and toxicity properties from distance-based graph signatures, a powerful way to represent geometric and physicochemical properties. pkCSM predictions are divided as estimates into five major classes: absorption (7 estimates), distribution (4), metabolism (7), excretion (2), and toxicity (10) [337].

The selected compounds were entered in the database using their SMILES structure formats (http://biosig.unimelb.edu.au/pkcsm).

3.2.5.3 *In silico* screening with PubChem

PubChem is the Molecular Libraries Roadmap (MLR) of the US National Institutes of Health (NIH); this public webserver provides information about chemical and physical properties, biological activities, safety and toxicity and literature citations for chemical substance. Chemical information and assay data are deposited by individual contributors, then filtered through a special standardization [338].

The data in PubChem organizes into: *(i)* substance SID includes chemical substance descriptions *(ii)* compound CID contains unique chemical structures extracted from the Substance database *(iii)* BioAssayAID stores the descriptions of biological assay experiments and bioactivity data for substances tested in the assays. The issue is 98% of PubChem compounds do not have archived BioAssay database, because scientific articles report data for active compounds.

The PubChem search (https://pubchem.ncbi.nlm.nih.gov/search/) allow the search for the selected molecules by simple entry of their SMILES formats, or keywords or text in the search box.

3.2.6 Evaluation of neurotoxic or neuroprotective effects *in vitro*

3.2.6.1 Development of a 3D cell culture model

For the *in vitro* toxicity tests, we proposed to apply a 3D model, based on spheroids auto-assembled in lab-molded agarose microwells, that might be more relevant than 2D models. Despite its considerable challenges, the micro-molded hydrogels are described as applicable with modest laboratory equipment, cost effective and reproducible [224] (section 1.6.2.2.1, p.42). The model of Dingle YT et al. (2015) [339] was applied with modification regarding the source of cells (postnatal rat for Dingle et al vs prenatal rat or mouse); cells were obtained according to a protocol of the Neuroscience department of UMONS.

3.2.6.1.1 Cell source and culture

Primary cultures of dissociated forebrain were isolated from BL6 mouse embryo at day 17 (E17) when neurogenesis and morphological differentiation into cells has taken place so they can develop morphologically and functionally in culture.

Set-up prior to harvest

1- 17 days prior to day of neuron isolation: breeding of BL6 mice was scheduled between adult mice for 24 h, to generate prenatal pups for neuron harvest.

2- The day prior to neurons isolation:

    a) Preparation of 3D micro petri dishes

    To obtain agarose hydrogels micro-wells with round-bottomed recesses, 330 µl of molten agarose 2 % in sterile saline (0.9 % w/v NaCl) were pipetted in 24-well plates 3D Petri Dish® (#24–35-large,#24–96-small MicroTissues®), each micro-mold forming 35 or 96 micro-wells. Upon solidification, the agarose was carefully removed, transferred to a standard 24-well plate (Figure 3.12) and equilibrated with complete cell culture medium (24 h, 37°C). Since the agarose hydrogel is transparent, the spheroids can be easily viewed using a standard inverted microscope.

    b) Sterilize the dissection instruments

    They were wrapped in aluminum foil and heated at 180°C for 2 h.
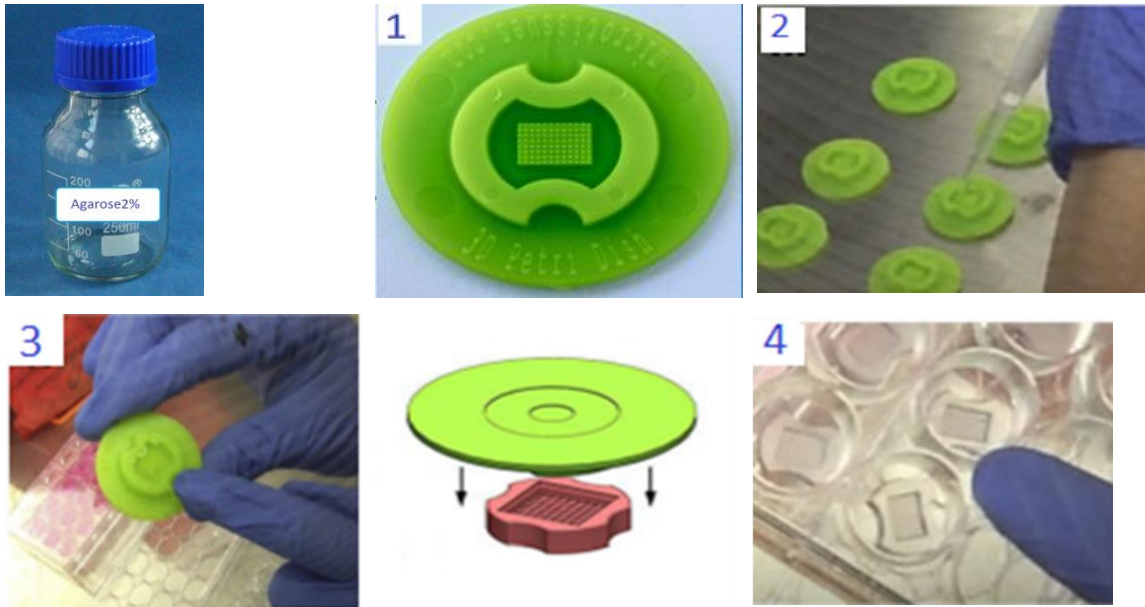
Figure 3.12 The successive steps for the preparation of the agarose hydrogels: add 330 µL of agarose 2 % in saline solution to micro-molds, wait for solidification then tranfer to 24-wells plate (adapted from [340]

Dissection of mouse forebrain Tissue

The initial dissection was completed outside laminar flow hood, but the subsequent steps of trituration and harvesting were done in maximum sterile conditions within a hood rated for cell culture that was sterilized by UV for 30 min before dissection.

The pregnant mouse at approximately 17 days post-fertilization was euthanized by decapitation. The embryos were recovered via cesarean section using fine scissors and forceps, placed in a 100×20 mm petri dish containing cold HBSS on ice; the amniotic sac was removed, and the embryos transferred to a new petri dish with cold HBSS on ice.

The head was cut from eyes to back of the neck with Vannas -Tübingen spring scissors and the cranium opened by peeling out the skin of skull from back to forward; the whole brain was removed from the head cavity using the #7 curved forceps and was placed in a 60×15 mm petri dish containing cold HBSS on ice; this work was repeated on all embryos.

Under a binocular magnifier, the brain was cut following the median longitudinal fissure, to separate the hemispheres, cutting off and discarding the brainstem and cerebellar tissues.

The meninges that cover each hemisphere were removed by grasping a small section with sterile forceps, pulling gently away, and transferred into a 60×15 mm petri dish containing cold HBSS on ice (Figure 3.13).

Tissue Dissociation

The collected brain tissues were transferred to a 15-ml conical tube containing 1mL of HBSS and gently triturated by pipetting with sterile rounded Pasteur pipette ~10 -15 times, avoiding bubbles; another 1 mL of HBSS was added, the suspension was triturated again until visual homogeneity.

The suspension was filtered with a cell strainer (40 µm pore size, BD Biosciences); another 1 mL of HBSS was added over the strainer, then 10 mL of Neurobasal® media with 10 % FBS were gently added, and the cell suspension was centrifuged (312 g, 10 min, 4°C).

The supernatant was discarded, and the cells resuspended in complete Neurobasal medium at room temperature (Neurobasal® Electro Medium supplemented with 2 % B-27® electrophysiology, 0.25 % Glutamax®, 1 % FBS, 0.5 % streptomycin-penicillin).

To determine the cells viability, 10 µL of the cell suspension were mixed with 10 µL of 0.4 % Trypan blue, and live cells were counted using a hemocytometer (Figure 3.13).

Day 1:
Prepare the cell culture plate by
preparing the agarose micro plates

Day 2:
Isolate the E17-18
embryos. Cut the skull.
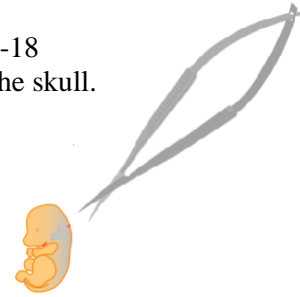
Remove the brains from the
heads and replace it in cold
HBSS (on ice)

Separate the
forebrain and discard
the brainstem and
cerebellum
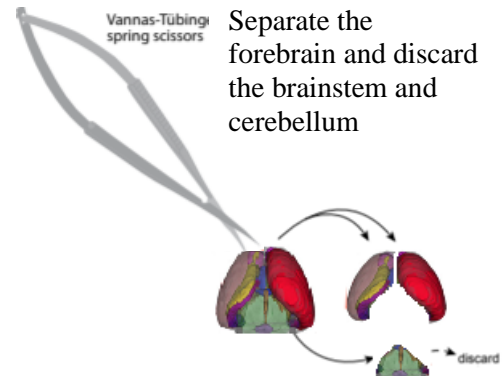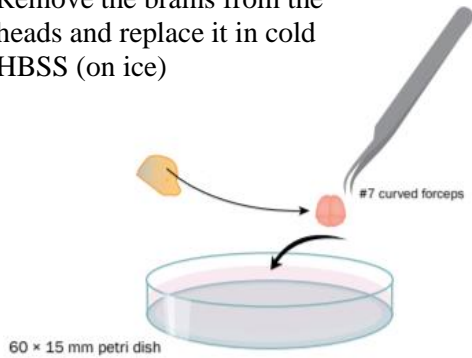
Peel off and discard
the meninges
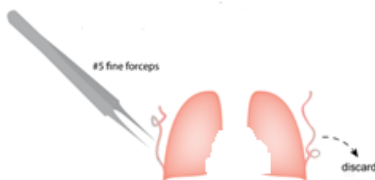
Transfer the hemispheres
(4 hemispheres per tube)

Gently triturate
Filtrate

Decant supernatant
Resuspend cells
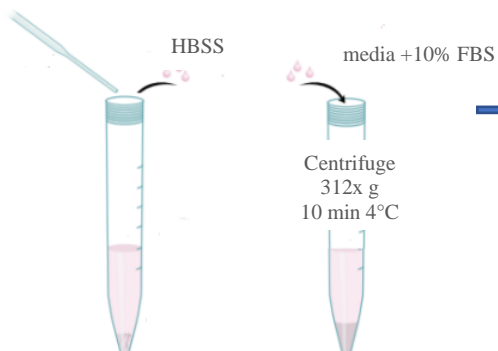
Count cells
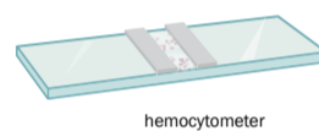
Figure 3.13: The protocol for obtaining the forebrain cells *(mainly cortical and hippocampal cells)* to be seeded
for neurosphere cultures (original).

Cell seeding

The cell suspension was diluted with warmed Complete Neurobasal Medium (at 37° C) to the desired seeding density, the major factor that conditions the future spheroid diameter.
To determine this factor, a series of seeding trials were performed. For large 3D micro-dishes, cells were seeded at densities based on Table 3.6 for spheres with estimated diameters of 200, 400, 500, 700 µm; for the small 3D micro-dishes, the densities of cells for 50, 100, 200, 300 µm were seeded as defined in Table 3.7.

For the continuation of the work, the diameter selection criteria depended on the reproducibility and handling easiness.

Table 3.6: The large 3D micro-dishes (24-35) with the cell seeding numbers for different spheroid diameters (based on Microtissues® protocol [340].

Estimatation of the cell seeding numbers for larger spheroids in 3D micro-dishes		#24–35	
		24 well plate Larger spheroids: 35	
Nominal spheroid diameter	Cells/spheroid	Total cells seeded (cells/75 µL)	
200	1000	35000/75µL	
400	8000	280000/75µL	**Large mold** (5 x 7) array 35 spheroids
500	15625	547000/75µL	
700	42875	1500000/75µL	

Table 3.7 : The small 3D micro-dishes (24-96) with the cell seeding numbers for different spheroid diameters (based on Microtissues® protocol [340].

Estimation of the cell seeding numbers for smaller spheroids in the 3D Petri Dish		#24–96	
		24 well plate Smaller spheroids: 96	
Nominal spheroid diameter	Cells/spheroid	Total cells seeded (cells/75 µL)	
50	15	35000/75µL	
100	125	12000/75µL	**Small mold** (8 x 12) array 96 spheroids
200	1000	96000/75µL	
300	3.375	324000/75µL	

3D neural spheroid culture

The medium equilibrating the agarose microwells was removed, 75 µl of the cells suspension were seeded into the agarose micro-dishes[13], the cells density depending on the chosen spheroid diameter (Table 3.6, Table 3.7); the cultures were then incubated in a 37°C, 5 % CO_2 humidified incubator (Figure 3.14).

After 30 min, 1 ml of warmed complete cell medium was added slowly (on the board of well-plate) and the plate was returned to incubator. Next day, the media was removed totally and replaced with fresh complete Neurobasal, then cells/spheroids were fed every 3- 4 days by removing half of the old media and replacing it with the same volume of fresh complete Neurobasal media

seeding chamber → Cells suspension seeded → Cells settled for 30 mins → Cells aggregated And assembled
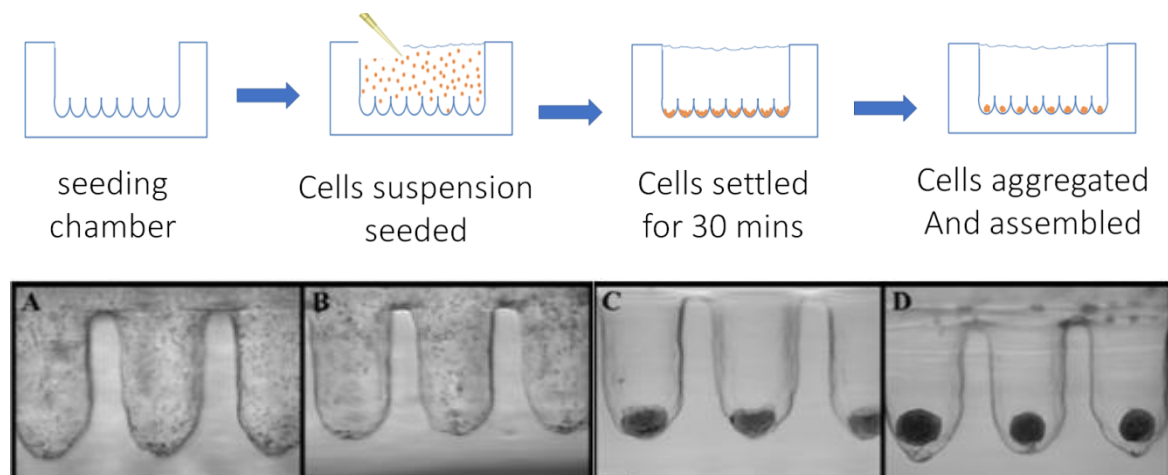
Figure 3.14: Cross-section of agarose hydrogels showing the steps of seeding the hydrogel chamber with cell suspension, followed by cells settling and aggregating to produce a neural spheroid (source [228])

3.2.6.1.2 Immunocytochemistry

The protocols of immunostaining and Clear[T2] clearing protocols were inspired from Dingle YT et al. (2015) [339] and from protocols of the UMONS Neuroscience department. After 2 weeks of neurons culturing, spheroids were washed 3 times with warmed (37°C) phosphate-buffered saline (PBS) pH 7.4, then were fixed overnight at room temperature with 4 % paraformaldehyde (PAF) in PBS pH 7.4, washed with PBS and stored in 0.07 % sodium azide PBS.

---

[13] 35 microwells/gel for the larger mold and 96 microwells/gel for the smaller mold

To permeabilize the spheroid and improve the penetration of antibodies, the spheroids were incubated in a solution of PBS containing 0.2 % Triton X-100 (1 h, 2 times), then in a blocking solution of casein 0.5 % and NH_4Cl 5% in PBS (2 h, room temperature). The spheroids were transferred to glass-bottom confocal slides or 12-well removable chambers slides by using a P-1000 pipette with end-cut tips (to minimize the damage to spheroids), incubated (48 h, RT) in primary antibodies diluted with the blocking solution (Table 3.7), washed with PBS/Triton X-100 0.2 % (1 h, 2 times) and incubated (48 h, RT) in secondary antibodies diluted with the blocking solution (Table 3.8).

To stain the DNA, the spheroids were then washed with PBS/Triton X-100 0.2 % (1 h, RT, 2 times), counterstained with 4′,6-diamidino-2-phenylindole (DAPI) 0.5 μg/mL in PBS/Triton X-100 0.2 % (1 h, RT), then rinsed with PBS.

For Clear[T2] clearing, the 3D spheroids were incubated with 25 % formamide/10 % PEG in PBS for 10 min, then 50 % formamide/20 % PEG in PBS for 5 min, followed by 50 % formamide/20% PEG in PBS for 60 min as the final mounting solution.

Table 3.8: Primary and secondary antibodies for immunohistochemistry

Antibodies	Host	Reactivity	Class	Dilution
Primary				
MAP2[14]	Rabbit	Human, Mouse, Rat	Polyclonal	1:200
Anti-Tau[15]	Mouse	Human, Mouse, Rat	Monoclonal	1:100
GFAP[16]	Mouse	Human, Mouse	Monoclonal	1:200
GFAP	Rabbit	Human, Mouse, Rat	Polyclonal	1:250
Iba-1[17]	Rabbit	Human, Mouse, Rat	Polyclonal	1:200
Anti-β-Tubulin[18]	Mouse	Human, bovine, Rat	Monoclonal	1:100
Secondary				
Alexa fluor 594	Goat	Mouse	Polyclonal	1:200
Alexa fluor 488	Goat	Rabbit	Polyclonal	1:200
Alexa fluor 594	Goat	Mouse	Polyclonal	1:200
Alexa fluor 488	Goat	Rabbit	Polyclonal	1:200

---

[14] Microtubule-associated protein 2 (MAP2) is a neuronal protein, interacts with microtubules to maintain the structure of dendrites.

[15] Tau is a family of microtubule-associated proteins thought to regulate the stability and organization of microtubules in neuronal cells.

[16] Glial fibrillary acidic protein (GFAP) is a type III intermediate filament protein that is expressed by numerous cell types of the central nervous system, including astrocytes.

[17] Ionized calcium binding adaptor molecule 1 (Iba-1) is a microglia/macrophage-specific calcium-binding protein

[18] β-Tubulin III, is protein expression that is restricted to neuron

3.2.6.2 Characterization of the spheroids

3.2.6.2.1 Spheroids diameter

Diameter measurements allowed following the culture development; spheroid bottom-view phase contrast images were taken by a DP 200 camera connected to a Zeiss axiovert 25 inverted microscope with 2x, 5x, and 10x objectives.
Spheroid diameters were measured using the Fiji software [341] after calibration with a reference scale bar; 3 independent measures were performed, and 18 spheroids were measured for each experiment.

3.2.6.2.2 Scanning electron microscopy of spheroids

To study cell morphology, and visualize 3D cell-to-cell relationships, scanning electron microscopy (SEM) was previously proposed, 3D SEM images being described as a reliable method to visualize and analyze 3D cell parameters, such as spreading and cell volume [342]. This technique applies a focused beam of high-energy electrons to generate a variety of signals at the surface of a solid, providing high-resolution, three-dimensional imaging for microstructure morphology, useful for evaluating the surface topography and composition of a sample.

The spheroids were fixed in 4 % PAF in PBS (24 h, 6°C), rinsed (3 X 1 h, RT) with PBS in an orbital shaker at 30 rpm to remove the fixing solution and dehydrated at room temperature in an ascending series of ethanol (EtOH) in PBS (50 %, 70 %, 90 %, 95 %, and 99.9 %)[19].

This process was repeated with a chemical drying agent in ethanol until the sample is washed with pure drying agent. For that, spheroids were rinsed in a series of wash solution (EtOH - hexamethyldisilazane, 2 : 1, 1 : 1 and 1 : 2, v/v, 15 min each), then 3 times with 100 % hexamethyldisilazane (15 min each) and allowed to dry in a fume hood.

The dried samples were carefully mounted on an aluminum stub, using a double-sided tape, and coated with a very thin film of gold, using a sputter coater (JFC 1100E ion sputtering

---

[19] The sample was serially immersed into each EtOH solution (2 X 10 min, except for the final solution, that was incubated 15 min).

device) under vacuum and high voltage (10 mA) for 3 min, before SEM examination (Fig. 3.20).
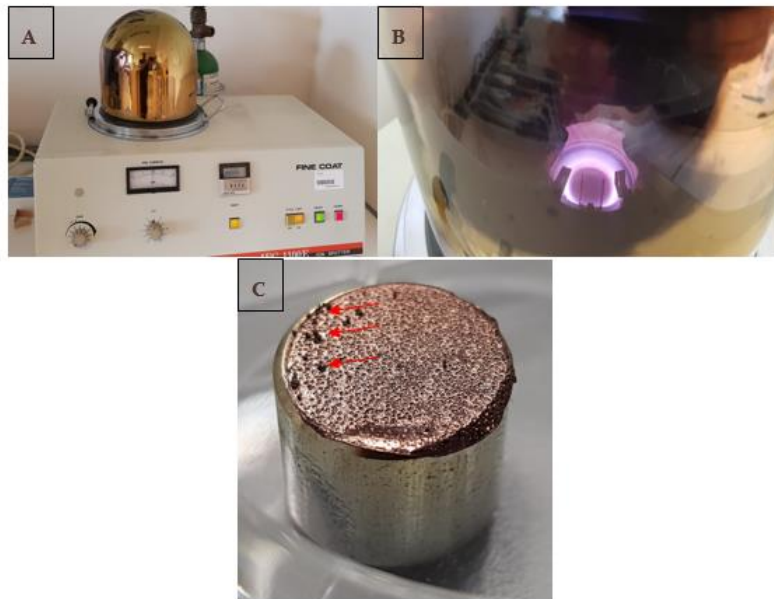
Figure 3.15: Mounting and preparing the spheroids for SEM observation (A) sputter coating device (B) The vacuum chamber of sputter device while coating the sample (C) the gold coated spheroids (marked by red arrows) (original images)

3.2.6.2.3 Identification of cell types present in spheroids

Imaging in epifluorescence microscopy

Using immunocytochemistry and fluorescence microscopy, the staining of neurospheres with DAPI, GFAP (mouse) and MAP2 (rabbit) antibodies (Table 3.8) yields two types of information that allow to (*i*) define the presence and position of cells (nuclei) including specific cells (neurons, glial cells) in spheroids; and (*ii*) quantify their presence, by determining the local concentration of fluorophores.

Fluorescence imaging of whole spheroids was performed on the Olympus IX 70 fluorescence microscope (Section 3.1.7, p.70); the 2x, 10x objectives were used.

For image processing and intensity measurements, the Fiji tool "Mean grey area" was applied to the different "colors" of each image (i.e. the different fluorescence acquired), after manually defining the spheres outline with the oval or polygone tool.

Data were acquired in 3 biologically independent experiments, with 3 technical replicates, for each of which 9 spheroids were measured (N=9); this allowed to quantify each type of cells in the spheroid and the reproducibility of cells ratios among the different cultures. The data were analyzed by one-way ANOVA with SigmaPlot 14a, considering the level of significance for $p < 0.05$.

Imaging in confocal microscopy

For high resolution imaging, confocal microscopy presents many advantages over epifluorescence microscopy by its ability to control the depth of field and collect sharp images of serial optical sections with the possibility to create 3D images.
This set-up was also used to identify the types of cells in our spheres.
The images were acquired using the Zeiss Laser Scanning confocal Microscope LSM 710 (Section 3.1.7).

Imaging the center of spheroids

To image the center of spheroid, the DIAPath (Digital Image Analysis in Pathology) unit at the Center for Microscopy and Molecular Imaging (CMMI, Gosselies; https://www.cmmi.be) allowed us access to their automated slicing, staining with hematoxylin/eosin and image acquiring. The fixed spheroids (Section 3.2.6.1.2, p.100) were transferred to a tube and centrifuged (5 min, 300g); the supernatants were discarded then 0.1 mL of a 1.5 % low melting point agarose gel solution was added; the suspension was gently mixed by pipetting up and down and refrigerated until gel solidification. The agarose pellet was carefully placed into a pre-labeled cassette that was transferred into the automated system.

3.2.6.2.4 Study of cytotoxicity on spheroids

Given the difficulty to apply a microscopic measurement to the spheroids, the method proposed by Pamies et *al*. 2018 [343] based on measuring a fluorescence in the culture media, was selected.
The evaluation of a compound effect was applied on day14 of culture; the medium was fully exchanged with a fresh medium containing the test compounds at concentrations of 50, 100

and 250 µM (prepared from a stock solution of 100 mM in DMSO; maximal DMSO concentration in contact with the spheroids, 0.25 %).

3.2.6.2.5 Evaluation of cell viability

To measure the cell viability, a resazurin assay was performed. Resazurin (7-hydroxy-3H-phenoxazin-3 one 10-oxide) is a blue dye used as a redox indicator for aerobic and anaerobic respiration. It is irreversibly reduced to fluorescent resorufin [344].
After 21 h exposure to the different concentrations of test compound, resazurin (50 µl of a 2 mg/ml stock solution in PBS) was directly added to the medium of 24-well plates (1 ml/well). After incubation for 3 h at 37°C, 5 % CO_2, 50 µl of the medium of each well were transferred to a 96-well plate and the fluorescence intensities were measured at 525 nm/580-640 nm (excitation/emission) with a multi-well fluorometric reader GloMax®-Multi+ Microplate Multimode reader (Promega, Inc).
The viability was calculated as below:

$$\text{Viability percentage} = \frac{\text{fluorescence x 100}}{\text{average fluorescence of negative control}}$$

These viability results were compared with the intensity of fluorescence corresponding to cells (DAPI), neurons (MAP2) and glial cells (GFAP) staining of spheroids after 24 h of exposure to the different concentration of test compounds (section 3.2.6.2.3, p.103).

All data are the means ± SD of 3 to 6 independent experiments performed with 3 technical replicates. The data were analyzed by one-way ANOVA with post-hoc Bonferroni test, using SigmaPlot 14a, considering the level of significance for $p < 0.05$.

3.2.6.2.6 Reactive oxygen species (ROS) measurement

The brain is vulnerable to oxidative stress that is incriminated in a pathophysiology, common to several diseases, that underpins neuronal cell death. Oxidative stress can be induced by an excessive generation of reactive oxygen species (ROS) or by dysfunction of the antioxidant systems.

To measure the reactive oxygen species (ROS), a highly sensitive fluorometric method described by Silveira et *al*. 2002 [345] was applied on the cultures at day 14, after the addition of tested compounds.

Measurement in culture medium

This method is based on the oxidation of 2′,7′- dichlorodihydrofluorescein (DCFH) to the fluorescent 2′,7′-dichlorofluorescein (DCF) by the free radicals generated in the medium. The DCFH was prepared in-house by hydrolysis of 2′,7′- dichlorodihydrofluorescein diacetate (DCFH-DA) as described by Cathcart and coworkers [346].

After 3, 5, 9, 24 h of exposure to test compounds, 50 µl of the medium were collected, transferred to a 96-wells plate and incubated with 50 µl of DCFH 10 µM (45 min, 37°C, 5 % CO_2). The fluorescence intensity was measured at 490 nm/510-570 nm (excitation/emission) in a multi-well fluorometric reader GloMax®-Multi+ Microplate Multimode reader (Promega, Inc).

Measurement in-cellulo

The ROS measurement was compared in the presence of DCFH and of DCFH-DA. DCFH-DA is widely used to detect intracellular oxidative stress; cell-permeable, it is hydrolyzed intracellularly to the DCFH carboxylate anion, locally oxidized into DCF by ROS. For this experiment, 5 µL of a 2 mM solution of DCFH-DA in DMSO were added to the culture media, immediately after exchanging the medium with a fresh medium containing the tested compound, to yield a DCFH-DA concentration of 10 µM. After 3, 5, 9, 24 hours, 50 µl of the medium were collected, transferred to a 96-well-plate. Then, the fluorescence intensity was measured at described in the previous section.

The two methods were compared, based on fluorescence intensities. All data come from 3 to 5 independent experiments performed with 3 technical replicates. To determine statistical significance, two and one-way ANOVA tests were performed with post-hoc Bonferroni test.

3.2.6.2.7 Study of apoptotic and necrotic effects

Apoptosis is the process of programmed cell death; it is a normal part of an organism's cellular balance, and it occurs normally during development and aging and as a homeostatic

mechanism to maintain cell populations in tissues. Necrosis is a highly pro-inflammatory form of cell death or premature death caused by several external sources, including injury, infection, cancer, infarction, poisons, and inflammation; it is an uncontrolled change in an organism's cell balance, so it, resulting in noticeable, negative symptoms. From this prospective studying the apoptosis and necrosis effect of our molecules was important.

- ✓ For the evaluation of apoptosis, different techniques have been proposed; the terminal deoxynucleotidyl transferase-mediated dUTP nick-end labeling (TUNEL) assay is applied to detect DNA degradation at the late stage of apoptosis [347], while the detection of caspases activation permits an earlier detection [348]. The activation of the caspase cascade was measured using the CellEvent Caspase 3/7 Assay Green Detection Reagent Kit (Invitrogen ™). The detection reagent is intrinsically non-fluorescent as a DEVD (Asp-Glu-Val-Asp) peptide inhibits the ability of the dye to bind to DNA. Upon activation of caspases 3/7 in apoptotic cells, the DEVD peptide is cleaved, allowing the dye to bind to DNA and produce fluorescent emission ~530 nm, measured using a standard FITC filter set.

- ✓ In parallel necrotic effects were evaluated by a propidium iodide test. When necrosis occurs, the cell membrane becomes porous and exposes DNA molecules to propidium iodide, a red-fluorescent intercalating agent that stains nucleic acids (DNA or RNA). Since the propidium is not permeant to live cells, it is commonly used to detect dead (necrotic) cells in a population.

On the 14th day of culture, we collected the neurospheres using a pipette and transferred them to slides with a removable 12-wells silicone chamber (Ibidi®). We replaced the entire medium with fresh medium with different concentrations of the studied molecule, staurosporine[20] at a concentration of 200 nM or hydrogen peroxide[21] at a concentration of 50 µM.

---

[20] Staurosporine is a potent inducer of apoptosis, activator of caspases 3/7, used as a positive control for apoptosis
[21] Hydrogen peroxide induces oxidative stress which mainly results in necrosis. The concentration of the H_2O_2 stock solution was verified by $KMnO_4$ redox titration; H_2O_2 dilute solutions were prepared extemporaneously

After 24 h, we acquired images with the Olympus IX70 microscope (3.1.7, p.70), in white light and with the filters FITC (λ absorption, 488 nm; λ emission, 530 nm) and rhodamine (λ absorption, 538 nm; λ emission, 617 nm).

The images were analysis by Fiji imageJ as described in 3.2.6.2.1 and 3.2.6.2.3 with background signal subtraction. The spheroids with diameters less than 340 µm or greater than 460 µm were excluded from the study (i.e. a tolerance of 15 % compared to the size expected from the inoculation density; exclusion percentages are stated along measurement results). Also, the overlapping and damaged spheroids were excluded.

3.2.6.3 Statistical procedures

To determine the statistical significance of our studies, the SigmaPlot 14 software (Systat Software Inc., San Jose, USA) was used. Both one-way and two-way ANOVA tests were performed, with a Shapiro-Wilk test for normality, a Brown-Forsythe test for equal variances and a post-hoc Bonferroni-test for post-hoc pairwise multiple comparisons. All data are given as means $\pm$ SD of at least 3 biologically independent experiments performed with 3 technical replicates. Statistical significance was classically set at $p < 0.05$.

3.2.7 Evaluation of neurotoxic or neuroprotective effects *in vivo*

To evaluate the effect of one of our compounds, a collaboration was developed with the laboratory of Richard Apps, School of Physiology, Pharmacology and Neuroscience, University of Bristol, Bristol, United Kingdom. Their research focuses on understanding the contributions of the mammalian cerebellum to the control of goal-directed movements and defense behaviors [349]. The research team uses a combination of anatomical, physiological and behavioral techniques to examine cerebellar structure-function relationships, with a focus on the climbing fiber system that plays a vital but enigmatic role in cerebellar function. They have developed a rat model with bilateral cannula chronic implantation for direct administration of neuroactive agents, which permits the substances to bypass the blood-brain barrier.

Miniature microdrives (weight, approximately 2.5 g) were built in house, each incorporating up to four independently movable electrodes (two to four bundles of 12.5 µm tungsten wires multitrodes) [350] (Figure 3.16).
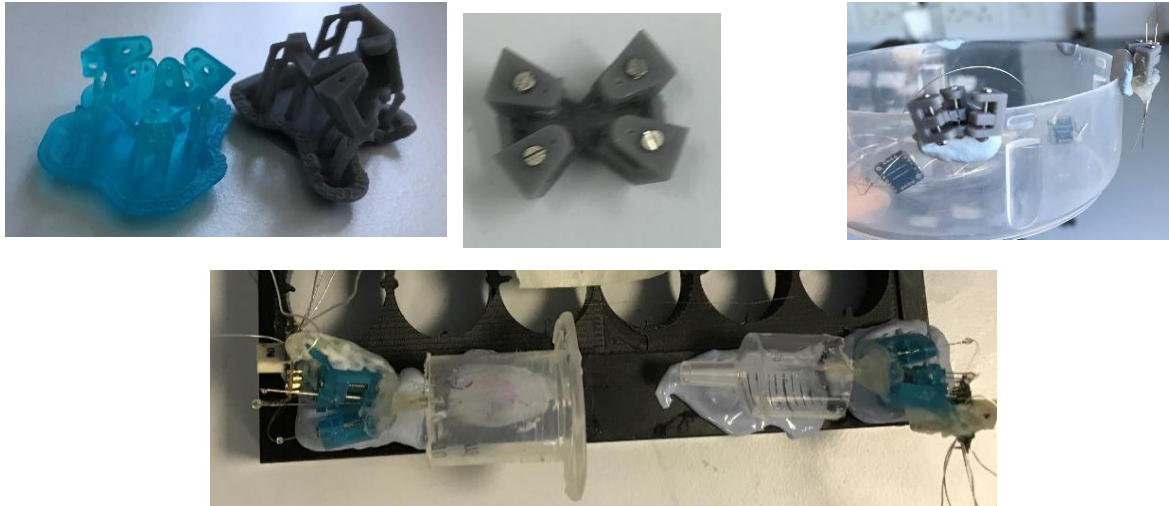
Figure 3.16: Steps of microdrive preparation, starting by 3D printing for the microdrive (tetrode supporter) followed by adding the contactor pins then the tetrodes (original images).

This method applies in vivo electrophysiological techniques to simultaneously record data from chronically implanted adult male Hood Lister rats (300 - 400g) (Figure 3.17) with:

1. Independently movable tetrodes[22] in the vermis of the cerebellar cortex, the medial cerebellar nuclei (CB), and in the ventral anterior nucleus/ventral lateral nucleus VL/VA complex of the thalamus (VM).
2. Bilateral surface electroencephalography (EEG) screws over the primary sensory (S1) and primary motor (M1) cortex.
3. Electromyography (EMG) wire implants in the triceps brachii and clavotrapezius (muscles known to be very well innervated by motor neurons)

Chronically implanted electrodes are connected to a Blackrock head stage with a built-in triaxial accelerometer.

---

[22]Tetrode is a quadruplet of electrodes that identifies the individual involvement of several neurons simultaneously
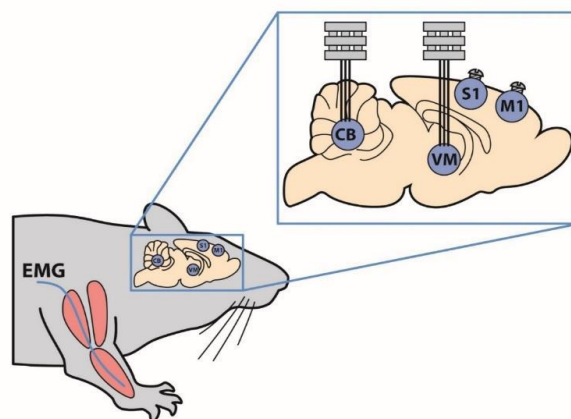
Figure 3.17: Schema representing the implantation of electrodes in a rat (source[351]).

Our compound was delivered to cerebellar nuclei with the bilateral and unilateral cannula. The unilateral cannula was implanted into the medial cerebellar nuclei, while the bilateral cannula was inserted into the cerebellum (two sides). The cannulas were already implanted, and a solution of 1μL of the molecule dissolved in saline at a concentration of 1mM was pumped into the cannula whilst the rat was awake and sat quietly on the experimenters' lap. The startup dose of our molecule was selected based on the harmaline dose known to produce a tremor (bolus administration).

Electrophysiological and acceleration recordings were acquired during waking behavior, to quantify the amplitude and frequency of tremor, using a tethered Blackrock recording system, which allows the rat to move freely around the cage during recording. Recordings were collected before and after administration of 1-benz -THIQ- 6,7-diol. The data was bandpass-filtered between 1 and 49 Hz and divided into resting, moving epochs.

4. Results

4.1 Preparation of overcooked meat samples

The choice of meat and the cooking methods were selected for a maximal generation of b-carbolines; a review by Pfau. et al. 2004 indicates that the contents of norharmane and harmane were the highest in broiled chicken (622 and 133 ng/g, respectively) and in flame broiled meat (795 and 169 ng/g) [97].

The beef meat was first broiled in lab oven at 270°C for 24 min, we notice the need to turn the slice to have homogenous cooking on both sides, and the meat was inedible (burned). Therefore, for chicken meat, we opted to broil it in lower temperature and longer time (200°C, 40 min) and turned it to obtain an homogenous brown color on both sides (Figure 4.1).

The meat was grinded in powerful ball mills (Figure 4.2) and the meat fond was collected with distilled water (250 mL H_2O_d for 1000 g of raw meat) and filtered on filter paper.

Figure 4.1: At left, the chicken broiled in domestic oven; at right, the beef broiled in laboratory oven.

Figure 4.2: Mixer mill MM400 by Retsch that offers efficient grinding for small samples by impact and friction. 10 g of sample were put in each grinding jar with metallic balls. Rapid radial oscillations in a horizontal position of the grinding jars, combined with the movement of the balls, resulted in a thorough milling of samples.

4.2 Extraction of overcooked meat and poultry

4.2.1 Extraction of β-carbolines by an alkaline detergent solution

The extraction was applied on different types of meat, the yield of raw extract, expressed on dry weight basis, was calculated from the following equation

$$\text{Yield (\%)} = (W1*100)/W2$$

Where, W1= weight of the extract residue obtained after solvent removal, W2= weight of the cooked meat.

The average yields of cooked beef and chicken meat were 1.34 % (Table 4.1) and 1.20 % (Table 4.2). For evaluating the recovery of alkaloids (Section 4.3.1, p.116), 10.0 g of cooked chicken where mixed with 1.2 mg each of the 4 standards, the weight of extract was 0.146 g and the Yield % was 1.46%.

The yield of extraction was low, but with a reasonable coefficient of variation (≤ 10 %).

Table 4.1: The yield of cooked beef meat extracted by an alkaline detergent solution.

	Weight of cooked beef meat	Weight of raw extract	Yield (%)
1	12.1 g	0.171 g	1.41 %
2	20.0 g	0.247 g	1.24 %
3	19.0 g	0.270 g	1.37 %
Mean			1.34 %
SD			0.09 %
CV (SD/Mean * 100)			7

Table 4.2: The yield of cooked chicken meat extracted by an alkaline detergent solution.

	Weight of cooked Chicken meat	Weight of extract	Yield (%)
1	10.0 g	0.136 g	1.36 %
2	13.0 g	0.148 g	1.14 %
3	13.6 g	0.153 g	1.13 %
Average			1.20 %
SD			0.13 %
CV			10

4.2.2 Extraction of β-carbolines by a general alkaloid method

The extraction was applied only on cooked chicken meat, based on the work of Louis ED et al. 2007 that indicates higher harmane levels in chicken compared to beef. The use of Soxhlet for the extraction permitted the use of a higher quantity of meat to increase the amount of extract. The yield of extract was calculated as above; the average yield was 0.05 %. For this method, the repetition was made by different experimenters Table 4.3.

Table 4.3: The yield of cooked chicken meet extract by a general alkaloid's method.

	Weight of cooked chicken meat	*Weight of alkaloid extract*	*Yield (%)*
1	150 g	0.076 g	0.051 %
2	150 g	0.081 g	0.049 %
3	150 g	0.073 g	0.049 %
Average			0.050 %
SD			0.001 %
CV			2

4.2.3 Extraction of volatile carbonyl compounds by Solvent Assisted Flavor Evaporation (SAFE)

This extraction was aimed at volatile carbonyl compounds; the choice of the SAFE method was based on its reputation to produce clean aroma extracts from complex matrixes at low temperatures. This method can be used on solid or liquid samples, but a high vacuum pump is needed (10^{-3} Pa); as our pump capacity was only 0.4 Pa, we decided to work with liquid samples, i.e. aqueous extracts of poultry meat and browned meat juices; the liquid extract was immediately treated without evaporating the solvent. The data are expressed in volumes of SAFE distillates (Table 4.4).

Table 4.4: The volume of extract by solvent assisted flavor evaporation (SAFE)

	Volume of samples	*Volume of SAFE distillate*
Aqueous sample[a]	22 mL	20.5 mL
Meat fond[b]	22 mL	20.3 mL
Deionized water[c]	22 mL	21.9 mL
Aldehydes standard solution[d]	22 mL	21.9 mL

[a] Overcooked poultry meat extracted with deionized water in a 1: 5 ratios (w/v)

[b] Browned meat juices from 1 kg chicken, collected with 250 mL distilled water

[c] Deionized water (procedural blank).

[d] "Aldehydes mixtures-556", containing 15 components, diluted at 40 ng/mL each

4.2.4 Extraction and isolation of volatile carbonyl compounds by headspace single-drop microextraction (HS-SDME) with droplet derivatization

Although the SAFE method is one of the best methods for volatile compounds, it requires continuous supervision, to ensure that liquid nitrogen is not totally evaporated. For this reason, we decided to compare the results with those of another method, headspace single-drop microextraction (HS-SDME), that allows a fast detection of volatile carbonyles in small quantities. The original method suggests the use of decane as solvent, but this was not adequate with our samples, as the decane peak overlapped many aldehyde peaks in the GC chromatogram. For this reason, we selected heptane as solvent. As the 2 µL microdroplet of heptane was evaporating during the in-vial equilibration phase, that was resolved by increasing the volume of droplet to 3 µL, without affecting its stability on the syringe tip; and so, we were able to collect ~ 1.5 µL for GC-MS injection[23].

4.2.5 Extraction and isolation of carbonyl compounds by condensation with a silica-gel supported reagent

This method was applied for the extraction of non-volatile carbonyles. The use of Soxhlet allowed the extraction of large amounts of meat and is followed by a condensation with a silica-supported reagent that is selective for carbonyl compounds. The extraction was applied on chicken and the yield of extract calculated as above; the average yield was 0.18 % (Table 4.5). The repetition was made by different experimenters.

Table 4.5: The yield of cooked chicken meet extracted by condensation with a silica-gel supported reagent

	Weight of cooked chicken meat	Weight of extract	Yield (%)
1	165 g	0.42 g	0.25 %
2	165 g	0.18 g	0.11 %
3	165 g	0.28 g	0.17 %
Average			0.18 %
SD			0.07%
CV			39

---

[23] Internal standard, methyl ethyl ketone

4.3 Characterization of extracts

4.3.1 Identification of β-carbolines

4.3.1.1 Thin-layer Chromatography analysis (TLC)

Extract of β-carbolines by an alkaline detergent solution

TLC was applied for the samples of overcooked beef and chicken meats to detect the presence of β-carbolines, by comparing the chromatograms of our samples and 4 standards (harmane, harmaline, harmine, harmalol). A molecule is considered tentatively identified by the presence of a spot in extract matching a reference spot by Rf value, similarity in fluorescence and coloration after pulverization with a chromogenic reagent.

The TLC was visualized under UV light at 254 nm (Figure 4.3-A); two dark grey quenching spots were detected on the sample's chromatograms, while the β-carboline alkaloid standards presented blue fluorescence at the same excitation wavelength.

After preliminary inspection, the chromatogram was analyzed by spraying with Dragendorff reagent (Figure 4.3-B). Spots of the meat samples turned orange-brown, showing almost similar color as the standards (harmane and harmine). However, the Rf values (Tab.4.6) differing from those of standards and the lack of fluorescence suggest that the spots detected in the samples are not our β-carboline alkaloids; HPLC was applied for confirmation of this suggestion (Section 4.3.1.2 p.120). Although considered quite indicative for alkaloids presence, the Dragendorff reagent is not entirely specific and many non-alkaloid compounds give a positive reaction, e.g. *(i)* amides [352]; *(ii)* non-nitrogenous compounds, notably aldehydes, ketones, lactones, ethers, esters, epoxides, and peroxides with an ethylene bond or free alkyl groups at the *β*-carbon [353]; and *(iii)* artifacts coming from reactions with nitrogenous compounds during an alkaline extraction [353].
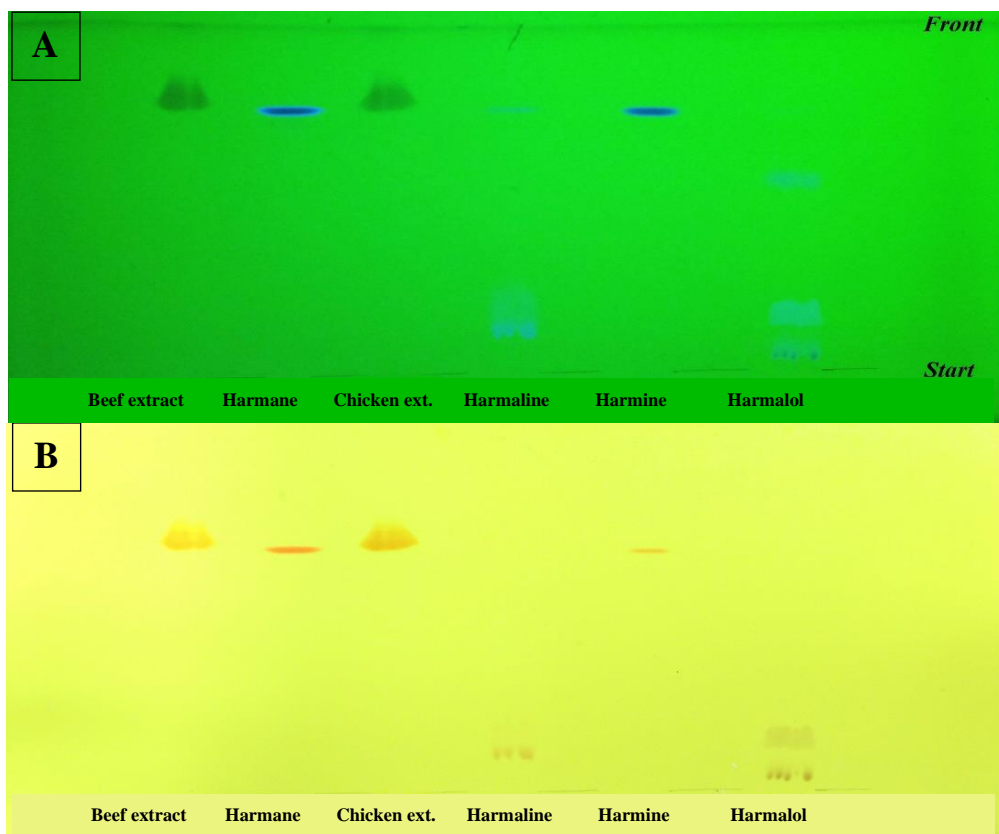
Figure 4.3: TLC plate (20cm×10cm), silica gel 60 F$_{254}$ of overcooked beef and chicken extracted by an alkaline detergent solution compared with β-carboline standards (1mM). (A) under UV light (254 nm) (B) under white light, after derivatization with Dragendorff reagent. Mobile phase, dichloromethane - methanol - 10% ammonia, 80 : 20 : 1.5 (v/v/v). (Note: the purity of the harmalol reference compound is only 80 %, explaining the multi-spots detection)

Table 4.6: Rf values of overcooked meat and chicken extracted by an alkaline detergent solution compared with reference standards. Data from (Figure 4.3).

Meat Samples	Migration distance (cm)	Rf	Attenuation or fluorescence (λ_{exc} 254nm)	Dragendorff reagent
Beef	6.2	0.81	dark grey	orange - brown
Chicken	6.2	0.81	dark grey	orange - brown
Harmane standard	5.9	0.77	blue fluorescence	orange
Harmaline standard	1.2	0.15	blue fluorescence	orange
Harmine standard	5.8	0.76	blue fluorescence	orange
Harmalol standard	1.6	0.21	blue fluorescence	orange

Based on the obtained result, a verification of the extraction efficiency was evaluated on:

1- A solution of 100 ng harmane extracted by the same alkaline detergent method, The TLC analysis shows the presence of harmane (at the same Rf and with the same fluorescence as a diluted reference (Figure 4.4, Table 4.7) which confirms the

efficiency of the method and the stability of this analyte during sample treatment. The spots corresponding to a1 (also present in the meat extract) appear to be artifacts coming from the extraction reagents.
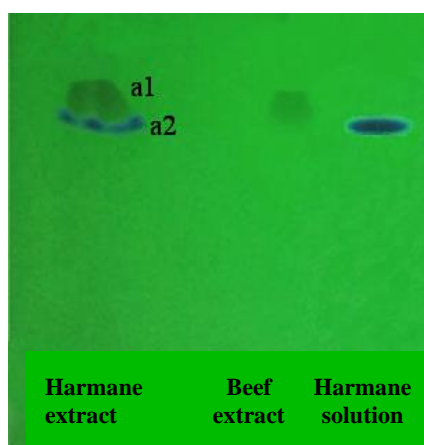
Figure 4.4: TLC plate (10cm×10cm), silica gel 60 F_{254} for the alkaline detergent extract of a 100 ng harmane standard solution, meat extract and harmane solution (100 ng/mL) under UV 254 nm light. Mobile phase, dichloromethane - methanol - 10 % ammonia, 80 : 20 : 1.5 (v/v/v)

Table 4.7: Rf values measured after extracting chicken meat spiked with harmane (data from Figure 4.4).

Samples		Migration distance (cm)	Rf
Harmane standard	a2	6.0	0.77
	a1	6.7	0.85
Sample meat extract		6.7	0.85
Harmane standard diluted		6.0	0.77

2- Extraction of reference standards (1.2 mg each of harmane, harmine, harmalol and harmaline) that were added to 10 g of chicken meat. The TLC analysis under UV 366 nm indicates the presence of the 4 standards in the sample spiked with standard references but at a very low concentration; a faint fluorescence is observed for the unspiked meat sample that could correspond to harmaline (Figure 4.5-A); while under UV 254 nm the spots were difficult to observe (Figure 4.5-B) for both samples, which was expected, given the low amounts spiked. On the TLC plate sprayed with Dragendorff's reagent (Figure 4.5-C), there was not a 100 % match between the samples and standards Rf, which could be due to an interference of meat extract components in chromatography.
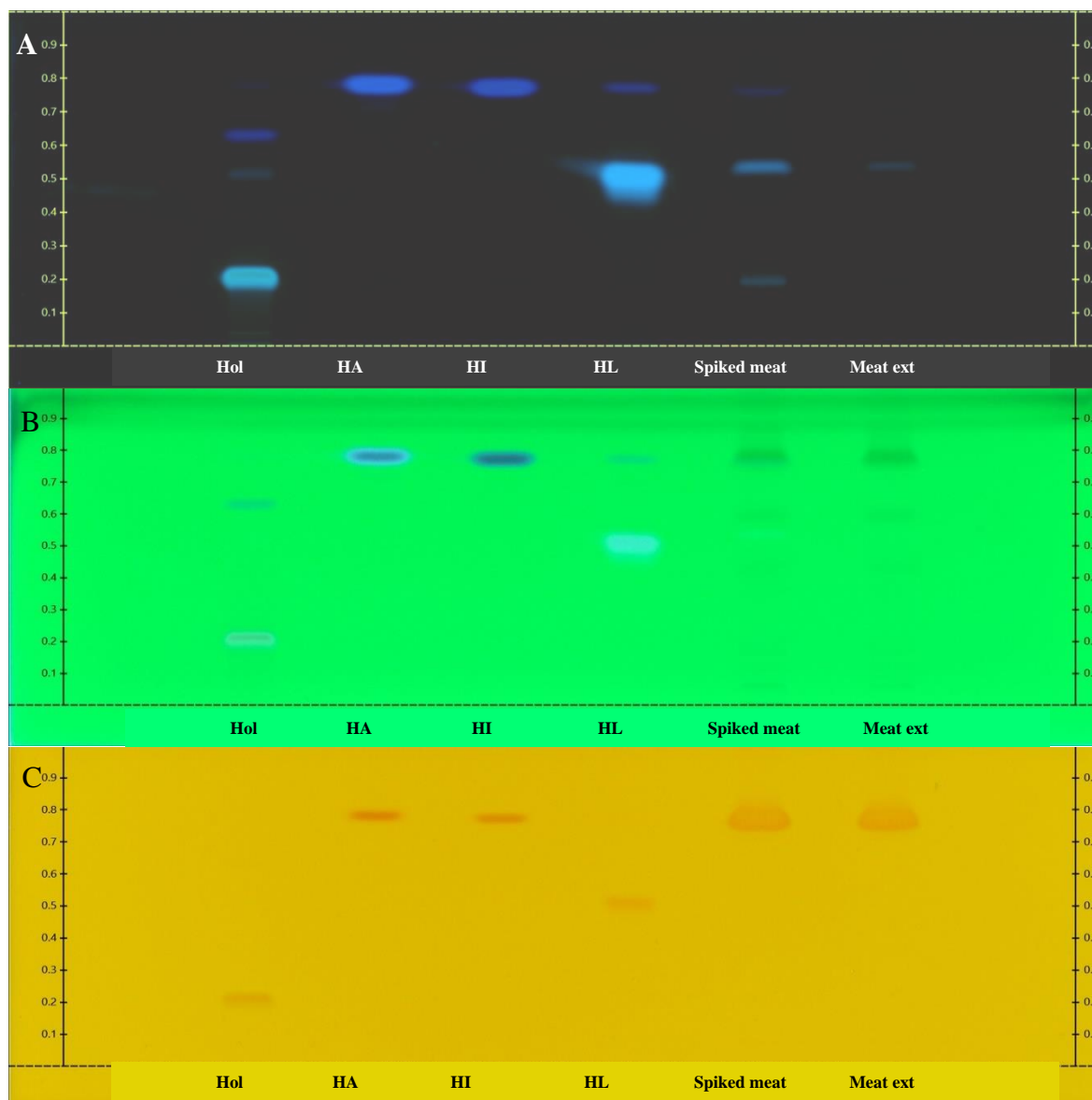
Figure 4.5: TLC plate (20cm×10cm), silica gel 60 F_{254} for the recovery of alkaloids spiked in overcooked chicken meat following extraction by an alkaline detergent solution. Tracks: harmalol (Hol), 2.7 mg/mL; harmane (HA), 1.82 mg/mL; harmine (HI), 2.12 mg/mL; harmaline (HL), 2.14 mg/mL; extract of spiked meat (10.0 g + 1.2 mg of each standard; extraction and dissolving the residue in 3 mL methanol; extract of unspiked meat. (A) under UV light (366 nm); (B) under UV light (254 nm); (C) under white light, after derivatization with Dragendorff's reagent. Mobile phase, dichloromethane - methanol - 10 % ammonia, 80 : 20 : 1.5 (v/v/v)

Extract of β-carbolines by a general alkaloid method

TLC allowed to compare the overcooked chicken meat alkaloid extract with the 4 standards (harmane, harmaline, harmine, harmalol). Under UV light at 254 nm (Figure 4.6-A), multiple attenuation spots were detected on the plate, while the β-carboline alkaloid standards presented blue fluorescence; also, the migration of two of the grey spots of the chicken meat sample were comparable to harmalol spots[24]. Upon derivatization with Dragendorff's reagent (Figure 4.6-B), only one spot of the chicken sample turned light orange, with a Rf value comparable to one of the harmalol spots.
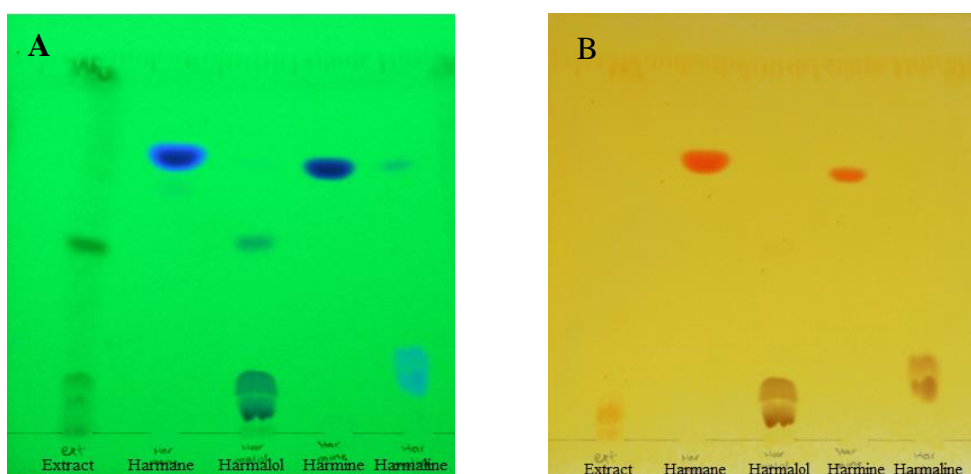
Figure 4.6: TLC plate (10cm×10cm), silica gel 60 F$_{254}$ for the overcooked chicken meat raw alkaloid extract (5 mg extract/mL), and methanolic solution of β-CAs standard (Hol, 2.7 mg/mL; HA, 1.82 mg/mL; HI, 2.12 mg/mL; HL, 2.14 mg/mL). (A) under UV light (254 nm) (B) under white light, after derivatization with Dragendorff's reagent. Mobile phase, dichloromethane - methanol - 10 % ammonia, 80 : 20 : 1.5 (v/v/v)

4.3.1.2 High Performance Liquid Chromatography (HPLC) of β-carbolines

The data obtained in TLC were not entirely conclusive about the presence of β-carbolines in our samples; for that we decided to examine the extracts by HPLC since it has an advantage over TLC in terms of resolution, sensitivity and quantification, in addition to a certain speed of analysis. So, our objective was to evaluate the eventual presence of the reference standards in the extract, in addition to defining the limit of detection of the standards in the extract.

---

[24] Note: the purity of the harmalol reference standard is only 80 %

Chromatograms of β-carbolines reference standards

We applied the method described in methods section 3.2.3.1.2, p.84 with the Agilent HPLC system.

The aim of this step was to build a standard database of retention times and determine the limit of detection for each standard; we selected different concentrations of our β-carboline standards and each one was injected in triplicate. A mix of standards was also injected to determine any overlap in peaks and eventually modify the mobile phase graduation to overcome the issue.

The chromatogram of standards (UV 254 nm; Figure 4.7); indicates a low resolution between harmaline and harmine, but we were not able to improve the separation on the column[25] used. 5 µL of a mix of standards at different concentrations (0.001 mM, 0.01 mM, 0.1 mM, 1 mM) were injected (Figure 4.8). Comparing with baseline noise, the detection limits[26] are about 0.045, 0.63, 2.98 and 3.12 ng injected for harmane, harmine, harmaline and harmalol, respectively. As literature data indicate their presence in overcooked chicken meat in the ng/g range (for harmane ~ 9 ng/g), we should be able to detect them, but with difficulties in their quantification [97, 323].

Extract of β-carbolines by an alkaline detergent solution

We applied the same method described in Section 3.2.3.1.2, p.84 with the Agilent HPLC system; the samples were filtered on 0.45 µm PTFE filter. The overcooked chicken extract, with or without spiking with the standards mix at 0.01 mM each, was diluted with 3 mL[27] ethanol (50 mg/mL), and 5 µL were injected (Figure 4.9). The two main peaks of the overcooked chicken extract (at 8.080 and 19.435 min) do not match with any peak of our standards; some minute peaks, barely distinguishable from baseline, are visible in the extract, while the mix standards were detectable in the spiked extract.

---

[25] Luna® 5µm phenyl-hexyl 100 Å, LC column 250 x 4.6 mm i.d. (from Phenomenex®)
[26] The LOD is the concentration at which the signal level of the substance reaches at least 3 times the signal noise of the baseline
[27] 3 mL was the minimum volume of solvent to dissolve the extract
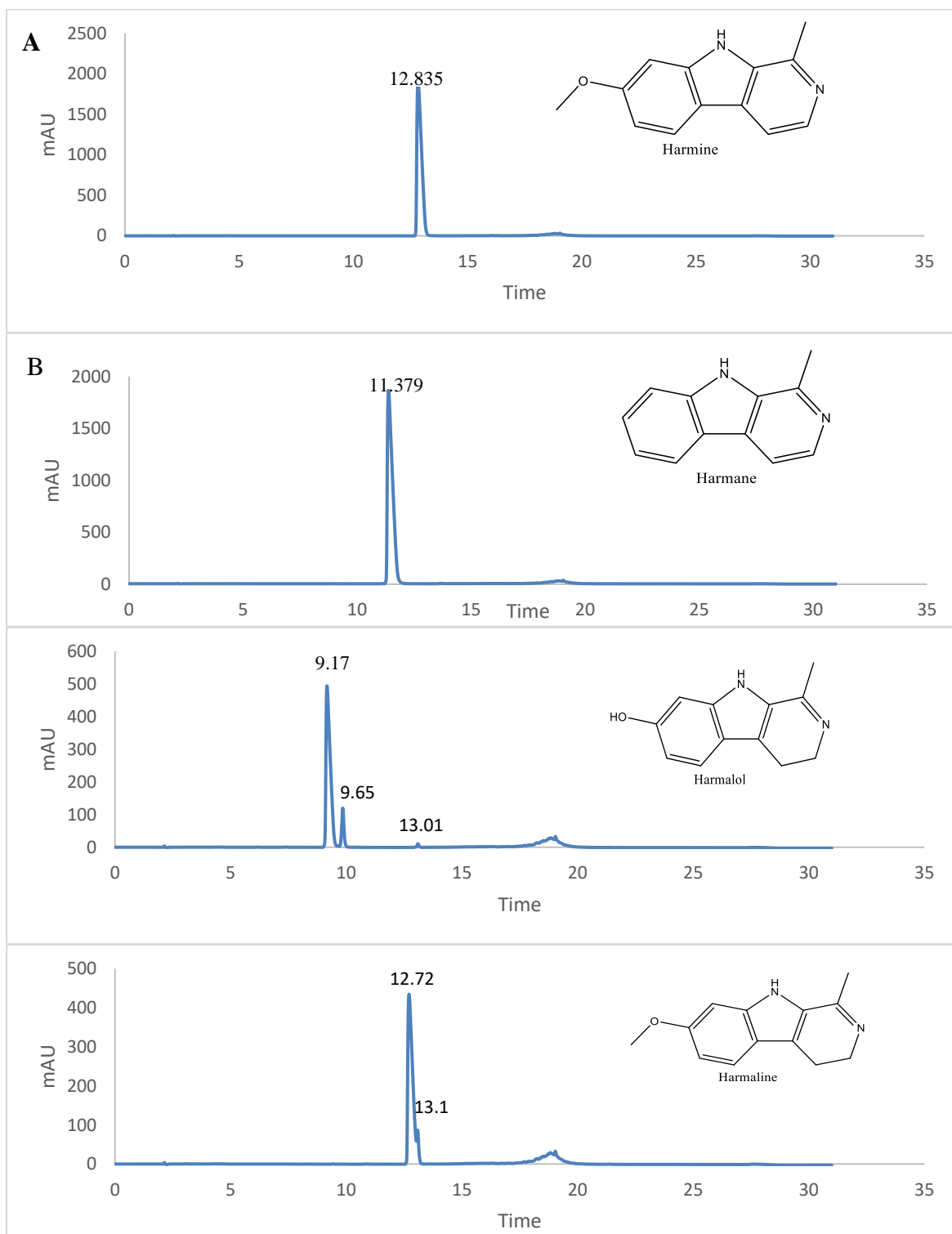
Figure 4.7: HPLC UV (254 nm) chromatogram for (A) Harmine 5mM, (B) Harmane 5mM (C) Harmalol 5mM, (D) Harmaline 5mM
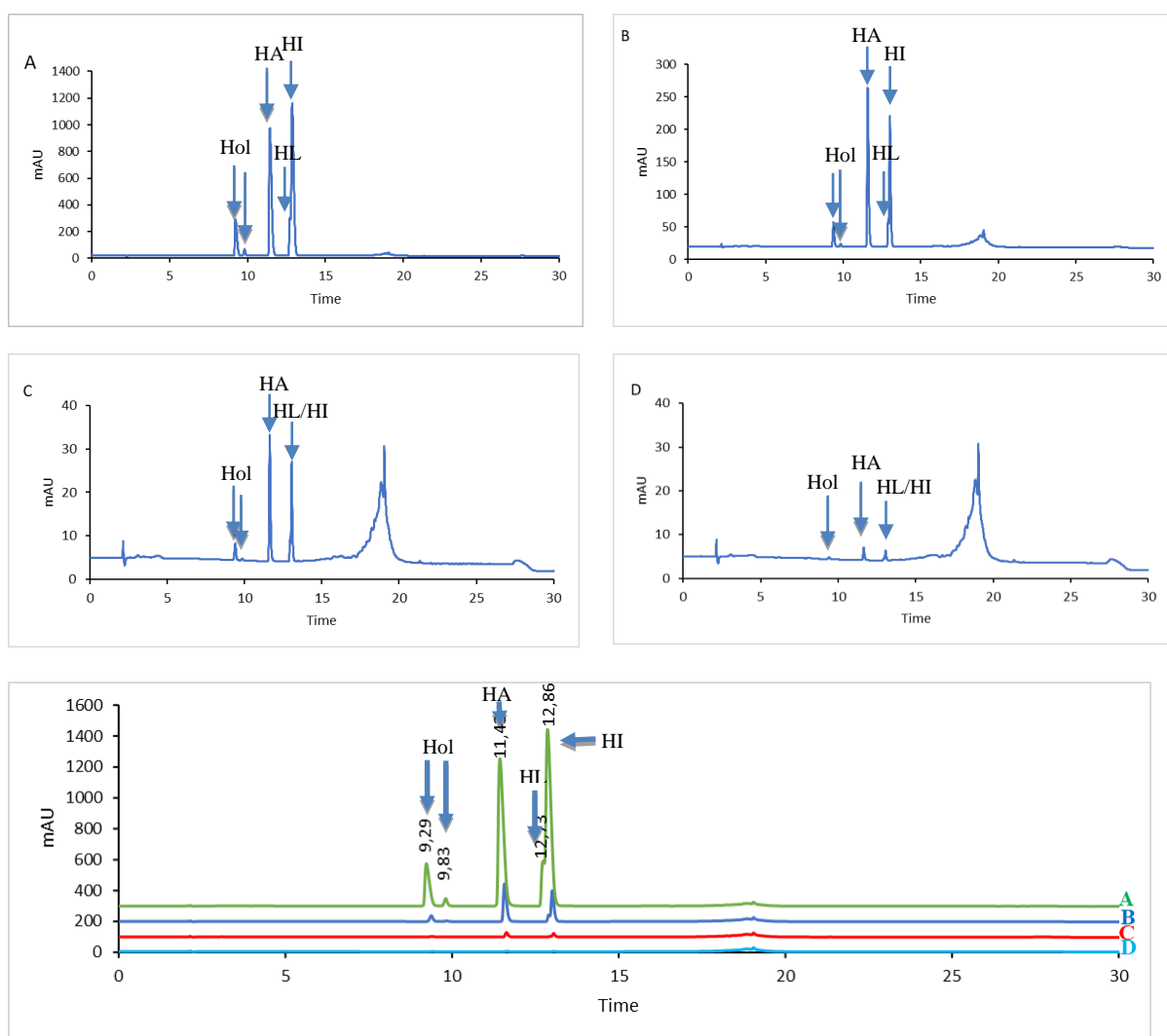
Figure 4.8: HPLC UV (254 nm) chromatogram for methanolic mix standard of harmane (HA) at 11.43 min, harmine (HI) at 12.86 min, harmaline (HL) at 12.73 min and harmalol (Hol) at 9.29, 9.83 min
(A) 1 mM (B) 0.1 mM (C) 0.01 mM (D) 0.001 mM
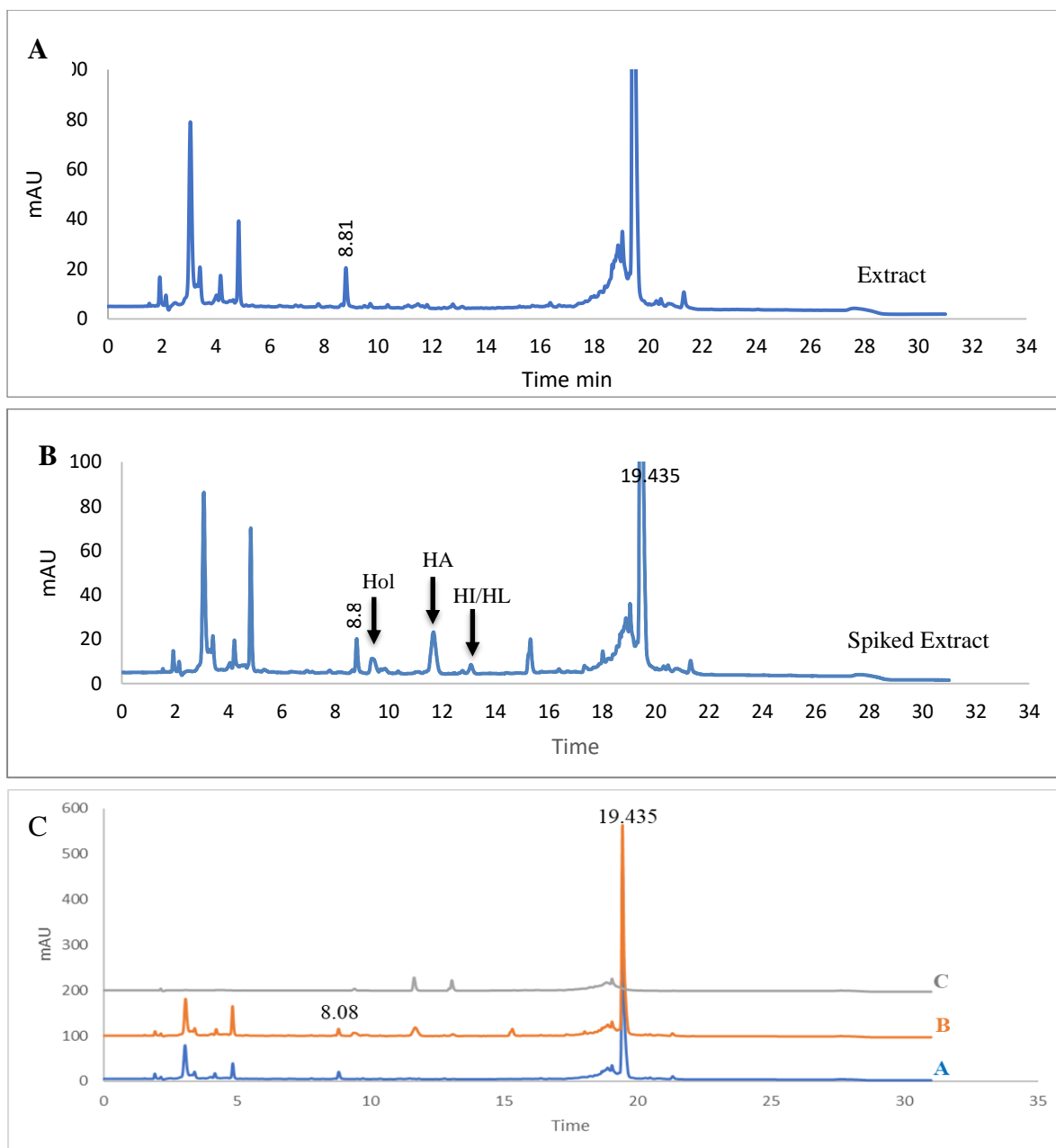
Figure 4.9: HPLC UV (254 nm) chromatogram for (A) chicken overcooked extract 50 mg/mL (B) chicken overcooked extract spiked with reference standards at 2 mM (C) Overlay of the chromatograms A and B with the standard mix (0.01 mM) (C).

Extract of β-carbolines by a general alkaloid method

We applied the same method described in Section 3.2.3.1.2, p.84 but with the Merck-Hitachi HPLC system; the samples were not filtered and injected at a concentration of 1.5 mg/mL, with and without spiking with the standard mix at 0.5 mM and comparison with the standard

mix at 1 mM. (Figure 4.10). Despite this specific extraction method, there was also no peak in the extracts matching the RT of the 4 β-carboline standards.
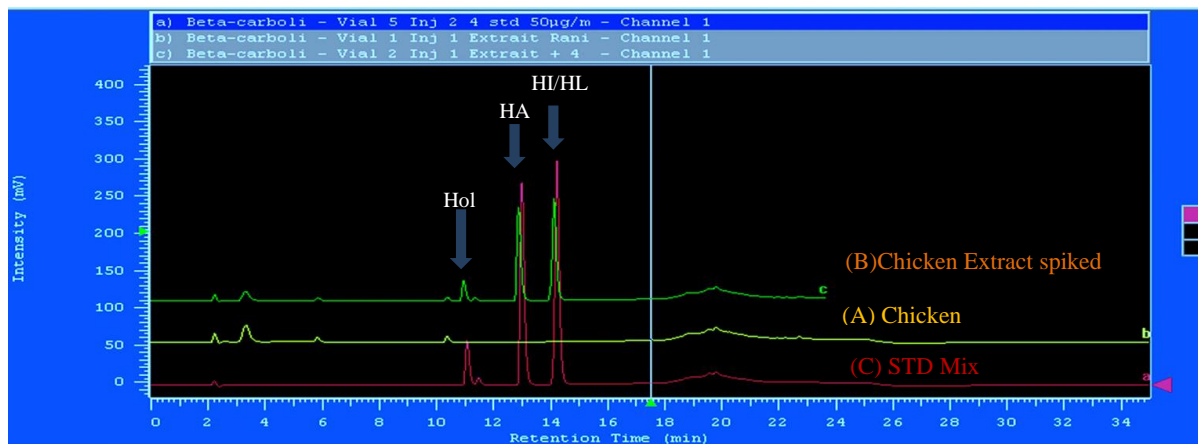
Figure 4.10: HPLC UV (254 nm) chromatogram for (A) chicken overcooked extract 1.5 mg/mL; (B) chicken overcooked extract spiked with standard mix at 0.5 mM; (C) standard mix at 1 mM.

4.3.2 Identification of carbonyl compounds in overcooked chicken meat

4.3.2.1 Derivatization with 4-hydrazino-N, N, N-trimethyl-4-oxobutanaminium iodide (HTMOB) and analysis by ESI-MS/MS

Synthesis of HTMOB

The synthesis included different steps; at each step, the identity of the intermediate product was controlled, either by mass spectrometry or by NMR spectroscopy.

Step 1: Esterification of butyric acid

The product of esterification of dimethylaminobutyric acid with ethanolethyl, 4-ethoxy-(dimethylamino) butanoate (Figure 4.11), was verified with an AutoSpec mass spectrometer, electron ion source (EI); the expected m/z 159 was present in the mass spectrometer as shown in Figure 4.12.

4-(dimethylamino)butanoic acid
$C_6H_{13}NO_2$; Mass: 131,09

4-ethoxy-(dimethylamino)butanoate
$C_8H_{17}NO_2$; Mass: 159,13
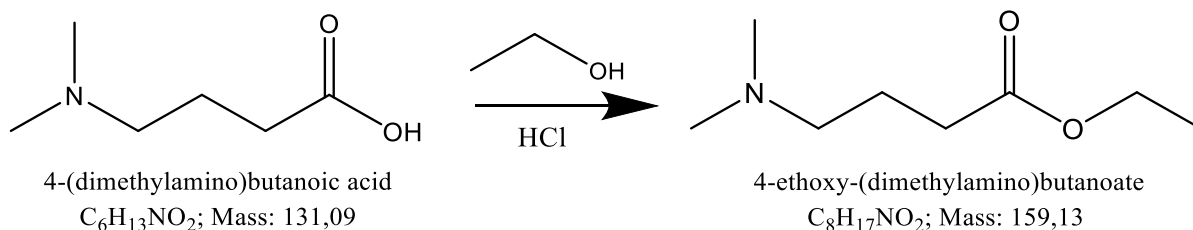
Figure 4.11: The reaction of 1st step of HTMOB synthesis, the esterification of dimethylaminobutyric acid with ethanol.
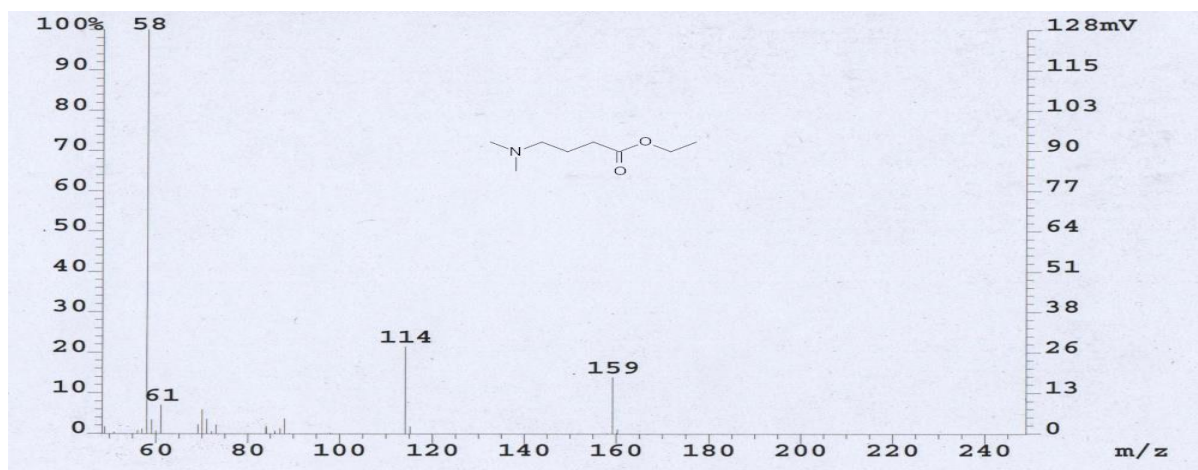
Figure 4.12: Mass spectrum for verification of 4-ethoxy-(dimethylamino) butanoate, *m/z* 159 ion (M$^+$) (Auto spec EI)

Step 2: Methylation - formation of a quaternary ammonium salt

The formed 4-ethoxy-*N,N,N*-trimethyl-4-oxobutan-1-aminium iodide Figure 4.13 yielded an ESI-MS mass spectrum (positive mode): *m/z* 174 (M$^+$) on the Quattro Premier Quadrupole mass spectrometer, indicating the effectiveness of methylation (Figure 4.14).

4-ethoxy-(dimethylamino)butanoate
$C_8H_{17}NO_2$; Mass: 159,13

4-ethoxy-*N,N,N*-trimethyl-4-oxobutan-1-aminium iodide
$C_9H_{20}INO_2$; Mass: 301,05; *m/z* : 174,15 (M$^+$)
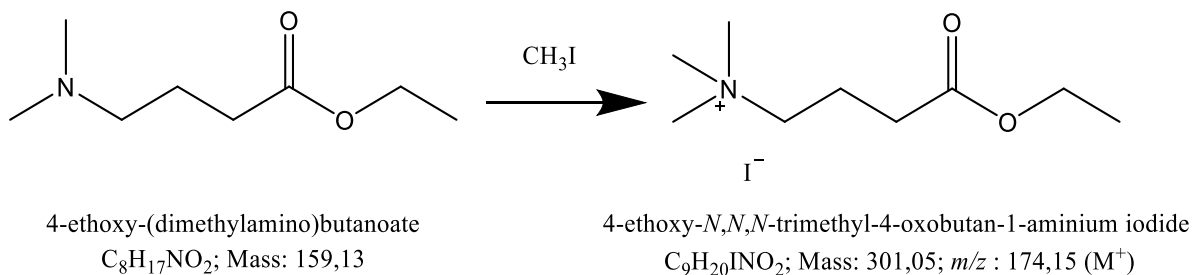
Figure 4.13: The reaction of 2nd step of HTMOB synthesis, the formation of 4-ethoxy-N,N,N-trimethyl-4-oxobutan-1-aminium iodide a quaternary ammonium salt, by adding iodomethane to ethyl dimethyl aminobutyrate the product of 1st step.
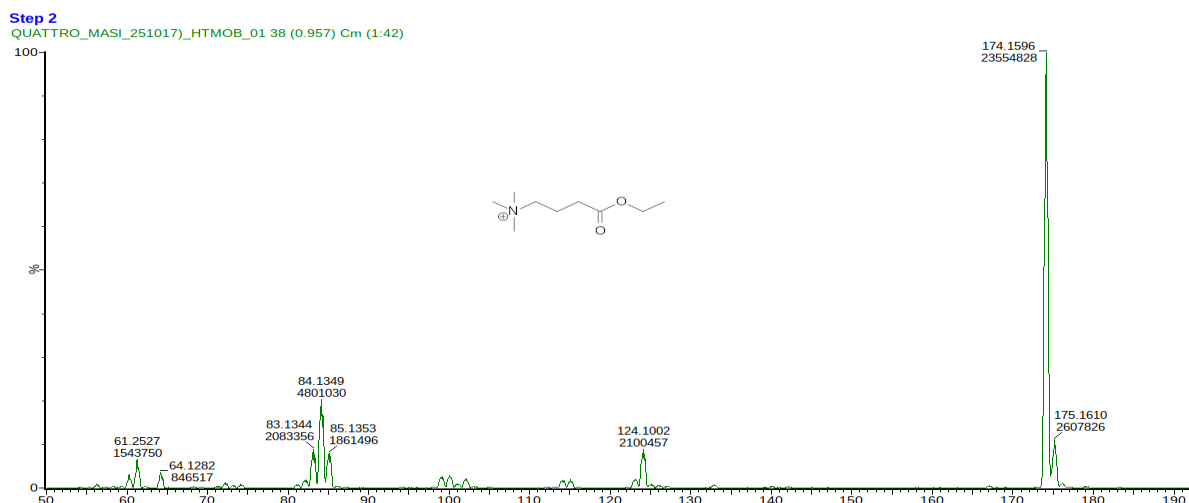
Figure 4.14: ESI-MS spectrum (by Quattro Premier Quadrupole mass spectrometer, positive mode) for the verification of 4-ethoxy-N, N, N-trimethyl-4-oxobutan-1-aminium iodide by looking for m/z 174 (M$^+$)

Step 3: Ester hydrazinolysis - formation of HTMOB

The formation of the 4-hydrazinyl-*N,N,N*-trimethyl-4-oxobutan-1-aminium iodide (Figure 4.15) was confirmed by mass spectrometry (Quattro Premier Quadrupole mass spectrometer ESI-MS in positive mode) at a m/z 160 (M$^+$) (Figure 4.16). Moreover, 1H NMR allowed confirmation of structure, the spectrum (Figure 4.17) being comparable with the spectrum described by Johnson DW (2007) [331]; the analysis of peaks is detailed in Table 4.8.

4-ethoxy-*N,N,N*-trimethyl-4-oxobutan-1-aminium iodide
$C_9H_{20}INO_2$; Mass: 301,05

4-hydrazinyl-*N,N,N*-trimethyl-4-oxobutan-1-aminium iodide
$C_7H_{18}IN_3O$; Mass: 287,05; m/z : 160,14 (M$^+$)
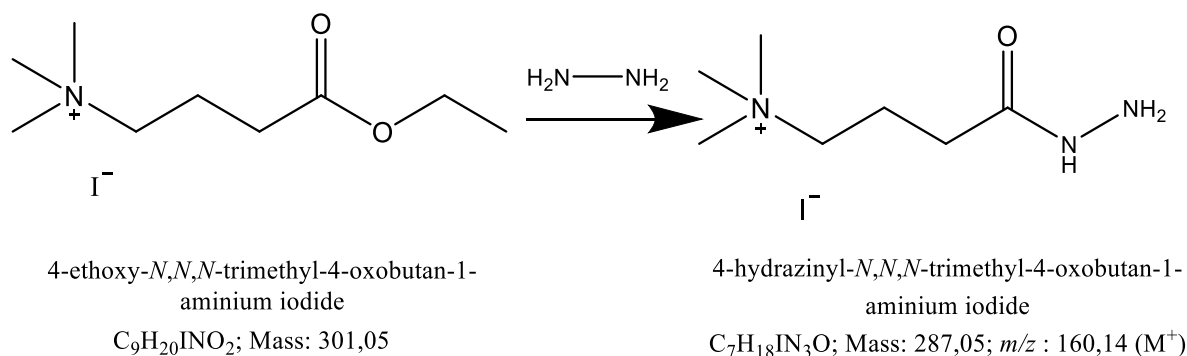
Figure 4.15: The reaction of 3rd step of HTMOB synthesis, the hydrazinolysis of 4-ethoxy-N,N,N-trimethyl-4-oxobutan-1-aminium iodide with hydrazine hydrate to form 4-hydrazinyl-*N,N,N*-trimethyl-4-oxobutan-1-aminium iodide.
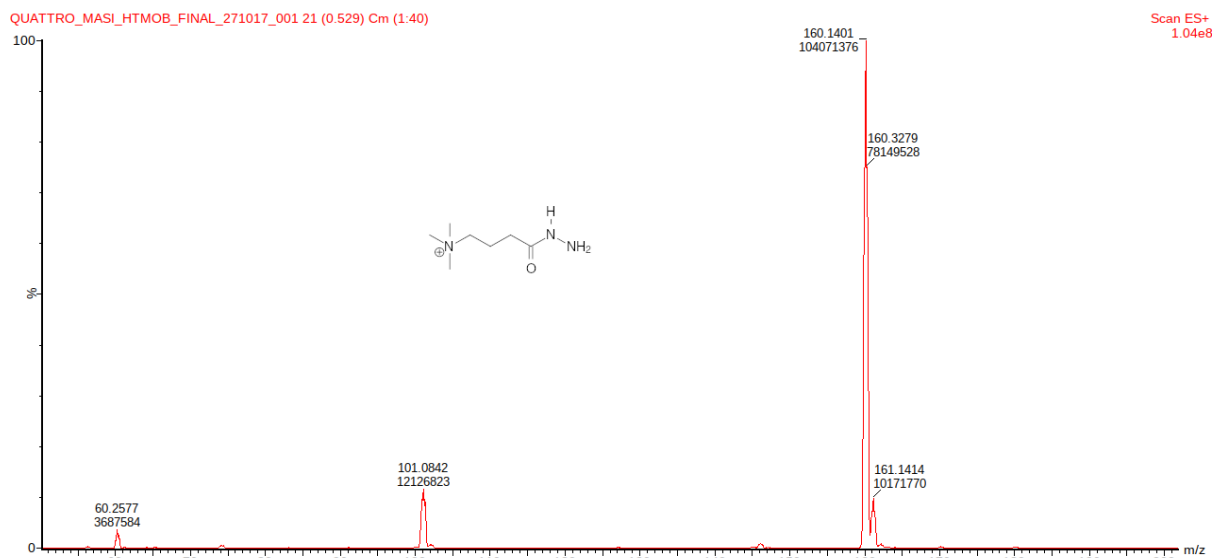
Figure 4.16: ESI-MS spectrum (Quattro Premier Quadrupole mass spectrometer, positive mode) verification of effective hydrazinolysis to produce 4-hydrazinyl-N, N, N-trimethyl-4-oxobutan-1-aminium iodide m/z 160 (M^+)
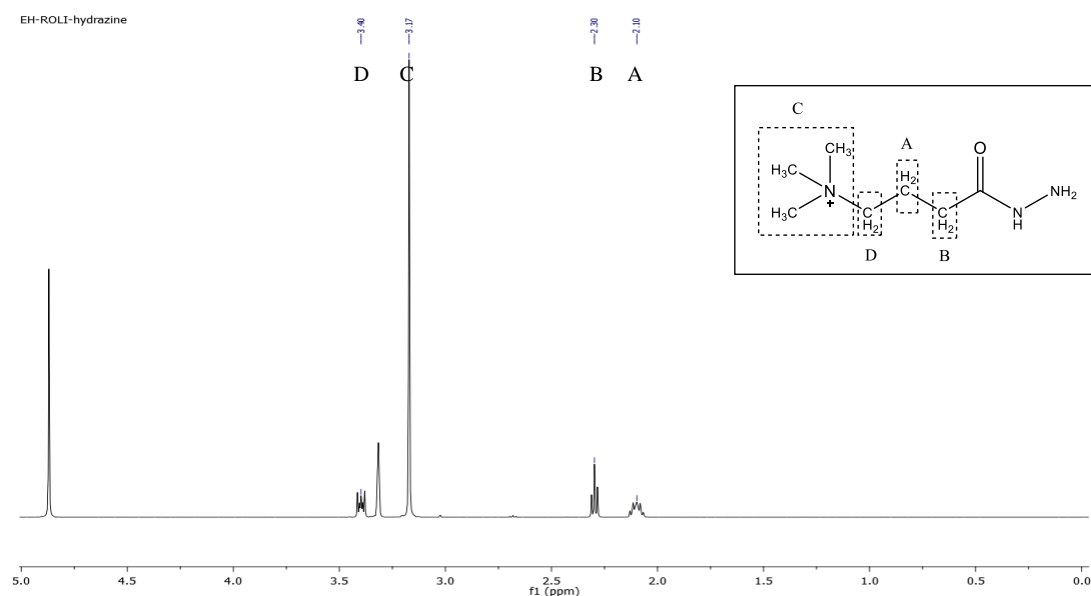
Figure 4.17: The 1H NMR spectrum of 4-hydrazinyl-N, N, N-trimethyl-4-oxobutan-1-aminium iodide (HTMOB) (in CD$_3$OD at 600 MHz)

Table 4.8: Analysis of the 1H NMR spectrum of 4-hydrazinyl-N, N, N-trimethyl-4-oxobutan-1-aminium iodide (of HTMOB) in CD$_3$OD (600 MHz)

	Functional Group	chemical shift δ Johnson DW (2007)	Pattern	chemical shift δ obtained	Pattern
A (2H)	NCH$_2$CH$_2$	2.08	multiplicity	2.10	multiplicity
B (2H)	CH$_2$CO	2.28	splitting	2.30	splitting
C (9H)	N(CH$_3$)$_3$	3.15	splitting	3.17	splitting
D (2H)	NCH$_2$CH$_2$	3.36	multiplicity	3.40	multiplicity

Derivatization of aldehydes and ketones with HTMOB

We first tested the HTMOB derivatization/identification method after modifying the original method described by Johnson DW (2007)[28];

✓ on benzaldehyde (Figure 4.18); the condensation of benzaldehyde with HTMOB produces a molecule with molecular mass of 248.18 Da, the loss of trimethylamine (59 Da) produces an ion with exact mass of 189.10. The ESI-MS/MS neutral loss 59 Da chromatogram revealed an abundant ion at *m/z* 189 that effectively corresponds to benzaldehyde.

✓ on overcooked chicken meat extract of non-volatile carbonyls (obtained by condensation with the silica-supported reagent, as per Section 3.2.2.5, p.80); the ion at *m/z* 160 of HTMOB is not apparent on the spectrum, indicating the probable total consumption of HTMOB to derivatize the carbonyl compounds of the extract (Figure 4.19).
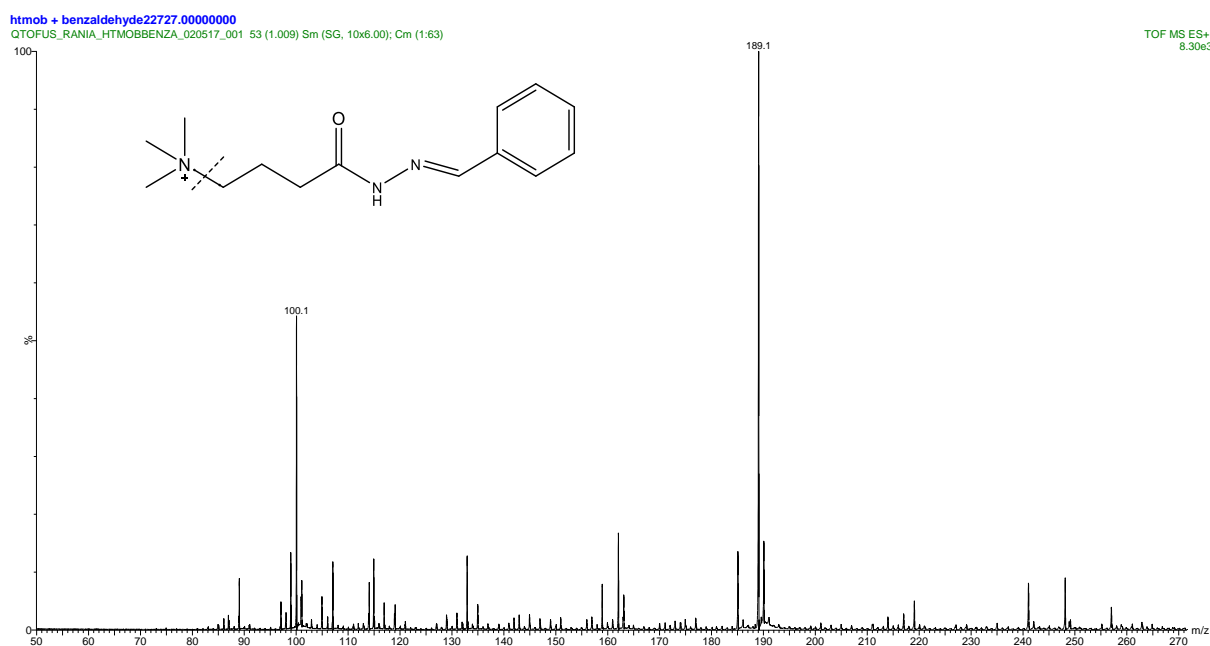
Figure 4.18: ESI-MS/MS neutral loss of 59 Da spectrum scan of HTMOB-derivatized benzaldehyde. The ion at *m/z* 189 (M^+H^+) corresponds to benzaldehyde.

---

[28] We applied HTMOB 100 mM in methanol containing 4 % glacial acetic acid at 75° C for 3h while the original method used HTMOB 10 mM in methanol containing 0.1 % formic acid at 20°C for 30 min
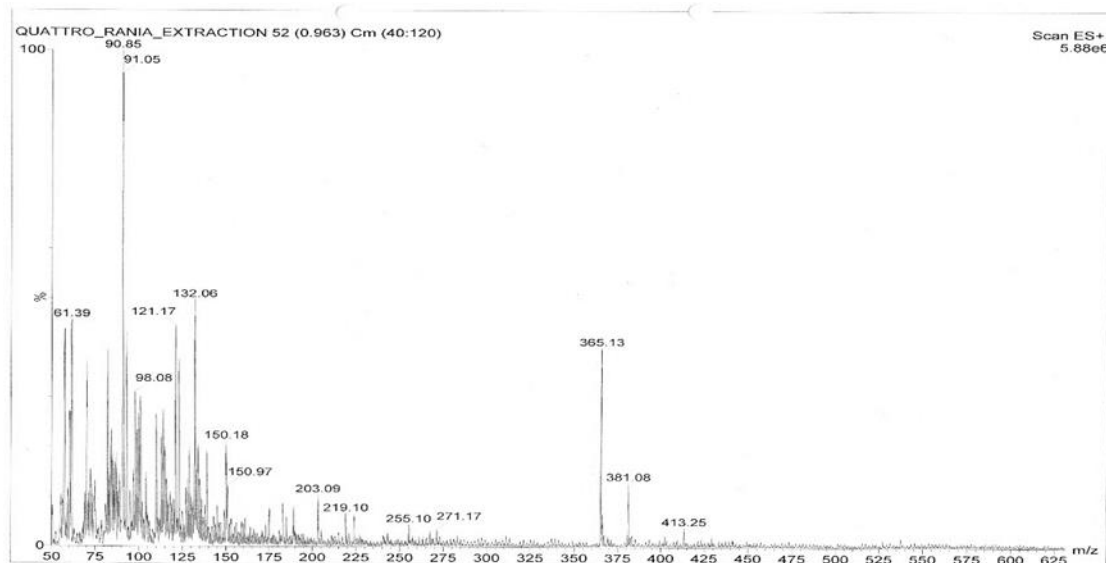
Figure 4.19: ESI-MS/MS neutral loss of 59 Da spectrum scan of HTMOB-derivatized with aldehydes chicken meat extract.

The derivatization conditions were then referred back to the original Johnson DW (2007) method with slight modifications[29] and, in collaboration with the S²MOS lab (Prof. P. Gerbaux and Mr. M. Simons), we developed a database of ESI-MS/MS full scan spectra and daughter scan spectra (for peaks that presented a neutral loss of 59 Da, corresponding to trimethylamine); this was done for 12 reference aldehydes, selected for their attested presence in cooked meats [332, 333]. The spectra are presented in annex 1 (section 8.1, p.254) and summarized in Table 4.9.

The process of identifying carbonyl compounds in our extracts consisted in defining the precursor molecular ion M^+ corresponding to a peak in the neutral loss scan[30], then examining the fragmentation spectrum (the daughter scan[31]) based on a comparison with the created database; 59 Da neutral loss and fragmentation patterns allowed to deduce the identities of peaks, as described by Johnson DW (2007).

Based on this methodology, the carbonyl extract obtained from overcooked meat chicken by condensation with silica-gel supported reagent (as per Section 3.2.2.5 p.80) (Figure 4.20) was analyzed, and the following aldehydes could be identified (Table 4.10):

---

[29] The injection solvent (acetonitrile/water/formic acid 50:50:0.25 v/v/v) was replaced by HPLC methanol to increase the sensitivity, and HTMOB was dissolved in methanol containing 1 % acid formic in place of 0.1 %
[30] Neutral loss scans are used for screening a group of compounds that give the same loss; and so, only the compounds that give the screened fragment are detected.
[31] Daughter scans are used for scanning the fragments that have actually lost 59 Da.

- ➢ Glycolaldehyde
- ➢ Isobutyraldehyde
- ➢ Isovaleraldehyde or 2-methylbutyraldehyde
- ➢ Phenylacetaldehyde

The same operation was repeated with the browned meat juices extract obtained by condensation with silica-gel supported reagent (as per Section 3.2.2.5, p.80) (Figure 4.21) and these aldehydes could be identified Table 4.11:

- ➢ 3-methylbutanal
- ➢ Isobutyraldehyde
- ➢ Acetaldehyde
- ➢ Formaldehyde

These analyses were repeated 3 times (technical replicates), yielding sensibly similar spectra that allowed to identify the same compounds. A summary of detected aldehydes in overcooked meat chicken and browned meat juices extracts is presented in Table 4.12.

Table 4.9: Characteristic ions of 12 selected reference aldehydes derivatized with HTMOB

Compound	m/z of fragment loss	m/z of parent ion M^+ (➜ minor peak in daughter scan)	m/z of major peak in M^+ daughter scan
Furfural	96.08	238.11	179.04
5-hydroxymethylfurfural	126.11	269.10	210.01
Acetaldehyde	44.05	186.08	126.98
Isobutyraldehyde	72.11	214.09	155.02
Isovaleraldehyde	86.13	228.12	169.14
2-Methylbutyraldehyde	86.13	228.24	169.10
Phenylacetaldehyde	120.14	262.34	203.27
3-Methylthiopropionaldehyde	104.17	246.14	187.14
Glyceraldehyde	90.08	231.98	173.11
Glycolaldehyde	60.05	202.22	143.12
Formaldehyde	30.03	172.16	113.19
Acrolein	56.06	198.06	139.07

Figure 4.20: Mass spectrum of the HTMOB- derivatized carbonyl extract obtained from overcooked chicken meat by condensation with silica-gel supported reagent. (A) ESI-MS full scan mode, (B) ESI-MS/MS neutral loss mode and (C) ESI-MS daughter scan (loss 59 Da)

Table 4.10: Analysis of ESI-MS/MS neutral loss of 59 Da spectrum of the HTMOB- derivatized carbonyl extract obtained from overcooked chicken meat by condensation with silica-gel supported reagent. Compounds were identified through the parent ion corresponding to the neutral loss scan, and the m/z of fragment in the daughter (59 Da loss) spectrum.

m/z of parent ion M^+ (full scan and neutral loss mode)	m/z of daughter ion M^+ (in daughter scan)	m/z of fragment loss	Identity of parent compound
160.56			HTMOB
173.58	114.01	31.74	/
182.89	123.54	39.67	/
184.12	124.91	41.88	/
201.87	141.83	60.02	Glycolaldehyde
204.51	144.84	62.66	/
213.96	214.50	71.98	Isobutyraldehyde
227.98	169.28	86.14	Isovaleraldehyde or 2-methylbutyraldehyde
242.12	183.65	100.81	/
262.12	202.57	120.07	Phenylacetaldehyde

Figure 4.21: Neutral loss 59 DA mass spectrum of the HTMOB- derivatized browned meat juices carbonyl extract obtained by condensation with silica-gel supported reagent. (A) ESI-MS full scan mode (above), (B) ESI-MS/MS neutral loss mode and (C) ESI-MS daughter scan (loss 59 Da)

Table 4.11: Analysis table of ESI-MS/MS neutral loss of 59 Da scans of browned meat juices sample. Compounds were identified through the parent ion corresponding to the neutral loss scan, and the *m/z* of fragment in the daughter (59 Da loss) spectrum.

m/z of parent ion M^+ (full scan and neutral loss mode	*m/z* of daughter ion M^+ (Daughter scan)	m/z of fragment loss	*Identity of parent compound*
160.17			HTMOB
254.18	193.92	112.03	
242.83	183.57	100.68	
240.20	181.01	98.54	
228.21	169.29	86.06	2- or 3-Methylbutanal
216.57	157.32	74.42	
214.26	155.81	72.06	Isobutyraldehyde
211.94	152.85	69.98	
200.25	139.86	58.06	
186.18	127.32	44.09	Acetaldehyde
182.75	123.51	40.06	
177.60	118.02	35.45	
175.14	116.14	32.99	
172.15	113.63	29.99	Formaldehyde

Table 4.12: Summary table of detected carbonyl compound in silica gel supported extraction; derivatized with HTMOB followed by ESI-MS-MS analysis

References aldehydes	Overcooked chicken meat	Browned chicken meat juice
Furfural	-	-
5-hydroxymethylfurfural	-	-
Acetaldehyde	-	+
Isobutyraldehyde	+	+
Isovaleraldehyde	+	+
2-Methylbutyraldehyde	+	+
Phenylacetaldehyde	+	-
3-Methylthiopropionaldehyde	-	-
Glyceraldehyde	-	-
Glycolaldehyde	+	-
Formaldehyde	-	+
Acrolein	-	-

4.3.2.2 Analysis of volatile carbonyl compounds by derivatization with PFBHA followed by Gas Chromatography-Mass Spectrometry

This derivatization with PFBHA was applied, following two different methods: (*i*) the EPA method 556 on the SAFE extract; and (*ii*) a direct derivatization by headspace single-drop microextraction (HS-SDME).

Derivatization of the SAFE extract

The PFBHA derivatization method was applied on a SAFE extract realized on *"Aldehydes mixtures-556"*, a mix of 15 aldehyde/ketone standards diluted at 40 ng/mL, to build, in our GC-MS conditions, a reference table of retention times (RT), Kovats retention indices (KRI) and mass spectra. In total ion chromatograms (TIC), the peaks corresponding to these reference standards were identified by their RT and KRI, according to EPA method 556, their C_6F_5-CH_2 fragment (characterized through an extracted-ion chromatogram (EIC) *m/z* 180.7-181.7) and a mass spectrum match in the NIST 2017 database (Annex 2, section 8.2.2, p. 261). Carbonyl analytes were tentatively identified by these same characteristics,

comparing the RTs, KRIs and fragmentations of reference peaks (Annex 2, section 8.2.2 p.261) with those in the chromatograms of the SAFE distillates obtained from aqueous extracts of browned chicken meat juice (Figure 4.22, Table 4.13), and overcooked chicken meat (Figure 4.23,Table 4.14); a blank injection allowed to identify eventual procedural oximes (Annex 2, section 8.2.1, p. 260) as recommended by EPA method 556. For any sample peak RT that was not corresponding to a reference peak, the MS spectrum was searched through the NIST database. Note that, as seen with the standard aldehydes mix, the suggested identification match probability seriously decreases with peak size

We were able to identify 8 aldehydes in browned chicken meat juice and 11 aldehydes in overcooked chicken meat aqueous extract SAFE distillates (Table 4.17)

- For the continuation of the work, a series of aldehydes presenting the higher response peaks and related to the standard references and/or yielding a high prediction match in the NIST database were selected, after deletion of peaks present in the procedural blank. These are:
    - ✓ Propionaldehyde
    - ✓ Isobutyraldehyde
    - ✓ Hexanal
    - ✓ Benzaldehyde
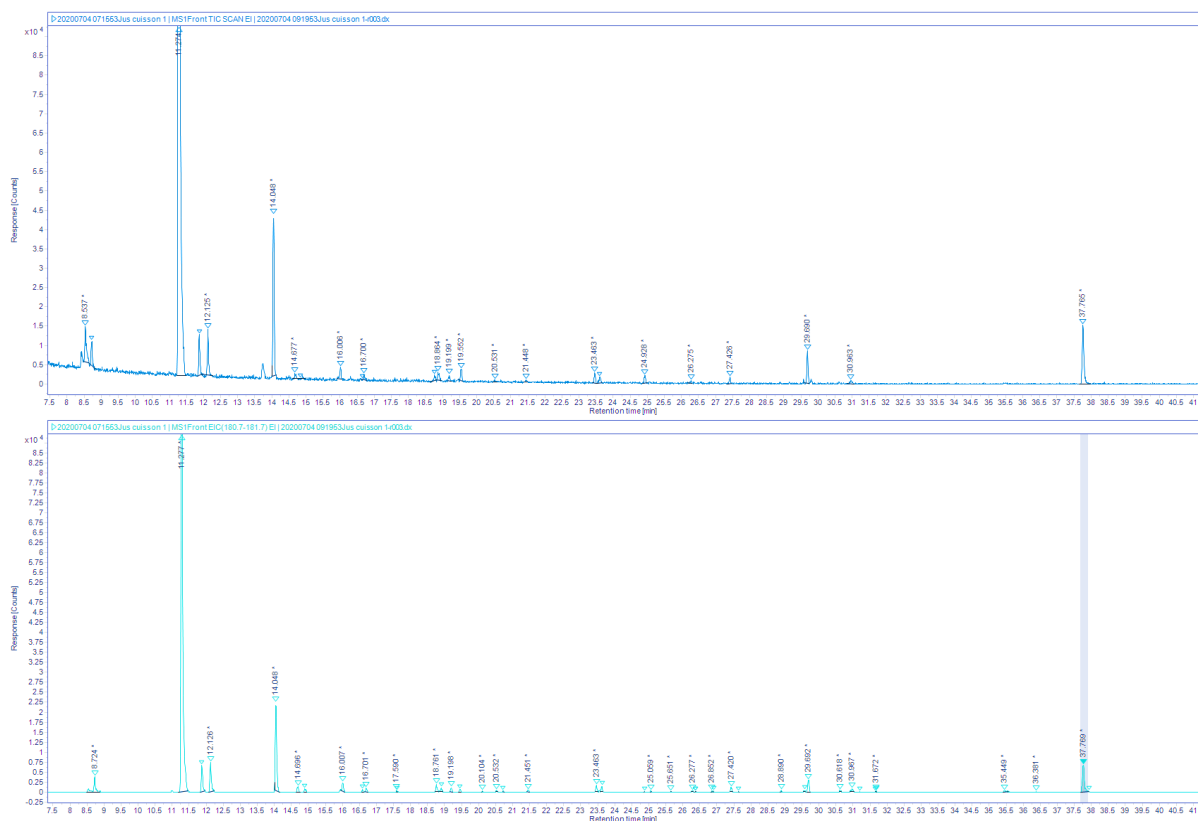
Figure 4.22: Total ion chromatogram (TIC) for the browned chicken meat juices extracted by SAFE and derivatized with PFBHA (up) and the extracted-ion chromatogram (EIC) 180.7-181.7 *m/z*.

Table 4.13: Identification of carbonyl compounds in browned chicken meat juices extracted by SAFE and derivatized with PFBHA based on comparision with reference standards RT, KRI and mass spectrum match in the NIST (probability).

Retention time T(min)	*Analytes*	*KRI*	*% Probability (NIST)*
8.530	Pentafluorobenzyl alcohol	1100.278	78.70 %
8.724	PFB hydroxylamine	1007.384	12.80 %
11.277	Formaldehyde oxime	1087.889	71.40 %
11.870	Acetaldehyde E	1004.974	54.30 %
12.128	Acetaldehyde Z	1013.440	46.20 %
14.049	Acetone oxime	1071.334	73.50 %
14.677	Propionaldehyde oxime (E)	1088.552	15.90 %
14.890	Propionaldehyde oxime (Z)	1094.225	/
16.070	Isobutyraldehyde oxime	1030.819	47.00 %
16.586	Methyl ethyl ketone oxime (E)	1046.631	/
16.700	Methyl ethyl ketone oxime (Z)	1050.058	5.60 %
17.631	Butyraldehyde oxime	1077.201	/
18.899	not identified	1014.802	
19.464	Crotonaldehyde oxime (E)	1033.059	/

Retention time T(min)	Analytes	KRI	% Probability (NIST)
20.530	Valeraldehyde oxime (E)	1066.106	/
23.463	Hexanal oxime (E)	951.984	13.20 %
23.626	Hexanal oxime (Z)	958.171	2.81 %
25.572	Cyclohexanone oxime	1028.913	/
26.277	Heptanal oxime (E)	1053.219	/
26.374	Heptanal oxime (Z)	1056.513	/
29.694	Benzaldehyde oxime	1324.239	62.90 %
37.768	Methylglyoxal bis-oxime	1088.428	3.90 %
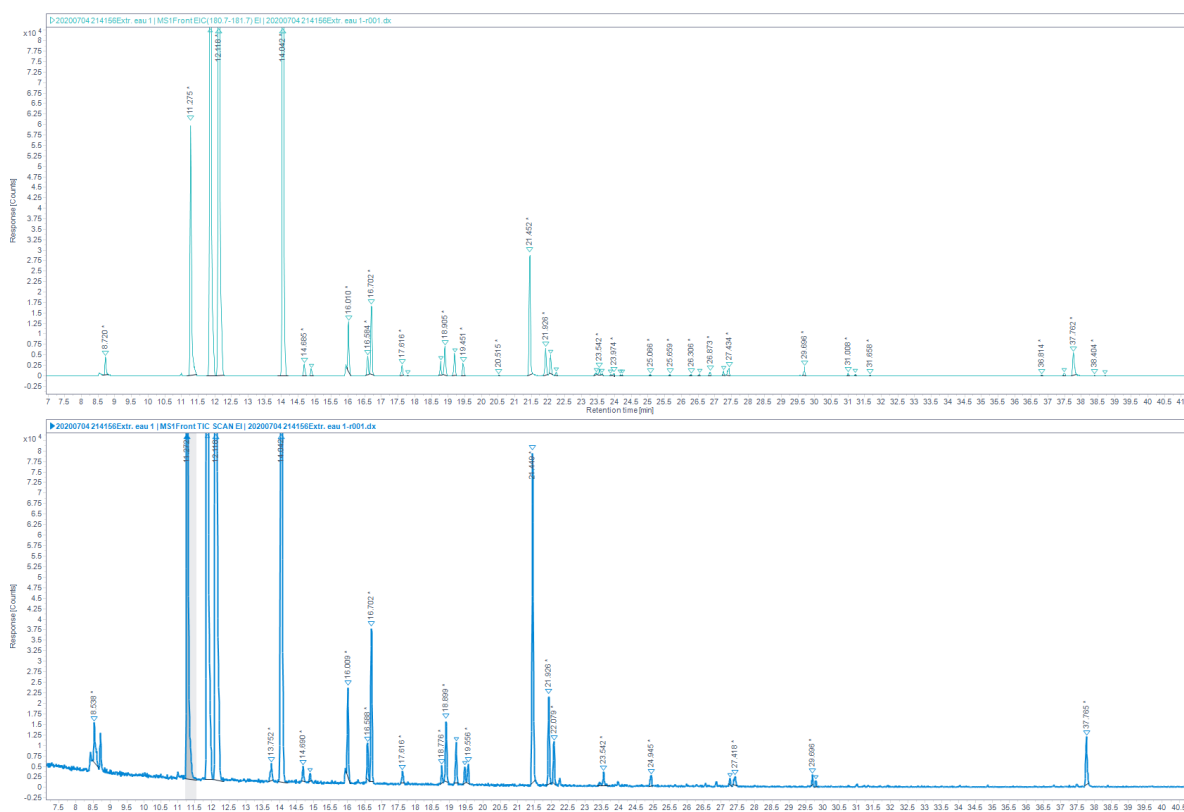
Figure 4.23: Total ion chromatogram (TIC) for the aqueous chicken sample extracted by SAFE and derivatized with PFBHA (up) and the extracted-ion chromatogram (EIC) 180.7-181.7 *m/z*.

Table 4.14: Identification of carbonyl compounds in overcooked chicken meat aqueous extract sample extracted by SAFE and derivatized with PFBHA based on RT compared with reference standards, KRI and mass spectrum match in the NIST (probability).

Retention time T(min)	Analytes	KRI	% Probability (NIST)
8.724	PFB hydroxylamine	1007.384	18.00 %
11.277	formaldehyde oxime	1087.889	68.00 %
11.870	acetaldehyde E	1004.974	42.20 %
12.128	acetaldehyde Z	1013.440	38.80 %
14.049	Acetone oxime	1071.334	75.10 %
14.690	Propionaldehyde oxime (E)	1088.901	67.70 %
14.890	Propionaldehyde oxime (Z)	1094.225	43.60 %
16.009	Isobutyraldehyde oxime	1028.916	51.20 %
16.586	Methyl ethyl ketone oxime (E)	1046.631	75.10 %
16.700	Methyl ethyl ketone oxime (Z)	1050.058	80.40 %
17.616	Butyraldehyde oxime!	1076.775	/
18.760	Butyraldehyde oxime!	1010.226	32.20 %
18.905	Butyraldehyde oxime!	1014.998	38.70 %
19.196	Butyraldehyde oxime!	1024.466	39.60 %
19.551	Crotonaldehyde oxime	1035.823	0.30 %
21.452	3-Methylpentanal oxime	1093.333	5.96 %
21.928	Crotonaldehyde oxime	1008.440	0.50 %
22.079	4-Methylpentanal oxime	1013.617	21.00 %
23.540	Hexanal oxime (Z)	1061.948	0.03 %
26.277	Heptanal oxime	1053.219	/
29.694	Benzaldehyde oxime	1073.020	6.40 %
31.672	Nonanal oxime	1046.457	/
37.768	Methyl glyoxal oxime	1088.428	3.40 %

Headspace single-drop microextraction (HS-SDME) with droplet PFBHA derivatization

The direct derivatization in the PFBHA hexane droplet was applied on the aqueous solution of the *"Aldehydes mixtures-556"*, a mix of 15 aldehyde/ketone standards diluted at 40 ng/mL, to build, in our derivatization and GC-MS conditions, a reference table of retention times (RT), Kovats retention indices (KRI) and mass spectra. The identification of analytes in total ion chromatograms (TIC) was performed as described here above based on the mix standard created database (Annex 3, section 8.3.2, p.264), and after the exclusion of peaks present in the procedural blank (Annex 3 section 8.3.1, p. 263).

Whenever a samples peak RT was not corresponding with any reference peaks, its MS spectrum was searched through the NIST database. Note that, as seen with the standard aldehydes mix, the suggested identification match probability seriously decreases with peak size.

With the microdroplet method, we were able to identify 9 aldehydes in the browned chicken meat juice juice (Figure 4.24, Table 4.15) and 4 in overcooked chicken meat aqueous extract (Figure 4.25, Table 4.16). A summary of detected aldehydes in overcooked meat chicken and browned meat juices extracts is presented in Table 4.17

For the continuation of the work, the aldehydes with the higher response peaks were selected. These are:

- for the browned chicken meat juice:
    - ✓ Propionaldehyde
    - ✓ Butyraldehyde
    - ✓ Hexanal
    - ✓ Benzaldehyde
- for the overcooked chicken meat aqueous extract:
    - ✓ Propionaldehyde
    - ✓ Hexanal
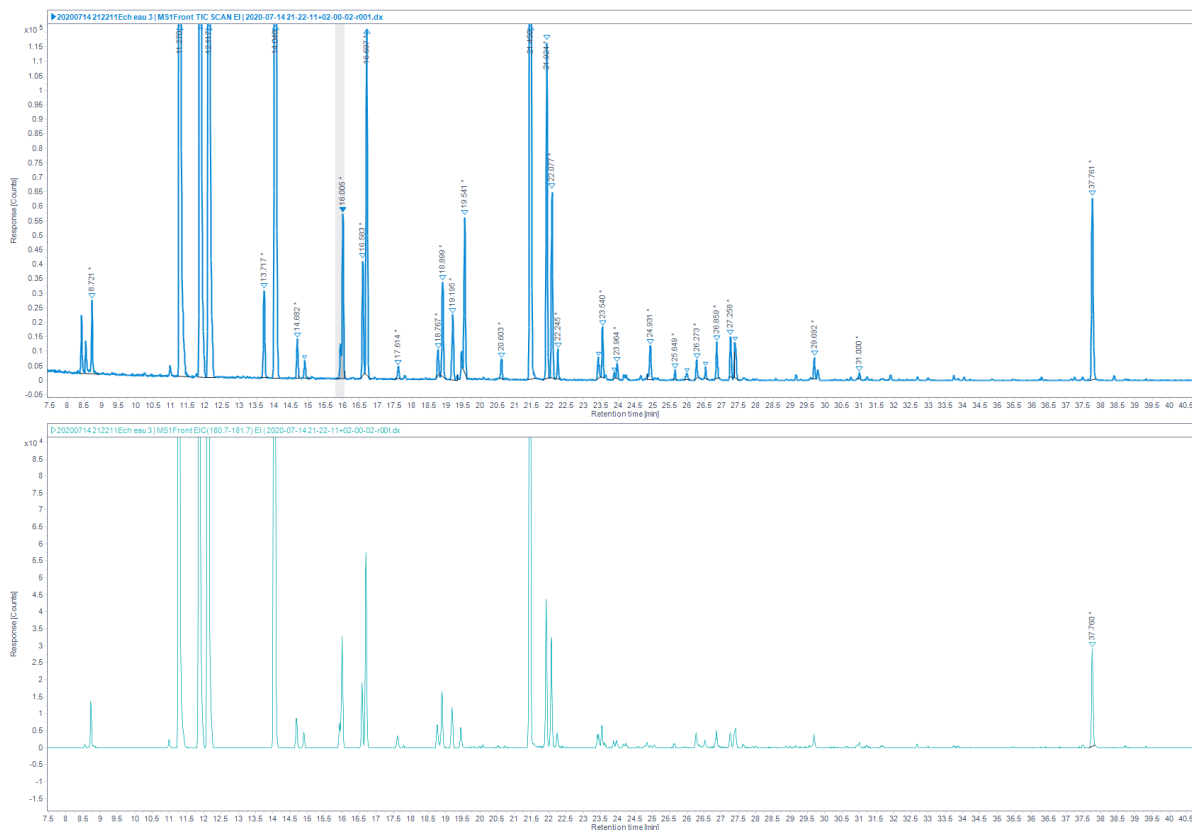
Figure 4.24: Total ion chromatogram (TIC) for browned chicken meat juices extracted by HS-SDME on PFBHA droplet (up) and the extracted-ion chromatogram (EIC) 180.7-181.7 EI (down).

Table 4.15: Identification of carbonyl compounds in browned chicken meat juices extracted by HS-SDME on PFBHA droplet, based on RT, KRI and fragmentation

Retention time T(min)	Analytes	KRI	%Probability (NIST)
11.870	Acetaldehyde oxime (E)	1004.974	52.70 %
12.128	Acetaldehyde oxime (Z)	1013.440	47.60 %
14.049	Acetone oxime	1071.334	75.20 %
14.676	Propionaldehyde oxime (E)	1088.525	63.70 %
14.889	Propionaldehyde oxime (E)	1094.199	65.50 %
16.009	Isobutyraldehyde oxime	1028.916	53.20 %
16.586	Methyl ethyl ketone oxime (E)	1046.631	84.20 %
16.690	Methyl ethyl ketone oxime (E)	1049.759	59.20 %
17.614	Butyraldehyde oxime (E)	1076.718	1.93 %
18.767	Pentanal (Valeraldehyde) oxime	1010.458	52.30 %
18.899	Valeraldehyde oxime	1014.802	20.60 %
19.190	Isovaleraldehyde oxime	1024.272	24.50 %
19.440	Crotonaldehyde oxime	1032.294	/
19.540	Cyclohexasiloxane	1035.474	35.30 %
21.452	1,3-Dihydroxypropanone oxime?	1093.333	24.90 %
21.928	1,3-Dihydroxypropanone oxime?	1008.440	38.30 %
22.080	Glycolaldehyde oxime!	1013.651	2.70 %
22.246	Glycolaldehyde oxime!	1019.301	10.80 %
23.470	Hexanal oxime (E)	1059.701	/
23.540	Cyclopentanone oxime	954.912	80.70 %
26.276	Heptanal oxime (E)	1053.185	/
26.860	5-Methoxy-2-pentanone oxime	1072.832	40.60 %
27.250	1,3-Dihydroxypropanone oxime?	1085.716	24.20 %
27.381	1,3-Dihydroxypropanone oxime?	1090.002	24.80 %
29.680	Benzaldehyde oxime	1072.528	72.90 %
31.000	Glycoaldehyde oxime or Phenylacetaldehyde oxime	1020.685	14.9 % 5.8 %
37.768	Methylglyoxal bis-oxime	1088.428	5.60 %
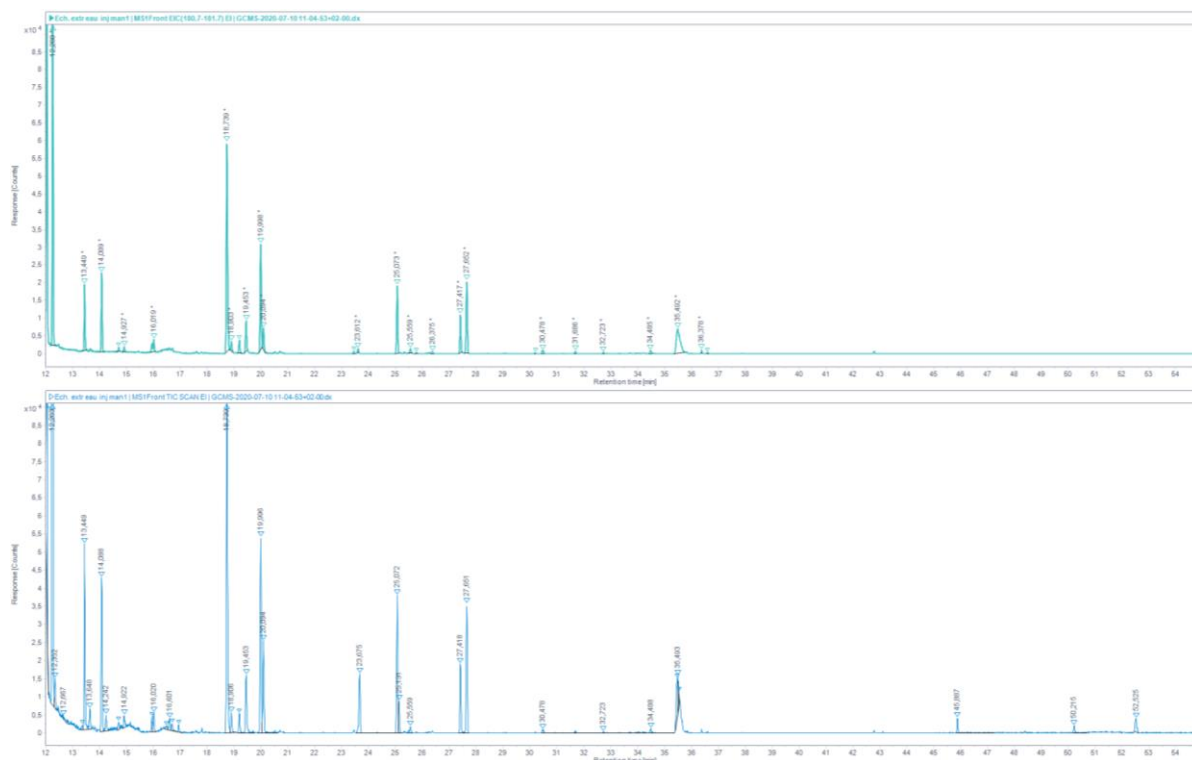
Figure 4.25: Total ion chromatogram (TIC) for aqueous chicken meat extract sample extracted by HS-SDME on PFBHA droplet (up) and the extracted-ion chromatogram (EIC) 180.7-181.7 EI (down).

Table 4.16: Identification of carbonyl compounds in overcooked chicken meat aqueous extract extracted by HS-SDME on PFBHA droplet, based on RT, KRI and fragmentation.

Retention time T(min)	Analytes	KRI	%Probability (NIST)
12.320	acetaldehyde Z	1019.625	52.30 %
13.462	Pentafluorobenzyloxime	1054.529	30.80 %
14.049	Acetone oxime	1071.334	67.70 %
14.686	Propionaldehyde oxime (E)	1088.793	0.67 %
14.900	Propionaldehyde oxime (Z)	1094.489	20.80 %
15.930	Isobutyraldehyde oxime	1026.441	46.40 %
16.002	Isobutyraldehyde oxime	1028.697	36.20 %
18.730	PFB hydroxylamine	1009.234	27.70 %
19.150	Crotonaldehyde oxime (E)	1022.979	< 0.01 %
19.453	Crotonaldehyde oxime (Z)	1032.708	< 0.01 %
19.990	Crotonaldehyde oxime (Z)	1049.586	0.25 %
23.457	Probably hexanal (E)	1059.283	/
23.612	Probably hexanal (Z)	1064.251	/
25.559	Not identified	1028.458	/

142

Table 4.17: Summary of volatile carbonyl compounds detected by SAFE and HS-SDME

Aldehydes mixtures-556	Browned chicken meat juice		Chicken meat	
	SAFE PFBHA[a]	HS-SDME[b]	SAFE PFBHA[a]	HS-SDME[b]
Benzaldehyde	+	-	+	+
Butyraldehyde	+	-	+	+
Crotonaldehyde	+	+	+	+
Cyclohexanone	+	-	-	-
Glycolaldehyde	-	-	+	-
Heptanal	+	-	+	+
Hexanal	+	+	+	+
Isobutyraldehyde	+	+	+	+
Isovaleraldehyde (3-Methylbutanal)	-	-	+	-
Nonanal	-	-	-	+
Octanal	-	-	-	-
Phenylacetaldehyde	-	-	+	-
Propionaldehyde	+	+	+	+
Valeraldehyde	+	-	+	-
2-methylbutyraldehyde	-	-	-	-

[a] SAFE distillate from the aqueous extract; derivatization with PFBHA followed by GC-MS analysis
[b] Direct derivatization by headspace single-drop microextraction followed by GC-MS analysis

4.4 Identification of carbonyl compounds likely to react with endogenous amines to form "artifactual" alkaloids

The results presented in Section 4.3.2 p.125 and Table 4.17, combined with literature data, allowed to select the aldehydes to be investigated in this section. Selected aldehydes were tested for their reactivity towards dopamine, serotonin, epinephrine, γ-aminobutyric acid (GABA), tryptophan and/or tryptamine. Only exemplative or positive data are presented in this Section.

4.4.1 Identification of artifact by TLC

A series of carbonyl compounds reference standards, selected from literature data and from the compounds detected here by SAFE and HS-SDME, were investigated for a possible condensation with biogenic amines. The occurrence of a reaction was confirmed on TLC plates, migrated in a mobile phase suited to β-carboline alkaloids, by observing the appearance of a new spot that is not present in either of the reactants and/or the disappearance of a reactant spot.

The aldehydes that were reacted with dopamine were analyzed by TLC in Figure 4.26 and are listed below:

- Glycolaldehyde
- 5-Hydroxymethylfurfural
- Glyceraldehyde
- 3-Methylthiopropioaldehyde
- Phenylacetaldehyde
- Formaldehyde

For serotonin, the reactions products were analyzed in Figure 4.27 for the following aldehydes:

- Glycolaldehyde
- 5-Hydroxymethylfurfural
- Glyceraldehyde

144

- Phenylacetaldehyde
- Formaldehyde

Tryptophan was reacted with Isovaleraldehyde and tryptamine with the following aldehydes Figure 4.28:

- Phenylacetaldehyde
- 2- Methyl butyraldehyde
- Glycolaldehyde

Hexanal demonstrated the ability to react with tryptamine, dopamine, and serotonin; benzaldehyde reacted with tryptamine (Figure 4.29, Figure 4.30).

As a result, 19 reactions were identified. A summary of the identified reaction in Table 4.18.

Table 4.18: Summary of identified condensation reaction between biogenic amines and aldehydes references selected based on literature and identified in SAFE and HS-SDME extraction (the reaction was not tested in cell with diagonal border)

	Dopamine	Serotonin	GABA	Nor-epinephrine	Tryptamine	Tryptophan
Acrolein	-	-	/	/	/	/
Acetaldehyde	-	-	-	-	-	-
Furfural	-	-	-	-	-	-
Glycolaldehyde	+	+	-	-	+	-
5-Hydroxymethylfurfural	+	+				
Glyceraldehyse	+	+				
Formaldehyde	+	+				
3-Methylthiopropioaldehyde	+					
2-methylbutyraldehyde	-	-	-	-	+	-
Isovaleraldehyde	-	-	-	-	-	+
Phenylacetaldehyde	+	+	-	-	+	-
Isobutyraldehyde	-	-	-	-	-	-
Benzaldehyde	-		-	-	+	-
Hexanal	+	+	-	-	+	-
Propionaldehyde	-	-	-	-	-	-
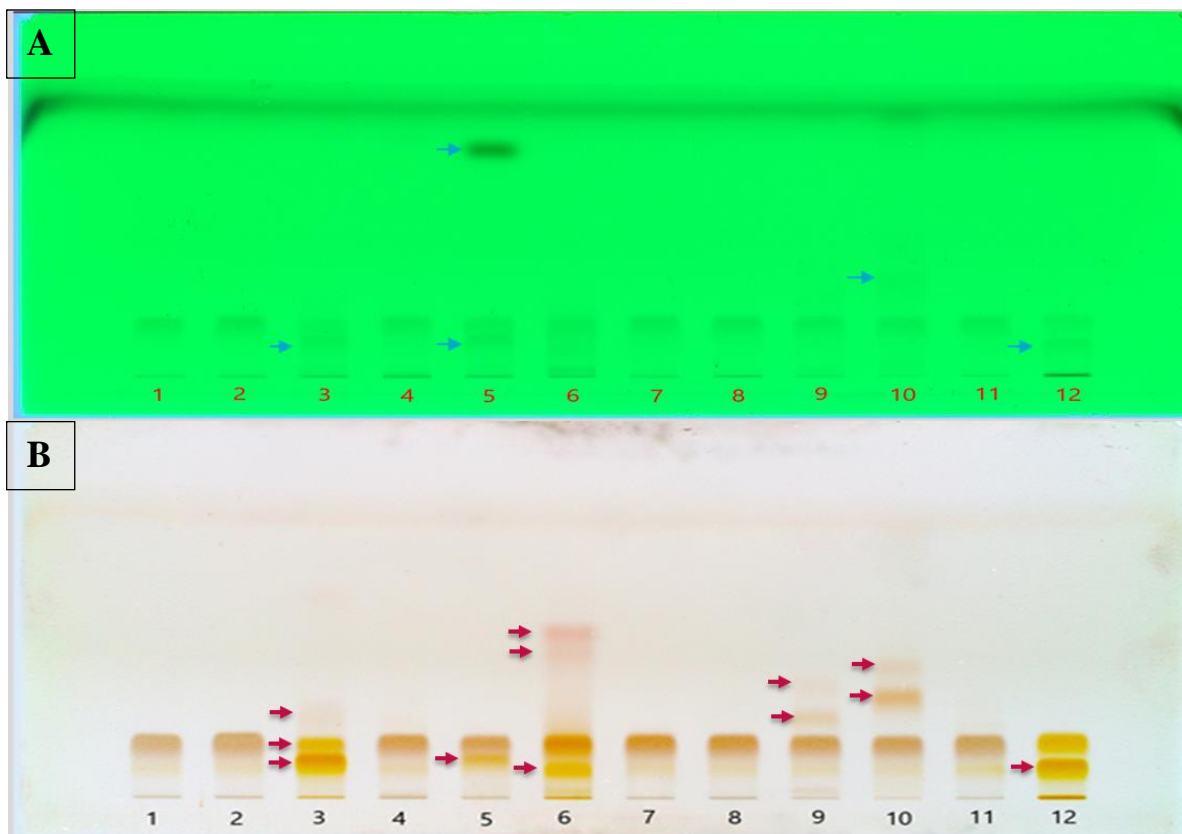
Figure 4.26: TLC plate (20cm×10cm), silica gel 60 F_{254} for verification of a potential reactivity between dopamine and aldehydes. Equimolar reactions (5 µM) at 37°C for 16 h. Mobile phase: ethyl acetate - acetic acid - methanol (6 : 2 : 2, v/v); sample application: 5 µL. (A) Plate visualized under UV light (254 nm); (B) Plate sprayed with a ninhydrin reagent, heated at 105°C for 5 min and visualized in white light. 1- Dopamine; 2- Dopamine 37°C; 3- Dopamine + Glycolaldehyde; 4- Dopamine + Acrolein; 5- Dopamine +5 Hydroxymethylfurfural; 6- Dopamine + Glyceraldehyde; 7-Dopamine + Acetaldehyde ;8- Dopamine + 2-Methylbutyraldehyde; 9- Dopamine + 3-Methylthiopropioaldehyde; 10- Dopamine + Phenylacetaldehyde ;11- Dopamine + Furfural; 12- Dopamine + Formaldehyde.
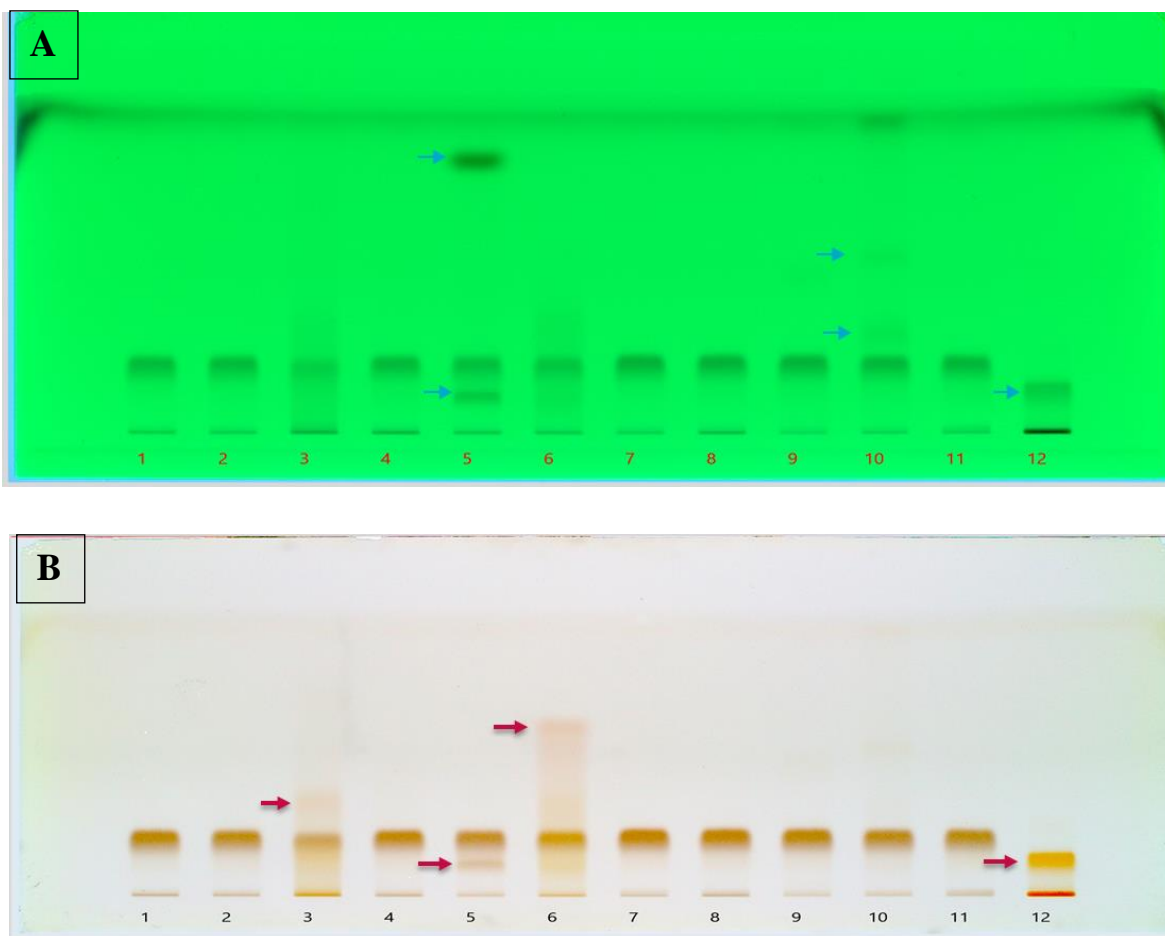
Figure 4.27: TLC plate (20cm×10cm), silica gel 60 F_{254} for verification of a potential reactivity between serotonin and aldehydes. Equimolar reactions (5 µM) at 37°C for 16 h. Mobile phase: ethyl acetate - acetic acid - methanol (6 : 2 : 2, v/v); sample application: 5 µL. (A) Plate visualized under UV light (254 nm); (B) Plate sprayed with a ninhydrin reagent, heated at 105°C for 5 min and visualized in white light; 1- Serotonin; 2- Serotonin 37°C; 3- Serotonin + Glycolaldehyde; 4- Serotonin + Acrolein; 5- Serotonin +5- Hydroxymethylfurfural; 6- Serotonin + Glyceraldehyde; 7- Serotonin + Acetaldehyde ;8- Serotonin + 2- Methylbutyraldehyde; 9- Serotonin + 3-Methylthiopropioaldehyde; 10- Serotonin + Phenylacetaldehyde ;11- Serotonin + Furfural; 12- Serotonin + Formaldehyde.
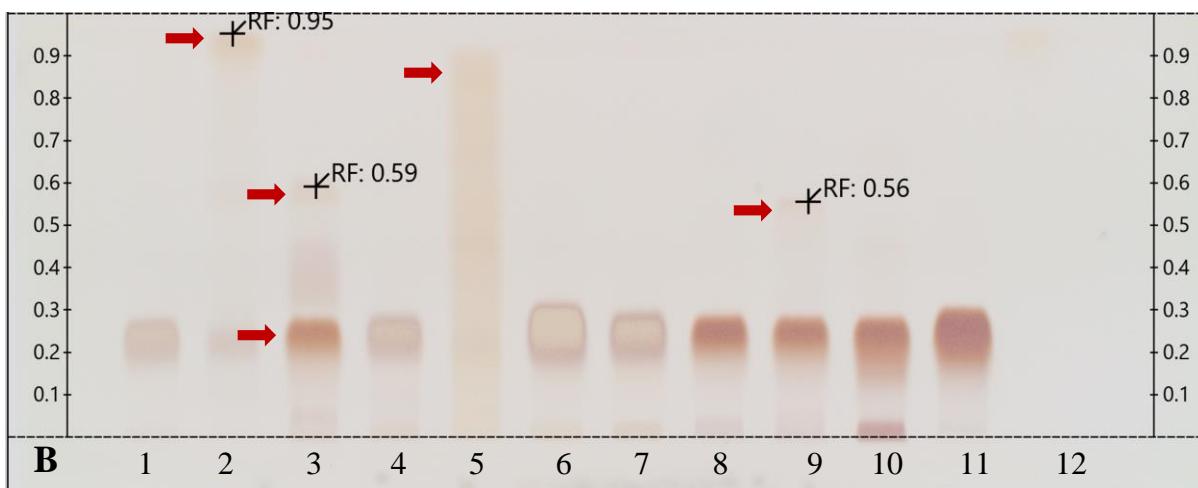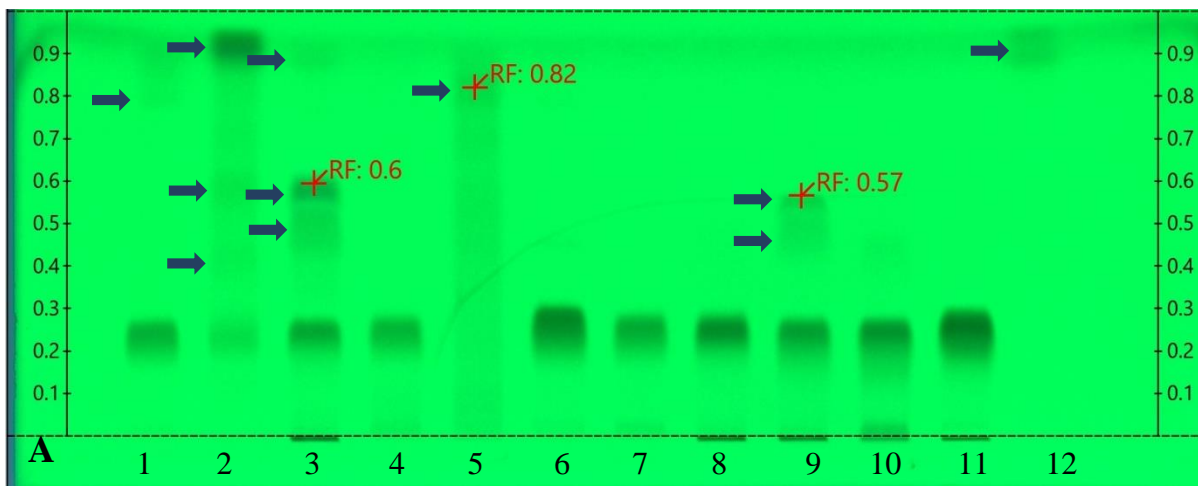
Figure 4.28: TLC plate (20cm×10cm), silica gel 60 F$_{254}$ for verification of a potential reactivity between tryptamine or tryptophan and aldehydes. Equimolar reactions (5 µM) at 37°C for 16 h. Mobile phase: ethyl acetate - acetic acid - methanol (6 : 2 : 2, v/v); sample application: 5 µL. (A) Plate visualized under UV light (254 nm); (B) Plate sprayed with a ninhydrin reagent, heated at 105°C for 5 min and visualized in white light; 1- Tryptamine + Phenylacetaldehyde (Aqueous medium); 2- Tryptamine + Phenylacetaldehyde (methanolic medium) 3- Tryptamine + 2- methylbutyraldehyde; 4- Tryptamine + Isovaleraldehyde; 5- Tryptamine + Glycolaldehyde; 6- Tryptamine; 7- Tryptophan + Phenylacetaldehyde 8- Tryptophan + 2- methylbutyraldehyde; 9- Tryptophan + Isovaleraldehyde; 10- Tryptophan + Glycolaldehyde; 11- Tryptophan; 12- Phenylacetaldehyde.
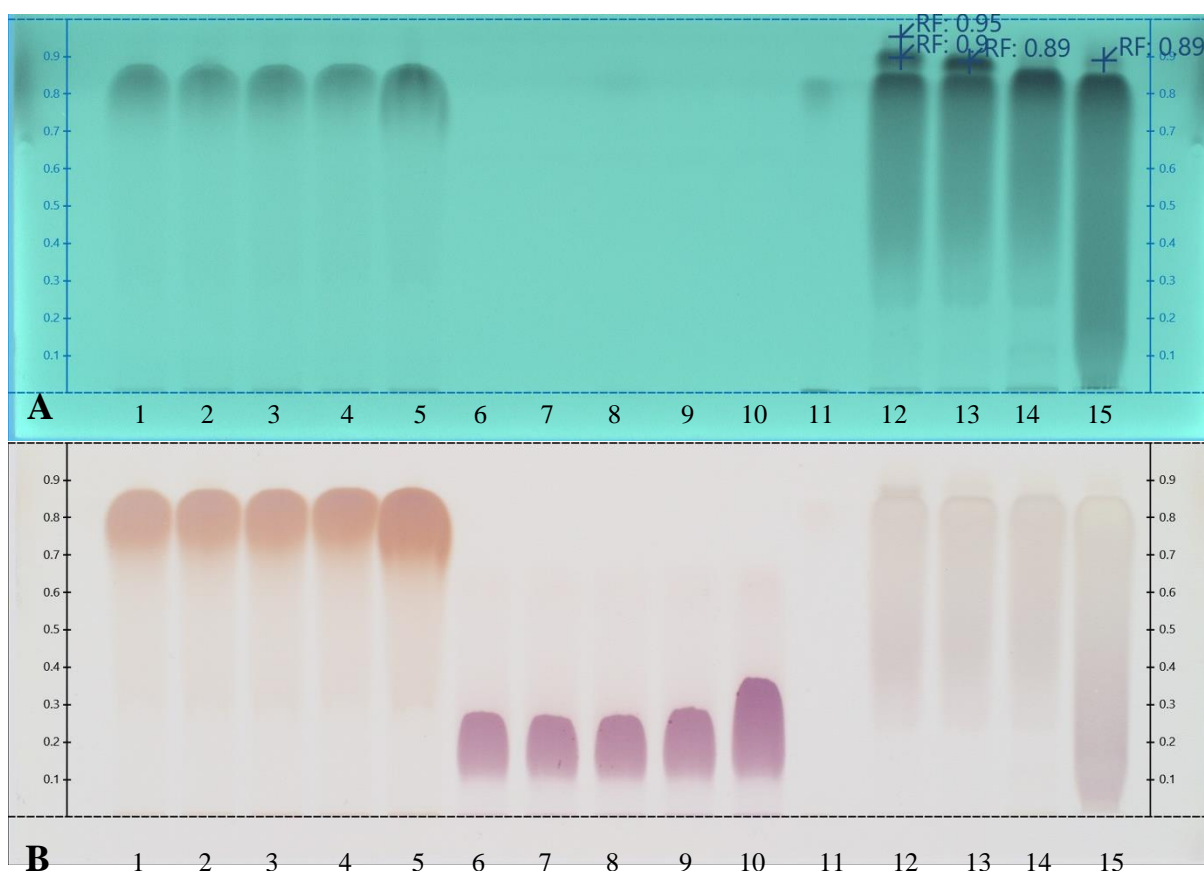
Figure 4.29: TLC plate (20cm×10cm), silica gel 60 F254S or verification of a potential reactivity between norepinephrine, GABA or tryptamine dopamine and aldehydes. Equimolar reactions (5 µM) at 37°C for 16 h. Mobile phase: ethyl acetate - acetic acid - methanol (8 : 2 : 2, v/v); sample application: 5 µL. (A) Plate visualized under UV light (254 nm); (B) Plate sprayed with a ninhydrin reagent, heated at 105°C for 5 min and visualized in white light.; 1- Propionaldehyde + Norepinephrine; 2- Hexanal + Norepinephrine; 3- Benzaldehyde + Norepinephrine; 4- Isobutyraldehyde + Norepinephrine; 5- Norepinephrine; 6- Propionaldehyde + GABA; 7- Hexanal + GABA; 8- Benzaldehyde + GABA; 9- Isobutyraldehyde + GABA; 10- GABA; 11- Propionaldehyde + Tryptamine; 12- Hexanal + Tryptamine; 13- Benzaldehyde + Tryptamine; 14- Isobutyraldehyde + Tryptamine; 15- Tryptamine.
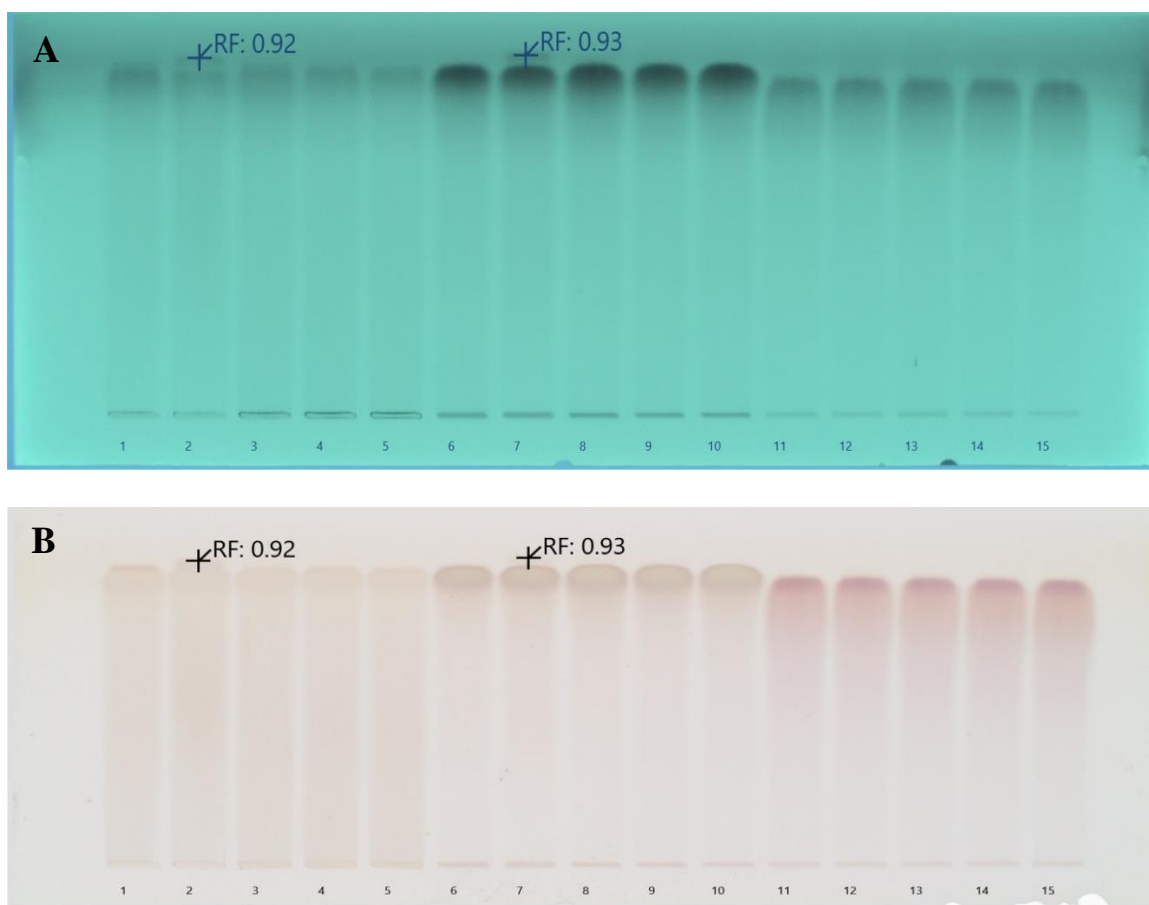
Figure 4.30: TLC plate (20cm×10cm), silica gel 60 F_{254S} for verification of a potential reactivity between dopamine, serotonin or epinephrine and aldehydes. Equimolar reaction (5 µM) at 37°C for 16 h. Mobile phase: ethyl acetate - acetic acid - methanol (8 : 2 : 2, v/v); sample application: 5 µL. (A) Plate visualized under UV light (254 nm); (B) Plate sprayed with a ninhydrin reagent, heated at 105°C for 5 min and visualized in white light.; 1- Propionaldehyde + dopamine; 2- Hexanal + dopamine; 3- Benzaldehyde + dopamine; 4- Isobutyraldehyde + dopamine; 5- Dopamine; 6- Propionaldehyde + Serotonin; 7- Hexanal + Serotonin; 8- Benzaldehyde + Serotonin; 9- Isobutyraldehyde + Serotonin; 10- Serotonin; 11- Propionaldehyde + Epinephrine; 12- Hexanal + Epinephrine; 13- Benzaldehyde + Epinephrine; 14- Isobutyraldehyde + Epinephrine; 15- Epinephrine.

4.4.2 Identification of reaction products by HPTLC/MS

The samples identified in section 4.4.1, p.144 for a positive reaction between an aldehyde and biogenic amines were applied on a MS TLC plate that was migrated in the same conditions; the spots corresponding to reaction products were localized under UV 254 nm. The plate was transferred to the TLC/MS interface and the marked spots were dialyzed one by one with 0.5 % formic acid in methanol for infusion in the mass spectrometer. After dialysis/infusion of all spots of interest, the plate was sprayed with ninhydrin to verify the correctness of spot localization. After subtracting the spectrum of a blank spot dialyzed in the same conditions, a specific mass was researched in the MS spectrum for each reaction, based on forecasted theorical reaction(s), taking in consideration that both the cyclic and acyclic reaction products may present the same mass. As our interest is focused on condensation reactions followed by spontaneous cyclization to produce β-carbolines or THIQ, further identification is then generally required.

- ✓ For the reactions with dopamine (Figure 4.31), 3 samples demonstrated the expected M^+H^+:
    - Dopamine + 5-hydroxymethylfurfural (Figure 4.32)
    - Dopamine + phenylacetaldehyde (Figure 4.33)
    - Dopamine + formaldehyde (Figure 4.34)

- ✓ For the reactions of reference aldehydes with serotonin (Figure 4.35), the expected M^+H^+ was not detected in any of analyzed spot.

- ✓ For the reactions of reference aldehydes with tryptamine (Figure 4.36), also a single sample yielded the expected M^+H^+:
    - Tryptamine + methylbutyraldehyde (Figure 4.37).

The major volatile aldehydes detected in GC-MS (Section 4.3.2.2, p.134) were also reacted with biogenic amines (Figure 4.38) and analyzed in the same conditions; the following samples confirmed the expected M^+H^+:

- Dopamine + hexanal (Figure 4.39)

151

- Serotonin + hexanal (Figure 4.40)

- Tryptamine + hexanal (Figure 4.41)

- Tryptamine + benzaldehyde (Figure 4.42)

As a result, 8 products of reaction were identified; we excluded 2 of them (*i*) the product of 5-hydroxymethylfurfural with dopamine, because we didn't detect this aldehyde in our extracts; and (*ii*) the product of formaldehyde with dopamine since a peak of formaldehyde is systematically detected in our procedural blanks[32]. In all, 6 products of reaction were selected for the continuation of the work (Table 4.19).

Table 4.19: Summary of the result of identification of artifact alkaloids of condensation of 8 carbonyl compounds with biogenic amines by TLC, the identify reaction were marked by + sign while the identified product was named, the products in white cells were excluded either it was not detected in extract or detected in blank procedure.

	Dopamine	Serotonin	Tryptamine	Tryptophan
Glycolaldehyde	+	+	+	-
5-Hydroxymethylfurfural	1-(5- hydroxy methyl furan)- THIQ- diol	+		
Glyceraldehyse	+	+		
Formaldehyde	THIQ- diol	+		
3-Methylthiopropioaldehyde	+			
2-methylbutyraldehyde	-	-	+	-
Isovaleraldehyde	-	-	-	+
Phenylacetaldehyde	1-benz-THIQ-diol	+	1-isobutyl DHβCa	-
Benzaldehyde	-		1-phenyl-DHβCa	-
Hexanal	1-pentyl-THIQ-diol	1-pentyl-THβCa-ol	1-pentyl-DHβCa	-

Considering the above reactions and comparing the size of the many aldehyde peaks in the various extracts we analyzed by chromatography and the result of in silico prediction (section 4.5 p.164), we decided to continue the work with 1-benzyl-1,2,3,4-tetrahydroisoquinoline-

---

[32] This aldehyde is a well-known environmental contaminant

6,7-diol (1-Benz-THIQ-diol), the product of condensation between dopamine and phenylacetaldehyde. Since further identification is needed to ensure that the detected product is effectively the cyclic alkaloid, and as we could not obtain enough product for NMR structure determination, we tried to find a commercial source for the putative reaction product. We could purchase the 1-Benz-THIQ-diol molecule and compare it to our reaction product by TLC then by HPTLC/MS; the Rf and mass spectra were practically identical, confirming the likely identity of our reaction product (Figure 4.43, Figure 4.44, Figure 4.45)
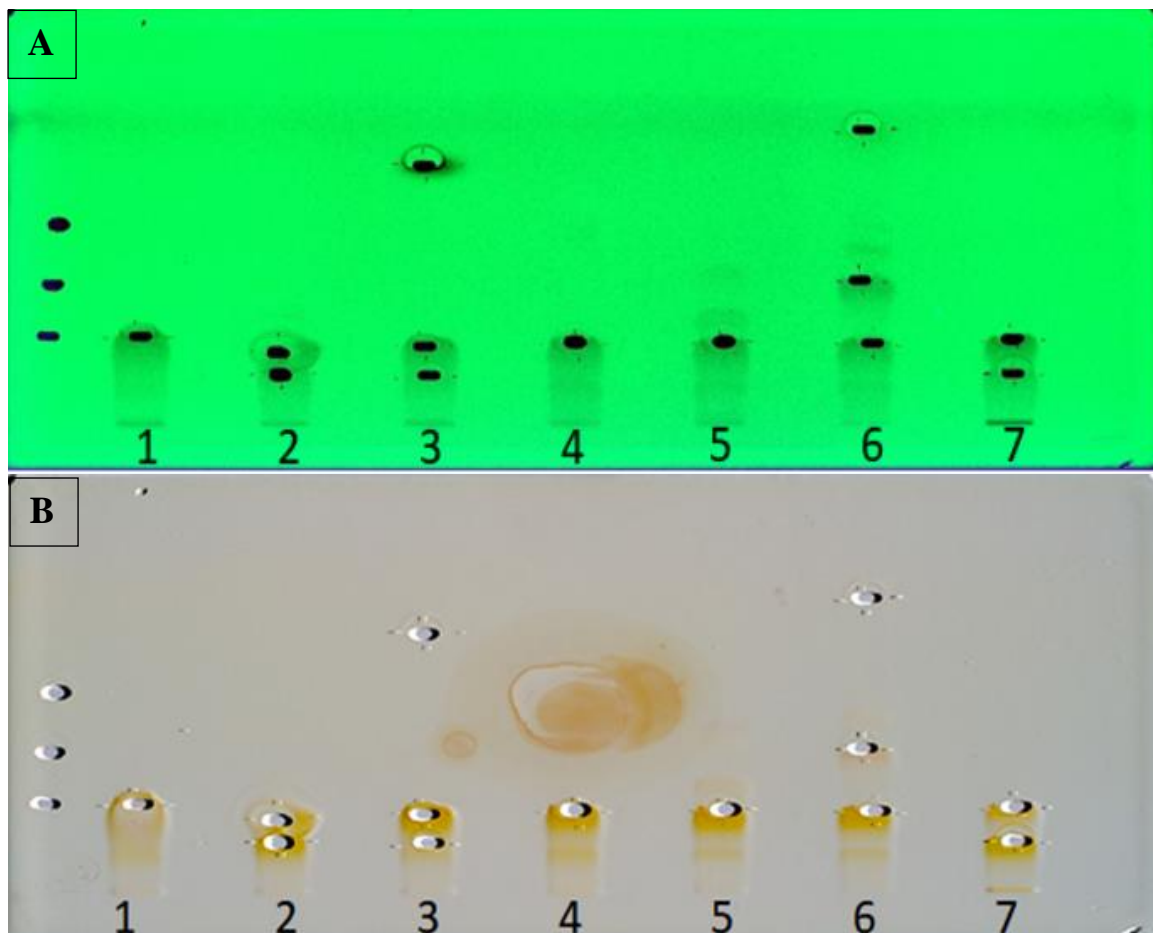
Figure 4.31: HPTLC/MS (20cm×10cm), silica gel 60 F_{254} grade silica plate for the reaction products of between dopamine and aldehydes. Equimolar reactions (50 µM) at 37°C for 16 h. Mobile phase: ethyl acetate - acetic acid - methanol (6 : 2 : 2, v/v); sample application: 5 µL. Plate visualized after spot elution (A) under UV light (254 nm), (B) under white light after spraying a ninhydrin reagent and heating at 105°C for 5 min. Dialyzed spots appear as ovoid holes. 1- Dopamine; 2- Dopamine + Glycolaldehyde; 3- Dopamine + 5-Hydroxymethylfurfural; 4- Dopamine + 3-Methylthiopropioaldehyde; 5- Dopamine + Glyceraldehyde; 6- Dopamine + Phenylacetaldehyde; 7- Dopamine + Formaldehyde.
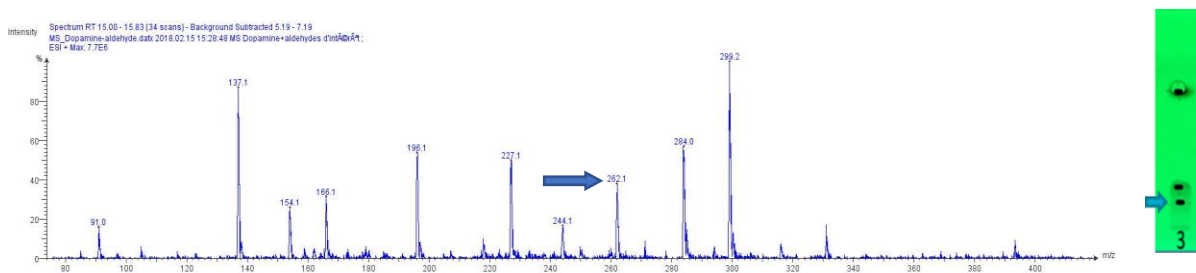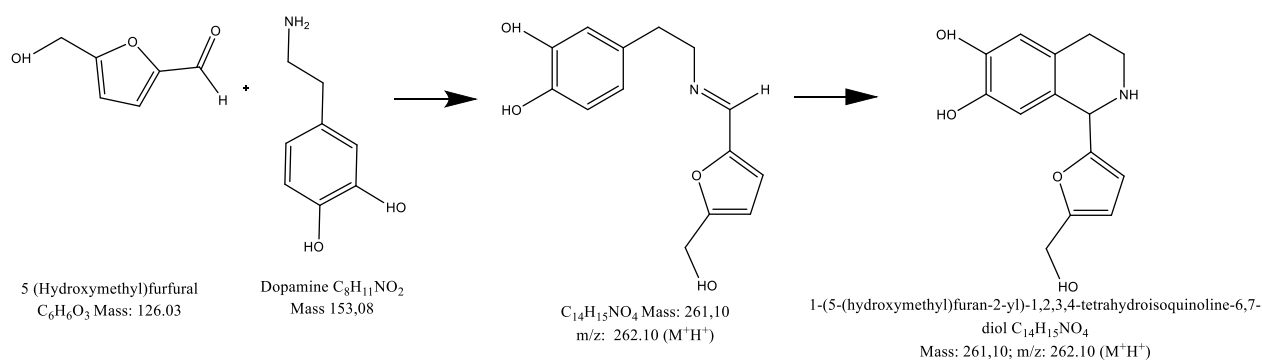
Figure 4.32: Expected reaction between dopamine and 5-hydroxymethylfurfural. Mass spectra obtained for the 1st spot of the reaction mixture on HPTLC plate indicates the presence of the expected m/z 262.1 (M+H+).
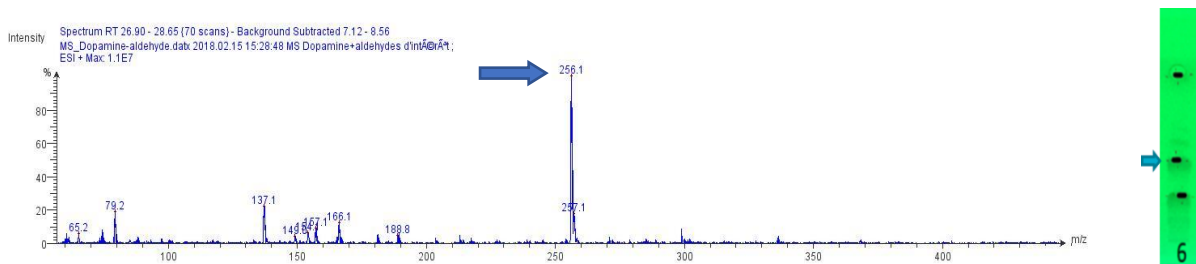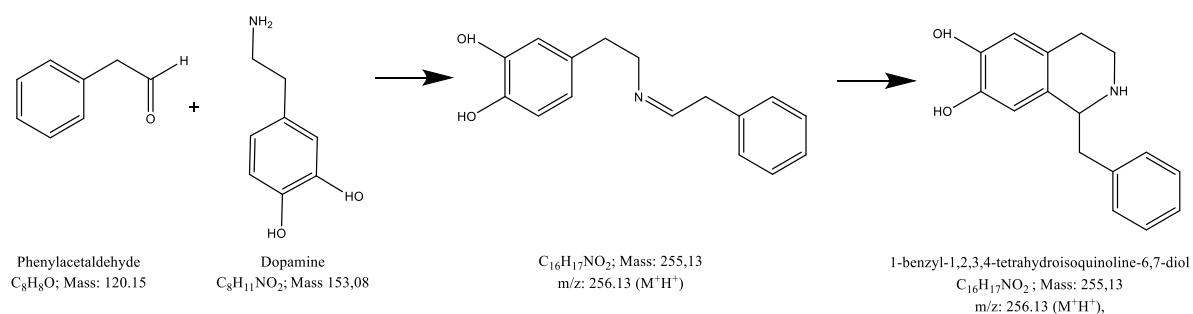
Figure 4.33: Expected reaction between dopamine and phenylacetaldehyde. Mass spectra obtained for the 2nd spot of the reaction mixture on HPTLC plate indicates the presence of the expected m/z 256.1 (M+H+).
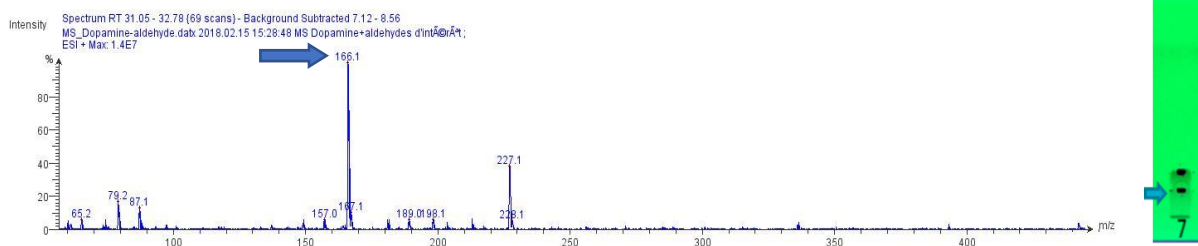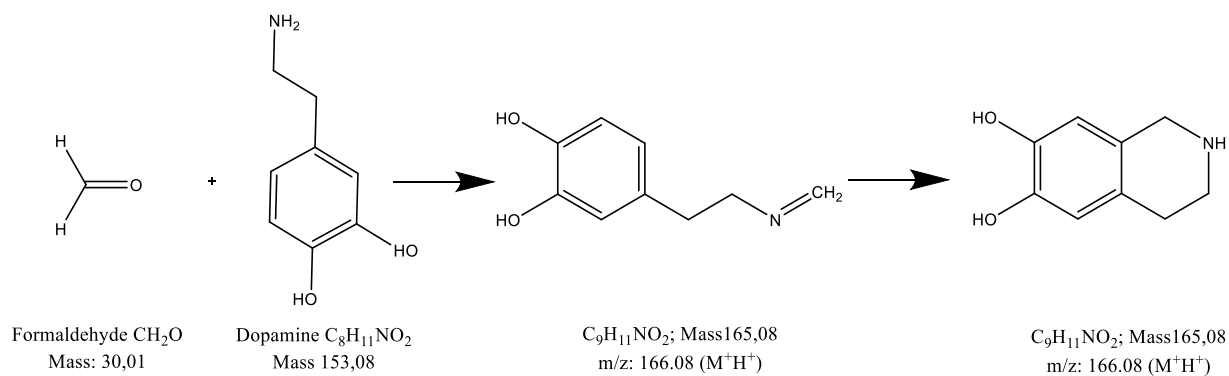
Figure 4.34: Expected reaction between dopamine and formaldehyde. Mass spectra for the 1st and 2nd spots of the reaction mixture on HPTLC plate indicates the presence of the expected m/z 166.1 (M^+H^+).
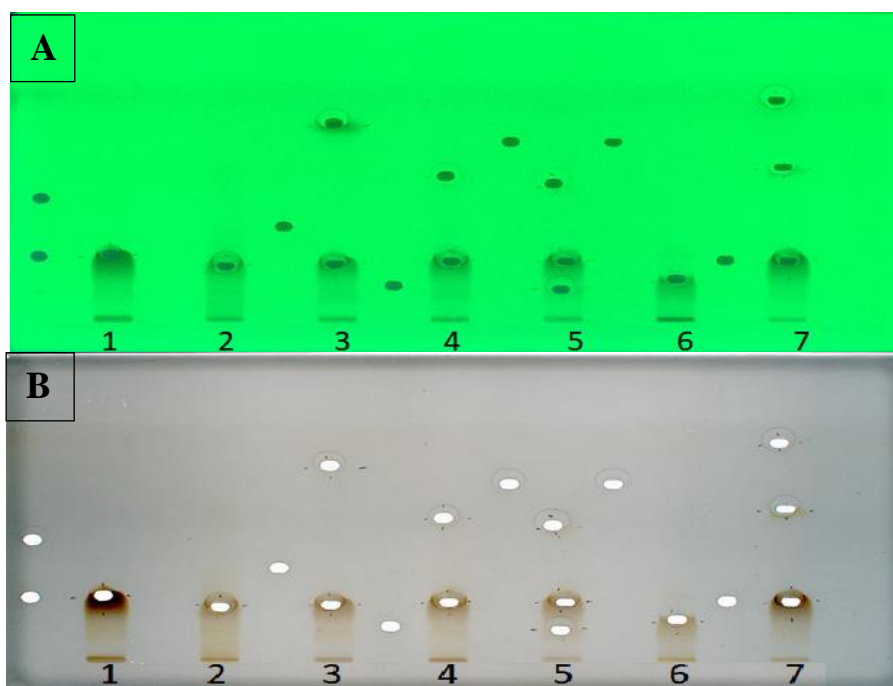
Figure 4.35: HPTLC/MS grade plate (20cm×10cm), silica gel 60 F_{254}, for the reaction products of between serotonin and aldehydes. Equimolar reactions (50 µM) at 37°C for 16 h. Mobile phase: ethyl acetate - acetic acid - methanol (6 : 2 : 2, v/v); sample application: 5 µL. Plate visualized after spot elution (A) under UV light (254 nm), (B) under white light after spraying a ninhydrin reagent and heating at 105°C for 5 min. Dialyzed spots appear as ovoid holes. 1- Serotonin; 2- Serotonin + Glycolaldehyde; 3- Serotonin +5 Hydroxymethylfurfural; 4- Serotonin + 3-Methylthiopropioaldehyde; 5- Serotonin + Glyceraldehyde; 6- Serotonin + Phenylacetaldehyde; 7- Serotonin + Formaldehyde.

155
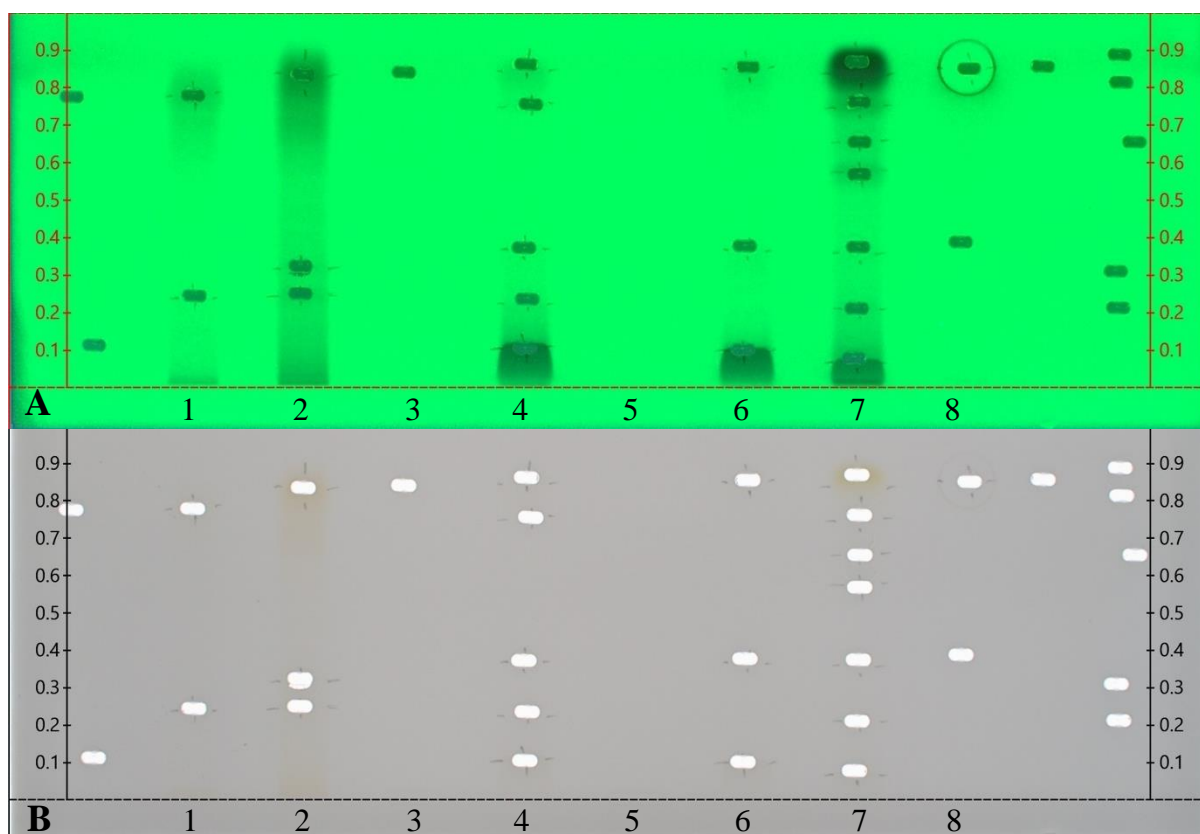
Figure 4.36: HPTLC/MS grade plate (20cm×10cm), silica gel 60 F_{254}, for the reaction products between tryptamine and aldehydes. Equimolar reactions (50 µM) at 37°C for 16 h. Mobile phase: ethyl acetate - acetic acid - methanol (8 : 2 : 2, v/v); sample application: 5 μL. Plate visualized after spot elution (A) under UV light (254 nm), (B) under white light after spraying a ninhydrin reagent and heating at 105°C for 5 min. Dialyzed spots appear as ovoid holes.

1- Tryptamine + Glycolaldehyde; 2- Tryptamine + Glycolaldehyde; 3- Glycolaldehyde; 4- Tryptamine + 2-methylbutyraldehyde; 5- 2- methylbutyraldehyde; 6- Tryptamine; 7- Tryptamine + Phenylacetaldehyde; 8- Phenylacetaldehyde.
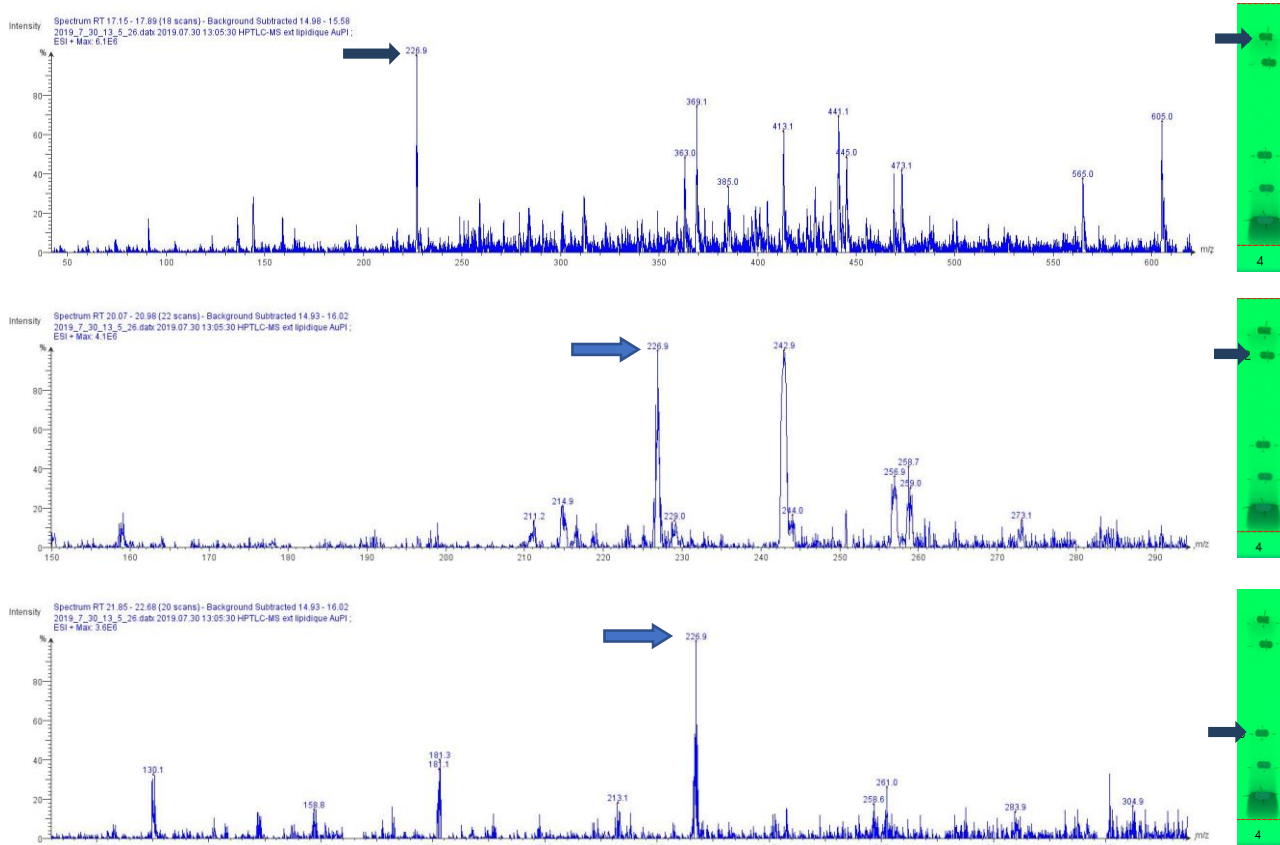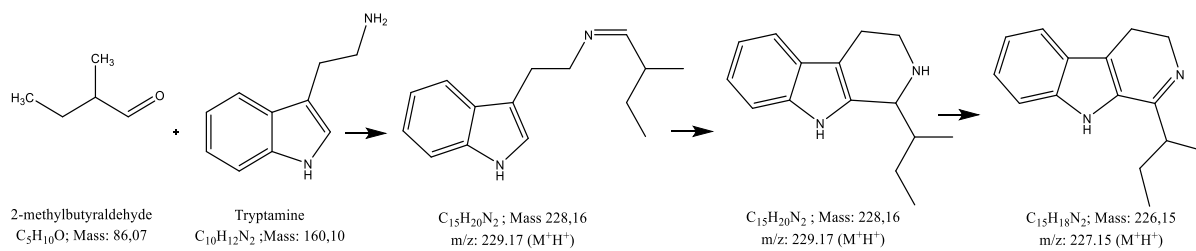
Figure 4.37: Expected reaction between methylbutyraldehyde and tryptamine. Mass spectra for the 1st, 2nd, and 3rd spots of the reaction mixture on HPTLC plate indicate the presence of the expected m/z 226.9 (M$^+$H$^+$).
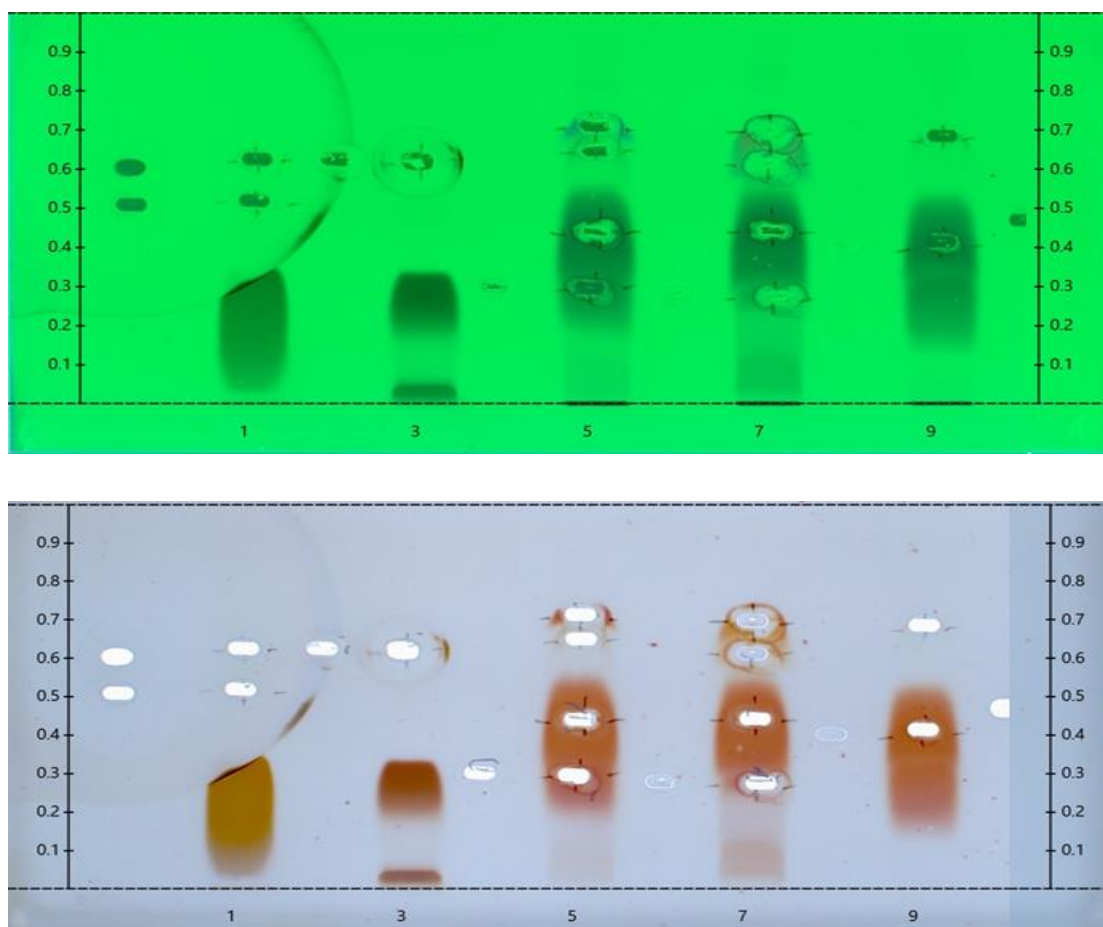
Figure 4.38: HPTLC/MS grade plate (20cm×10cm), silica gel 60 F_{254}, for the reaction products between volatile aldehydes and neurotransmitters. Equimolar reactions (50 µM) at 37°C for 16 h. Mobile phase: ethyl acetate - acetic acid - methanol (6 : 2 : 2, v/v); sample application: 5 µL. Plate visualized after spot elution (A) under UV light (254 nm), (B) under white light after spraying a ninhydrin reagent and heating at 105°C for 5 min. Dialyzed spots appear as ovoid holes.1-Hexanal + Dopamine; 3- Hexanal+ serotonin; 5-Hexanal + tryptamine; 7- Benzaldehyde + tryptamine; 9- tryptamine
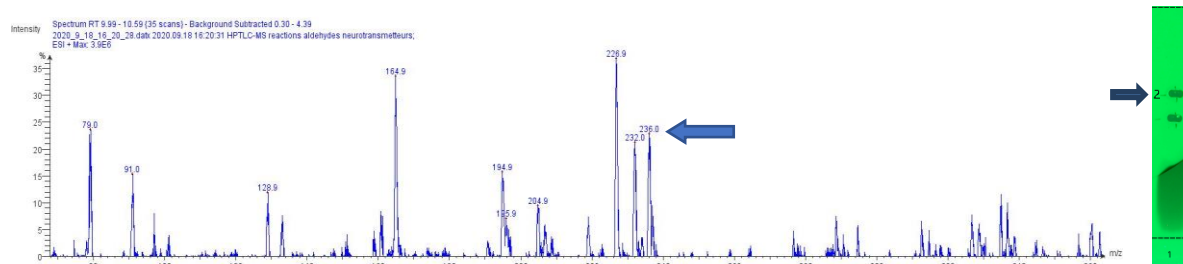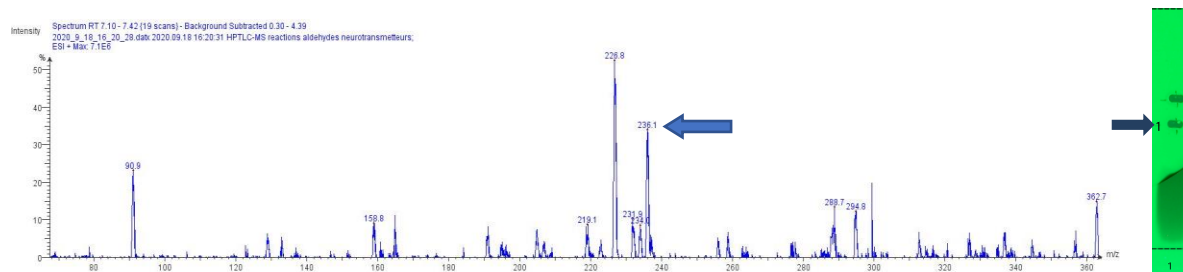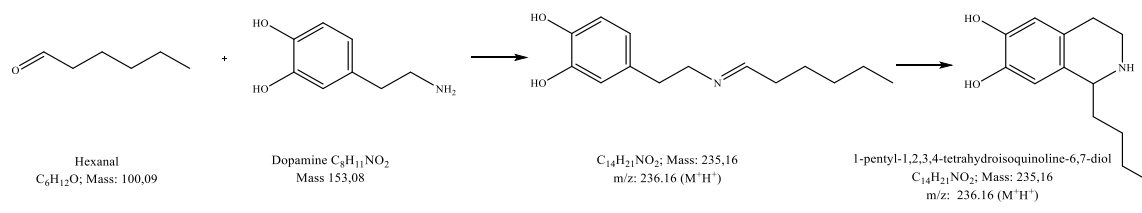
Figure 4.39: Expected reaction between dopamine and hexanal. Mass spectrum for the 1st and 2nd spots of the reaction mixture on HPTLC plate indicate the presence of the expected m/z 236.1 (M$^+$H$^+$).
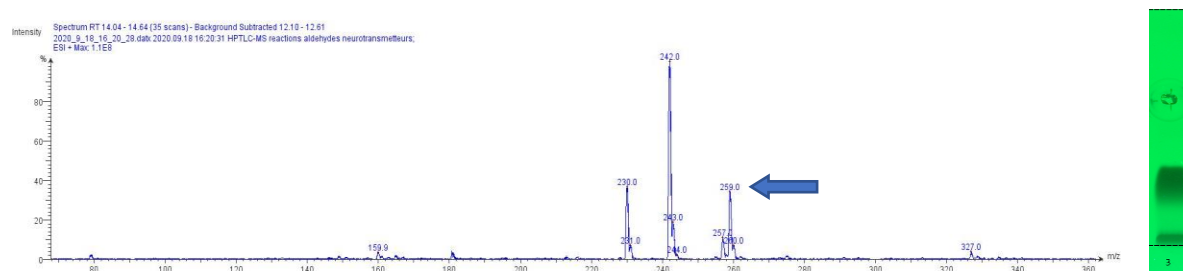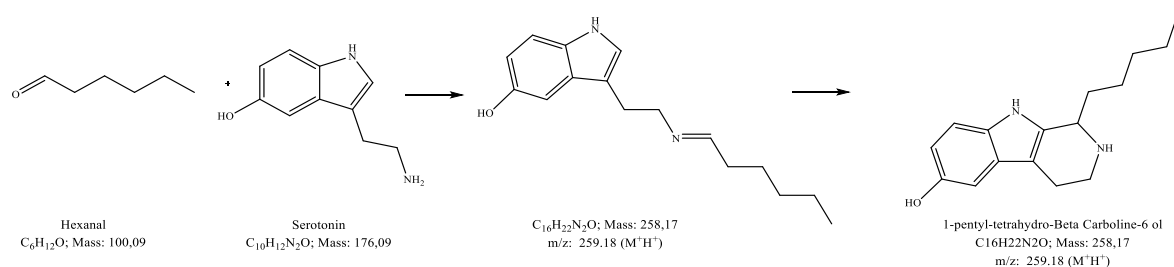
Figure 4.40: Expected reaction between serotonin and hexanal. Mass spectra for the spot of the reaction mixture on HPTLC plate indicates the presence of the expected m/z 259 (M$^+$H$^+$).
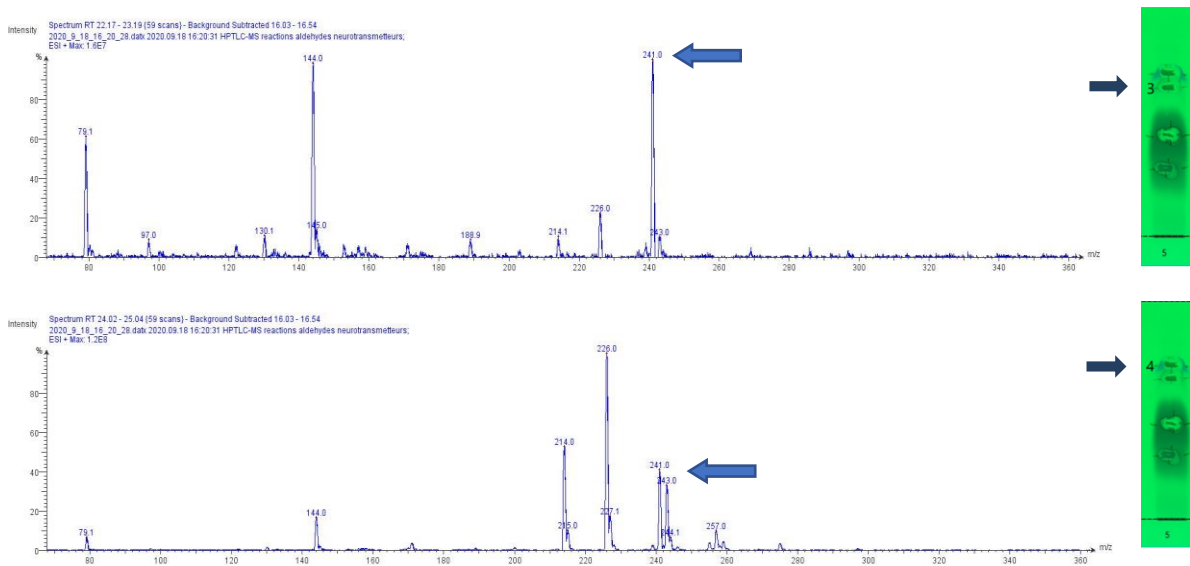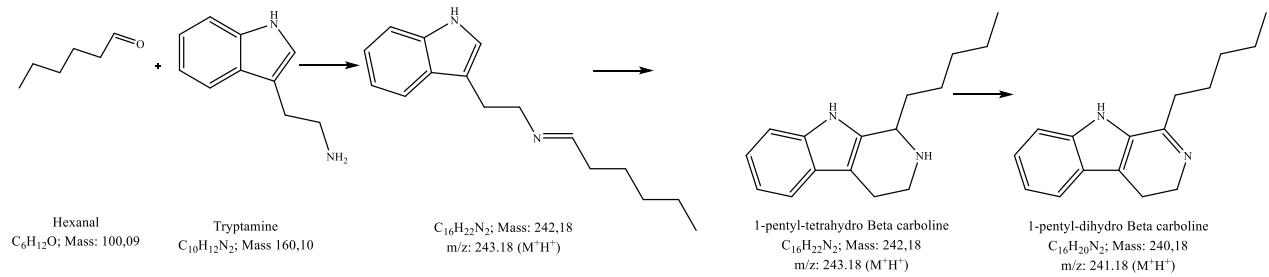
Figure 4.41: Expected reaction between tryptamine and hexanal. Mass spectra for the 3rd, and 4th spots of the reaction mixture on HPTLC plate indicate the presence of the expected m/z 241 (M+H+).
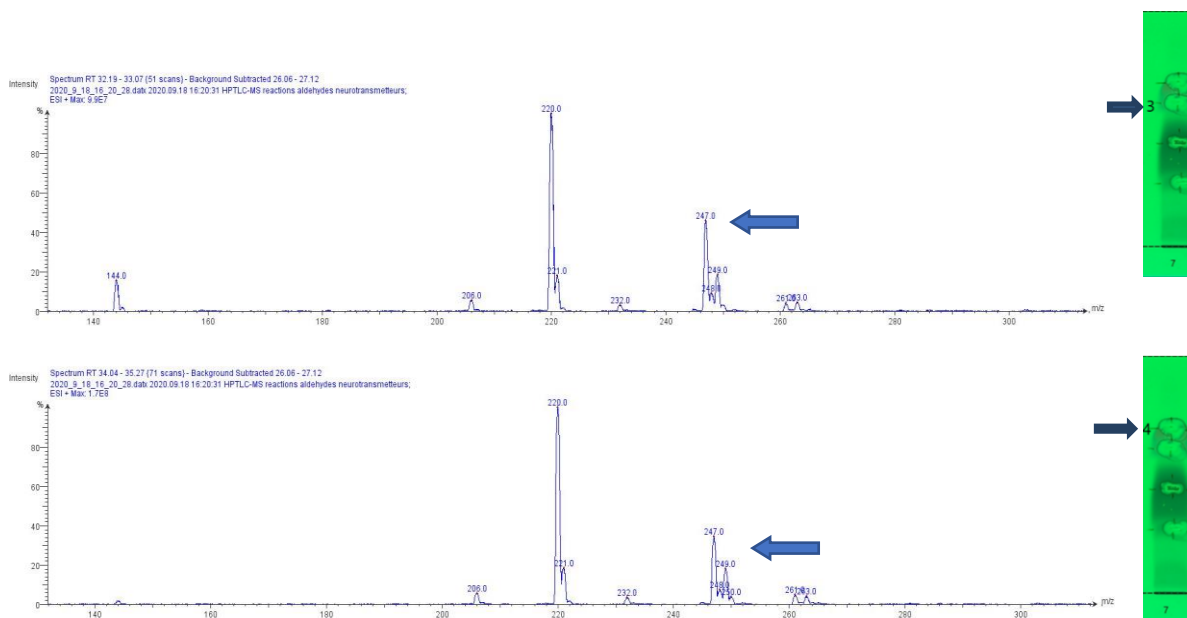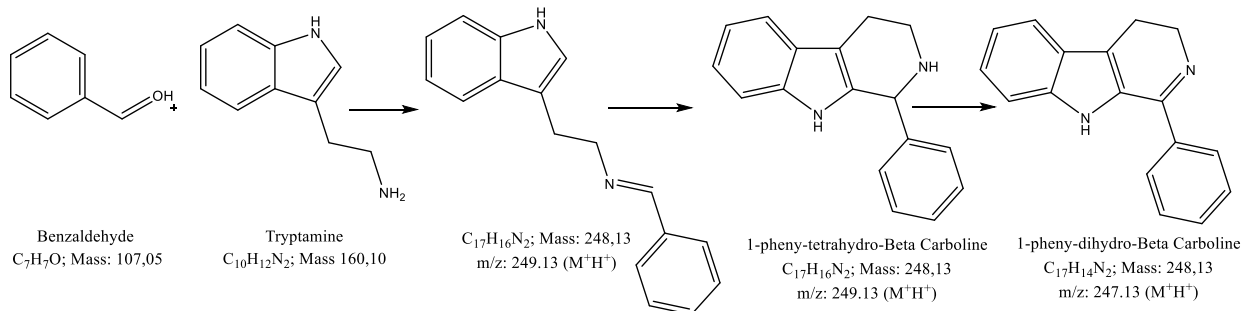
Figure 4.42: Expected reaction between tryptamine and benzaldehyde. Mass spectra for the 3rd, and 4th spots of the reaction mixture on HPTLC plate indicate the presence of the expected m/z 247 (M+H+).

A   **B**   **C**
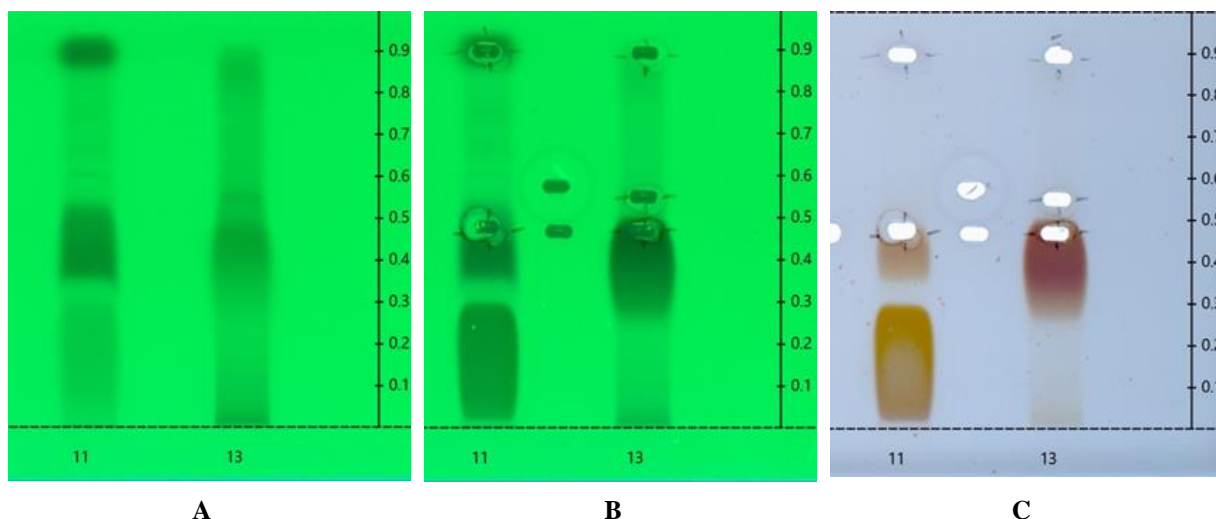
Figure 4.43: HPTLC/MS grade plate (20cm×10cm), silica gel 60 F_{254} for the comparison of the product of reaction between dopamine and phenylacetaldehyde to commercial 1-benzyl-1,2,3,4-tetrahydroisoquinoline-6,7-diol. Equimolar reactions (50 µM) at 37°C for 16 h. Mobile phase: ethyl acetate - acetic acid - methanol (6 : 2 : 2, v/v); sample application: 5 µL. Plate visualized before spot elution (A) under UV light (254 nm (B) under UV light (254 nm)) and after spot elution, (C) under white light after spraying a ninhydrin reagent and heating at 105°C for 5 min. Dialyzed spots appear as ovoid holes. 11- Phenylacetaldehyde + Dopamine; 13- commercial 1-benzyl-1,2,3,4-tetrahydroisoquinoline-6,7-diol
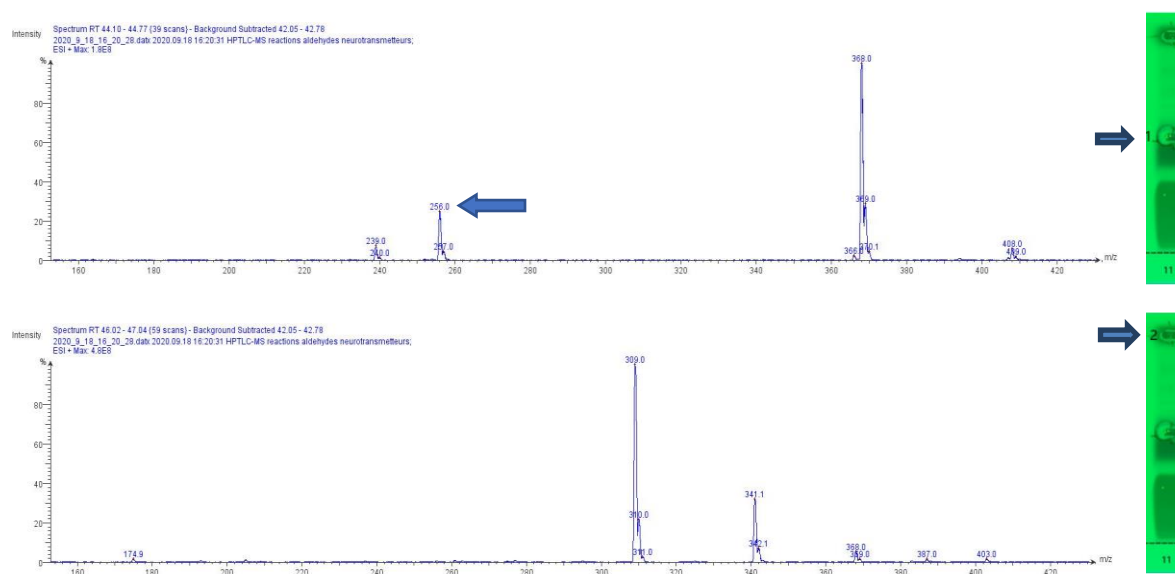
Figure 4.44 Mass spectra for the 1st and 2nd spots of the reaction mixture of Phenylacetaldehyde + Dopamine on HPTLC plate indicate the presence of the expected m/z 256 (M^+H^+) in the 1st spot.

162
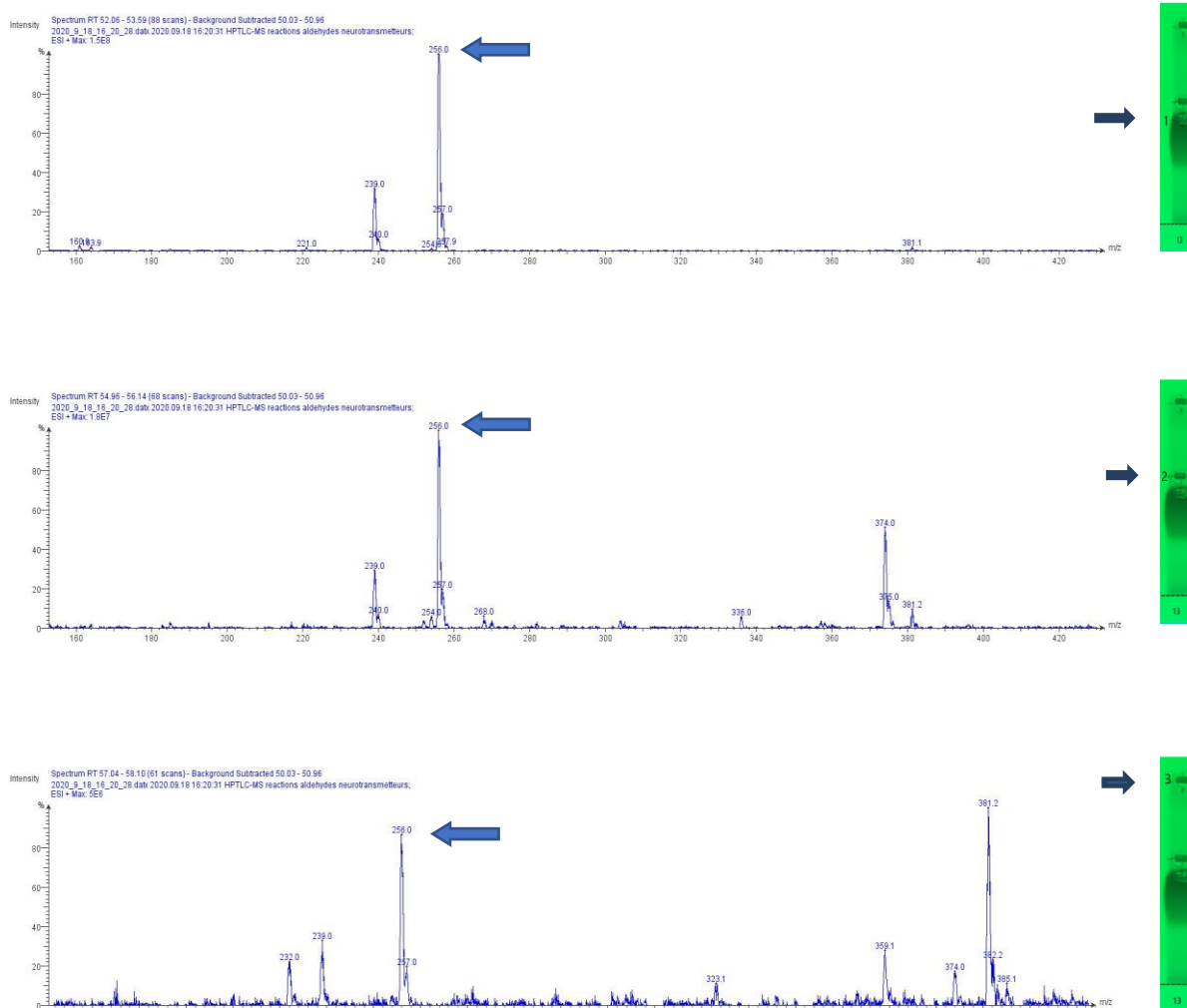
Figure 4.45: The mass spectra for the 3 spots obtained for commercial 1-benzyl-1,2,3,4-tetrahydroisoquinoline-6,7-diol indicate the presence of the expected m/z 256 (M^+H^+) in three spots, indicating the instability of the molecule, however the spectrum of 1st spot is the clearer.

4.5 *In-silico* prediction of neurotoxicity or neuroprotection effect

The *in-silico* prediction of toxicity was applied on the seven compounds, harmane and the selected compounds in section 4.4.2, p.151 and listed in Table 4.19; the smile formats were defined for all products (Table 4.20) as described in Section 3.2.5.1, p.93.

Table 4.20: List of selected compounds for *in-silico* studies

Compound	SMILE format	CAS number	Molecule depiction
Harmane	Cc2nccc3c1ccccc1[nH]c23	486-84-0	
1-Benz-6,7-diol-THIQ	Oc3cc2CCNC(Cc1ccccc1)c2cc3O	14919-82-5	
1-Isobutyl-DHβCa	CCC(C)/C1=N/CCc2c1[nH]c3ccccc23	1042288-34-5	
1-Pentyl-THIQ-diol	CCCCCC2NCCc1cc(O)c(O)cc12	392334-24-6	
1-Pentyl-THβCa-ol	CCCCCC1NCCc2c1[nH]c3ccc(O)cc23	2520628-82-2	
1-Pentyl-DHβCa	CCCCC/C1=N/CCc2c1[nH]c3ccccc23	n.a.	
1-Phenyl-DHβCa	c4ccc(/C1=N/CCc2c1[nH]c3ccccc23)cc4	10022-79-4	

4.5.1 *In-silico* prediction with eMolTox

The *in-silico* study was started with eMolTox web server[33], the compounds were transformed to smile format (Table 4.20), then the format inserted in the step 1 on eMolTox web server page and was asked for CNS toxic prediction from step 2.

Summary tables of results from the eMolTox database are listed[34] in Table 4.21 and

Table 4.22; the positive outcomes predicted for tested compounds are listed below:

✓ Harmane does not present a CNS toxic effect, based on eMolTox database. Its logP[35] is estimated at 3.025, indicating an ability to cross membranes and reach the central nervous system.

✓ 1-Benz-THIQ-diol: toxicity prediction defined a possible modulation of dopamine D1 receptor that might cause an injury to central nervous system, kidney and heart at p = 0.999 confidence. This is probably an inference from the catechol C_6-C_2-N structure.

✓ 1-Isobutyl-DhβCa is suggested to modulate adrenergic receptors α-2A and α-2B, in addition to serotonin 2b receptor. The injury affects the CNS and nervous system subsequently with 0.990 confidence.

✓ 1-Pentyl-THIQ-diol potentially modulates dopamine D1 and serotonin 1b receptors with 0.990 confidence. This is also probably an inference from the catechol C_6-C_2-N structure.

✓ 1-Pentyl-ThβCa-ol is predicted to modulate dopamine D1 and serotonin 1b receptors with confidence of 0.994 and 0.990

✓ 1-Pentyl-DhβCa is suggested to modulate adrenergic receptors α-2a and α-2b of the nervous system with confidence of 0.990.

---

[33] http://xundrug.cn/moltox/silicotox
[34] these tables do not present *(i)* the raw data corresponding to negative outcomes for all compounds; and *(ii)* the list of similarly structural compounds on which the prediction is based (complete data are available in Annex 4 section 8.4, p.265)
[35] LogP is the partition coefficient of a substance between an aqueous phase and a lipid phase. A negative value for logP means the compound has a higher affinity for the aqueous phase; when logP = 0 the compound is equally partitioned between the lipid and aqueous phases; a positive value for logP denotes a higher concentration in the lipid phase

✓ 1-Phenyl-DhβCa has a potential toxicity on nervous system with confidence of 0.980 by modulating the serotonin 2b receptor.

4.5.2 *In-silico* prediction with pkCSM

The *in-silico* prediction of pharmacokinetic properties (ADMET, i.e., absorption, distribution, metabolism, excretion and toxicity) was obtained from the pkCSM web server[36] for all compounds (Table 4.23), and below are the main prediction outcomes for absorption, distribution and toxicity:

1- Absorption:

All molecules are not water soluble (negative result for log S), which affects the absorption, but very well absorbed from the human intestine (Caco2 > 0.9 and intestinal absorption > 30 %). However, they are likely to be substrates of the P-glycoprotein.

2- Distribution:

All molecules are likely to present a high volume of distribution in tissue vs plasma (log VDss > 0.45), except 1-Phenyl-DhβCa but it is still not considered as low (log VDss < -0.15). On other hand, the fraction unbound to serum proteins is lower than the bound one, which negatively affects the cellular membrane diffusion or transport. Moreover, only harmane and 1-phenyl-DhβCa are considered readily to cross the blood brain barrier with log BB > 0.3. Although the CNS permeability factor, that takes in consideration the compound surface area, indicates that all compounds can penetrate (log PS > -2); 1-Benz-THIQ-diol and 1-pentyl-THIQ-diol are however less able to penetrate the CNS with (-3 < logPS < -2)[37].

3- Toxicity

The prediction of toxicity in pkCSM (
Table 4.23) assesses the mutagenic effects of molecules (AMES mutagenicity test), the toxic concentration (max recommended tolerated dose MRTD), lethal dosage (rat LD_{50}) for acute administration, lethal concentration LC_{50} (minnow toxicity), the

---

[36] http://biosig.unimelb.edu.au/pkcsm
[37] Compounds with Log PS < -3 are unable to enter the CNS

concentration to inhibit 50 % of *Tetrahymena pyriformis* growth (IGC50), the lowest observed adverse effect (LOADL) in rat by oral chronic administration, the risk of long QT syndrome induction, that results from the inhibition of potassium channels, represented by Herg, the hepatotoxicity and the skin sensitization; pkCSM however does not assess the neurotoxicity.

4.5.3 *In silico* screening with PubChem

The next step was the search of the molecules on PubChem[38]:

- ✓ Harmane is described *(i)* in the *"pharmacology and biochemistry"* sections, as mutagen and neurotoxin; *(ii)* in the *"toxicity"* section, harmane demonstrated behavioral altered sleep time when administered intraperitoneally; and *(iii)* in the *"associated disorders and diseases"* section, harmane is implied in neurodegenerative diseases and tremor [354]. As a result, the molecule is implicated in our area of interest (neurodegenerative diseases), but there is a paucity of data about its biological effects; for that, the investigation on such effects is needed for this compound.
- ✓ The search for 1-Benz-THIQ-diol in the section *"biological test results"* demonstrates that the molecule presents a binding affinity towards D2 and D1 dopamine receptors but at different concentrations, as shown in rat striatal synaptosomes [355] This affinity could explain a D1, D2 dopaminergic antagonist effect [356]. Knowing that dopamine antagonist agents are known to induce parkinsonism, dystonia, tics and tremor [357, 358], accordingly the compound was selected for further investigations.
- ✓ 1-Pentyl-THIQ-diol- presents in the *'literature'* section one article investigating the antimicrobial, antimalarial, cytotoxic, and anti-HIV potentiality of isoquinoline and benzylisoquinoline alkaloids [359].
- ✓ The search of 1-Phenyl-DhβCa demonstrates in *"biological test results"* section an antimicrobial activity [360].
- ✓ 1-Isobutyl-DhβCa, 1-Pentyl-6-ol-THβCa and 1-Pentyl-DHβCa do not exist in the PubChem database.

Table 4.21: eMolTOX profiles for Harmane, 1-Benz-THIQ-diol and 1- isobutyl-DHβCa

Action	Injury	Harmane		1-Benz-THIQ-diol		1-Isobutyl - DHβCa	
		Outcome	Confidence	Outcome	Confidence	Outcome	Confidence
Antagonist of the androgen receptor (AR) signaling pathway	Endocrine, Central nervous system	Inconclusive	0	Inconclusive	0	Inconclusive	0
Modulator of Dopamine D1 receptor	Central nervous system, Kidney, Heart	Negative	0.986	Positive	1	Inconclusive	0
Modulator of Histamine H1 receptor	Immune, Nervous system, Heart, Gastrointestinal	Negative	0.994	Negative	0.999	Negative	0.989
Modulator of GABA-A receptor; alpha-1/beta-3/gamma-2	Central nervous system	Inconclusive	0	Negative	0.994	Inconclusive	0
Modulator of Serotonin 7 (5-HT7) receptor	Nervous system, immune	Negative	0.993	Negative	0.994	Negative	0.983
Modulator of Neuronal acetylcholine receptor protein α-7 subunit	Central nervous system	Inconclusive	0	Inconclusive	0	Inconclusive	0
Modulator of Neuronal acetylcholine receptor; alpha3/beta4	Central nervous system	Negative	0.987	Negative	0.996	Inconclusive	0
Modulator of Alpha-2a adrenergic receptor	Heart, Nervous system, GI, pancreas	Inconclusive	0	Inconclusive	0	Positive	0.998
Modulator of Serotonin 2b (5-HT2b) receptor	Heart, Nervous system, Gastrointestinal	Inconclusive	0	Inconclusive	0	Positive	0.996
Modulator of Glutamate NMDA receptor	Central nervous system	Negative	0.983	Negative	0.986	Inconclusive	0
Modulator of Muscarinic acetylcholine receptor M5	Nervous system	Negative	0.994	Negative	0.989	Inconclusive	0
Modulator of Mu opioid receptor	NS, respiratory, GI, Heart, pancreas, Kidney	Negative	0.999	Negative	1.000	Negative	0.998
Antagonist of the glucocorticoid receptor (GR) signaling pathway	Endocrine, immune, Nervous system	Inconclusive	0	Inconclusive	0	Inconclusive	0
Modulator of Serotonin 3a (5-HT3a) receptor	Gastrointestinal, Heart, CNS	Inconclusive	0	Negative	0.989	Inconclusive	0
Agonist of the androgen receptor (AR) signaling pathway	Endocrine, Central nervous system	Inconclusive	0	Inconclusive	0	Negative	0.992
Modulator of Serotonin 2c (5-HT2c) receptor	Nervous system	Negative	0.986	Negative	0.992	Positive	0.980
Modulator of Dopamine transporter	Nervous system	Negative	0.998	Negative	0.984	Inconclusive	0
Modulator of Neuronal acetylcholine receptor protein α-4 subunit	Central nervous system	Inconclusive	0	Inconclusive	0	Negative	0.995
Modulator of GABA-A receptor; anion channel	Central nervous system	Negative	0.990	Inconclusive	0	Negative	0.993
Activator Alzheimer's amyloid precursor	Central nervous system	Inconclusive	0	Inconclusive	0	Inconclusive	0
Modulator of Alpha-2b adrenergic receptor	Heart, Nervous system	Inconclusive	0	Inconclusive	0	Positive	0.996
Modulator of GABA-A receptor; alpha-3/beta-3/gamma-2	Central nervous system	Negative	1.000	Negative	0.996	Inconclusive	0
Modulator of Serotonin 1b (5-HT1b) receptor	Nervous system, Heart	Negative	0.981	Negative	0.997	Inconclusive	0
Modulator of Sigma opioid receptor	Nervous system	Negative	0.997	Inconclusive	0	Negative	0.995
Modulator of Serotonin 1a (5-HT1a) receptor	Nervous system, Heart, endocrine	Negative	0.998	Negative	0.999	Negative	0.990
Modulator of Serotonin 2a (5-HT2a) receptor	Nervous system, blood, Heart	Inconclusive	0	Negative	0.996	Inconclusive	0
Modulator of Norepinephrine transporter	Heart, Nervous system	Negative	0.998	Negative	0.986	Inconclusive	0
Modulator of Monoamine oxidase A	Pharmaco-kinetics, Central nervous system	Inconclusive	0	Inconclusive	0	Inconclusive	0
Antagonist of the androgen receptor (AR) signaling pathway	Endocrine, Central nervous system	Inconclusive	0	Inconclusive	0	Inconclusive	0
Modulator of Serotonin transporter	CNS, blood, Heart, Gastrointestinal	Negative	0.997	Negative	0.996	Inconclusive	0
Modulator of GABA-A receptor; anion channel	Central nervous system	Negative	0.981	Negative	0.994	Inconclusive	0
Agonist of the glucocorticoid receptor (GR) signaling pathway	Endocrine, immune, Nervous system	Inconclusive	0	Inconclusive	0	Inconclusive	0

Table 4.22: eMolTOX profiles for 1-Pentyl-THIQ-diol, 1-Pentyl-THβCa-ol, 1-Pentyl-DhβCa, and 1-Phenyl-DhβCa

Action	Injury	1-Pentyl-THIQ-diol		1-Pentyl-THβCa-ol		1-Pentyl-DHβCa		1-Phenyl-DHβCa	
		Outcome	Conf.	Outcome	Conf.	Outcome	Conf.	Outcome	Conf.
Antagonist of the AR signaling pathway	Endocrine, Central nervous system	Inconclusive	0	Inconclusive	0	Inconclusive	0	Inconclusive	0
Modulator of Dopamine D1 receptor	Central nervous system, Kidney, Heart	Positive	0.998	Positive	0.995	Inconclusive	0	Inconclusive	0
Modulator of Histamine H1 receptor	Immune, Nervous system, Heart, GI	Negative	0.996	Negative	0.999	Inconclusive	0	Inconclusive	0
Modulator of GABA-A receptor; α-1/β-3/γ-2	Central nervous system	Negative	0.996	Inconclusive	0	Inconclusive	0	Inconclusive	0
Modulator of Serotonin 7 (5-HT7) receptor	Nervous system, immune	Negative	0.997	Inconclusive	0	Inconclusive	0	Inconclusive	0
Modulator of Neuronal AChR protein α-7 subunit	Central nervous system	Inconclusive	0	Inconclusive	0	Inconclusive	0	Inconclusive	0
Modulator of Neuronal acetylcholine receptor; α3/β4	Central nervous system	Inconclusive	0	Negative	0.983	Inconclusive	0	Negative	0.987
Modulator of Alpha-2a adrenergic receptor	Heart, Nervous system, GI, pancreas	Inconclusive	0	Inconclusive	0	Positive	0.988	Inconclusive	0
Modulator of Serotonin 2b (5-HT2b) receptor	Heart, Nervous system, Gastrointestinal	Inconclusive	0	Inconclusive	0	Inconclusive	0	Inconclusive	0
Modulator of Glutamate NMDA receptor	Central nervous system	Inconclusive	0	Inconclusive	0	Negative	0.984	Inconclusive	0
Modulator of Muscarinic acetylcholine receptor M5	Nervous system	Negative	0.986	Inconclusive	0	Inconclusive	0	Inconclusive	0
Modulator of Mu opioid receptor	NS, respiratory, GI, Heart, pancreas, Kidney	Negative	1.000	Inconclusive	0	Negative	0.999	Negative	1
Antagonist of the GR signaling pathway	Endocrine, immune, Nervous system	Inconclusive	0	Inconclusive	0	Inconclusive	0	Inconclusive	0
Modulator of Serotonin 3a (5-HT3a) receptor	Gastrointestinal, Heart, CNS	Negative	0.988	Inconclusive	0	Inconclusive	0	Inconclusive	0
Agonist of the androgen receptor signaling pathway	Endocrine, Central nervous system	Inconclusive	0	Inconclusive	0	Negative	0.998	Inconclusive	0
Modulator of Serotonin 2c (5-HT2c) receptor	Nervous system	Negative	0.993	Inconclusive	0	Inconclusive	0	Inconclusive	0
Modulator of Dopamine transporter	Nervous system	Negative	0.983	Inconclusive	0	Inconclusive	0	Inconclusive	0
Modulator of Neuronal ACh protein α-4 subunit	Central nervous system	Inconclusive	0	Inconclusive	0	Negative	0.991	Inconclusive	0
Modulator of GABA-A receptor; anion channel	Central nervous system	Inconclusive	0	Negative	0.996	Negative	0.984	Inconclusive	0
Activator Alzheimer's amyloid precursor	Central nervous system	Inconclusive	0	Inconclusive	0	Inconclusive	0	Positive	0.984
Modulator of Alpha-2b adrenergic receptor	Heart, Nervous system	Inconclusive	0	Inconclusive	0	Positive	0.987	Positive	0.984
Modulator of GABA-A receptor; α-3/β-3/γ-2	Central nervous system	Negative	0.995	Negative	0.993	Negative	0.98	Negative	0.981
Modulator of Serotonin 1b (5-HT1b) receptor	Nervous system, Heart	Negative	0.983	Positive	0.989	Inconclusive	0	Inconclusive	0
Modulator of Sigma opioid receptor	Nervous system	Negative	0.994	Inconclusive	0	Inconclusive	0	Negative	0.984
Modulator of Serotonin 1a (5-HT1a) receptor	Nervous system, Heart, endocrine	Negative	0.996	Inconclusive	0	Negative	0.99	Negative	0.991
Modulator of Serotonin 2a (5-HT2a) receptor	Nervous system, blood, Heart	Negative	0.987	Inconclusive	0	Inconclusive	0	Inconclusive	0
Modulator of Norepinephrine transporter	Heart, Nervous system	Negative	0.989	Inconclusive	0	Inconclusive	0	Negative	0.983
Modulator of Monoamine oxidase A	Pharmaco-kinetics, CNS	Inconclusive	0	Inconclusive	0	Inconclusive	0	Inconclusive	0
Antagonist of the AR signaling pathway	Endocrine, Central nervous system	Inconclusive	0	Inconclusive	0	Inconclusive	0	Inconclusive	0
Modulator of Serotonin transporter	CNS, blood, Heart, Gastrointestinal	Negative	0.996	Negative	0.988	Inconclusive	0	Inconclusive	0
Modulator of GABA-A receptor; anion channel	Central nervous system	Negative	0.992	Negative	0.989	Inconclusive	0	Inconclusive	0
Agonist of the GR signaling pathway	Endocrine, immune, Nervous system	Inconclusive	0	Inconclusive	0	Inconclusive	0	Inconclusive	0

Table 4.23: ADMET profiles for the 7 selected compounds based on pkCSM prediction

Property	Model Name	Unit	Harmane	1-Benz-THIQ-diol	1-Isobutyl THβCa	1-Isobutyl DHβCa	1-Pentyl-THIQ-diol	1-Pentyl-ThβCa-ol	1-Pentyl-DHβCa	1-Phenyl DHβCa
Absorption	Water solubility	Numeric (log mol/L)	-3.326	-3.096	-3.226	-4.06	-2.243	-3.159	-4.453	-4.364
	Caco2 permeability	Numeric (log Papp in 10-6 cm/s)	1.467	1.205	1.416	1.436	1.244	1.268	1.431	1.499
	Intestinal absorption (human)	Numeric (% Absorbed)	94.395	90.092	91.442	93.263	91.645	90.203	91.881	93.442
	Skin Permeability	Numeric (log Kp)	-2.698	-2.952	-2.698	-2.414	-2.786	-2.813	-2.481	-2.801
	P-glycoprotein substrate	Categorical (Yes/No)	Yes	Yes	Yes	Yes	Yes	Yes	Yes	Yes
	P-glycoprotein I inhibitor	Categorical (Yes/No)	No	No	No	No	No	No	No	No
	P-glycoprotein II inhibitor	Categorical (Yes/No)	No	No	No	No	No	No	No	No
Distribution	VDss (human)	Numeric (log L/kg)	0.595	1.081	1.292	0.729	1.043	1.395	0.895	0.242
	Fraction unbound (human)	Numeric (Fu)	0.263	0.223	0.322	0.191	0.389	0.383	0.137	0.090
	BBB permeability	Numeric (log BB)	0.373	0.109	0.226	0.189	0.092	0.124	0.288	0.321
	CNS permeability	Numeric (log PS)	-1.897	-2.053	-1.449	-1.791	-2.313	-1.393	-1.596	-0.931
Metabolism	CYP2D6 substrate	Categorical (Yes/No)	No	Yes	Yes	Yes	No	Yes	Yes	Yes
	CYP3A4 substrate	Categorical (Yes/No)	No	Yes	Yes	Yes	No	No	Yes	Yes
	CYP1A2 inhibitor	Categorical (Yes/No)	Yes	No	Yes	Yes	No	Yes	Yes	Yes
	CYP2C19 inhibitor	Categorical (Yes/No)	No	No	No	Yes	No	No	Yes	Yes
	CYP2C9 inhibitor	Categorical (Yes/No)	No	No	No	No	No	No	No	No
	CYP2D6 inhibitor	Categorical (Yes/No)	Yes	Yes	Yes	No	No	Yes	No	No
	CYP3A4 inhibitor	Categorical (Yes/No)	Yes	No	No	No	No	No	No	Yes
Excretion	Total Clearance	Numeric (log ml/min/kg)	0.475	1.069	1.165	0.471	1.218	1.337	0.515	0.465
	Renal OCT2 substrate	Categorical (Yes/No)	No	Yes	Yes	Yes	No	Yes	Yes	No
Toxicity	AMES toxicity	Categorical (Yes/No)	Yes	Yes	Yes	Yes	No	No	No	Yes
	Max. tolerated dose (human)	Numeric (log mg/kg/day)	-0.081	0.109	-0.123	-0.021	-0.012	-0.388	0.131	0.194
	hERG I inhibitor	Categorical (Yes/No)	No	No	No	No	No	No	No	No
	hERG II inhibitor	Categorical (Yes/No)	No	Yes	No	No	No	Yes	No	No
	Oral Rat Acute Toxicity (LD50)	Numeric (mol/kg)	2.900	2.605	2.859	2.438	2.395	2.670	2.357	2.364
	Oral Rat Chronic Toxicity (LOAEL)	Numeric (log mg/kg bw/day)	1.152	1.518	2.318	1.763	2.226	2.550	1.728	1.922
	Hepatotoxicity	Categorical (Yes/No)	No	No	Yes	Yes	No	No	Yes	No
	Skin Sensitization	Categorical (Yes/No)	No	Yes	Yes	No	Yes	No	Yes	No
	T. pyriformis toxicity	Numeric (log ug/L)	0.549	1.095	0.837	1.745	0.732	0.640	2.066	1.096
	Minnow toxicity	Numeric (log mM)	0.680	1.114	-0.357	-0.322	0.344	-0.121	-0.727	0.289

4.6 *In vitro* evaluation of neurotoxicity and neuroprotection

4.6.1 Development of a 3D cell culture model

To define optimal conditions, monodispersed cortical cells obtained from mice embryos were seeded in the micro-molded agarose wells at different seeding densities in the small (8x12 array) and large (7x5 array) mold-casted gels.

The hydrogel microwells facilitated the assembling of cells, while preventing the agglomeration between spheroids; the aggregation of cells in spheroids was noticed at day 4.

After several cell cultures with different spheroid diameters (Figure 4.46, Figure 4.47), we determined that:

- In the casting of micro-molded agarose wells, if the surface is not absolutely flat, the size homogeneity of spheroids developing within the micro-well is affected.
- Media changing after 24 h is a crucial step for the good development of spheroid.
- The spheroids with diameter of 50, 100 µm in the small molds and 200 µm in the large mold are not reproducible.
- The spheroids with diameter of 300 µm in the small mold and 500, 700 µm in the large mold were difficult to harvest.
- The spheroids with 200 µm in the small molds and 400 µm in the large molds are the best diameters, both for size reproducibility and harvest easiness.

For the continuation of the work, we supposed that the biggest spheroids will be more representative of the real cell environment; and so, the spheroids with 400 µM of diameter obtained at a seeding density of 8000 cells/micro-well from large (7x5 array) mold-casted gels were our choice
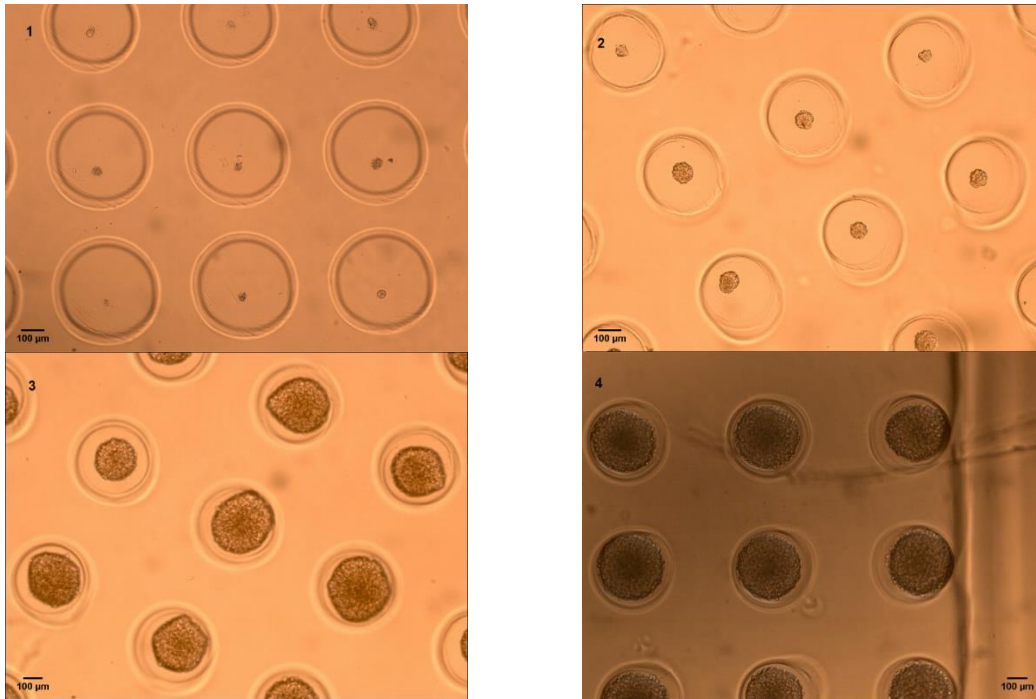
Figure 4.46: Visible light contrast microscopy images of neurosphere in small micro-wells with 5x magnification at day 14, with seeding of monodispersed mice embryos cortical cells at initial densities of: (1) 15 cells/spheroid and 50 µm of diameter, (2) 125 cells/spheroid and 100 µm of diameter, (3) 1000 cells/spheroid and 200 µm of diameter, (4) 3,375 cells/spheroid and 300 µm of diameter. (The scale bar represents 100 µm).
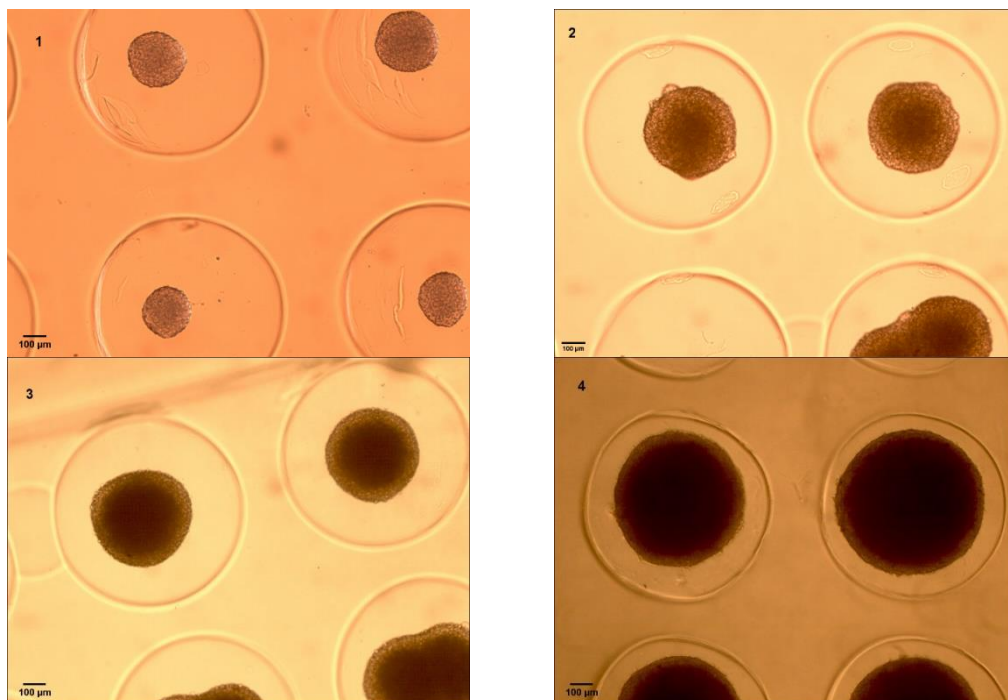
Figure 4.47: Visible light contrast microscopy images of neurosphere in large micro-wells with 5x magnifications at day 14, with seeding of monodispersed mice embryos cortical cells at initial densities of: (1) 1000 cells/spheroid and 200 µm of diameter, (2) 8000 cells/spheroid and 400 µm of diameter, (3) 15,625 cells/spheroid and 500 µm diameter, (4) 42,875 cells/spheroid and 700 µm diameter. (The black scale bar represents 100 µm).

172

4.6.2 Characterization of t neurospheres

4.6.2.1 Spheroid's diameter

Monodispersed cortical cells were seeded in the large micro-molded hydrogels at seeding densities of 8k cells per microwell. Spheroid diameters at first day in vitro (1 DIV) ranged from 500 – 700 µm; the hydrogel microwells facilitated the assembly of spheroids and we noticed their aggregation from 4 DIV. Spheroid diameter increased from 8 DIV to 11 DIV; between 11 and 14 DIV, a lesser diameter growth was observed (Figure 4.48, Figure 4.49).

The diameter measurement, of 3 biologically independent experiments performed with 3 technical replicates, indicated a mean of 626 ± 81 µm at first day, 363 ± 39 µm at day 4, 356 ± 39 µm at day 8, and 394 ± 37 µm at day 14 (Figure 4.49).

A two-way analysis of variance (ANOVA) for diameters with factors "*time*" and "*culture*" indicates that the differences in the mean values among the different days are greater than would be expected by chance ($P \leq 0.001$) (Figure 4.49), while the differences between cultures are not statistically significant ($P = 0.664$) (Figure 4.50), but the interaction *(day x culture)* is statistically significant ($P \leq 0.001$) (Figure 4.51).

The pairwise multiple comparisons (Bonferroni-test) for factors (*culture x time*) indicate that there is not a significant statistical difference between C1 and C3 at all days, and between the three cultures at day 11 (Figure 4.51).
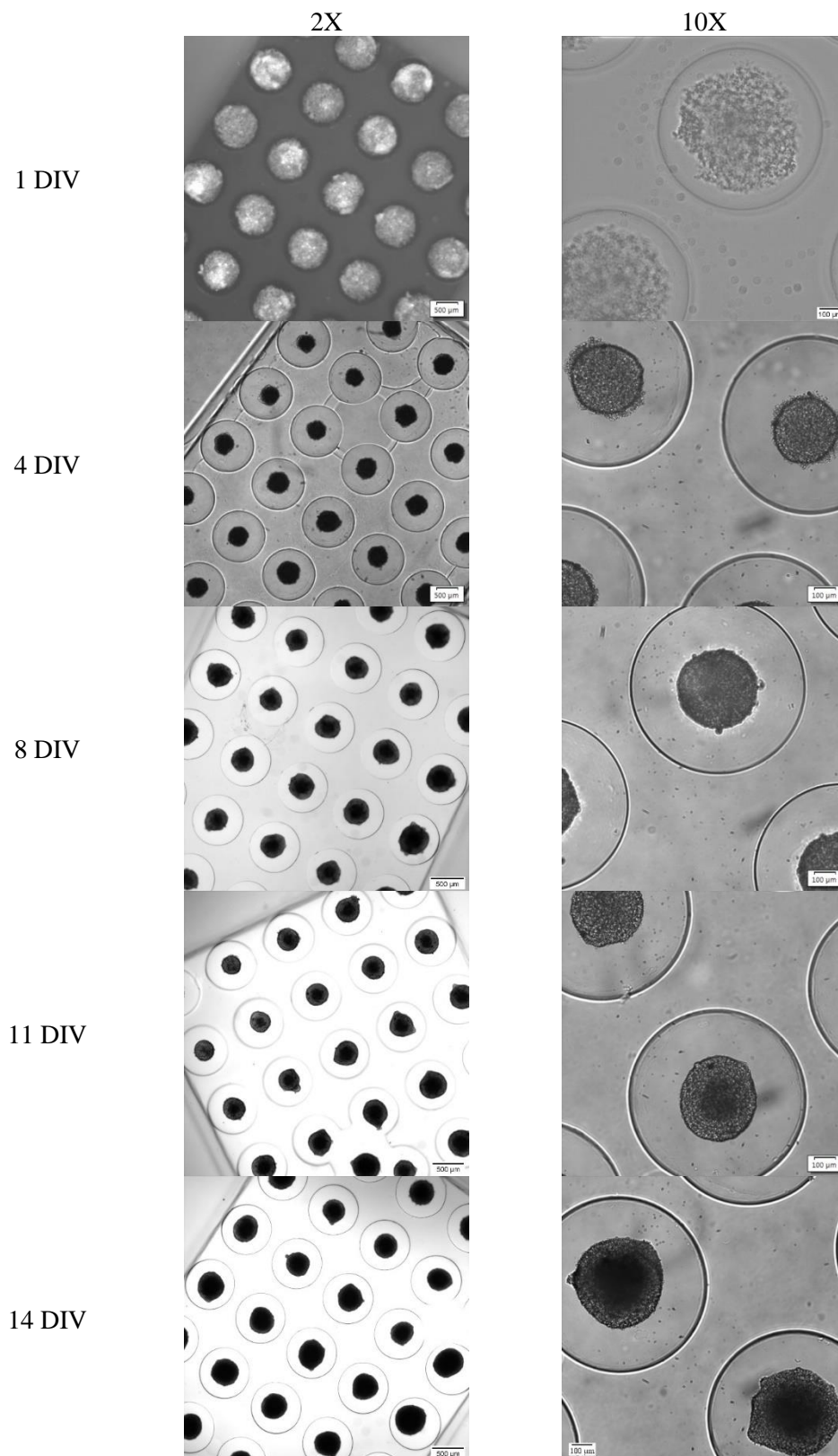
Figure 4.48: Visible light contrast microscopy images for the development of neural spheroids with seeding monodispersed mice embryos cortical cells at initial densities of 8,000 cells/spheroid with 2X and 10X magnifications from day in vitro (DIV) 1 to 14. (Scale bar represents 100µm for 10X µm and 500µm for 2X).
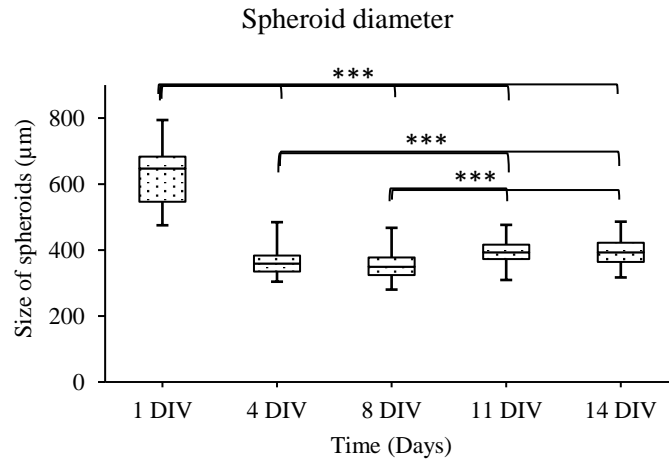
Figure 4.49: Spheroid diameters (8,000 monodispersed mice embryos cortical cells/spheroid) from 1 DIV to 14 DIV from 3 independent experiments with 3 technical replicates (N=54 spheroids measured for each DIV). The diameter decreases with the aggregation between 1 DIV and 4DIV (P < 0.001), the mean diameters were stable between 4 DIV and 8 (P = 1), to increase till 11 DIV (P < 0.001), then they were stable to 14 DIV (P = 1).
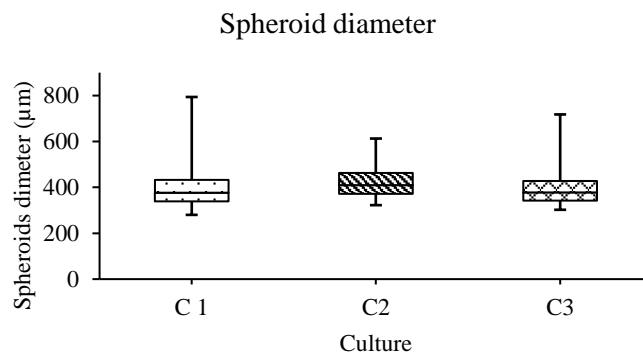
Figure 4.50: Total spheroid diameters per culture from 1 DIV till 14 DIV, data from 3 independent experiments with 3 technical replicates (N=90 spheroids measured in each experiment), the difference was not statically significant for the factor "culture" (ANOVA 2-ways, P = 0.664)
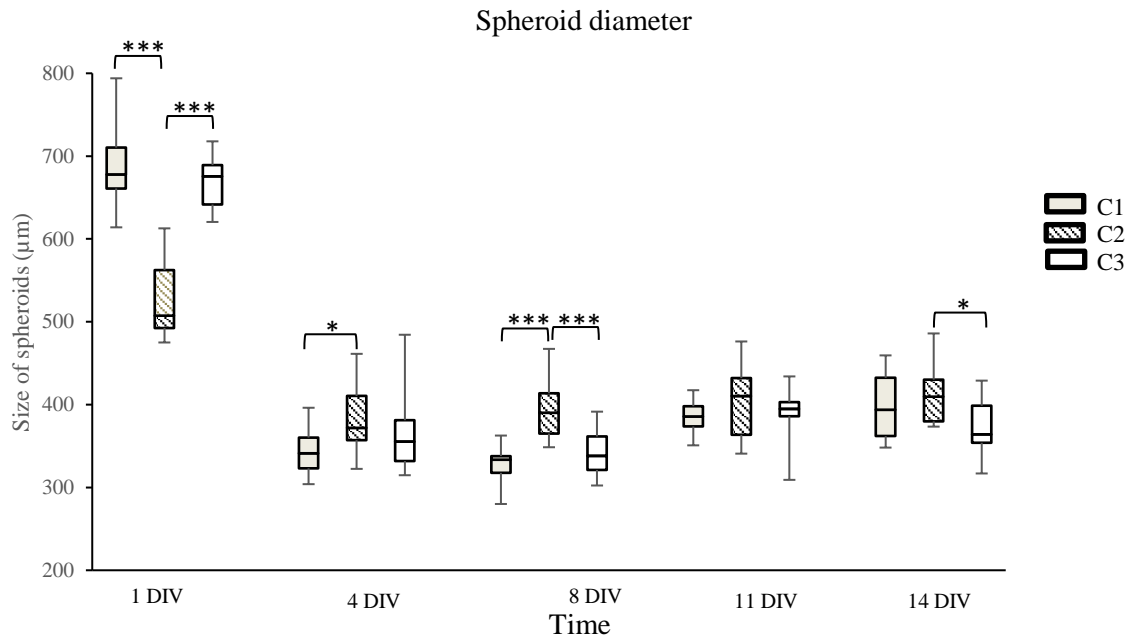
Figure 4.51: Spheroid diameters from 1 DIV to 14 DIV from 3 independent experiments (N=18 spheroids measured on each day per experiment). The pairwise comparisons for factor (*day x culture*) indicate that diameters statistically differ between cultures at different times except for 11 DIV; at 1 DIV the difference between C2 and both C1and C3 (P < 0.001) at 4 DIV between C1 and C2 (P = 0.02) at 8 DIV between C2 and both C1and C3 (P<0.001) at 14 DIV between C2 and C3 (P = 0.047).

4.6.2.2 Spheroid structure

By scanning electron microscopy

The appearance of spheroids was analyzed by SEM. SEM images have a characteristic 3D appearance and are useful for evaluating the surface structure of the spheroids, from which we observed two types of morphologies (Figure 4.52): (*i*) Spheroids with hyper-cellularized surface (*ii*) spheroids with more regular shape and structure, with dispersed cells.

The cells of the hyper-cellularized spheroids (Figure 4.52-B, C) present irregular membranes probably damaged by the fixing solution (PAF 4%) or in dehydration or drying steps. The presence of smooth then porous sections and incomplete spheres (Figure 4.53) seems to support this hypothesis. While the spheroids with highest diameter might be not fully dehydrated which probably explains their more regular shape.
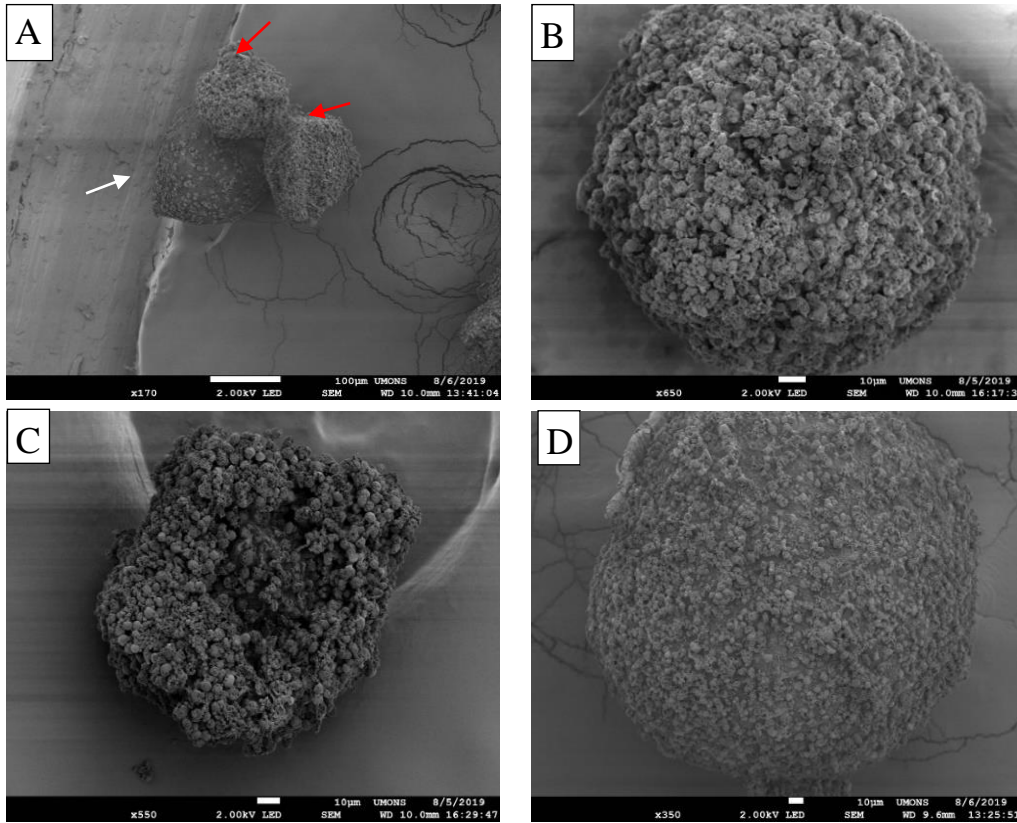
Figure 4.52 : SEM images of the two types of spheroids observed. Spheroid with a hyper-cellularized surface (A, red arrows; B, C) and spheroids with a more regular, well-shaped surface (A, white arrow; D). (The white scale bar represents 100 µm in A and 10 µm in B,C and D).
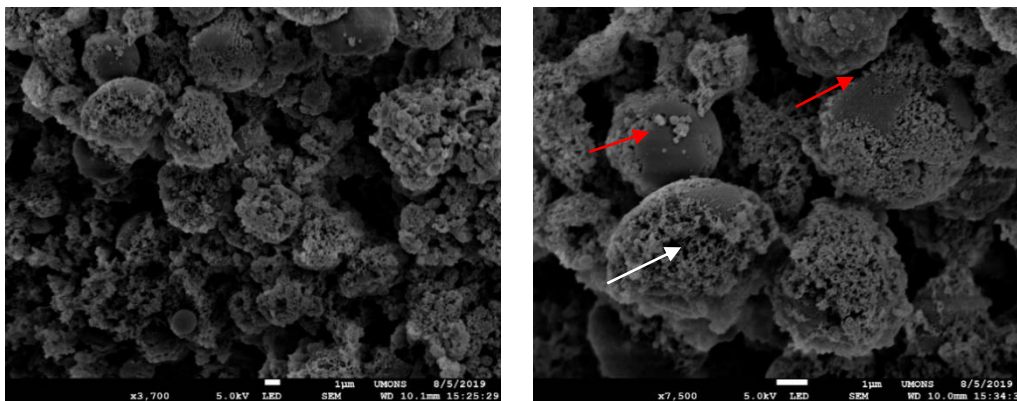
Figure 4.53: Hyper-cellularized spheroid with an irregular membrane with smooth then porous areas (red arrows) and deformed shape cells (white arrow) (The white scale bar represents 1 µm).

The spheroids present numerous extensions that may correspond to axons and dendrites. The cells were based on an extracellular matrix organized in the form of superimposed layers, while the cellular extensions were organized in a complex architecture lining the surface of

the spheroid. Complex tree networks of cellular extensions appeared on only well shaped spheroid whilst bundles were seen on hyper-cellularized surface (Figure 4.54, Figure 4.55).
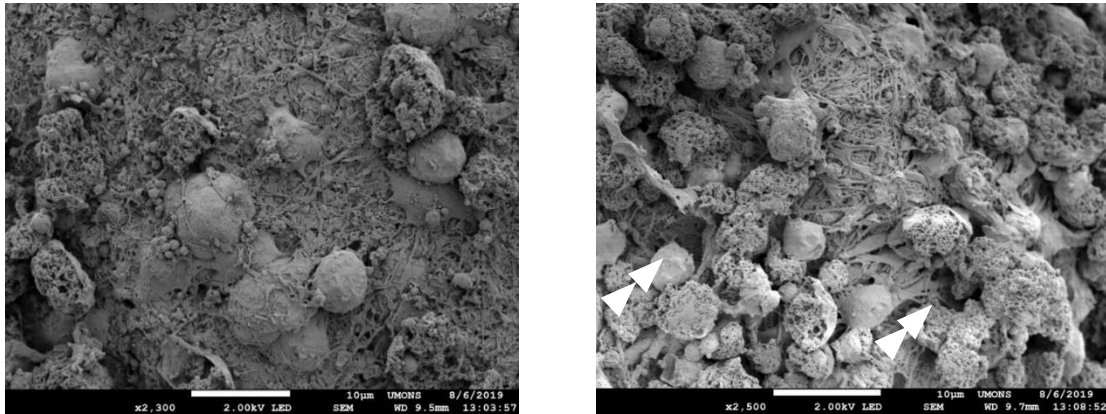
Figure 4.54: Complex tree network lining the hyper-cellularized surface of spheroid, with micro-pores (white arrow) on the surface, suggesting that there could be some channel-like structures in the spheroid. (The white scale bar represents 10 µm).
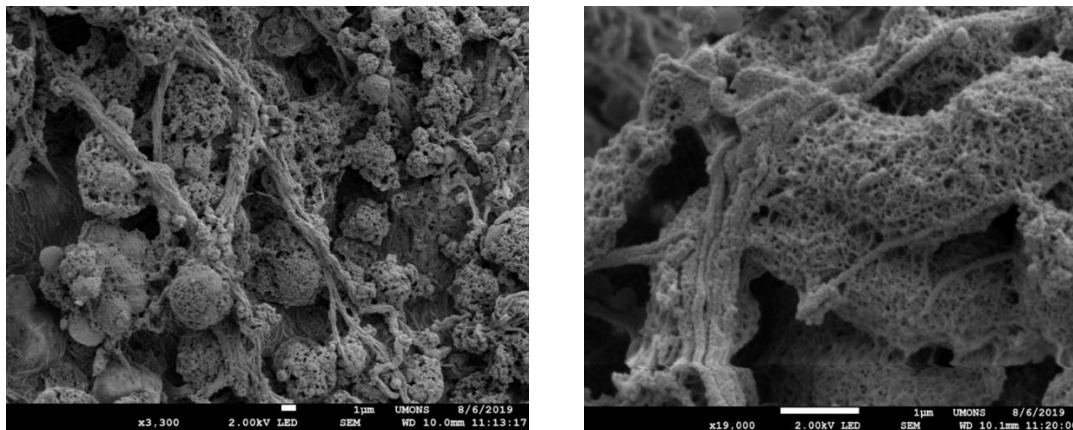
Figure 4.55: Bundles of cellular extensions grouped into complex structured and oriented networks on the hyper-cellularized surface of spheroid. (The white scale bar represents 1 µm).

4.6.2.3 Identification and quantification types of cells

By fluorescence microscopy

CNS markers-based immunocytochemistry coupled to fluorescence microscopy allowed to identify neuronal cells by tracing dendrites through MAP2 expression (microtubule-associated protein 2), astrocytes through GFAP expression (Glial Fibrillary Acidic Protein) and nuclei through DAPI staining (4′,6-diamidino-2-phenylindole) (Figure 4.56). Normalizing the fluorescence intensity based on cell numbers is unrealistic in 3D. And so, even though it is not ideal, we selected to normalize the fluorescence based on spheroid

diameter by hypothesizing that spheroids with close diameters have similar radii and close cell numbers.
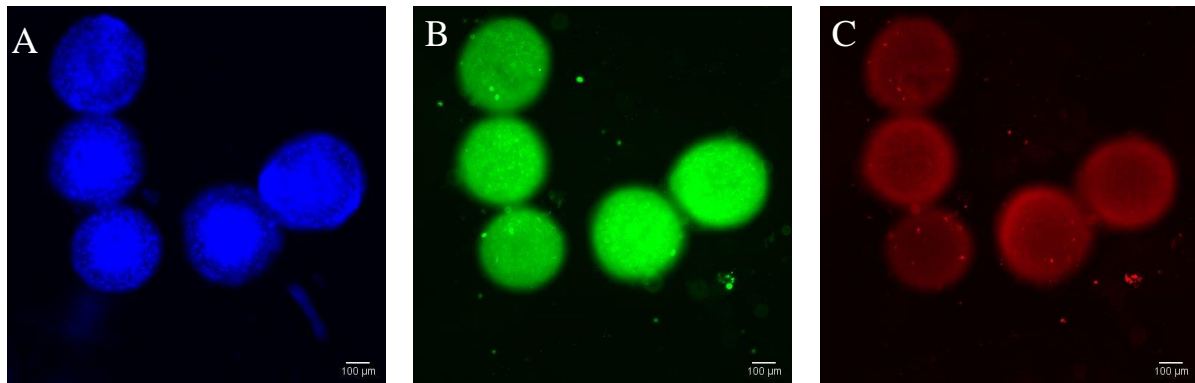
Figure 4.56: Fluorescence microscopy images (Olympus IX 70 and x10 objective) of neuronal spheroids after immunostaining with Mouse GFAP monoclonal antibodies (astrocytes), Rabbit MAP2 polyclonal antibodies (neurons), Goat anti-mouse IgG Alexa fluor 488 and Goat anti- rabbit IgG 594, followed with nucleus staining by DAPI. (A) the nuclei with DAPI, (B) the glial cells with GFAP and (C) the neurons with MAP2. (The white scale bar represents 100 µm)

To determine the variability of types of cell proportion among the different cultures, the intensities of fluorescence were measured for the different biomarkers and compared in 3 biologically independent experiments with 3 technical replicates.

The mean fluorescence intensities of DAPI that represent the nuclei were 46102 ± 4815 (SD), 37737 ± 8829 and 37152 ± 1054 x10^3 u., respectively (Figure 4.57). The data were normally distributed (Shapiro-Wilk test) with equal variances (Brown-Forsythe test); a one-way ANOVA analysis indicated that the P -value for the difference between the groups was 0.059 (NS), which indicates that the proportion of nuclei in our neurosphere do not differ from culture to culture.

The average measurements of fluorescence intensities of GFAP, that represent the glial cells, were 42902 ± 5719 (SD), 35947 ± 5078, and 42903 ± 10101 u. respectively (Figure 4.58). As data are not normally distributed (Shapiro-Wilk test, $P < 0.050$), a Kruskal-Wallis one way ANOVA on ranks was applied, indicating that the differences in the median values among the different cultures are not statistically different ($P = 0.077$). This indicates that there was a slight but not significant difference in glial cells fluorescences in our spheroids from culture to culture.

179

The average measurements of fluorescence intensities of MAP2, that represent the neurons, were 23121 ± 6614 (SD), 25770 ± 5943, and 23164 ± 3531 x10^3 u. respectively (Figure 4.59). The data were normally distributed (Shapiro-Wilk test) with equal variances (Brown-Forsythe test); a one-way ANOVA analysis indicated that the P -value for the difference between the groups was 0.052 (NS). So, the proportions of fluorescence due to neuron were not significantly different between cultures.
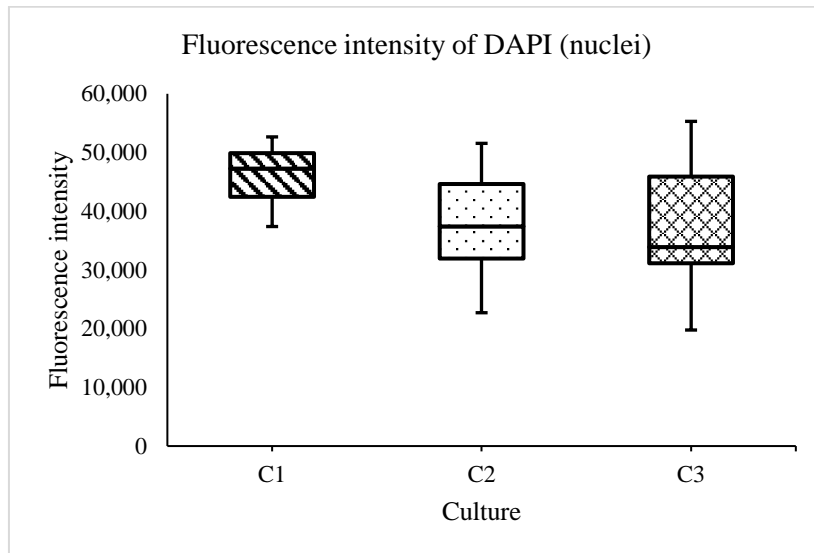
Figure 4.57: Mean values of DAPI fluorescence intensities in 3 biologically independent experiments performed with 3 technical replicates (N=9) (bar in the box represents the mean of data); there was not a statistically significant difference between the experiments (ANOVA; P = 0.059).
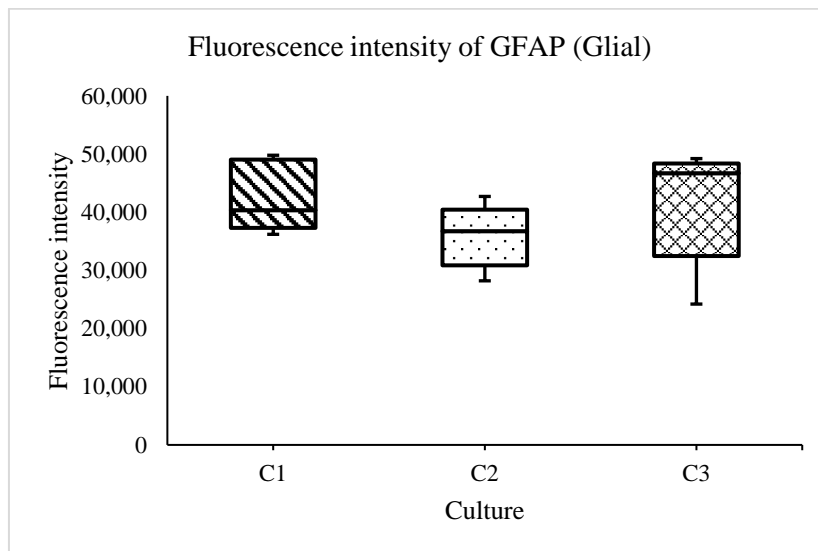
Figure 4.58: Mean values of GFAP fluorescence intensities in 3 biologically independent experiments performed with 3 technical replicates (N=9) (bar in the box represents the mean of data), there was not a statistically significant difference between the three experiments (Kruskal-Wallis; P = 0.077).
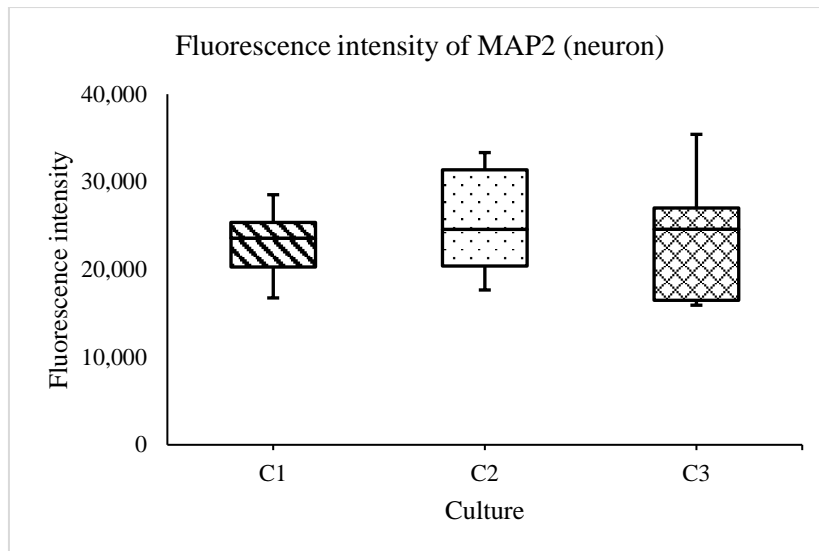
Figure 4.59: Mean values of MAP2 fluorescence intensities in 3 biologically independent experiments performed with 3 technical replicates (N=9) (bar in the box represents the mean of data); there was not a statistically significant difference between the three experiments (ANOVA; P = 0.052).

By Confocal microscopy

The confocal microscopy images showed that neurons and glial cells formed complex 3D structures in the spheroids. The neurons were stained by anti-neuronal antibodies, including MAP2, beta III tubulin and TAU; the glial cells (astrocytes cells were marked by GFAP and the microglia cells by IBA-1 (ionized calcium binding adapter molecule 1) (Figure 4.60).

The confocal images yield higher sensitivity than fluorescence images, better signal-to-noise ratios, and higher X, Y, and Z resolution while maintaining ± high-throughput data. However, the imaging penetration depth, increased light absorption and light scattering did not allow us to gather information from more than 100 µM of depth.

A water immersion objective with 40X magnification is supposed to enable higher resolution and details at deeper depth; but its use was more challenging as the 400 µM average diameters of spheroids were too big for 40X. For smaller spheroids, we were able to obtain a better resolution, but the depth could not surpass 100 µm, even when applying clearing techniques (Figure 4.61).

As a result, the confocal images were used for identification only, as it was challenging to obtain high-quality images from the deep with our thick 3D neuronal spheroids.

20x GFAP +DAPI	20x GFAP	20x DAPI
20x MAP2 + IBA2	20x IBA2	20x MAP 2
20x GFAP +TAU	20x TAU	20x GFAP
20 x Class III β-tubulin + DAPI	20 x Class III β-tubulin	20 x DAPI
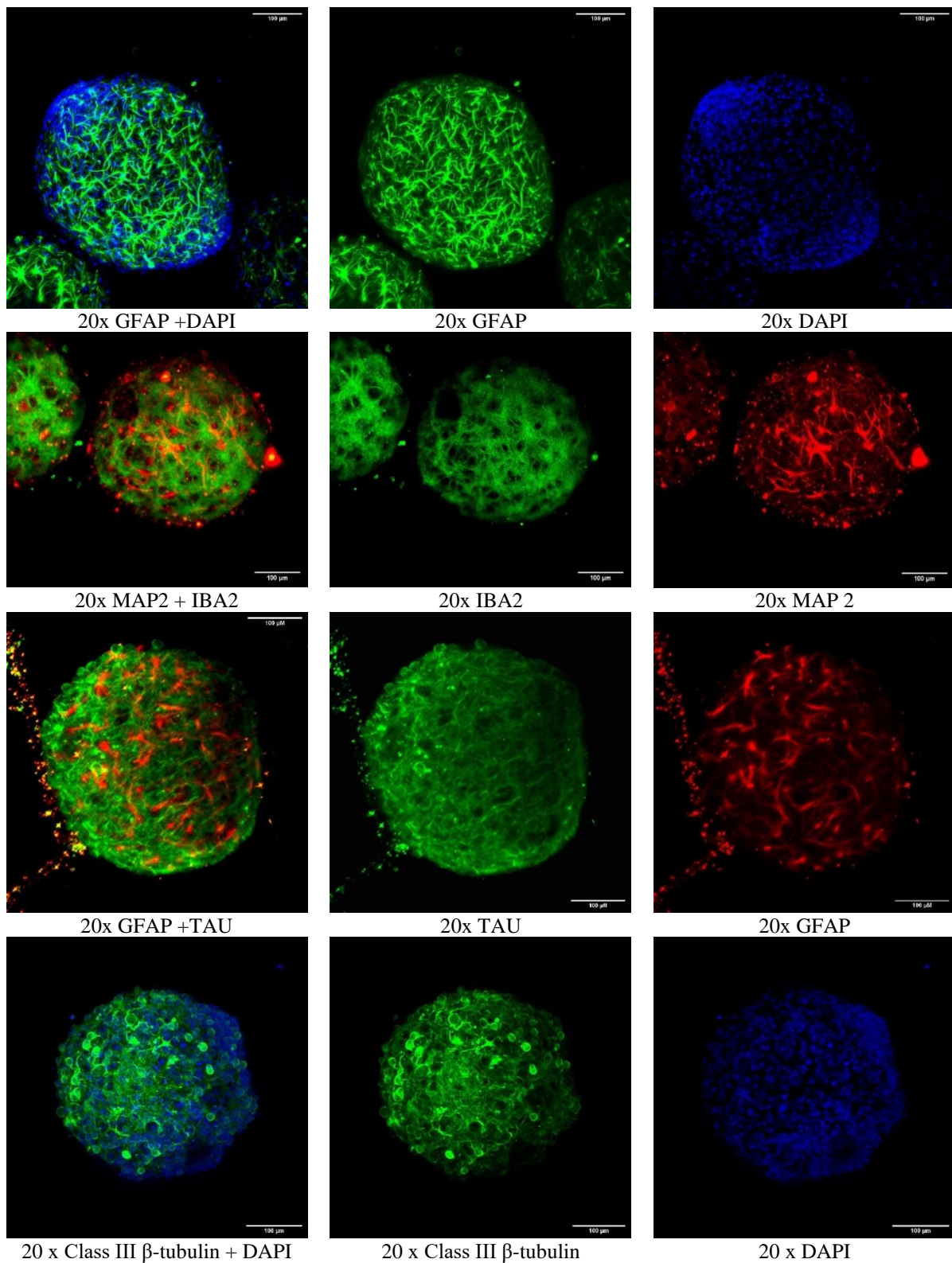
Figure 4.60: Confocal images with 20X objective at day 14 indicate that the neural spheroids contain CNS cell types, including astrocytes (GFAP), microglia (IBA2), and neurons represented by their dendrites (MAP2) and microtubules (Class III β-tubulin). Nuclei were counterstained with DAPI. (The white scale bar represents 100 µm).

182
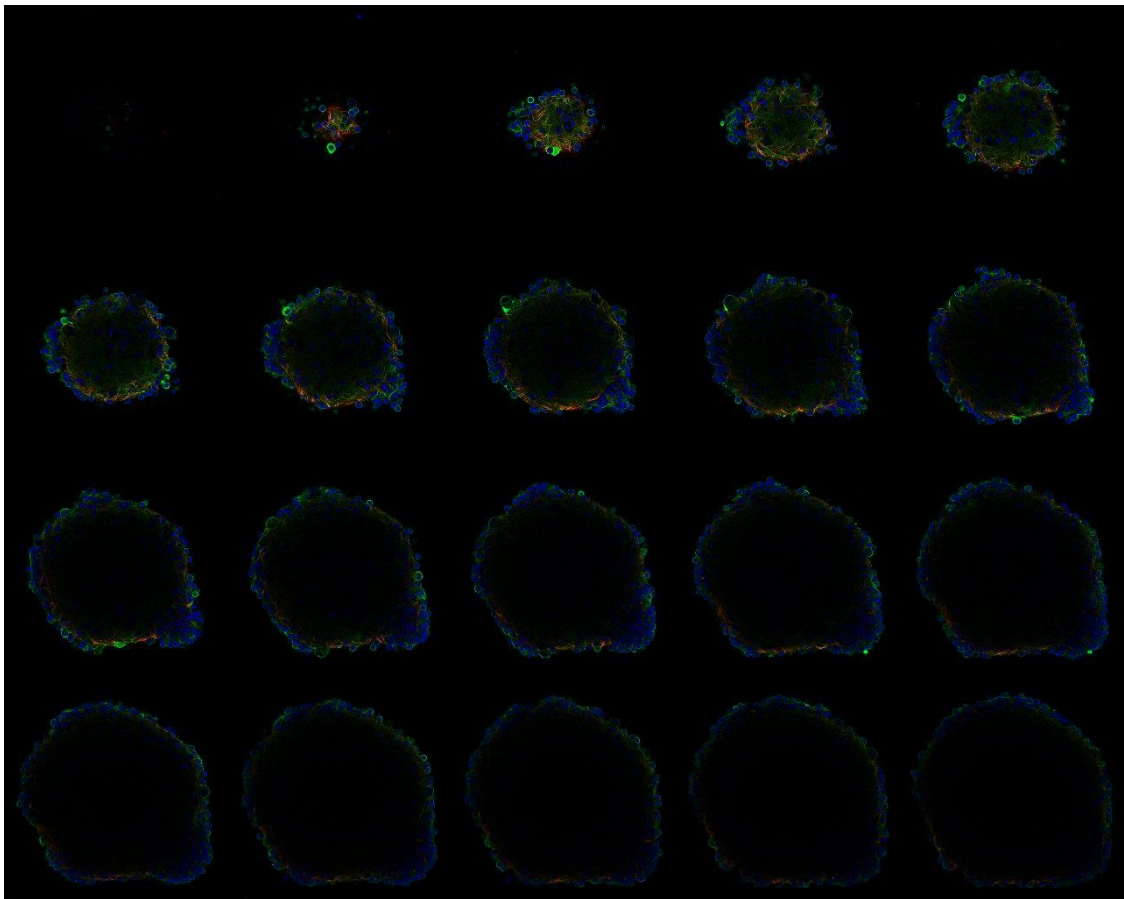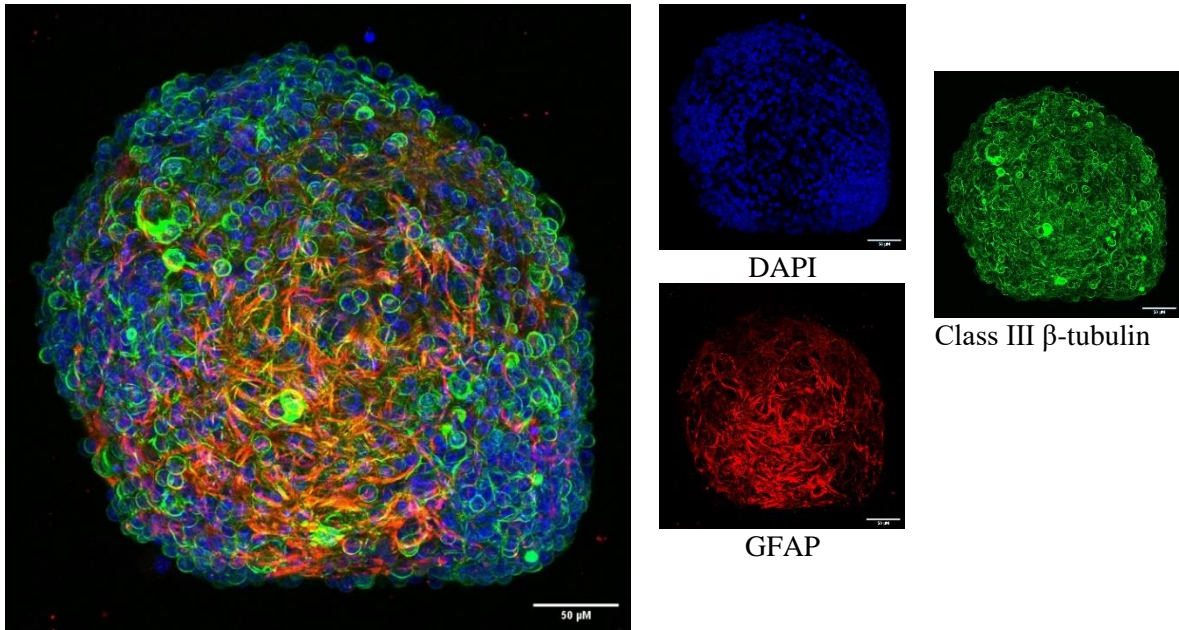
Figure 4.61: Confocal images obtained with a water immersion 40X objective at day 14: (A) the different types of cells in neural spheroids including neurons (Class III β-tubulin, green), astrocytes (GFAP, red) and nuclei (DAPI, blue). (B) The 20 stacks of the composite image above illustrate the dark center, indicating the challenges to high-quality deep imaging within a 3D spheroid. (The white scale bar represents 50 µm).

By sectioning/staining and visible microscopy

The dark centers observed in spheroids confocal imaging raise the question as whether these are due to a light penetration issue or to the occurrence of necrotic centers and/or central acellular matrices?

To clarify this, an automated slices sectioning followed by hematoxylin/eosin staining and examination under visible light was applied on neuronal spheroids; obtained images indicate that there is no necrosis in the center but fewer cells that seem embedded in a loose connective tissue (Figure 4.62)
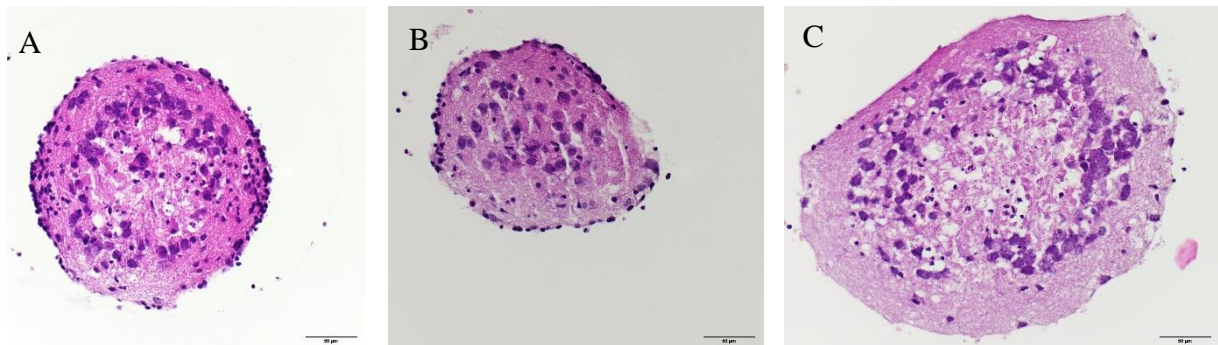
Figure 4.62: Visible light images with 40X objective for different slices of 14 DIV neuronal spheroids stained (A and B at 100 µm depth while C at 200 µm) with hematoxylin and eosin. Cell nuclei are colored in shades of blue and purple and connective tissue is colored in shades of pink. The center of spheroids contains cells but fewer, the cell bodies being larger than in the periphery. The extracellular matrix was denser in the periphery than in the center. (The black scale bar represents 50 µm)

4.6.3 Study of Cytotoxicity effects

4.6.3.1 Evaluation of cell viability

Evaluation of cell viability with harmane

After exposure to increasing concentrations of harmane (50, 100, 250 µM) for 24 h, the 3D neural spheroids showed a decrease in cell viability (resazurin test) which was correlated to harmane concentration, down to 27 % reduction at 250 µM harmane (Figure 4.63). As data were normally distributed (Shapiro-Wilk test) (p = 0.848), these were compared by a two-way ANOVA test, with the factors *"harmane concentration"* and *"experience"*, the difference was statistically significant for the *harmane concentration* factor (P < 0.001) and was not statistically significant for factors *"experience"* and "*harmane concentration x experience*" (P= 0.402 and 0.121, respectively). A post-hoc pairwise t-tests (Bonferroni correction) indicated that the differences were statistically significant for both 250 µM and 100 µM versus the control group with P < 0.001 and P = 0.006, respectively (Figure 4.63).
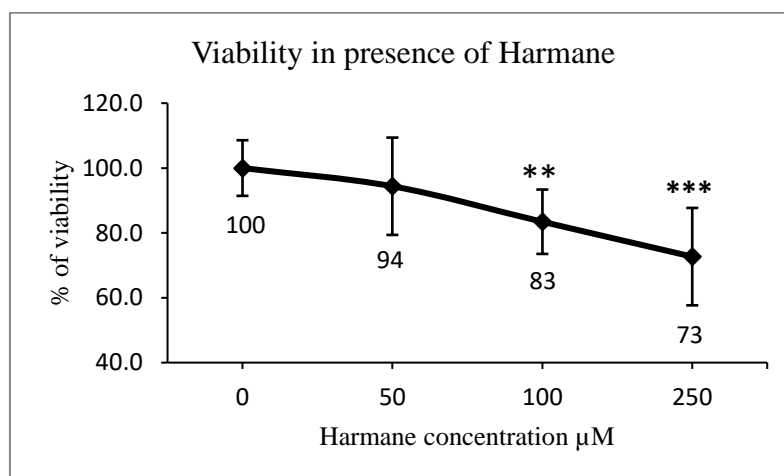
Figure 4.63: Cell viability after 24 h exposure to different concentrations of harmane; data from 6 biologically independent experiments performed with 3 technical replicates (resazurin viability test; mean ± SD) (N=18). There is a clear trend in viability reduction with harmane concentration. There was a statistically significant difference between the conditions negative control and harmane 100 and 250 µM (ANOVA test P values = 0.06 and < 0.001, respectively).

For verification of these resazurin viability data, we measured the intensity of fluorescence of neurons (MAP2), glial cells (GFAP) and nuclei (DAPI) after 24 h exposure to different concentrations of harmane. We noticed a reduction in the intensity of fluorescence for the 3 stains, that corresponds with the increase of harmane concentrations (Figure 4.64).

A two-way ANOVA analysis was applied with factors *"harmane concentration"*, *"experience"* and indicate that there was a statistically significant difference for factor "*harmane concentration*" (P <0.001 for nuclei, neurons, and glial cells). The differences for factor "*experience"* were not statistically significant for nuclei and glial cells (P = 0.524, 0.375 respectively); while it was statistically significant for the fluorophore of neurons (P = 0.014). The factor *"harmane concentration x experience"* was statistically significant for neurons (P = <0,001) and not significant for nuclei and glial cell (P = 0.2 and 0.4 respectively).
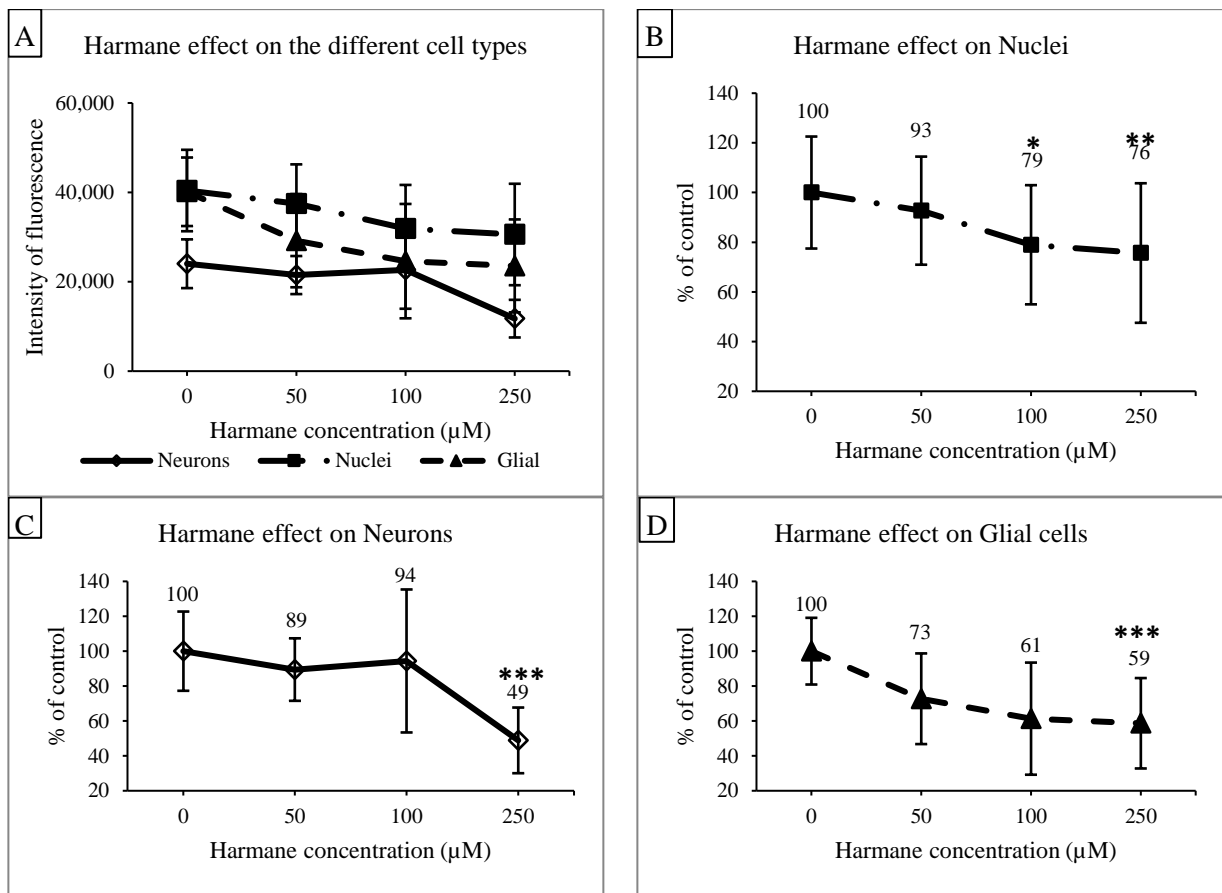
Figure 4.64: Fluorescence intensities after 24 h exposure to different concentrations of harmane, data from 3 biologically independent experiments performed with 3 technical replicates (mean ± SD) (N = 12). (A) Absolute fluorescence intensities. There is a clear trend in reduction with the higher harmane concentrations. (B) Fluorescence of DAPI (nuclei), relatively to the control condition; there was a statistically significant difference between control group and harmane 100 and 250 µM. (P=0.01 and 0.002, respectively). (C) Fluorescence of MAP2 (neurons), relatively to the control condition; there was a statistically significant difference for all groups vs. harmane 250 µM., (P < 0.001); (D) Fluorescence of GFAP (glial cells), relatively to the control condition; the difference was statistically significant for all groups vs. harmane 250 µM (P < 0.001).

Despite the huge variability inherent to this experiment (variability that inevitably arises from the different variabilities we have investigated, i.e. the sizes of spheroids, cf Section 4.6.2.1, p.173, and the distribution of the different types of cells, cf Section 4.6.2.3, p.178, the absolute fluorescence intensities indicate a clear, but non-significant, trend in reduction with harmane concentration (Figure 4.64, Figure 4.64-A). When expressed in percentages of control fluorescence, the trends appear clearer and the cytotoxic effect of harmane is significant for total cells (nuclei) at 100 and 250 µM (Figure 4.64-B) and for neurons and glial cells at 250 µM (Figure 4.64_C and D).

Evaluation of cell viability with 1-Benz-THIQ-diol

After exposure to increasing concentrations of 1-Benz-THIQ-diol (50, 100, 250 µM) for 24 h, the 3D neural spheroid showed a slight decrease in viability (resazurin test), which was not 1-Benz-THIQ-diol concentration-dependent. The mean values of percentage of viability based on control group were 90.6 ± 22.6 (SD), 84.9 ± 12.1 and 93.1 ± 12.6 % for 1-Benz-THIQ-diol 50, 100 and 250 µM, respectively (Figure 4.65). A two-way ANOVA analysis for factors *"treatment "*, *"experience"* and *"treatment x experience" indicates* there is no statistically significant difference among the different *treatments* ($P = 0.150$), the different *experiences* ($p = 0.051$) and no interaction *experience-treatment* ($P = 0.880$).
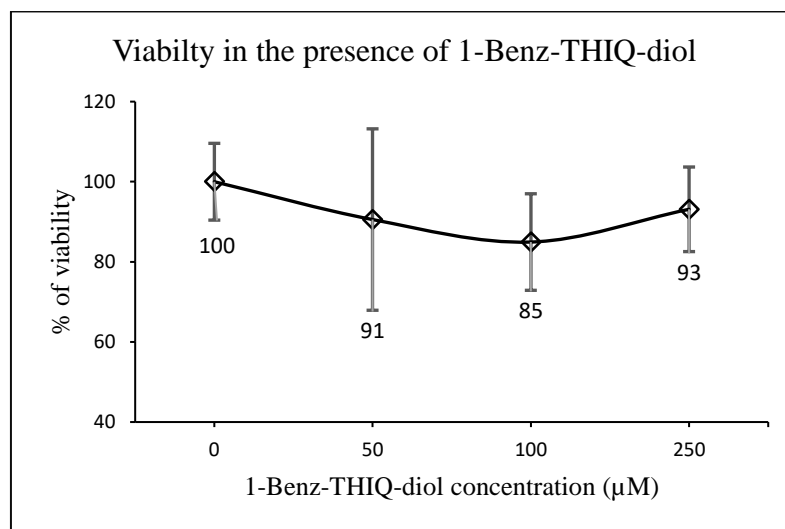

Figure 4.65: Viability after 24 h exposure to different concentrations of 1-Benz-THIQ-diol, data from 4 biologically independent experiments performed with 3 technical replicates (resazurin viability test; mean ± SD) (N=12). There is no significant difference between concentrations (ANOVA; P = 0.150).

4.6.3.2 Reactive oxygen species (ROS) measurement

Evaluation of ROS in the culture medium of spheroids exposed to harmane

After 3, 5, 9, 24 h exposure of spheroids to increasing concentrations of harmane (50, 100, 250 µM), the medium was collected and mixed with 2′,7′- dichlorodihydrofluorescein (DCFH); after 45 min, the fluorescence of oxidized DCF was measured. The fluorescence intensities indicate a variation in ROS production with time, independently of exposure to harmane, and no effect of harmane concentration (two-way ANOVA, $P < 0.001$ for the factor *"time"* and $P = 0.765$ for the factor *"concentration"*; $P = 0.948$ for the interaction *"time"* x *"concentration"*) (Figure 4.66).
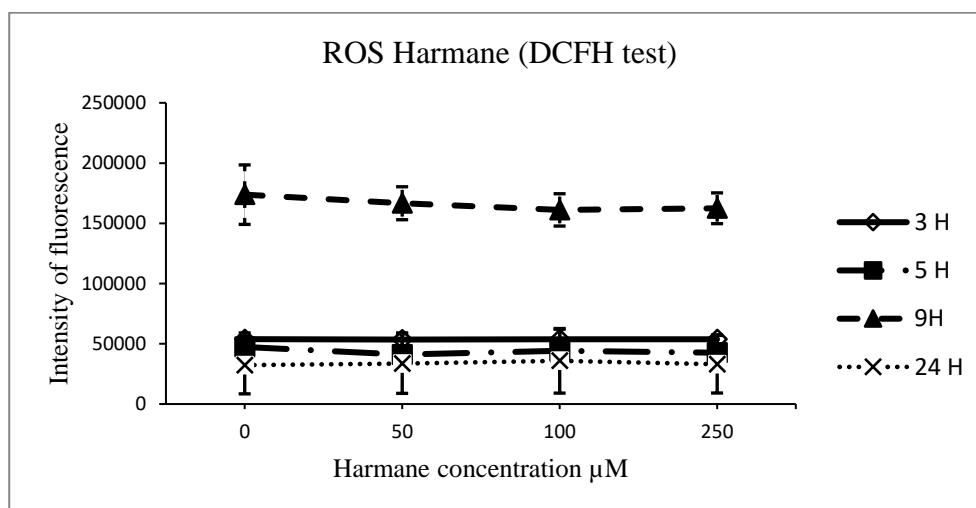
Figure 4.66: ROS production measured with a DCFH test after 3, 5, 9, 24 h exposure to different concentrations of harmane (0, 50,10, 250 µM), data from 3 biologically independent experiments performed with 3 technical replicates (mean ± SD) (N=9). The difference was not statistically significant for the different treatments (P = 0.765) but was statistically significant for the different levels of time (P = <0,001). The considerable fluorescence intensities measured at time 9 h are explained by a different setting of the fluorescence reader at that time point.

Evaluation of ROS in spheroids exposed to harmane

Cells were exposed to harmane in the presence of 2′,7′- dichlorodihydrofluorescein diacetate (DCFH-DA) and the intensity of DCF fluorescence was measured in the medium after 3, 5, 9, 24 h of exposure to different concentrations of harmane. The fluorescence intensities indicate a slight variation in ROS production with time and with harmane concentration (two-way ANOVA, $P < 0.001$ for the factor *"time"* and $P = 0.011$ for the factor *"concentration"*; $P = 0.76$ for the interaction *"time"* x *"concentration"*) (Figure 4.67). Even though we

188

excluded the 9 h measurement, there is still significant difference in factor *time* between 3 and 24 h; moreover, for the factor concentration, the difference was significant between harmane 250 µM and the negative control. In this experiment however, the measured fluorescence intensities are much lower compared to the previous tests, indicating that only a small fraction of DCF effectively diffuses from spheroids to the medium; it could be interesting to lyse the spheroids to measure the total DCF, but this was particularly difficult to achieve.
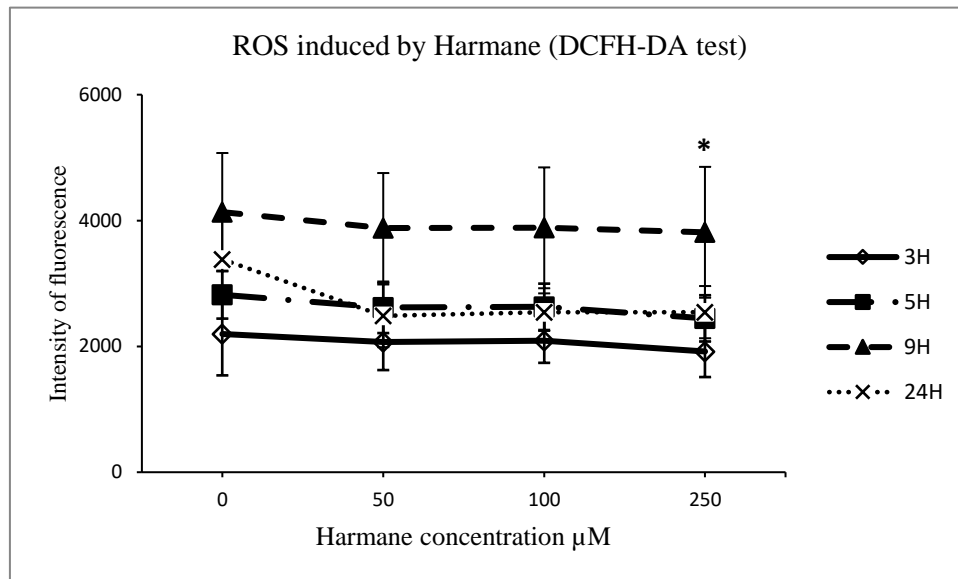
Figure 4.67: ROS production measured with a DCFH-DA test after 3, 5, 9, 24 h exposure to different concentrations of harmane (0, 50,10, 250 µM), data from 3 biologically independent experiments performed with 3 technical replicates (mean ± SD) (N=9), the difference was statistically significant according to time (P < 0.001) and for the different treatments at different times for harmane 250 µM vs control (P = 0.010). The considerable fluorescence intensities measured at time 9 h are explained by a different setting of the fluorescence reader at that time point.

Spheroids exposed to harmane: comparison of ROS in the culture medium and in spheroids

To compare the measurement of DCF intensities between the two tests (DCFH, measurement of ROS in medium; DCFH-DA, measurement of ROS in spheroids) at different times (3 biologically independent experiments performed with 3 technical replicates at 4 time levels; N = 9), the measured intensities were expressed as percentages of control (Figure 4.68).

These were compared by a three-way ANOVA test, with the factors *"time", "harmane concentration"* and *"test"*, with post-hoc pairwise t-tests (Bonferroni correction). For factor

time, there is no significant difference (P = 0.065); conversely, the differences were statistically significant for factors *test* (P < 0.001) and *harmane concentration* (P < 0.001). For pairwise comparisons, there is no statistically significant interactions between *"Time x Harmane concentration"* (P = 0.943) *and "Test x Harmane concentration"* (P = 0.053), while there is a statistically significant interaction between *"Time x Test"* (P = <0,001). A pairwise comparisons isolate which group(s) statistically differ from other; *(i)* two tests at 24 h (P < 0.001); *(ii)* two tests within 250 µM concentration (P = 0.005).
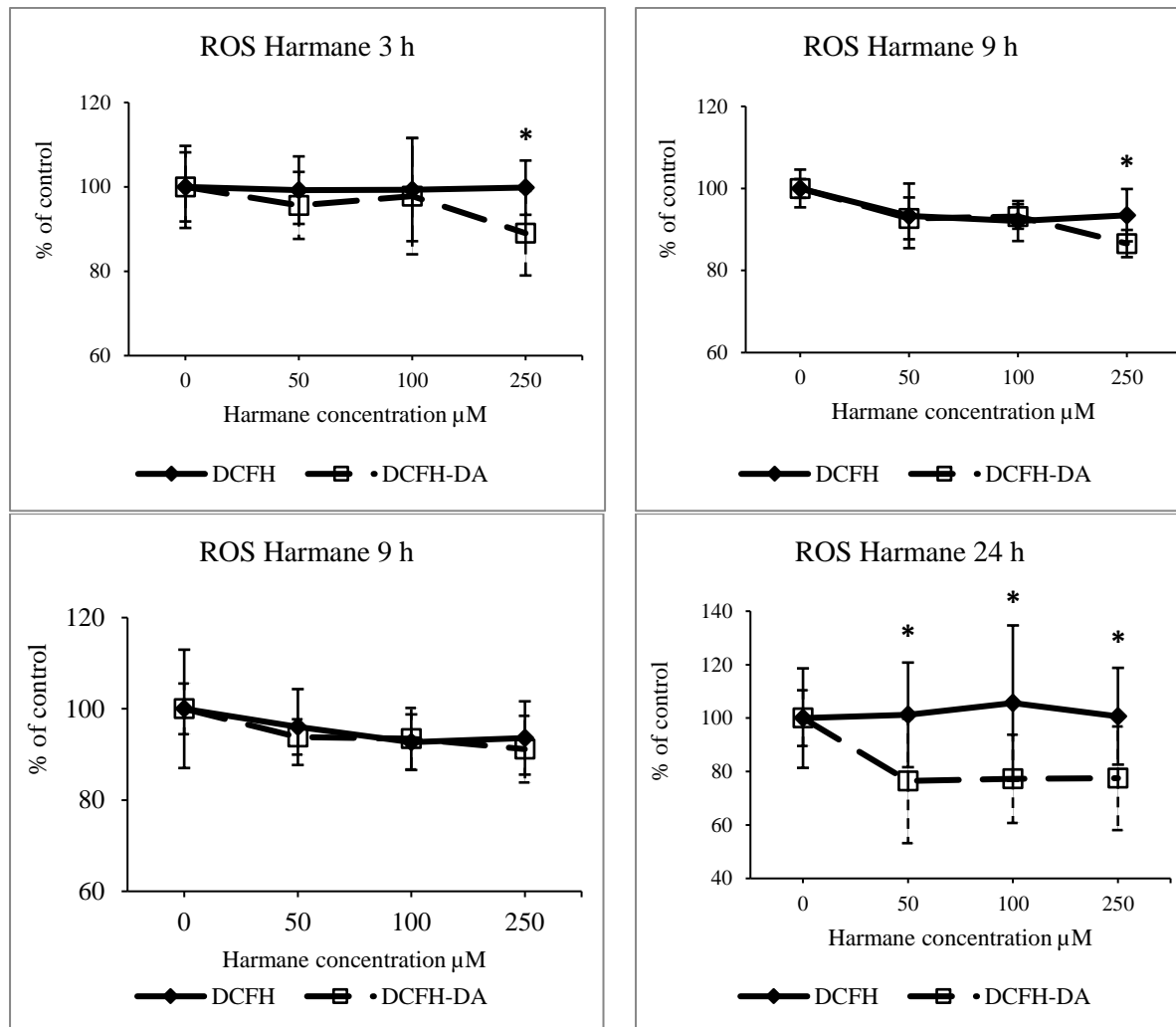
Figure 4.68*:* ROS production (percentage of control) of DCFH test compared with DCFH-DA test, after the exposure to different concentrations of harmane at different times, data from 3 biologically independent experiments performed with 3 technical replicates (mean ± SD). After 3, 5 and 9 h there was no statistically significant difference between the two tests (one-way ANOVA P = 0.090, 0.280 and 0.631, respectively); while the difference was statistically significant after 24 h (P < 0.001). The comparison for the different treatments at different times (N = 9) between the 2 tests indicates a significant difference *(i)* for 250 µM after 3, 5 and 24 h (P= 0.015, 0.011 and 0.018); *(ii)* for 100 µM after 24 h (P = 0.02); and *(iii)* for 50 µM after 24 h (P = 0.027).

Evaluation of ROS in culture medium of spheroids exposed to 1-Benz-THIQ-diol

As indicated by the DCFH-DA experiment here above, it seems that only a small fraction of oxidized DCF effectively diffuses from spheroids to the medium, making difficult the interpretation of these data. And so, for 1-Benz-THIQ-diol, only the DCFH test was applied after 24 h of exposure to the compounds, on 5 biologically independent experiments performed with 3 technical replicates (Figure 4.69). There is no significant effect of 1-Benz-THIQ-diol on the generation of ROS as measured here (two-way ANOVA, $P = 0.348$ factor *"Treatment"*; $P = 0.391$ for the interaction *"Culture"* x *"Treatment"*), while the difference was statistically significant for factor *"Culture"* ($P = 0.013$) and the pairwise comparisons (Bonferroni t-test) indicate that the difference was significant between C1 and C2 ($P = 0.014$).
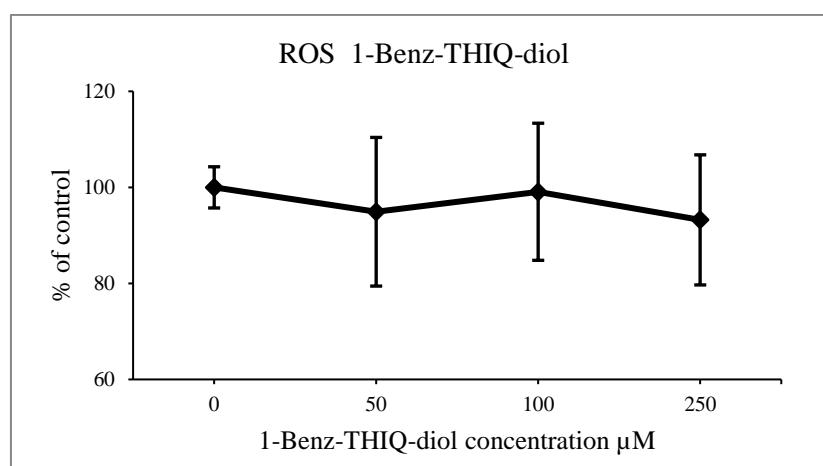
Figure 4.69: ROS production (percentage of control) after 24 h exposure to different concentrations of 1-Benz-THIQ-diol, data from 5 biologically independent experiments performed with 3 technical replicates (mean ± SD) (N=15). There was no significant difference between the treatments (two-way ANOVA, $P = 0.115$).

4.6.3.3 Study of apoptosis and necrosis on spheroids

Over the 2420 neurosphers produced, after harvesting, *(i)* 39 were excluded from the experiment because of induced damage while pipetting to transfer the spheroid (bubble in the medium or damaged surface); and *(ii)* 63 were excluded, being smaller than 340 µm or larger than 460 µm; this size range (400 µm ± 15 %) was arbitrarily selected to reduce the interference of diameters on measurements, the percentage of excluded spheroids was 4.17 %. Alterations in cell morphology occur in both necrotic and apoptotic cells and can be determined by assessment of staining using fluorescent stains and fluorescence microscopy (Figure 4.70, Figure 4.71).
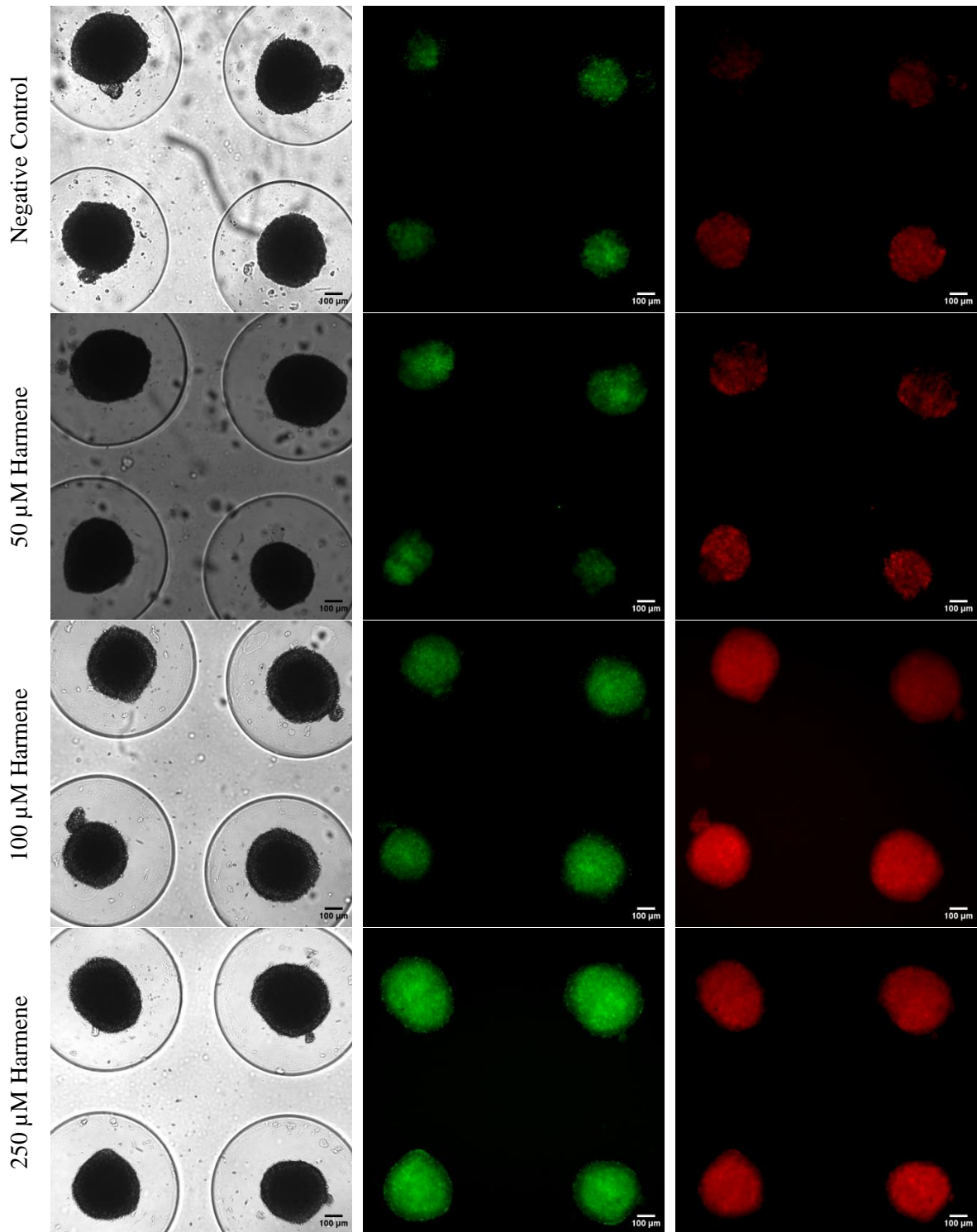
Figure 4.70: Phase-contrast and fluorescence microscopy images (Olympus IX 70 and x10 objective) of neuronal spheroids after exposure to different harmane concentrations (0, 50, 100 and 250 µM). The phase-contrast images were used to define the acceptable spheroids, the caspases 3/7 in apoptotic cells induce a green-fluorescence, the propidium iodide stains nucleic acids in necrotic cells with a red-fluorescence. (The scale bar represents 100 µm).
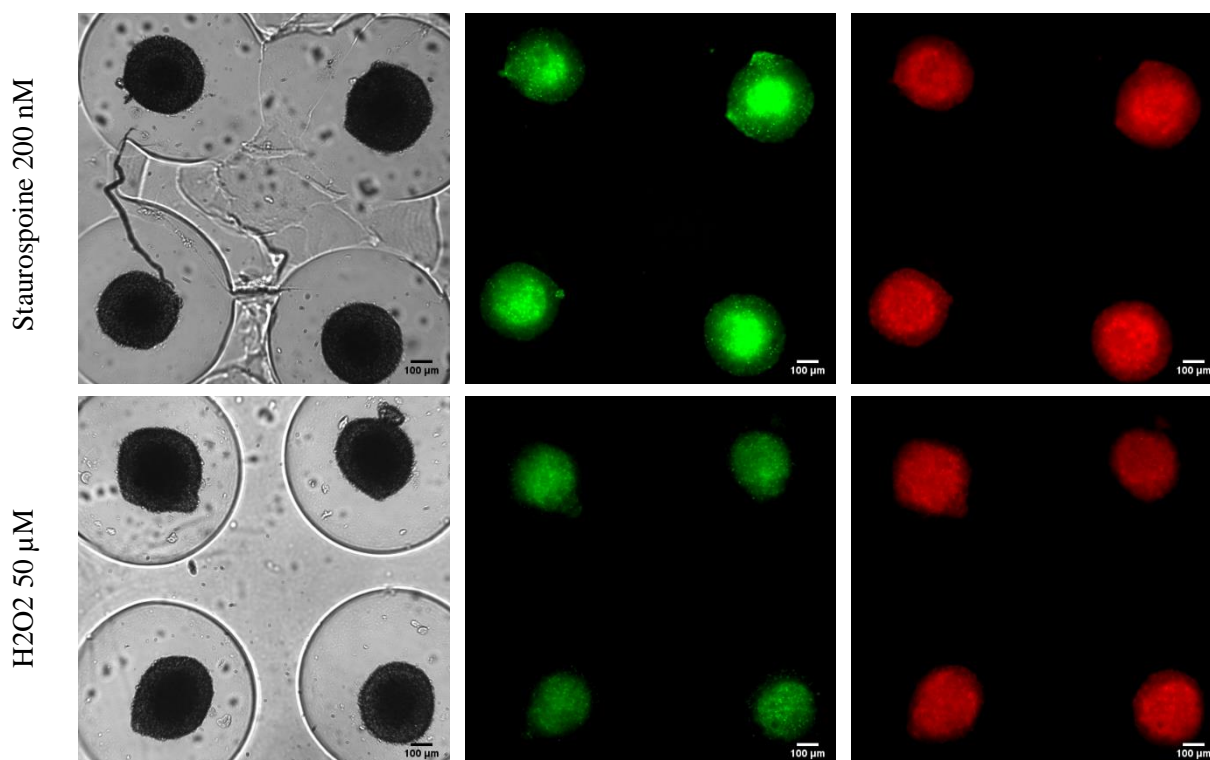
Figure 4.71: Phase-contrast and fluorescence microscopy images (Olympus IX 70 and x10 objective) of neuronal spheroids after exposure to staurosporine 200 nM and H_2O_2 50 µM. The phase-contrast images were used to define the acceptable spheroids, the caspases 3/7 in apoptotic cells induce a green-fluorescence, the propidium iodide stains nucleic acids in necrotic cells with a red-fluorescence. (The scale bar represents 100 µm).

Measurement of apoptosis

For apoptosis, we measured the fluorescence intensity induced by the activation of the caspase cascade in neurospheres after 24 h exposure to different concentration of harmane (0 to 250 µM), staurosporine 200 nM (apoptosis positive control) or hydrogen peroxide H_2O_2 50 µM (necrosis positive control) (Figure 4.70, Figure 4.71). The fluorescence intensity increased with the increased concentration of harmane. A two-way ANOVA analysis was applied for the factor *"treatment"*, *"culture"* and for the interaction *"treatment"* x *"culture"* indicating that the differences were statistically significant for all factors ($P < 0.001$) Figure 4.72). A post-hoc Bonferroni t-test showed a statistically significant difference between the negative control group and harmane 250 µM and staurosporine 200 nM ($p < 0.001$).
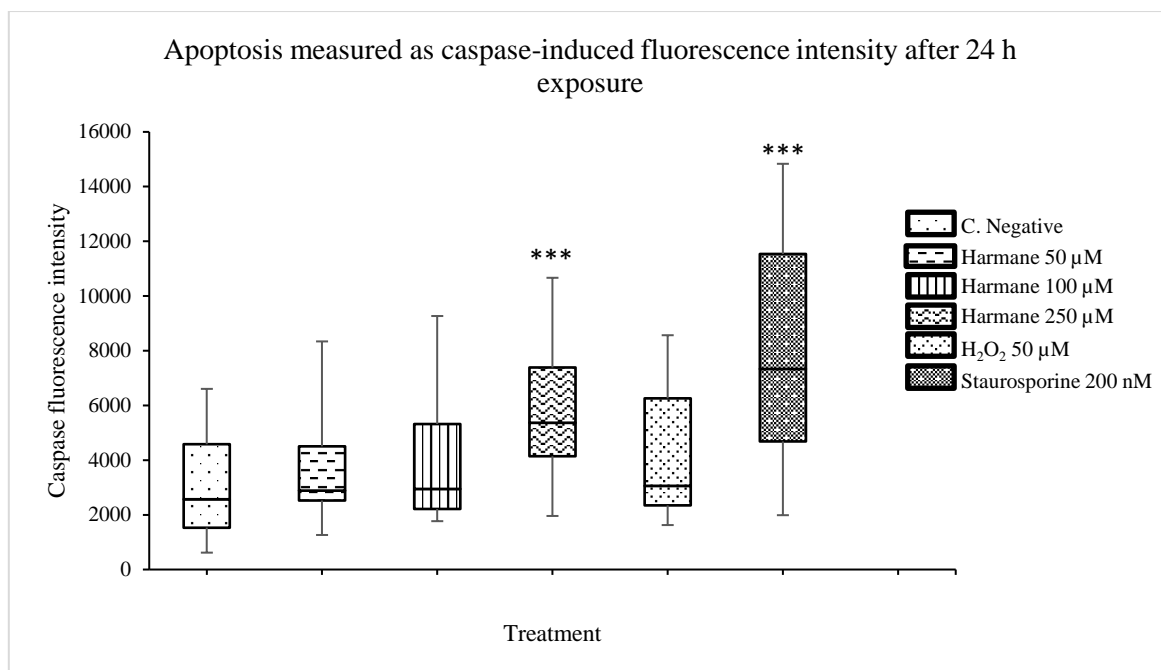
Figure 4.72: The caspase-induced fluorescence intensity after 24 h exposure to different concentrations of harmane, staurosporine and H_2O_2, data from 3 biologically independent experiments performed with 3 technical replicates (bar in the box represents the median of data) (Number of measured spheroids: 35 control negative, 35 harmane 50 µM, 42 harmane 100 µM, 32 harmane 250 µM, 44 H_2O_2, 41 staurosporine). There was a statistically significant difference between negative control and both harmane 250 µM and staurosporine 200 nM (P<0.001).

Measurement of necrosis

To assess necrosis, we measured the fluorescence intensity of propidium iodide in the same conditions as for caspase. We observed an increase in the propidium iodide fluorescence in spheroids exposed to different treatments compared to the control group (Figure 4.73). A two-way ANOVA analysis for the factors *"treatment"*, *"culture"* and for the interaction *"treatment"* x *"culture"* indicates that the differences were statistically significant for the three factors (P < 0.001). A post-hoc Bonferroni t-test showed a statistically significant difference between the staurosporine 200 nM and all other treatment, (P < 0.001), hydrogen peroxide 50 µM versus negative control (P = 0.031) and harmane 250 µM versus negative control and harmane 50 µM (P < 0.01).

The difference between cultures is significant in both tests (apoptosis and necrosis), but the treatment affects all cultures in the same levels; in other word the increase of necrosis and apoptosis were related to increased concentration of harmane; both for apoptosis and

194

necrosis, staurosporine 200 nM was a good positive control (with a much higher its effect on apoptosis, compared to necrosis) while H_2O_2 50 µM was not.
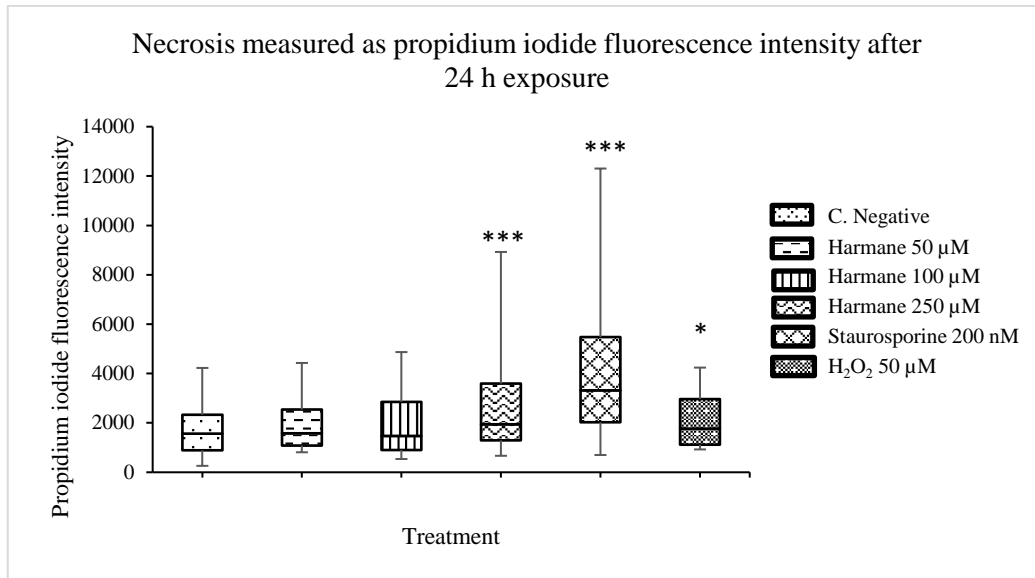
Figure 4.73: The propidium iodide fluorescence intensity after 24 h exposure to different concentrations of harmane, staurosporine and H_2O_2, data from 3 biologically independent experiments performed with 3 technical replicates (Number of measured spheroids: 35 control negative, 35 harmane 50 µM, 42 harmane 100 µM, 32 harmane 250 µM, 44 H_2O_2, 41 staurosporine). There was a statistically significant difference between control negative and harmane 250 µM ($P < 0.001$), staurosporine 200 nM ($P < 0.001$) and H_2O_2 ($P = 0.03$).

4.7 *In vivo* evaluation of neurotoxicity or neuroprotection of 1-Benz-THIQ-diol

Unfortunately, due to Covid-19 it was not possible to repeat the measures to statistically compare the frequency power and coherence, before and after administration of 1-benzyl -TIQ- 6,7-diol; therefore, the results below are to be considered as purely preliminary.

Delivery to cerebellum via a unilateral cannula

In the case of infusing 1-Benz-THIQ-diol through a unilateral cannula, the comparison of EEG data, collected before and after the infusion, indicates a general but non-significant decrease in the amplitude of the EEG signal across frequencies (Figure 4.74). However, the post-experiment immunohistochemistry of this rat cerebellum indicated a mis-position of the cannula that was in fact in the cerebellar cortex rather than in the medial cerebellar nucleus (Figure 4.75).
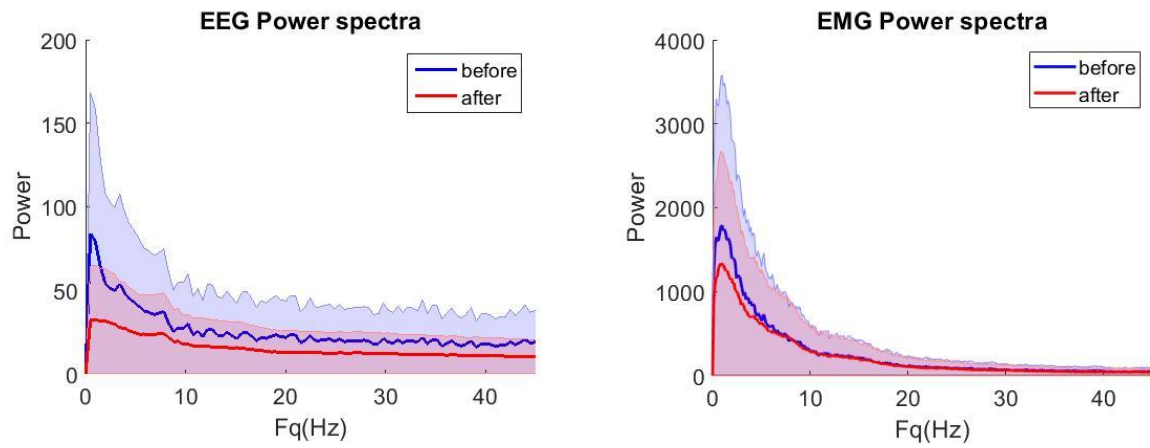
Figure 4.74: Effect of 1-benzyl -TIQ- 6,7-diol infused in unilateral cannula. The data are divided into "resting" and "moving" epochs. There was a slight decrease in the power after the infusion of compound at the tremor frequency on EMG and EEG power spectra.
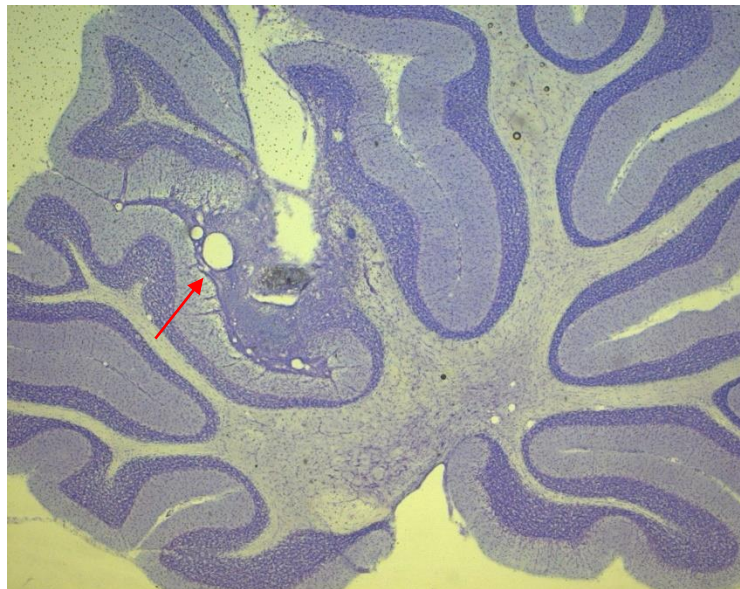
Figure 4.75: Immunohistochemical analysis of rat cerebellum displaying the approximate location of electrode recording sites (arrow) in cerebellar cortex.

Delivery to cerebellum via a bilateral cannula

The compound did not have any effect on behavior of animals, when delivered to the cerebellar nuclei through a bilateral cannula. The analysis of EEG and EMG signal plots and kinematic sensors (in particular gyroscopes and accelerometers) (Figure 4.76) indicates no difference in the signals and the frequency spectrum of acceleration caused by movements before and after infusion. However, double peaks were detected, indicating a tremor with a frequency between 7-10 Hz (close to ET tremor frequency).
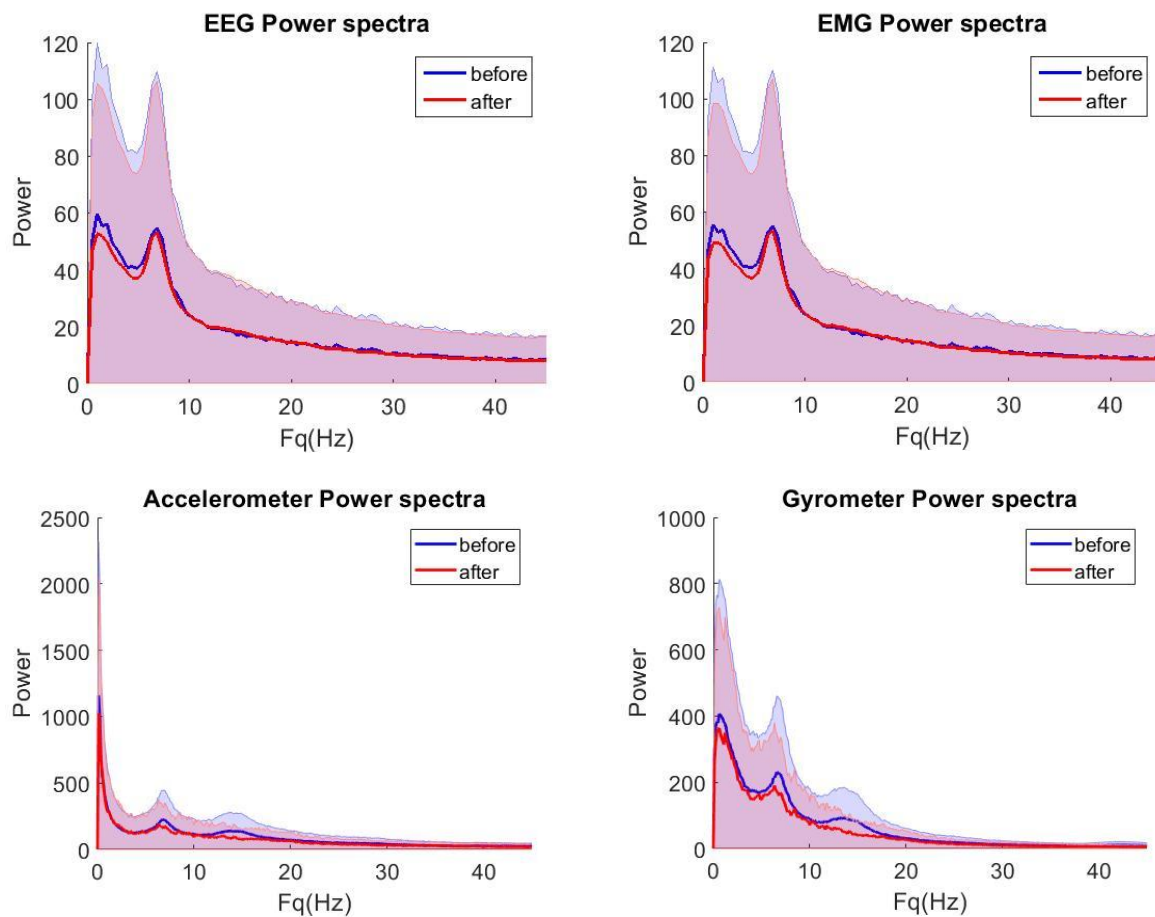
Figure 4.76_: Effect of 1-Benz-THIQ-diol infused in bilateral cannula. The data are divided into "resting" and "moving" epochs. There was no difference between before/after the infusion of compound on tremor frequency, on EMG, EEG, accelerometer, and gyrometer power spectra.

5. Discussion

ET is a widespread neurodegenerative disease whose etiology is still unclear, while both genetic and environmental factors are suspected. Many findings support the heterogeneity of essential tremor pathology [28, 361], which makes it challenging to define the role of a specific neurotoxin or a particular factor in its etiology.

The Maillard reaction, the major chemical reaction responsible for the brown color and attractive flavor of cooked foods, has desirable consequences in food industry, but some negative effects on the aliment nutritional value and the consumer's health. The end products of Maillard reaction (MRPs) or its intermediary antinutritive compounds are suspected of toxicological effects in animal models, and have been implicated in diseases, notably in neurodegenerative disorders [362-364]. Cooked protein foods, like meat, are a major dietary source for heterocyclic amines (HCAs) and carbonyl compounds that have been linked to neurodegenerative diseases, including essential tremor [365-367]. As with other MRPS, their quantity in cooked meats varies according to meat type and cooking practices, i.e. temperature, duration, the presence of water and the concentration of sugar and amino acids, while their identity depends on the reacted sugars and amino acids [97].

In the present work, we aim at investigating the dietary epidemiology of Essential Tremor, through the study of overcooked meats and the development of a strategy to identify Maillard reaction products (MRPs) possibly implicated in ET.

5.1 Preparation of overcooked meat samples

The preparation of our samples aimed at developing a brown color, that results from the condensation of amino compounds and sugar fragments in the meat into brown pigments called melanoidins, as indicator of Maillard reaction occurrence. By contrast with some studies in the literature, we have chosen to develop an overcooking method that yields a meat remaining consumable, typical of what can be achieved in daily (over)cooking.

5.2 Extraction of overcooked samples

We have investigated both β-carbolines and carbonyl compounds as (*i*) the β-carboline harmane is described as a potent neurotoxin and has been proposed as an environmental etiology for ET, due to its elevated concentration in the blood and brain of patients [40, 41,

99] and its identification in cooked foods; (*ii*) the injection of the β-carboline harmaline has a high tremorgenic effect in animals; and (*iii*) β-carbolines are both exogenous and endogenous in origin; and so we were interested in their carbonyl compounds precursors and their possible reaction with endogenous amines.

5.2.1 Extraction of β-carbolines

The amounts of β-carbolines in cooked meat are very low (at ppb level, i.e. 0.1 - 9.6 ng/g) as mentioned in a 2004 review by Pfau [97]; moreover, they exist in complex matrices that impose difficult extraction processes, involving multi-steps techniques.

We applied two different methods for the extraction of β-carbolines from beef and chicken meat, taking into account their pH-dependent solubilities. In both methods, we used an alkaline solution to digest the matrix and liberate the β-carbolines, followed by extraction with organic solvents since free alkaloids are lipophilic.

1- *Extraction of β-carbolines by an alkaline detergent solution*

This method, described by Louis ED et al. 2007 to quantify harmane in barbecued/grilled meat samples [323], was applied with slight modifications: (*i*) the discarding of a protease inhibitor cocktail, based on preliminary assays that showed no difference between the extraction w/o protease inhibition; (*ii*) the use of diethyl ether instead of methyl t-butyl ether based on their close polarities (polarity indexes, 2.5 and 2.8, respectively).

The yield of extracts (w/w) was low (as expected) and the dispersion of yields for the 3 extractions was acceptable (CV ≤ 10 %). This method could be considered as simple as only depending on the selectivity of organic solvents, but it does not include any step of purification from other possible organic-soluble impurities.

2- *Extraction of β-carbolines by a general alkaloid method*

For this extraction, we made the choice to continue working with one kind of meat "the chicken", our choice was based on the work of Louis et al. (2007) [323] in the determination of the concentrations of five β-carbolines (ng/g) in three meat types

"beef, hamburger and chicken", where the concentration of harmane was higher in the chicken meat.

To increase the size of our samples, and subsequently the amount of extract, and considering the fair thermic stability of β-carbolines, we used a Soxhlet apparatus that allowed a continuous reflux extraction with limited amounts of solvent.

This method included purification steps through partitioning with acidic aqueous solution, that gives the advantage, over the previous alkaline detergent extraction, of higher selectivity; this was reflected by the much lower yields of the alkaloid totum extract. The dispersion of extract means was acceptable with a CV of 2 %.

5.2.2 Extraction of carbonyl compounds

Carbonyl compounds play an important role in the meat flavor, also they are very reactive towards oxidoreductive, polymerization and amine-condensation transformations and represent intermediates in a lot of biochemical reactions. Our interest was focused on the possibility of aldol condensation of carbonyl compounds with amino groups of meat constituents or endogenous amines to produce heterocyclic amines (i.e. artifactual and endogenous alkaloids, respectively). The production of carbonyl compounds in heated meat might be as result of Maillard reaction, Strecker reaction (that is perceived as a reaction within the Maillard reaction), lipid oxidation, degradation of thiamine, or even bacterial action [332, 368].

For carbonyl compounds extraction, we used different methods to extract the volatile and non-volatile aldehydes from chicken cooked meat:

1- *Extraction of volatile carbonyl compounds by Solvent Assisted Flavor Evaporation (SAFE)*

This method was described as one of the best methods for "clean" aroma extracts at low temperature, with high efficiency of extraction for the most volatiles compounds [369]. The samples in SAFE apparatus are preferably in liquid state, although the method can be applied directly on matrixes, but with the need for a high vacuum

$(< 10^{-3}$ Pa) pump. Considering the available equipment, an aqueous extract of chicken meat samples was distillated, in addition to the browned chicken meat juices.

The amount of solvent used in this method is minimal and the complexity of the work is considered low, provided that the system is correctly handled and set, which is not so straightforward as described. Still, a continuous supervision of the extraction is needed to ensure that all parameters (temperature and vacuum) are well applied and maintained and to control the size of samples dropping to avoid the reflux of non-volatile compounds; also, as liquid nitrogen is so volatile, there is a need to adjust its level to maintain the temperature of the cold trap.

2- *Extraction and analysis of volatile carbonyl compounds by headspace single-drop microextraction (HS-SDME) with droplet derivatization*

The HS-SDME technique allowed the isolation of numerous volatile carbonyl compounds with small sample volume and very few steps.

This method needs precision in application and definition of the best parameters for the samples, including selection of a solvent with a polarity adequate for all volatile compounds, of the temperature and stirring rate applied during the process; also the volume of organic solvent in the syringe depends on the viscosity of the solvent and its temperature of evaporation. On the other hand, this technique is fast, inexpensive, and ensures reliable results [326, 327].

We slightly modified the original method by changing the organic solvent decane to heptane (as the decane peak overlapped many aldehyde peaks in the GC chromatogram), and the volume of injection was increased to 3 µL to compensate the heptane evaporation.

3- *Extraction and isolation of lower-polarity carbonyl compounds by condensation over a silica-gel supported reagent*

In this method we based on a Soxhlet apparatus to extract the carbonyl compounds from the chicken meat samples in an organic solvent and followed by specific isolation through condensation with a semicarbazide to separate the carbonyl compounds from other extracted impurities.

This method is adequate for the extraction of lower-polarity carbonyl compounds; the Soxhlet advantages (automated renewal of fresh warm solvent over a series of extraction processes without requiring handling and filtration) are combined with a selective condensation with a semicarbazide-silica reagent to ensure the isolation of carbonyl compounds. However, this condensation-desorption is a long procedure that cannot be sped up by agitation, requires huge volumes of solvent and presents some variability (CV% for carbonyl totum > 10 %). Also, the need to evaporate the large volumes of solvent (toluene) is time consuming and absolutely not adequate to recover volatile aldehydes [370].

5.3 Characterization of extracts

5.3.1 Identification of β-carbolines

5.3.1.1 Thin-layer chromatography analysis (TLC) of β-carbolines

TLC is a semi-specific method of analysis; despite its low-resolution, it is frequently used as a preliminary screening technique, offering valuable data regarding the identity of the components existing in a sample. Therefore, the results obtained by TLC should be confirmed by other analytical methods.

In our work, the identification by TLC relied on the visual comparison with reference standards of Rfs, of colors/fluorescences under UV exposure and, upon chemical pulverization with Dragendorff's reagent, under visible light. Although considered quite indicative for alkaloids presence, the Dragendorff reagent is not entirely specific and many non-alkaloid compounds give a positive reaction, e.g. *(i)* amides [352]; *(ii)* non-nitrogenous compounds, notably aldehydes, ketones, lactones, ethers, esters, epoxides, and peroxides with an ethylene bond or free alkyl groups at the β-carbon [353]; and *(iii)* artifacts coming from reactions with nitrogenous compounds during an alkaline extraction [353]. Therefore, the obtained results need to be confirmed with another method such as HPLC.

TLC analysis of β-carbolines extracted by an alkaline detergent solution

In this method of extraction, we were not able to confirm the presence of any of our standards in our samples; (*i*) the Rf of the compound detected in both beef and chicken meat extract is close to the Rf of harmane and harmine; (*ii*) the orange coloration of the extract spot with Dragendorff indicates the probable presence of an alkaloid (as we mention above, it is not entirely specific); and (*iii*) there was no color match under UV light.

For that, a verification of the efficiency of the method of extraction and detection was needed.

1- By alkaline detergent treatment of a methanolic solution of harmane, in concentration adapted to the expected concentration of our samples and comparison on TLC plate with meat sample extract and diluted harmane standard at the same concentration.
The TLC showed the efficacy of the extraction method since the spot of extracted harmane has (*i*) the same Rf as diluted harmane; (*ii*) the same color under UV light, but with an intensity of fluorescence lower than the diluted harmane, which could be explained as a partial loss of harmane through the extraction. Still, the treated harmane solution has the same grey spot as the meat sample, which can be explained as an artifactual effect from the alkaline detergent.
To conclude, the first identification indicates a probable loss of compounds of interest during extraction.

2- The identification of the role of meat matrix in the extraction method. The four standards were spiked in overcooked chicken meat (1.2 mg each/10 g) and extracted. The TLC indicates that (*i*) the blue fluorescence has disappeared for the spiked sample under $UV_{254\,nm}$ light but is still faintly apparent under $UV_{366\,nm}$; (*ii*) the Rf and coloration of the Dragendorff-positive spot were similar in spiked and unspiked extract, confirming the artifact from the extraction detergent (seen in step 1).
This second step of verification clearly indicates an important role that meat matrix plays in hindering this extraction method at the levels spiked.

Based on these results that indicate a huge interference of the meat matrix on the extraction, interference that was not apparent from published data obtained with this method [323], we decided to test another method of extraction, specific for alkaloids. For this method, a higher

amount of meat sample also allowed to increase the extracted quantity of β-carbolines and so their probable detectability.

TLC analysis of β-carbolines extracted by a general alkaloid method

A TLC comparison between the chicken meat extract and the 4 β-carbolines standards indicates similarity of Rf between one spot of the extract and harmalol; however, the extract spot did not show the blue fluorescence of harmalol under $UV_{254\,nm}$ light and a different color upon reaction with Dragendorff's reagent; this may be explained by a difference in concentrations.

Based on above, there was high probability that the extract contained harmalol, but this needs to be confirmed by another method.

5.3.1.2 High Performance Liquid Chromatography (HPLC) of β-carbolines

Chromatograms of β-carbolines reference standards

The chromatography of reference standards in different concentrations indicates the difficulty to detect, with our DAD UV system, the standards in concentrations less or equal to 1 µM, which correspond to about 0.2 µg/mL (200 ng) of each standard.

HPLC analysis of β-carbolines extracted by an alkaline detergent solution

The extract did not show a peak matching with one of our β-carbolines standards. According to literature [323], the expected concentration of harmane in our samples should be 84.8 ± 98.6 ng/10 g; comparing with the detection limit of our reference standards makes it difficult to determine their presence in our sample, especially considering the extraction losses we have shown (Section 5.2.1).

In the original paper describing the method of extraction [323], the authors have spiked the meat and the extraction buffer with harmane and harmine standards (100 ng/g of chicken meat and 100 ng/2 mL buffer) before extraction, calculating the harmane[39] recovery (102.6 %) from the ratios of peaks measured in the two extracts. Based on our observation of

---

[39] In this paper, we notice that recovery data for harmine are not presented. Also, the recovery seems to be obtained from a single experiment at a single spike point and this spike is way higher than the levels actually measured in meats (12 – 26 times higher).

the meat matrix role in extraction losses, this recovery appears quite surprising, especially considering the inclusion in the method of a *"removal of top-layer fat tissues"* in alkaline conditions. Indeed, at alkaline pH, β-carbolines are lipophilic and have all chances to be extracted by the fat layer.

HPLC analysis of β-carbolines extracted by a general alkaloid method

Despite the elevated amount of extracted meat to increase the possibility to detect the 4 β-carbolines standards, we were not able to confirm the presence of harmalol; also, no other β-carboline could be detected. This should be further explored with a more sensitive detection method (fluorescence).

5.3.1.3 Conclusion regarding the determination of β-carbolines in meats

Given the difficulties in measuring such low amounts of β-carbolines in meat, we decided to investigate overcooked meats for compounds that could be implicated in the generation of biologically active artifactual endogenous alkaloids, and we focused our attention on carbonyl compounds.

5.3.2 Identification of carbonyl compounds

Carbonyl compounds have special interest for their toxicity and carcinogenicity that relate to their ability to adduct or react with endogenous amines, proteins or nucleic bases [371, 372]. Many studies examined their (trace) presence in air, water, beverage, or food; as such, different sensitive methods were developed to identify and quantify nanogram amounts of carbonyl compounds, making profit of various derivatization reagents capable to capture small (a)polar carbonyl molecules [373-376].

For the identification of carbonyl compounds in our meat samples, we applied different derivatization strategies and chromatographic methods.

5.3.2.1 Derivatization with PFBHA followed by Gas Chromatography-Mass Spectrometry (GC-MS)

GC/MS is widely used for the characterization of carbonyl compounds in biological fluids for its sensitivity, selectivity, specificity, and rapidity; the derivatization with PFBHA reduces cleanup steps and yields oximes, stable at elevated temperatures and amenable to GC analysis [330, 377, 378].

This derivatization with PFBHA was applied, following two different methods: *(i)* the EPA method 556 [379] on the SAFE extract; and *(ii)* a direct derivatization by headspace single-drop microextraction (HS-SDME) [327].

Both methods require very small quantities of organic solvents; the micro-extraction procedure is particularly fast and convenient but does not include any washing step that could reduce the levels of eventually extracted interferants.

The identification of analytes in the sample chromatograms was based on a search in the NIST[40] library, taking into account the match probabilities, and on a comparison of peaks retention times (RT) with those of aldehyde standards, both pure and included in laboratory-fortified blanks; based on the variations of standards RT in a triplicate measurement, a slight window of accepted RTs was defined. From these RTs, we computed Kovats retention indexes (KRIs) as a second dimension for identification; through comparison with the retention times of aliphatic alkanes, KRIs convert the retention times to constants (retention indexes). Although we were not able to locate a bibliographic reference for PFBoximes KRIs, most of them are included in the NIST library.

We noticed in the procedural blanks important peaks for formaldehyde, acetaldehyde, and a small peak identified as methyl glyoxal; the well-known atmospheric contaminants formaldehyde and acetaldehyde [379] were excluded when analyzing our samples.

---

[40] The National Institute of Standards and Technology (NIST) is a mass Spectrometry Data Center, a Group in the Biomolecular Measurement Division (BMD) of the U.S. Department of Commerce. NIST develops evaluated mass spectral libraries and provides related software tools. These products are intended to assist compound identification by providing reference mass spectra for GC/MS (70 keV electron ionization) and LC-MS/MS (by tandem mass spectrometry) as well as gas phase retention indices for GC.

We could identify *(i)* 9 and 11 aldehydes in the SAFE extracts of browned chicken meat juice and aqueous chicken extract; and *(ii)* 8 and 4 aldehydes in the HS-SDME extract of browned chicken meat juice and aqueous chicken extract, respectively Table 5.1.

Comparison of these two analytical methods indicates a very good agreement between the 2 methods for the identification of volatile aldehydes. The SAFE technique allows a clearer chromatogram (better signal to noise ratio). However, HS-SDME is way faster and requires much less steps. As these 2 analytical methods are limited to volatile compounds, we investigated a further method to identify low-polarity and low-volatility carbonyl compounds.

Four of these aldehydes were selected for the continuation of this work (propionaldehyde, isobutyraldehyde, hexanal, benzaldehyde); the criteria of selection were based on the height of peaks, considered as an indication of the preeminence of a given aldehyde in our samples. We however discarded formaldehyde and acetaldehyde, well-known environmental contaminants [380, 381] that are not so characteristic of overcooked meat samples. Identification of carbonyl compounds likely to react with endogenous amines to form "artifactual" alkaloids.

5.3.2.2   Derivatization with 4-hydrazino-N, N, N-trimethyl-4-oxobutanaminium iodide (HTMOB), ESI-MS/MS

For this method, the carbonyl compounds were extracted from overcooked chicken meat according to the technique discussed in section 5.2.2-3 (reaction with a silica gel-supported semicarbazide). The identification of extracted carbonyl compounds was aided by derivatization with HTMOB, a modified Girard derivatizing reagent. This HTMOB derivatization presents a series of advantages over methods based on Girard T reagent, that is a universal ESI-MS/MS product ion, with a constant mass loss regardless of molecule size, yielding a high intensity signal, which improves the analytical sensitivity [331].

As HTMOB is commercially unavailable, we performed the synthesis in our lab, based on the description of Johnson DW (2007). As shown by NMR and MS, we obtained a relatively pure product a preliminary test with benzaldehyde showed that the synthesized HTMOB could be used as a sensitive reagent and allowed to fine-tune the derivatization conditions. The ESI-MS-MS analysis of HTMOB-reacted overcooked chicken meat carbonyl extract

(silica gel extract) provided a rapid and clean neutral loss 59 spectrum but indicated the need to create a database of carbonyl standards to aid in peaks identification. The few compounds identified by this method in overcooked chicken meat and browned chicken meat juices are presented in Table 5.1.

Table 5.1 : Summary of carbonyl compounds detected by the three analytical methods

	Browned chicken meat juice			Chicken meat		
	SAFE PFBHA[a]	HS-SDME[b]	Silica-gel [c]	SAFE PFBHA[a]	HS-SDME[b]	Silica-gel [c]
Benzaldehyde	+	-	-	+	+	-
Butyraldehyde	+	-	-	+	+	-
Crotonaldehyde	+	+	-	+	+	-
Cyclohexanone	+	-	-	-	-	-
Glycolaldehyde	-	-	-	+	-	+
Heptanal	+	-	-	+	+	-
Hexanal	+	+	-	+	+	-
Isobutyraldehyde	+	+	+	+	+	+
Isovaleraldehyde (3-Methylbutanal)	-	-	+	+	-	+
Nonanal	-	-	-	-	+	-
Octanal	-	-	-	-	-	-
Phenylacetaldehyde	-	-	-	+	-	+
Propionaldehyde	+	+	-	+	+	-
Valeraldehyde (Pentanal)	+	-	-	+	-	-
2-methylbutyraldehyde	-	-	+	-	-	+

[a] SAFE distillate from the aqueous extract; derivatization with PFBHA followed by GC-MS analysis
[b] Direct derivatization by headspace single-drop microextraction followed by GC-MS analysis
[c] Silica-gel supported extraction; derivatization with HTMOB followed by ESI-MS-MS analysis
Blue cells indicate compounds common to SAFE, HS-SDME and/or silica-gel analyses
Pink cells indicate compounds identified by only one method

5.4 Identification of carbonyl compounds likely to react with endogenous amines to form "artifactual" alkaloids

Carbonyl compounds constitute an organic group that includes many different compounds with structural diversities and differences in chemical reactivity. Their mechanism of toxicity in neurodegenerative diseases, more specifically essential tremor, might correspond to their ability to non-enzymatically interact with endogenous amines to form artefactual compounds, notably β-carboline and isoquinoline alkaloids [150, 382, 383]. Therefore, there was an importance to verify the possibility that the carbonyl compounds identified in our meat extracts react with biogenic amines. This was tested by simple equimolar incubation at 37°C in an aqueous medium (some solubility issues in water were resolved by using slight proportions of methanol). The reaction was applied on standard aldehydes in place of the complex meat extracts, which facilitated the analysis by molecule, the determination of both reactants concentrations, and the identification of reaction products.

We examined the possibility of condensation reactions followed by spontaneous cyclization to produce an isoquinoline ring (reaction with dopamine, epinephrine, or norepinephrine) or a β-carboline ring (reaction with serotonin or tryptamine). The verification of reaction possibility was performed using TLC techniques and the reaction products were tentatively identified by TLC/MS. It should be noted that TLC/MS is unable to precise whether a cyclisation has effectively taken place as the molecular weight (m/z) is the same for cyclic and non-cyclic molecules; thus, further verification will be needed for reaction products of interest.

The identification of possible reaction products was applied for detected carbonyl compounds (Section 5.3.2) that were reacted with 6 endogenous amines (dopamine, serotonin, epinephrine, γ-aminobutyric acid (GABA), tryptamine, and tryptophan). As a result, 4 of the tested carbonyl compounds were demonstrated able to spontaneously condensate with amines, with 6 reaction products yielding the m/z corresponding to expected reaction products. For some reactions, we noticed the presence of the desired m/z in different TLC spots (Section 4.2.3.2); as we mention above, TLC/MS cannot give us information about the nature of molecule (aliphatic or cyclic) and further verification, by comparison of Rfs with

reference standard and by isolation followed by NMR elucidation of structure, is needed for the molecules of interest.

According to the *in silico* predicted toxicity of likely reaction products (Section 4.2.4), the experimental work was continued with the major reaction product between dopamine and phenylacetaldehyde, i.e. the 1-benzyl-1,2,3,4-tetrahydroisoquinoline-6,7-diol (1-benz-6,7-diol THIQ). Our trials to purify enough 1-benz-6,7-diol THIQ for NMR analysis were unsuccessful, the yield of synthesis being quite low and the purification particularly difficult due to an apparent reversibility of the reaction. After many difficulties, we managed to obtain the molecule from a commercial source (Chemieliva Pharmaceutical Co., Ltd, purity 95) and the comparison of TLC Rfs and MS confirmed that 1-benz-6,7-diol THIQ is effectively a major product of reaction when incubating dopamine with phenylacetaldehyde at 37°C. Given the phenylacetaldehyde pharmacokinetic properties (predicted by pkCSM: log P, 1.428[41]; log BB[42], 0.169; log PS[43], -1.724), the compound has a good probability to cross the blood-brain barrier and to encounter dopamine in brain tissues. Moreover, given the very high concentrations of dopamine in the gastrointestinal tract (production by enteric neurons and intestinal epithelial cells), and thus in hepatic portal vein [384], there is also a high probability of local condensation with alimentary phenylacetaldehyde to yield 1-benz-6,7-diol THIQ.

5.5 In silico prediction of neurotoxic or neuroprotective effects of tentatively identified reaction products

The practice of "*in silico* toxicology" is necessary to identify and classify potential risks for molecules, in a cost effective and timely manner. Different methodologies can be used as preliminary screening tools to identify potential toxicant effect and prioritize compounds for further testing by standard laboratory procedures [385, 386].

---

[41] This log P indicates an ability to cross biological membranes
[42] A compound with log BB > 0.3 is considered to readily cross the blood-brain barrier, while molecules with log BB < -1 are considered poorly distributed to the brain
[43] A compound with log PS > -2 is considered to penetrate the central nervous system

It is beneficial to use the results of several expert toxicity systems to reduce the risks of false negative predictions. In this work, the neurotoxicity was predicted for 7 molecules using the publicly available web server e-MolTOx and the results were crosslinked with the biological activities gathered from PubChem. In addition, the pharmacokinetic properties (ADMET) were predicted *in silico*, using the pkCSM web server.

For harmane, the e-MolTOx algorithms do not predict a neurotoxicity; by contrast, the data repertoried in PubChem describe harmane as a neurotoxin and suggests its implication in neurodegenerative diseases, seizures and tremor while the acute toxicity section mentions *"altered sleep time"*. These diverging results of toxicity between a predictor and limited experimental data might be explained by the lack of toxicology-related experimental datasets; in fact, further investigation on harmane neurotoxicity is needed.

For 1-benz-6,7-diol THIQ, eMolTox predicts a modulation of dopamine receptor D1, while PubChem data indicate binding with dopamine receptors D1 and D2 and an agonist activity on α1B-, β1- and β2-adrenergic receptors. The affinity with dopamine receptors could explain a D1, D2 dopaminergic antagonist effect [356]. Considering the compound predicted pharmacokinetic properties (pkCSM: log P, 2.527; log BB, 0.109; log PS, -2.053) and knowing that dopamine antagonists are known to induce parkinsonism, dystonia, tics and tremor [357, 358], the compound was accordingly selected for further investigations.

For the other compounds, e-Mol-TOX predicts modulation effects for the following receptors; (*i*) serotonin (2a, 2b and 2c) by 1-isobutyl -1,2,3,4-tetrahydro-1H-β -carboline; (*ii*) serotonin 2a by 1-pentyl-1,2,3,4-tetrahydro-β-carboline; (*iii*) dopamine D1 and serotonin 1b by 1-pentyl-1,2,3,4-tetrahydro- 6, hydroxy-β-carboline; (*iv*) dopamine D1 by pentyl-1,2,3,4-tetrahydroisoquinoline-6,7-diol; and finally (*v*) serotonin 2b and α2A adrenergic by 1-phenyl-1,2,3,4-tetrahydro-β-carboline. In PubChem, these molecules are either not described or no toxicology data are listed.

The ADMET distribution analyzed by pkCSM indicate that some of these molecules readily cross the blood-brain barrier (harmane, 1-pentyl THβCa and 1-phenyl THβCa); the others present less favorable properties but some (i.e. 1-benz-6,7-diol THIQ) will most probably penetrate the CNS. It should be noted that these predictions of permeability do not consider

an eventual transport mechanism and are purely based on molecular weight, lipophilicity, hydrogen bonding, and other variables that regulate the diffusion of molecules through a membrane [387].

Taking in consideration that *in silico* toxicology is built on data sets from previous biological work and on structural similarities with known toxicants, they do not yield certitudes, but provide rapid analysis and prediction. Although the different methodologies and the application of *in silico* approaches rapidly evolve, there is still considerable work needed to increase their potential, in particular by generating biological data to comfort and expand the necessary datasets [388].

5.6 In vitro evaluation of neurotoxicity and neuroprotection

ET is a complex pathology with potentially varied environmental determinants. Food cooking, through Maillard reaction, notably generates β-CAs but also aldehydes that can condense with endogenous amines to form β-CAs and isoquinolines. The role and importance of β-carboline alkaloids in the pathogenesis need to be clarified. Harmane is the molecule with the higher evidence so far in terms of pathogeny [365] but analogous compounds could present a synergistic action or even be more active. In addition, the role of isoquinolines in neurodegenerative disorders and their long term neurotoxic effects need further examination [389].

Unfortunately, *(i)* the lack of clear mechanisms for ET development impedes biochemistry-based studies; and *(ii)* animal models do not reproduce human tremor perfectly, remain expensive and raise ethical issues. 3D neural spheroids represent a promising future in research for neurological diseases as they will allow to carry out screening studies to identify toxicological effects of environmental factors, including harmane/harmaline derivatives and analogues or THIQs and derivatives. In addition, the primary location of the CNS sites involved in the generation of ET remains highly debated. It is possible to select brain structures during cell harvesting for seeding and so to produce organoids specific to parts of the brain, possibly leading to specific architectural and/or functional models. This theoretical prospect would permit the study of β-carboline alkaloids or THIQs in cells from the

cerebellum, cortex or brainstem, possibly providing additional evidence to support the key-role of one target rather than another.

5.6.1   Development of 3D Cell culture model

The 3D cell cultures and organoids are growingly being used to bridge the gap between *in vitro* 2D cell cultures and *in vivo* animal models. There is a consensus that 3D models are more physiologically relevant than biochemical assays and 2D cell cultures, as they more closely represent the microenvironments, cell-to-cell interactions, and biological processes that occur in vivo [390-392]. However, the 3D neuronal cultures remain challenging for many technical aspects. Notably, these 3D spheroids sizes must be controlled because of the lack of circulatory system that may cause central necrosis zones due to a lack of oxygen and nutrients. This limitation is a key point in the development of 3D neural spheroids as it may jeopardize the sensitivity of toxicity screening tests [393]. To circumvent these problems, advanced culture techniques, based on growing neurons either in microfluidic circuitry [231] or in co-culture with blood capillaries [394], have been proposed; these are however much more technically challenging. Involved technologies are also proposed for high-throughput workflow, accuracy, precision, culture manipulation and integrity. However, such methods are still largely artistic, not standardized, and not accessible in all laboratories [395].

We chose to apply a 3D neurosphere culture based on a non-scaffold technique, that needs reasonable lab equipment and is stated to offer reproducible cultures, using prenatal mice neural cells and agarose-molded wells. We developed our method by testing different microwell diameters and cell densities. Based on the reproducibility and ease of harvesting, our preferred diameter was 400 µm in "large" molds (i.e. 800 µm diameter, 800 µm depth).

Although this method requires a simple lab equipment, it needs a very careful and precise experimenter as different factors affect the quality and quantity of spheroids, starting from the set-up prior to culture and ending by spheroid harvest: *(i)* the quality of agarose micro-well shapes[44] affects the distribution of cells and thus the diameter of spheroids; *(ii)* the pre-culture equilibration with the medium; *(iii)* the dissection and dissociation of cortical tissues

---

[44] that strongly depends on the horizontality of casting surface

influence the quality of neurons seeded; *(iv)* the time needed for cells to settle and aggregate before adding the total volume of medium; *(v)* and the regular and timely medium renewing.

5.6.2   Characterization of obtained spheroids

Different parameters were measured to characterize our 3D neural spheroid cultures and to investigate their reproducibility:

- ***Spheroid diameters***
  Spheroid size was controlled by altering the number of seeded cells. The measurements of spheroid diameters indicated that the spheroids were well aggregated at 4 DIV, with a growth observed between 8 and 11DIV; depending on growth time, measured diameters were slightly different from culture to culture but came to be uniform at 11 DIV.
  Our experience indicates that different parameters can be improved to yield a reproducible diameter culture: (*i*) make sure that the agarose mold does not form a curved contact surface with the plate; (*ii*) automatize cell counting; and (*iii*) suspend very well the cells before seeding.

- ***Spheroid surface structure***
  The characterization of surface structure by SEM reflexed the intricacy of cell-to-cell connections, with complex surfaces, and a bundle of axons and dendrites.

- ***Identification and quantification of cell types present in spheroids***
  To obtain biological information, CNS markers-based immunocytochemistry coupled to fluorescent dyes was realized, both in epifluorescence and confocal microscopies. Histological staining with observation under white light was also applied to visualize the centers of spheroids.
  By epifluorescence microscopy
  The analysis of fluorescence microscopy images indicated that our 3D neural spheroid cultures comprise all brain cell types, including glial, microglial and neural cells. Moreover, the quantitative fluorescence intensities corresponding to the different markers was invariable between the cultures, demonstrating a high reproducibility in terms of proportions of cell types in spheroids.

215

Quantifying the fluorescence of spheroids is challenging and needs optimization and attention to increase the robustness of assays and the compatibility with high-throughput screening. In 2D cell cultures, the signals are typically normalized based on the field of view or numbers of cells; neither are applicable in spheroids for which the method of fluorescence signals normalization must reflect the variables of width, length and height radii of spheroids [396].

In our work, the attention to the staining methods, their optimization and normalization of the fluorescence signals were taken in consideration to reduce the errors and enhance sensitivity. The duration of spheroid staining was increased, the signal was normalized by eliminating the size-based differences in fluorescence and, to do so, we analyzed the spheroids within narrow ranges of radii.

Applying flow cytometry analysis would undoubtedly be be more precise for the quantification of cell types, but our trials indicated that properly dissociating a neurosphere is quite challenging.

By confocal microscopy
The confocal microscopy provides the highest sensitivity and X, Y and Z resolution imaging with high-throughput data acquisition.
Still, the imaging of 3D neural spheroids remains challenging: *(i)* the inability of imaging optics to penetrate deep into the 3D structure to provide relevant information (light scattering and absorption limit confocal imaging at depths around 100 µm); *(ii)* the density and diameter of the 3D spheres remain key parameters for accessibility to imaging optics; *(iii)* further challenge remains in the measurement (segmentation and quantification) of relevant 3D parameters in the reconstituted images, if possible in a medium- to high-throughput manner [397].
The use of some techniques allowed us to improve the confocal: *(i)* the use of a water immersion objective, that improves the resolution as its higher numerical aperture allows to capture more light and smaller focal depth reduces the background light and light scattering compared to air objectives; *(ii)* optical clearing techniques to remove the lipid and protein molecules that contribute to light scattering effects, and thus homogenize refractive indices within spheroids [398].

We applied these 2 techniques to enable fluorescent imaging deep within the sphere. The obtained confocal spheroid images enlighten the complexity of structure and illustrate the intricate architecture of spheroids microenvironment with highest sensitivity. Nevertheless, the still limited penetration depth raises the question about cell viability in the center of spheroids (Figure 4.69). Also, analyzing confocal images, e.g., for measuring connections, axons or dendrites sizes remains complicated and requires further expertise.

By sectioning, staining and visible microscopy

As the spheroids centers appear dark in confocal images, the need to get information on its constitution appeared obvious; indeed, the applicability of the model will vary whether this "invisible" area reflects a necrotic area, as a result of oxygen and nutrients privation, or an optical problem in penetrating the 3D structure.

To visualize the spheroids centers, we applied a traditional histological embedding/sectioning/staining [399], with an hematoxylin and eosin (H&E) stain that highlights a broad range of cytoplasmic, nuclear, and extracellular matrix features. The observation of multiple H&E stained histological slices at different depths of spheroids, including the center, indicated that the dark centers were due to light penetration issue, and that necrosis is limited. Compared to the rest of the spheroid, the center appears to contain more connective tissue and fewer cells.

This slicing technique might be the best to analyze the complexity of the spheroids and could be completed by staining the slices with different antibodies. But this method certainly reduces the analytical throughput and the advantages of 3D imaging.

5.6.3 Study of cytotoxicity on spheroids

For cytotoxicity assays, we have tested harmane and 1-benz-6,7-diol THIQ at different concentrations, over 24 h.

Harmane, a natural β-carboline, is described as both a neurotoxic and neuroprotective molecule; it is notably a strong inhibitor of myeloperoxidase [329] , a key player in neuroinflammation [400], a monoamine oxidase inhibitor [401] and an antioxidant considered as a likely chemoprotective agent [402]. The harmane neurotoxicity has been

related to its dopaminergic effects [403] and a series of data incriminate harmane exposure in the pathogenesis of ET [402].

Also, THIQs have been described as neurotoxic and neuroprotective molecules [153]. 1-benzyl-1,2,3,4-tetrahydroisoquinoline (1-benz THIQ), a close relative to our tested molecule (1-benz-6,7-diol THIQ) (Figure 5.1), is suspected in the pathogenesis of Parkinson disease; it has a role in dopaminergic neurons death by decreasing the concentration of dopamine in tyrosine hydroxylase-positive cells [404], inhibiting the respiratory chain, inducing the formation of ROS [405], increasing lipid peroxidation and activating caspase-3 to induce apoptosis [406].However, these effects are suggested to be concentration-dependent, and low benzyl-1,2,3,4-tetrahydroisoquinoline concentration was shown to exhibit neuroprotective activity [407]. Another close relative is tetrahydropapaveroline (Figure 5.1), the neurotoxic THIQ that has been related to Parkinson's disease and alcoholism, through its ability to produce ROS that can cause a dopaminergic neuronal death and DNA damage [408, 409].
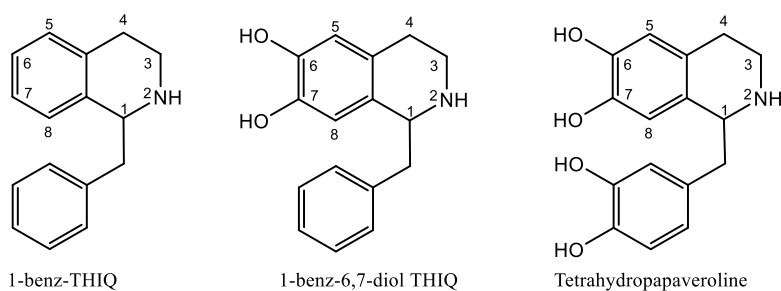
Figure 5.1: structure of 1-benz THIQ, 1-benz-6,7 diol THIQ and tetrahydropapaveroline

5.6.3.1 Evaluation of cell viability

The 'resazurin reduction test' has been broadly used as an indicator of cell viability in several types of assays, in which resazurin (blue and nonfluorescent) is reduced to resorufin (pink and highly fluorescent) by transfer of electrons from $NADPH + H^+$ to resazurin by mitochondrial enzymes; although the reduction takes place within cells, the resorufin is excreted in the medium [410, 411]. This test is considered a simple method for measuring cell proliferation and cytotoxicity that can be quantified by spectrophotometry of culture medium.

Evaluation of cell viability in the presence of harmane

The application of this test on 3D spheroids raises a question whether the cell-cell interaction inhibits resazurin uptake and reduces the reduction activity [411]. For that, we applied a verification method for the test, by comparing the resazurin measures of viability with the measure of neurons (MAP2), glial cells (GFAP) and nuclei (DAPI) fluorescences.
The resazurin assay indicates a harmane concentration-based trend in spheroids viability decrease after 24 h, with a reduction significant at 100 and 250 µM.
Moreover, the measurement of intensity fluorescence for neurons, glia, and nuclei, in spheroids exposed to different concentrations of harmane, indicates a similar reduction of viability, particularly for DAPI, i.e. a measurement of nuclei numbers.
These results confirm the neurotoxic effect of harmane and the suitability of a simple resazurin assay to measure the cells viability in spheroids.

Evaluation of cell viability in the presence of 1-benz-6,7-diol THIQ

The application of the resazurin test on spheroids exposed to different concentration of 1-benz-6,7-diol THIQ does not indicate a statistically significant reduction in viability.
This result confirmed previous result that demonstrated the relation of neurotoxicity effect of benz-6,7-diol THIQ with cell types, more specifically the neurotoxic effect is related to dopaminergic neurons [404].

5.6.3.2 Reactive oxygen species (ROS) measurement

ROS are notably generated during mitochondrial electron transport; they are highly reactive species and their excessive generation can lead to damages such as protein and lipid oxidation and DNA breakage and adduction. In the central nervous system (CNS), microglia correspond to local immune cells that produce ROS and/or cytokines in response to various stimuli [412]. The chronic activation of microglia may cause neuronal damage through the persistent release of potentially cytotoxic molecules, including ROS [413]. It is therefore critical to study ROS generated within cells, which could also be reflected by ROS leakages into the culture medium [343, 414].

The assay we selected for ROS measurement was based on 2′,7′- dichlorodihydrofluorescein (DCFH) for analysis of extracellular ROS and 2′,7′- dichlorodihydrofluorescein diacetate (DCFH-DA) for intracellular ROS. DCFH-DA is widely used to detect intracellular ROS, it is cell permeable and hydrolyzed intracellularly to DCFH that can be oxidized to the fluorescent dichlorofluorescein (DCF).

We encountered many difficulties in ROS measurement; in future experiments, the method should ideally be modified by using culture media without phenolsulfonphthalein (phenol red).

Evaluation of ROS in the presence of Harmane

For leaked ROS measurement, there was no significant difference in the mean values between the control conditions and the different harmane treatments, at the different incubation times tested (up to 24 h).

For intracellular ROS measurement, we were not able to detect any significant signal in cells by fluorescence microscopy, for all tested harmane concentrations and incubation times. We measured in parallel the fluorescence of the culture medium, with the hypothesis that DCFH could be released from damaged cells; the result indicates a likely reduction in ROS after 24h exposure to 250 µM of harmane.

The comparison of leaked ROS, measured in the cell medium, by direct incubation with DCFH and after incubation with DCFH-DA, indicates that there was a significant difference in the measurements, especially after 24 h contact with harmane. This result could be tentatively explained by a slow and non-specific release of DCFH from cells.

Evaluation of ROS in the presence of 1-benz-6,7-diol THIQ

The evaluation of leaked ROS after 24 h contact does not show any difference for all tested concentrations of 1-benz-6,7-diol THIQ.

5.6.3.3 Study of apoptosis and necrosis

The reduction of viability with harmane demands to analyze whether the cytotoxicity is due to an apoptotic or necrotic effect; apoptosis is an active cell death mechanism, programmed

and related to internal cellular factors, while necrosis is a passive death, uncontrolled and depending on extracellular factors [415].

To investigate an eventual apoptotic role of harmane, we measured the caspase cascade, more specifically the fluorescence intensity generated by the cleavage of a caspase 3-7 substrate (positive control, staurosporine 200 nM); caspases are part of a family of proteases and part of them are involved in apoptosis. On the other hand, we determined an eventual necrotic effect by a propidium iodide test (positive control, H_2O_2 50 µM); this fluorophore has the ability to stain the DNA of necrotic cells and with damaged membrane. Both tests require fluorescence measurement, with normalization of fluorescence intensity to spheroid diameter, carefully delineating by hand the measurement area.

In our hands, staurosporin is clearly a pro-apoptotic agent, but part of cells stained also with propidium iodide; spheroids appeared quite resistant to H_2O_2, that yielded only a weak necrotic effect. In 2D neuronal cultures, this H_2O_2 concentration typically yields ∼50% of necrotic cell death after incubation of 12h. [416]. This observation might relate to selectively toxic effect of H_2O_2 on immature neurons culture (6 DIV) compared with mature neurons culture (20 DIV) [417]. This may be worth of further investigation for eventual survival mechanisms as this type of resistance may question the relevance of data obtained on 2D cultures. On the other hand, it is possible that the toxicant is not evenly distributed within the spheroid, biasing the concentrations to which cells are really exposed to. The test indicates that harmane has both apoptotic and necrotic effects, with a probable predominance of necrosis. As fluorescence measurements are quite challenging, yielding a high heterogeneity of data, it would be advantageous to use another method like flow cytometry; but, despite our efforts, we could not manage to successfully apply flow cytometry on spheroids (problems of cells dissociation).

5.7 In vivo study of 1-benz-6,7-diol THIQ

The acute exposure to β-carboline derivatives (harmane, harmine and harmaline) has been examined in animals and demonstrated a severe tremorgenic effect [418, 419]. In order to study a possible implication of 1-benz-6,7-diol THIQ in the genesis of the tremors, an *in-vivo* test was needed. We took into consideration *(i)* the ADMET prediction that the molecule may

cross blood brain barrier by passive diffusion, although its structure is not ideal (Section 5.5); and *(ii)* the likeliness of the aldehyde precursor to enter the brain and form the alkaloid 1-benz-6,7-diol THIQ *in situ*. And so, in experimental rat models, we decided to apply the alkaloid directly to the brain with intracerebellar cannula implantation, a method to administer neuroactive agents requiring bypassing the blood-brain barrier. The implanted unilateral and bilateral cannula allows injection of substances into one side or both sides of cerebellum.

The bilateral infusion did not indicate any change in power, but tremor frequencies was noticed. due to the infusion of 1-benz-6,7-diol THIQ while the unilateral infusion indicated a decrease in the amplitude of the EEG signal across frequencies. Unfortunately, the histological analysis of the cerebellum after unilateral cannula implantation indicated that the recording electrode had in fact been wrongly inserted into the cerebellar cortex and not in the medial cerebellar nucleus. These latter results are then doubtful. Also, the implanted rats had undergone a previous experiment for a month, which has probably affected his behavior; we could notice the rat getting bored and sitting quietly rather than actively moving around the cage.

The data presented here are to be considered as very preliminary results, indicative of what can be achieved to link compounds of interest to the pathology of essential tremor.

6. Conclusions and Perspectives

6.1 The challenges tackled in this work

Despite many studies, essential tremor (ET), one of the most prevalent neurological diseases, remains poorly known; the aetiology is not clear and both genetic and environmental factors are suggested to play a role. Till now, the β-carboline alkaloid harmane is the molecule the most often implicated in the disease with the demonstration of elevated concentrations in ET patients blood [39-42, 104]; nevertheless, its exposure sources and role in the pathogenesis are not clear. Harmane is normally present in the mammalian brain and is also widespread among the plant kingdom, so its origin might be exogenous and endogenous. Overcooked meats are regularly implicated as a major source of β-carbolines [97, 323], but actual data are still lacking or not solid.

Reducing the number of animals that are used in research is very demanding but requires better *in vitro* systems; indeed, the classically used 2D cultures do not meet all the researchers need, as they do not represent the real *in vivo* environment in which cells spatially and chemically interact; their lack in predictivity increases the cost and failure rate of clinical trials and this is especially the case in neurosciences. Recently, 3D cell cultures have received much attention, as these are closer to tissue models; they are being used growingly in the hope to bridge the gap between *in vitro* 2D cell cultures and *in vivo* animal models. There is a consensus that 3D models are physiologically relevant, as they more closely represent the microenvironments, cell-to-cell interactions, and biological processes that occur *in vivo*. Still the challenges with 3D models reside in end-point measurements.

6.2 The development of our methodology

The present work aims at investigating the eventual implication of dietary compounds in ET. We began by exploring the levels of β-carboline alkaloids in overcooked meats to verify whether the actual levels are as low as described (3.8 – 8.5 ng/g [97, 323]). After many trials (documented in the thesis and followed by a further series of extraction trials, undocumented here), we concluded that the -carbolines are effectively extremely low and not easily accessible to the analytical equipment available in the laboratory. We also raise some doubts on the alleged link between overcooked meat β-carbolines and essential tremor; it is

noticeable that this link, pledged for by different authors [102, 323, 420, 421], is attributed to *"lifelong exposure with brain accumulation of these highly lipophilic compounds"*. Our doubts are comforted by the lack of link between essential tremor and tobacco smoking (tobacco smoke contains β-carbolines; 1 cigarette corresponds to 3.6 µg harmane [422]) or using the medicinal plant *Peganum harmala* L. (rich in β-carboline alkaloids; the seeds contain harmaline, harmine, harmalol, harmane and harmol at 3.8, 2.93, 0.12, 0.03 and 0.02 %, respectively [329].

Given the difficulties and the dubious interest in measuring such low amounts of β-carbolines in meat, we then decided to develop a methodology for investigating overcooked meats for compounds that could be implicated in the generation of biologically active artifactual endogenous alkaloids. Such reactions have already been shown for formaldehyde, acetaldehyde [423] (formation of salsolinol, [424]) and 2-hydroxy-4-methoxybenzaldehyde [334]. We then focused our attention on carbonyl compounds produced during the Maillard reaction in overcooked meats, one of their important dietary sources. We investigated and developed a study methodology following these steps:

- ✓ Extract and identify the volatile and non-volatile carbonyl compounds produced by meat overcooking;
- ✓ Select major compounds and investigate their reactivity with endogenous amines;
- ✓ Identify reaction products;
- ✓ Investigate *in silico* their predicted pharmacokinetic and toxicological properties on the central nervous system;
- ✓ Investigate *in vitro* their eventual toxicity on a 3D organoid model;
- ✓ Test their possible tremorgenic involvement in a *in vivo* model.

The suitability of the methodology has been studied for a major aldehyde identified in overcooked chicken meat.

6.3 Our major findings and their possible implications

6.3.1 Maillard carbonyls as endogenous alkaloid precursors

A series of volatile and non-volatile carbonyl compounds have been identified in overcooked chicken meat and browned chicken meat cooking juices. By analysing the possible reactivity of major identified compounds with biogenic amines to form βCAs or isoquinolines, this thesis has shown the possibility of direct condensation at 37°C in very simple reaction conditions; these conditions do not consider eventual *in vivo* interferences that may accelerate or prevent the reaction but also possibly increase its yield (gastrointestinal pH, lipid or protein mediators, metals, bacterial or human enzymes). This result demonstrates the meat as an alkaloid precursors source.

Considering all the tested aldehydes, a series of alkaloid reaction products have been shown by TLC analysis. The work was pursued for a major aldehyde identified in overcooked chicken meat (phenylacetaldehyde, the Strecker degradation product of phenylalanine) and its condensation product with dopamine, i.e. the alkaloid 1-benzyl-1,2,3,4-tetrahydroisoquinoline-6,7-diol (1-benz-6,7-diol THIQ). In addition to this compound, quite a number of reaction products remain to be further identified and investigated; the methodology we developed appears quite well suited to study all these alkaloids.

6.3.2 Development of a 3D neurosphere model

The 3D neurosphere model presented in this work has shown its ability to yield a reproduce 3D culture, using simple materials and routine laboratory equipment. Despite the challenges in 3D culture and data obtaining, this 3D neurosphere model mimics a neuronal microenvironment, allowing a fine study of neurodegenerative disorders and the effect of chemicals on the brain.

Our 3D model is intended for the development of tests to study a wide range of neurotoxic or neuroprotective agents. The results indicate that, although fluorescence measurement is challenging, it is still possible to evaluate cell viability, major death mechanisms (apoptosis versus necrosis), and oxidative stress. Considerable work is still needed to *(i)* better

characterize the model by defining the neurosphere growth, in terms of stem cells proliferation (nestin stain) and cells apoptosis along its development, and the cells microenvironment using western blotting; *(ii)* ameliorate the applied tests; *(iii)* study the chronic effect of molecules on cultures, considering MPTP as positive control; and *(iv)* to develop more intricate measurement points (synaptic signaling, electrophysiological measurements, gene and protein expression, measurement of functions for specific cells, local NO•, prostaglandins and cytokines production…) that are quite challenging in this type of model. Our work opens the door to go beyond the obstacles with modest laboratory equipment and suggests possible answers, at least for the tests we investigated so far.

6.3.3 *In vitro* study of harmane and 1-benzyl-1,2,3,4-tetrahydroisoquinoline-6,7-diol

The two alkaloids were tested in our neurosphere model for cytotoxicity and oxidative stress induction. Obtained results support the role of harmane as a neurotoxic agent but at a high concentration, hardly compatible with its content in overcooked meat, which is not in favor of the *"meat harmane hypothesis"* unless *(i)* lifelong exposure would manage to accumulate so much harmane in the brain that could be tested by measering the effect of chronic exposure to harmane throughout culture development; or *(ii)* mechanisms at play are more subtle than cell impairment. Our data moreover do not support a possible neuroprotective property for harmane. Further studies are required to elucidate the biological activities of harmane and to decipher, via *in vitro* tests, an eventual relationship with ET disorder. And further research is needed to determine the causes and consequences of elevated blood concentrations of harmane shown in ET patients.

So far, our *in vitro* data do not support an eventual neurotoxic effect for 1-benz-6,7-diol THIQ.

6.3.4 *In vivo* study of 1-benzyl-1,2,3,4-tetrahydroisoquinoline-6,7-diol

We had the chance to perform a few tests in the University of Bristol. Due to the Covid situation, it was not possible to properly study 1-benz-6,7-diol THIQ, but the very preliminary experiments we could perform indicate that this extension of our methodology

constitutes an indispensable tool to link *in vitro* data with tremorgenic activity and mechanisms.

6.4   Conclusions and perspectives

This research clearly illustrates that, despite the challenges in 3D culture and data obtaining, our 3D neurosphere model mimics a neuronal microenvironment; upon developing further measurement points and cultures from specific parts of the brain, the model could allow a fine study of neurodegenerative disorders and the effect of chemicals on the brain.

But ET is a neurodegenerative disease that progresses within time, and our research was limited to the study of short-term effects of molecules on 3D spheroids; for better understanding the implications of these molecules in ET, future studies should address mid- to +/- long-term effects of the molecules on the spheroids, for example by regular addition of test molecules to the culture media along spheroid life; to study effects on brain development (a possible mimic of plasticity?), exposure may possibly start during spheroid growth, maybe even starting on culture day 1.

We also raise the question whether an animal source of cells is the best model, especially for CNS diseases, considering the complexity of the brain in humans compared to rodents. It would be interesting to investigate 3D models based on human stem cells that may be more relevant to diseases like ET, where genetics play a role and could transfer the research on another level.

To better understand the etiology of ET and the roles of β-carboline and isoquinoline alkaloids in this disease, we also suggest comparing their effects on induced pluripotent stem cells (iPSC)[45] obtained from ET patient, healthy family member and healthy person.

---

[45] Induced pluripotent stem cells (iPSC) are a type of pluripotent stem cell (PSC) that can be obtained by reprogramming somatic cells through artificial expression of key transcription factors under specific culture conditions. Their differentiation into different cell types can be achieved under other specific conditions.

7. References

[1].Jankovic J. Essential tremor: clinical characteristics. Neurology. 2000;54(11 Suppl 4):S21-5.

[2].Brennan KC, Jurewicz EC, Ford B, Pullman SL, Louis ED. Is essential tremor predominantly a kinetic or a postural tremor? A clinical and electrophysiological study. Movement Disorders. 2002;17(2):313-6.

[3].Louis ED. Diagnosis and Management of Tremor. CONTINUUM: Lifelong Learning in Neurology. 2016;22(4, Movement Disorders):1143-58.

[4].Gasparini M, Bonifati V, Fabrizio E, Fabbrini G, Brusa L, Lenzi GL, et al. Frontal lobe dysfunction in essential tremor. Journal of Neurology. [journal article]. 2001;248(5):399-402.

[5].Deuschl G, Elble R. Essential tremor--neurodegenerative or nondegenerative disease towards a working definition of ET. Movement Disorders. 2009 October;24(14):2033-41.

[6].Sengul Y, Sengul HS, Yucekaya SK, Yucel S, Bakim B, Pazarcı NK, et al. Cognitive functions, fatigue, depression, anxiety, and sleep disturbances: assessment of nonmotor features in young patients with essential tremor. Acta Neurologica Belgica. [journal article]. 2015;115(3):281-7.

[7].Louis ED, Huey ED, Gerbin M, Viner AS. Depressive traits in essential tremor: impact on disability, quality of life, and medication adherence. European Journal of Neurology. 2012;19(10):1349-54.

[8].Louis ED. Essential Tremor and Other Forms of Kinetic Tremor. In: Grimaldi G, Manto M, editors. Mechanisms and Emerging Therapies in Tremor Disorders. New York, NY: Springer New York; 2013. p. 167-201.

[9].Louis ED. Chapter 33 - Essential tremor. In: William JW, Eduardo T, editors. Handbook of Clinical Neurology: Elsevier; 2011. p. 433-48.

[10].Benito-Leon J, Bermejo-Pareja F, Louis ED. Incidence of essential tremor in three elderly populations of central Spain. Neurology. 2005;64(10):1721-5.

[11].Louis ED, Ferreira JJ. How common is the most common adult movement disorder? Update on the worldwide prevalence of essential tremor. Movement Disorders. 2010;25(5):534-41.

[12].Schnitzler A, Munks C, Butz M, Timmermann L, Gross J. Synchronized brain network associated with essential tremor as revealed by magnetoencephalography. Movement Disorders. 2009;24(11):1629-35.

[13].Contarino MF, Groot PF, van der Meer JN, Bour LJ, Speelman JD, Nederveen AJ, et al. Is there a role for combined EMG-fMRI in exploring the pathophysiology of essential tremor and improving functional neurosurgery? PLOS One. 2012;7(10):1.

[14].Boscolo Galazzo I, Magrinelli F, Pizzini FB, Storti SF, Agosta F, Filippi M, et al. Voxel-based morphometry and task functional magnetic resonance imaging in essential tremor: evidence for a disrupted brain network. Scientific Reports. 2020 2020/09/15;10(1):15061.

[15].Filip P, Lungu OV, Manto MU, Bareš M. Linking Essential Tremor to the Cerebellum: Physiological Evidence. Cerebellum. 2016;15(6):774-80.

[16].Louis ED. Essential tremor as a neuropsychiatric disorder. Journal of the Neurological Sciences. 2010;289(1–2):144-8.

[17].Simantov R, Snyder SH, Oster-Granite M-L. Harmaline-induced tremor in the rat: Abolition by 3-acetylpyridine destruction of cerebellar climbing fibers. Brain research. 1976 1976/09/10/;114(1):144-51.

[18].Montigny CD, Lamarre Y. Effects Produced by Local Applications of Harmaline in the Inferior Olive. Canadian Journal of Physiology and Pharmacology. 1975 1975/10/01;53(5):845-9.

[19].Hallett M, Dubinsky RM. Glucose metabolism in the brain of patients with essential tremor. Journal of the Neurological Sciences. 1993;114(1):45-8.

[20].Fang W, Lv F, Luo T, Cheng O, Liao W, Sheng K, et al. Abnormal regional homogeneity in patients with essential tremor revealed by resting-state functional MRI. PLOS One. 2013;8(7):e69199-e.

[21].Louis ED, Lenka A. The Olivary Hypothesis of Essential Tremor: Time to Lay this Model to Rest? Tremor Other Hyperkinet Mov (N Y). 2017;7:473-.

[22].Axelrad JE, Louis ED, Honig LS, Flores I, Ross GW, Pahwa R, et al. Reduced Purkinje Cell Number in Essential Tremor: A Postmortem Study. Archives of Neurology. 2008;65(1):101-7.

[23].Grimaldi G, Manto M. Is essential tremor a Purkinjopathy? The role of the cerebellar cortex in its pathogenesis: Movement Disorders. 2013 Nov;28(13):1759-61. doi: 10.1002/mds.25645. Epub 2013 Sep 30.

[24].Louis ED. From Neurons to Neuron Neighborhoods: the Rewiring of the Cerebellar Cortex in Essential Tremor. Cerebellum (London, England). 2014;13(4):501-12.

[25].Louis ED. Re-thinking the biology of essential tremor: From models to morphology. Parkinsonism & Related Disorders. 2014;20, Supplement 1:S88-S93.

[26].Bhalsing KS, Saini J, Pal PK. Understanding the pathophysiology of essential tremor through advanced neuroimaging: A review. Journal of the Neurological Sciences.335(1):9-13.

[27].Novellino F, Cherubini A, Chiriaco C, Morelli M, Salsone M, Arabia G, et al. Brain iron deposition in essential tremor: a quantitative 3-Tesla magnetic resonance imaging study. Movement Disorders. 2013 Feb;28(2):196-200.

[28].Louis ED, Faust PL, Vonsattel JP, Honig LS, Rajput A, Robinson CA, et al. Neuropathological changes in essential tremor: 33 cases compared with 21 controls. Brain. 2007;130(Pt 12):3297-307.

[29].Bonuccelli U. Essential tremor is a neurodegenerative disease. Journal of Neural Transmission. 2012;119(11):1383-7.

[30].Kronenbuerger M, Tronnier VM, Gerwig M, Fromm C, Coenen VA, Reinacher P, et al. Thalamic deep brain stimulation improves eyeblink conditioning deficits in essential tremor. Experimental Neurology. 2008;211(2):387-96.

[31].Klebe S, Stolze H, Grensing K, Volkmann J, Wenzelburger R, Deuschl G. Influence of alcohol on gait in patients with essential tremor. Neurology. 2005;65(1):96-101.

[32].Kurtis MM. Essential tremor: is it a neurodegenerative disease? No. Journal of Neural Transmission. 2012;119(11):1375-81.

[33].Louis ED, Diaz DT, Kuo SH, Gan SR, Cortes EP, Vonsattel JPG, et al. Inferior Olivary nucleus degeneration does not lessen tremor in essential tremor. Cerebellum Ataxias. 2018;5(1):018-0080.

[34].Boecker H, Weindl A, Brooks DJ, Ceballos-Baumann AO, Liedtke C, Miederer M, et al. GABAergic dysfunction in essential tremor: an 11C-flumazenil PET study. Journal of Nuclear Medicine. 2010;51(7):1030-5.

[35].Gironell A, Figueiras FP, Pagonabarraga J, Herance JR, Pascual-Sedano B, Trampal C, et al. Gaba and serotonin molecular neuroimaging in essential tremor: A clinical correlation study. Parkinsonism & Related Disorders.18(7):876-80.

[36].Cross AJ, Misra A, Sandilands A, Taylor MJ, Green AR. Effect of chlormethiazole, dizocilpine and pentobarbital on harmaline-induced increase of cerebellar cyclic GMP and tremor. Psychopharmacology. 1993;111(1):96-8.

[37].Louis ED. Environmental Epidemiology of Essential Tremor. Neuroepidemiology. 2008;31(3):139-49.

[38].Ong Y-L, Deng X, Tan E-K. Etiologic links between environmental and lifestyle factors and Essential tremor. Ann Clin Transl Neurol. 2019;6(5):979-89.

[39].Louis ED, Zheng W, Mao X, Shungu DC. Blood harmane is correlated with cerebellar metabolism in essential tremor: a pilot study. Neurology. 2007;69(6):515-20.

[40].Louis ED, Jiang W, Pellegrino KM, Rios E, Factor-Litvak P, Henchcliffe C, et al. Elevated blood harmane (1-methyl-9H-pyrido[3,4-b]indole) concentrations in essential tremor. Neurotoxicology. 2008;29(2):294-300.

[41].Louis ED, Benito-León J, Moreno-García S, Vega S, Romero JP, Bermejo-Pareja F, et al. Blood harmane (1-methyl-9H-pyrido[3,4-b]indole) concentration in essential tremor cases in Spain. Neurotoxicology. 2013 2013/01/01/;34:264-8.

[42].Louis ED, Jiang W, Gerbin M, Mullaney MM, Zheng W. Relationship between blood harmane and harmine concentrations in familial essential tremor, sporadic essential tremor and controls. Neurotoxicology. 2010;31(6):674-9.

[43].Wilms H, Sievers J, Deuschl G. Animal models of tremor. Movement Disorders. 1999;14(4):557-71.

[44].Rappaport MS, Gentry RT, Schneider DR, Dole VP. Ethanol effects on harmaline-induced tremor and increase of cerebellar cyclic GMP. Life Sciences. 1984;34(1):49-56.

[45].Hideto M, Tomomi K, Ai S, Tameko K, Tomoyoshi K. A species-specific difference in the effects of harmaline on the rodent olivocerebellar system. Brain research. 2006;1068 1:94-101.

[46].Handforth A. Linking Essential Tremor to the Cerebellum-Animal Model Evidence. Cerebellum. 2016;15(3):285-98.

[47].Roffler-Tarlov S, Beart PM, O'Gorman S, Sidman RL. Neurochemical and morphological consequences of axon terminal degeneration in cerebellar deep nuclei of mice with inherited Purkinje cell degeneration. Brain research. 1979;168(1):75-95.

[48].Kralic JE, Criswell HE, Osterman JL, O'Buckley TK, Wilkie ME, Matthews DB, et al. Genetic essential tremor in γ-aminobutyric acid(A) receptor α1 subunit knockout mice. Journal of Clinical Investigation. 2005;115(3):774-9.

[49].Jankovic J, Noebels JL. Genetic mouse models of essential tremor: are they essential? Journal of Clinical Investigation. 2005;115(3):584-6.

[50].Gutierrez-Merino C, Lopez-Sanchez C, Lagoa R, Samhan-Arias AK, Bueno C, Garcia-Martinez V. Neuroprotective actions of flavonoids. Current Medicinal Chemistry. 2011;18(8):1195-212.

[51].Deng H, Xie W-J, Le W, Huang M-S, Jankovic J. Genetic analysis of the GABRA1 gene in patients with essential tremor. Neuroscience Letters. 2006;401:16-9.

[52].Sartore RC, Cardoso SC, Lages YV, Paraguassu JM, Stelling MP, Madeiro da Costa RF, et al. Trace elements during primordial plexiform network formation in human cerebral organoids. PeerJ. 2017;8(5).

[53].Elble RJ. Tremor: clinical features, pathophysiology, and treatment. Neurol Clin. 2009;27(3):679-95.

[54].Zesiewicz TA, Elble R, Louis ED, Hauser RA, Sullivan KL, Dewey RB, Jr., et al. Practice parameter: therapies for essential tremor: report of the Quality Standards Subcommittee of the American Academy of Neurology. Neurology. 2005;64(12):2008-20.

[55].Abila B, Wilson JF, Marshall RW, Richens A. The tremorolytic action of beta-adrenoceptor blockers in essential, physiological and isoprenaline-induced tremor is mediated by beta-adrenoceptors located in a deep peripheral compartment. British Journal of Clinical Pharmacology. 1985;20(4):369-76.

[56].Sweetman SC, editor. Martindale: The complete drug reference. 36th Revised edition ed. London: Pharmaceutical Press 2009.

[57].Cleeves L, Findley LJ. Propranolol and propranolol-LA in essential tremor: a double blind comparative study. Journal of Neurology, Neurosurgery, and Psychiatry. 1988;51(3):379-84.

[58].Koller WC. Dose-response relationship of propranolol in the treatment of essential tremor. Archives of Neurology. 1986;43(1):42-3.

[59].Koller WC. Long-acting propranolol in essential tremor. Neurology. 1985;35(1):108-10.

[60].Tolosa ES, Loewenson RB. Essential tremor: treatment with propranolol. Neurology. 1975;25(11):1041-4.

[61].Leigh PN, Jefferson D, Twomey A, Marsden CD. Beta-adrenoreceptor mechanisms in essential tremor; a double-blind placebo controlled trial of metoprolol, sotalol and atenolol. Journal of Neurology, Neurosurgery, and Psychiatry. 1983;46(8):710-5.

[62].Guan XM, Peroutka SJ. Basic mechanisms of action of drugs used in the treatment of essential tremor. Clinical Neuropharmacology. 1990;13(3):210-23.

[63].Findley LJ, Cleeves L, Calzetti S. Primidone in essential tremor of the hands and head: a double blind controlled clinical study. Journal of Neurology, Neurosurgery, and Psychiatry. 1985;48(9):911-5.

[64].O'Suilleabhain P, Dewey RB, Jr. Randomized trial comparing primidone initiation schedules for treating essential tremor. Movement Disorders. 2002;17(2):382-6.

[65].Serrano-Duenas M. Use of primidone in low doses (250 mg/day) versus high doses (750 mg/day) in the management of essential tremor. Double-blind comparative study with one-year follow-up. Parkinsonism & Related Disorders. 2003;10(1):29-33.

[66].Taylor CP, Gee NS, Su TZ, Kocsis JD, Welty DF, Brown JP, et al. A summary of mechanistic hypotheses of gabapentin pharmacology. Epilepsy Research. 1998;29(3):233-49.

[67].Gironell A, Kulisevsky J, Barbanoj M, Lopez-Villegas D, Hernandez G, Pascual-Sedano B. A randomized placebo-controlled comparative trial of gabapentin and propranolol in essential tremor. Archives of Neurology. 1999;56(4):475-80.

[68].Ondo WG, Jankovic J, Connor GS, Pahwa R, Elble R, Stacy MA, et al. Topiramate in essential tremor: a double-blind, placebo-controlled trial. Neurology. 2006;66(5):672-7.

[69].Riss J, Cloyd J, Gates J, Collins S. Benzodiazepines in epilepsy: pharmacology and pharmacokinetics. Acta Neurologica Scandinavica. 2008;118(2):69-86.

[70].Gunal DI, Afsar N, Bekiroglu N, Aktan S. New alternative agents in essential tremor therapy: double-blind placebo-controlled study of alprazolam and acetazolamide. Neurological Sciences. 2000;21(5):315-7.

[71].Ceravolo R, Salvetti S, Piccini P, Lucetti C, Gambaccini G, Bonuccelli U. Acute and chronic effects of clozapine in essential tremor. Movement Disorders. 1999;14(3):468-72.

[72].Knudsen K, Lorenz D, Deuschl G. A clinical test for the alcohol sensitivity of essential tremor. Movement Disorders. 2011;26(12):2291-5.

[73].Bushara KO, Goldstein SR, Grimes GJ, Jr., Burstein AH, Hallett M. Pilot trial of 1-octanol in essential tremor. Neurology. 2004;62(1):122-4.

[74].Nahab FB, Wittevrongel L, Ippolito D, Toro C, Grimes GJ, Starling J, et al. An open-label, single-dose, crossover study of the pharmacokinetics and metabolism of two oral formulations of 1-octanol in patients with essential tremor. Neurotherapeutics. 2011;8(4):753-62.

[75].Haubenberger D, Nahab FB, Voller B, Hallett M. Treatment of Essential Tremor with Long-Chain Alcohols: Still Experimental or Ready for Prime Time? Tremor and Other Hyperkinetic Movements. 2014;4:tre-04-211-4673-2.

[76].Nahab FB, Handforth A, Brown T, Shin C, Quesada A, Dong C, et al. Octanoic acid suppresses harmaline-induced tremor in mouse model of essential tremor. Neurotherapeutics. 2012;9(3):635-8.

[77].Abdulrahman AA, Faisal K, Meshref AA, Arshaduddin M. Low-dose acute vanillin is beneficial against harmaline-induced tremors in rats. Neurological Research. 2017;39(3):264-70.

[78].Schuurman PR, Bosch DA, Bossuyt PM, Bonsel GJ, van Someren EJ, de Bie RM, et al. A comparison of continuous thalamic stimulation and thalamotomy for suppression of severe tremor. New England Journal of Medicine. 2000;342(7):461-8.

[79].Nagaseki Y, Shibazaki T, Hirai T, Kawashima Y, Hirato M, Wada H, et al. Long-term follow-up results of selective VIM-thalamotomy. Journal of Neurosurgery. 1986;65(3):296-302.

[80].Selby G. Stereotactic surgery for the relief of Parkinson's disease. 2. An analysis of the results in a series of 303 patients (413 operations). Journal Neurological Sciences. 1967;5(2):343-75.

[81].Matsumoto K, Shichijo F, Fukami T. Long-term follow-up review of cases of Parkinson's disease after unilateral or bilateral thalamotomy. Journal of Neurosurgery. 1984;60(5):1033-44.

[82].Boockvar JA, Telfeian A, Baltuch GH, Skolnick B, Simuni T, Stern M, et al. Long-term deep brain stimulation in a patient with essential tremor: clinical response and postmortem correlation with

stimulator termination sites in ventral thalamus. Case report. Journal of Neurosurgery. 2000;93(1):140-4.

[83].Hubble JP, Busenbark KL, Wilkinson S, Penn RD, Lyons K, Koller WC. Deep brain stimulation for essential tremor. Neurology. 1996;46(4):1150-3.

[84].Koller W, Pahwa R, Busenbark K, Hubble J, Wilkinson S, Lang A, et al. High-frequency unilateral thalamic stimulation in the treatment of essential and parkinsonian tremor. Annals of Neurology. 1997;42(3):292-9.

[85].Pahwa R, Lyons KL, Wilkinson SB, Carpenter MA, Troster AI, Searl JP, et al. Bilateral thalamic stimulation for the treatment of essential tremor. Neurology. 1999;53(7):1447-50.

[86].Benabid AL, Benazzouz A, Hoffmann D, Limousin P, Krack P, Pollak P. Long-term electrical inhibition of deep brain targets in movement disorders. Movement Disorders. 1998;3:119-25.

[87].Niranjan A, Kondziolka D, Baser S, Heyman R, Lunsford LD. Functional outcomes after gamma knife thalamotomy for essential tremor and MS-related tremor. Neurology. 2000;55(3):443-6.

[88].Young RF, Jacques S, Mark R, Kopyov O, Copcutt B, Posewitz A, et al. Gamma knife thalamotomy for treatment of tremor: long-term results. Journal of Neurosurgery. 2000;3:128-35.

[89].Siderowf A, Gollump SM, Stern MB, Baltuch GH, Riina HA. Emergence of complex, involuntary movements after gamma knife radiosurgery for essential tremor. Movement Disorders. 2001;16(5):965-7.

[90].Popa T, Russo M, Vidailhet M, Roze E, Lehericy S, Bonnet C, et al. Cerebellar rTMS stimulation may induce prolonged clinical benefits in essential tremor, and subjacent changes in functional connectivity: an open label trial. Brain Stimulation. 2013;6(2):175-9.

[91].Grimaldi G, Argyropoulos GP, Bastian A, Cortes M, Davis NJ, Edwards DJ, et al. Cerebellar Transcranial Direct Current Stimulation (ctDCS): A Novel Approach to Understanding Cerebellar Function in Health and Disease. Neuroscientist. 2016;22(1):83-97.

[92].Helvaci Yilmaz N, Polat B, Hanoglu L. Transcranial Direct Current Stimulation in the Treatment of Essential Tremor: An Open-Label Study. Neurologist. 2016;21(2):28-9.

[93].Shih LC, Pascual-Leone A. Non-invasive Brain Stimulation for Essential Tremor. Tremor and Other Hyperkinetic Movements. 2017;7:458.

[94].BRUNETON J. Pharmacognosie - Phytochimie - Plantes médicinales. Paris: Lavoisier TEC & DOC; 2016.

[95].Aniszewski T. Chapter 3 - Biology of alkaloids. In: Aniszewski T, editor. Alkaloids (Second Edition). Boston: Elsevier; 2015. p. 195-258.

[96].Aniszewski T. Chapter 7 - Problems of alkaloids in nature and human activity. In: Aniszewski T, editor. Alkaloids (Second Edition). Boston: Elsevier; 2015. p. 421-38.

[97].Pfau W, Skog K. Exposure to beta-carbolines norharman and harman. Journal of Chromatography B Analytical Technologies in the Biomedical and Life Sciences. 2004;802(1):115-26.

[98].Louis ED, Zheng W. Beta-carboline alkaloids and essential tremor: exploring the environmental determinants of one of the most prevalent neurological diseases. Scientific World Journal. 2010;10:1783-94.

[99].Louis ED, Factor-Litvak P, Liu X, Vonsattel JP, Galecki M, Jiang W, et al. Elevated brain harmane (1-methyl-9H-pyrido[3,4-b]indole) in essential tremor cases vs. controls. Neurotoxicology. 2013;38:131-5.

[100].Higgins D, Burack M, Lein P, Banker G. Mechanisms of neuronal polarity. Current Opinion in Neurobiology. 1997;7(5):599-604.

[101].Kolasiewicz W, Kuter K, Wardas J, Ossowska K. Role of the metabotropic glutamate receptor subtype 1 in the harmaline-induced tremor in rats. Journal of Neural Transmission. 2009;116(9):1059-63.

[102].Louis ED, Keating GA, Bogen KT, Rios E, Pellegrino KM, Factor-Litvak P. Dietary epidemiology of essential tremor: meat consumption and meat cooking practices. Neuroepidemiology. 2008;30(3):161-6.

[103].Li S, Liu W, Teng L, Cheng X, Wang Z, Wang C. Metabolites identification of harmane in vitro/in vivo in rats by ultra-performance liquid chromatography combined with electrospray ionization quadrupole time-of-flight tandem mass spectrometry. Journal of Pharmaceutical and Biomedical Analysis. 2014;92:53-62.

[104].Louis ED, Michalec M, Jiang W, Factor-Litvak P, Zheng W. Elevated blood harmane (1-methyl-9H-pyrido[3,4-b]indole) concentrations in Parkinson's disease. Neurotoxicology. 2014;40:52-6.

[105].Murkovic M. Chemistry, formation and occurrence of genotoxic heterocyclic aromatic amines in fried products. European Journal of Lipid Science and Technology. 2004;106(11):777-85.

[106].Murkovic M. Formation of heterocyclic aromatic amines in model systems. Journal of Chromatography B Analytical Technologies in the Biomedical and Life Sciences. 2004;802(1):3-10.

[107].Ronner B, Lerche H, Bergmuller W, Freilinger C, Severin T, Pischetsrieder M. Formation of tetrahydro-beta-carbolines and beta-carbolines during the reaction of L-tryptophan with D-glucose. Journal of Agricultural and Food Chemistry. 2000;48(6):2111-6.

[108].Herraiz T, Galisteo J. Naturally-occurring tetrahydro-beta-carboline alkaloids derived from tryptophan are oxidized to bioactive beta-carboline alkaloids by heme peroxidases. Biochem Biophys Res Commun. 2014;451(1):42-7.

[109].Collins MA, Neafsey EJ. Beta-carboline analogues of N-methyl-4-phenyl-1,2,5,6-tetrahydropyridine (MPTP): endogenous factors underlying idiopathic parkinsonism? Neurosci Lett. 1985;55(2):179-84.

[110].Wernicke C, Schott Y, Enzensperger C, Schulze G, Lehmann J, Rommelspacher H. Cytotoxicity of beta-carbolines in dopamine transporter expressing cells: structure-activity relationships. Biochemical Pharmacology. 2007;74(7):1065-77.

[111].Storch A, Hwang Y-I, Gearhart DA, Beach JW, Neafsey EJ, Collins MA, et al. Dopamine transporter-mediated cytotoxicity of β-carbolinium derivatives related to Parkinson's disease: relationship to transporter-dependent uptake. Journal of Neurochemistry. 2004;89(3):685-94.

[112].Collins MA, Neafsey EJ. β-Carboline Derivatives as Neurotoxins. In: Moser A, editor. Pharmacology of Endogenous Neurotoxins: A Handbook. Boston, MA: Birkhäuser Boston; 1998. p. 129-49.

[113].Matsubara K, Gonda T, Sawada H, Uezono T, Kobayashi Y, Kawamura T, et al. Endogenously occurring beta-carboline induces parkinsonism in nonprimate animals: a possible causative protoxin in idiopathic Parkinson's disease. Journal of Neurochemistry. 1998;70(2):727-35.

[114].Herraiz T, Guillen H, Galisteo J. N-methyltetrahydro-beta-carboline analogs of 1-methyl-4-phenyl-1,2,3,6-tetrahydropyridine (MPTP) neurotoxin are oxidized to neurotoxic beta-carbolinium cations by heme peroxidases. Biochemical and Biophysical Research Communications. 2007;356(1):118-23.

[115].Herraiz T, Chaparro C. Human monoamine oxidase enzyme inhibition by coffee and beta-carbolines norharman and harman isolated from coffee. Life Sciences. 2006;78(8):795-802.

[116].Wernicke C, Hellmann J, Zięba B, Kuter K, Ossowska K, Frenzel M, et al. 9-Methyl-β-carboline has restorative effects in an animal model of Parkinson's disease. Pharmacological Reports. 2010;62(1):35-53.

[117].Herraiz T, Chaparro C. Human monoamine oxidase is inhibited by tobacco smoke: beta-carboline alkaloids act as potent and reversible inhibitors. Biochem Biophys Res Commun. 2005;326(2):378-86.

[118].Scott WK, Zhang F, Stajich JM, Scott BL, Stacy MA, Vance JM. Family-based case-control study of cigarette smoking and Parkinson disease. Neurology. 2005;64(3):442-7.

[119].Emerit J, Edeas M, Bricaire F. Neurodegenerative diseases and oxidative stress. Biomed Pharmacother. 2004;58(1):39-46.

[120].Cataldo JK, Prochaska JJ, Glantz SA. Cigarette smoking is a risk factor for Alzheimer's disease: An analysis controlling for tobacco industry affiliation. Journal of Alzheimer's disease : JAD. 2010;19(2):465-80.

[121].Sun P, Zhang S, Li Y, Wang L. Harmine mediated neuroprotection via evaluation of glutamate transporter 1 in a rat model of global cerebral ischemia. Neuroscience Letters. 2014;583:32-6.

[122].Li Y, Sattler R, Yang EJ, Nunes A, Ayukawa Y, Akhtar S, et al. Harmine, a natural beta-carboline alkaloid, upregulates astroglial glutamate transporter expression. Neuropharmacology. 2011;60(7-8):1168-75.

[123].Allaman I, Belanger M, Magistretti PJ. Astrocyte-neuron metabolic relationships: for better and for worse. Trends in Neurosciences. 2011;34(2):76-87.

[124].Błaszczyk JW. Parkinson's Disease and Neurodegeneration: GABA-Collapse Hypothesis. Frontiers in Neuroscience. [Hypothesis & Theory]. 2016 2016-June-09;10(269).

[125].Buddhala C, Hsu CC, Wu JY. A novel mechanism for GABA synthesis and packaging into synaptic vesicles. Neurochemistry International. 2009;55(1-3):9-12.

[126].Salazar P, Tapia R. Epilepsy and hippocampal neurodegeneration induced by glutamate decarboxylase inhibitors in awake rats. Epilepsy Research. 2015;116:27-33.

[127].Huff CL, Morano RL, Herman JP, Yamamoto BK, Gudelsky GA. MDMA decreases glutamic acid decarboxylase (GAD) 67-immunoreactive neurons in the hippocampus and increases seizure susceptibility: Role for glutamate. Neurotoxicology. 2016;57:282-90.

[128].Manto M, Laute MA. A possible mechanism for the beneficial effect of ethanol in essential tremor. European Journal of Neurology. 2008;15(7):697-705.

[129].Monsef HR, Ghobadi A, Iranshahi M, Abdollahi M. Antinociceptive effects of Peganum harmala L. alkaloid extract on mouse formalin test. Journal of pharmacy & pharmaceutical sciences. 2004;7(1):65-9.

[130].Farouk L, Laroubi A, Aboufatima R, Benharref A, Chait A. Evaluation of the analgesic effect of alkaloid extract of Peganum harmala L.: Possible mechanisms involved. Journal of Ethnopharmacology. 2008 2008/02/12/;115(3):449-54.

[131].Pathan A. Peganum harmala: A Phyto-pharmacological Review. 2012;2012:01-2.

[132].Kim H, Sablin SO, Ramsay RR. Inhibition of monoamine oxidase A by beta-carboline derivatives. Archives of Biochemistry and Biophysics. 1997;337(1):137-42.

[133].Moura D, Rorig C, Vieira D, Henriques JA, Roesler R, Saffi J, et al. Effects of β-carboline alkaloids on the object recognition task in mice. Life Sciences. 2006;79:2099-104.

[134].Wiart C. Chapter 1 - Alkaloids. In: Wiart C, editor. Lead Compounds from Medicinal Plants for the Treatment of Neurodegenerative Diseases. San Diego: Academic Press; 2014. p. 1-188.

[135].McNaught KS, Carrupt PA, Altomare C, Cellamare S, Carotti A, Testa B, et al. Isoquinoline derivatives as endogenous neurotoxins in the aetiology of Parkinson's disease. Biochemical Pharmacology. 1998;56(8):921-33.

[136].Niwa T, Takeda N, Kaneda N, Hashizume Y, Nagatsu T. Presence of tetrahydroisoquinoline and 2-methyl-tetrahydroquinoline in Parkinsonian and normal human brains. Biochemical and Biophysical Research Communications. 1987 1987/04/29/;144(2):1084-9.

[137].Mogi M, Harada M, Kojima K, Kiuchi K, Nagatsu T. Effects of systemic administration of 1-methyl-4-phenyl-1,2,3,6-tetrahydropyridine to mice on tyrosine hydroxylase, L-3,4-dihydroxyphenylalanine decarboxylase, dopamine beta-hydroxylase, and monoamine oxidase activities in the striatum and hypothalamus. J Neurochem. 1988;50(4):1053-6.

[138].Nagatsu T, Yoshida M. An endogenous substance of the brain, tetrahydroisoquinoline, produces parkinsonism in primates with decreased dopamine, tyrosine hydroxylase and biopterin in the nigrostriatal regions. Neuroscience Letters. 1988 22 April;87(1):178-82.

[139].Nagatsu T. Isoquinoline neurotoxins in the brain and Parkinson's disease. Neuroscience Research. 1997 1997/10/01/;29(2):99-111.

[140].Suzuki K, Mizuno Y, Yoshida M. Inhibition of mitochondrial respiration by 1,2,3,4-tetrahydroisoquinoline-like endogenous alkaloids in mouse brain. Neurochemical Research. 1990 1990/07/01;15(7):705-10.

[141].Storch A, Ott S, Hwang Y-I, Ortmann R, Hein A, Frenzel S, et al. Selective dopaminergic neurotoxicity of isoquinoline derivatives related to Parkinson's disease: studies using heterologous expression systems of the dopamine transporter. Biochemical Pharmacology. 2002 2002/03/01/;63(5):909-20.

[142].Maruyama W, Naoi M, Kasamatsu T, Hashizume Y, Takahashi T, Kohda K, et al. An endogenous dopaminergic neurotoxin, N-methyl-(R)-salsolinol, induces DNA damage in human dopaminergic neuroblastoma SH-SY5Y cells. Journal of Neurochemistry. 1997;69(1):322-9.

[143].Naoi M, Maruyama W, Dostert P, Hashizume Y, Nakahara D, Takahashi T, et al. Dopamine-derived endogenous 1(R),2(N)-dimethyl-6,7-dihydroxy-1,2,3,4-tetrahydroisoquinoline, N-methyl-(R)-salsolinol, induced parkinsonism in rat: biochemical, pathological and behavioral studies. Brain Research. 1996 1996/02/19/;709(2):285-95.

[144].Maruyama W, Nakahara D, Ota M, Takahashi T, Takahashi A, Nagatsu T, et al. N-Methylation of Dopamine-Derived 6,7-Dihydroxy-1,2,3,4-Tetrahydroisoquinoline, (R)-Salsolinol, in Rat Brains: In Vivo Microdialysis Study. Journal of Neurochemistry. 1992 1992/08/01;59(2):395-400.

[145].Morikawa N, Naoi M, Maruyama W, Ohta S, Kotake Y, Kawai H, et al. Effects of various tetrahydroisoquinoline derivatives on mitochondrial respiration and the electron transfer complexes. Journal of Neural Transmission. 1998 1998/09/01;105(6):677-88.

[146].Ohta S, Tachikawa O, Makino Y, Tasaki Y, Hirobe M. Metabolism and brain accumulation of tetrahydroisoquinoline (TIQ) a possible parkinsonism inducing substance, in an animal model of a poor debrisoquine metabolizer. Life Sciences. 1990;46(8):599-605.

[147].Lorenc-Koci E, Wójcikowski J, Kot M, Haduch A, Boksa J, Daniel WA. Disposition of 1,2,3,4,-tetrahydroisoquinoline in the brain of male Wistar and Dark Agouti rats. Brain research. 2004 2004/01/23/;996(2):168-79.

[148].Antkiewicz-Michaluk L, Rommelspacher H. Isoquinolines And Beta-Carbolines As Neurotoxins And Neuroprotectants: New Vistas In Parkinson's Disease Therapy2012.

[149].Kotake Y, Taguchi R, Okuda K, Sekiya Y, Tasaki Y, Hirobe M, et al. Neuroprotective effect of 1-methyl-1,2,3,4-tetrahydroisoquinoline on cultured rat mesencephalic neurons in the presence or absence of various neurotoxins. Brain Research. 2005;8(2):143-50.

[150].Antkiewicz-Michaluk L, Wąsik A, Michaluk J. 1-Methyl-1,2,3,4-tetrahydroisoquinoline, an endogenous amine with unexpected mechanism of action: new vistas of therapeutic application. Neurotoxicity Research. 2014;25(1):1-12.

[151].Kurnik-Łucka M, Latacz G, Martyniak A, Bugajski A, Kieć-Kononowicz K, Gil K. Salsolinol—neurotoxic or Neuroprotective? Neurotoxicity Research. 2020 2020/02/01;37(2):286-97.

[152].Naoi M, Maruyama W, Kasamatsu T, Dostert P. Oxidation of N-methyl(R)salsolinol: involvement to neurotoxicity and neuroprotection by endogenous catechol isoquinolines. Journal of Neural Transmission Supplementa. 1998;52:125-38.

[153].Peana AT, Bassareo V, Acquas E. Not Just from Ethanol. Tetrahydroisoquinolinic (TIQ) Derivatives: from Neurotoxicity to Neuroprotection. Neurotoxicity Research. 2019 2019/11/01;36(4):653-68.

[154].USDA. Agricultural research service Npgs. Germplasm Resources Information Network (GRIN-Taxonomy). Beltsville, Maryland: National Germplasm Resources Laboratory; 2021; Available from: http://www.narc.gov.jo/gringlobal/taxonomydetail.aspx?id=9852. Accessed 24 May

[155].Yuan N-N, Cai C-Z, Wu M-Y, Su H-X, Li M, Lu J-H. Neuroprotective effects of berberine in animal models of Alzheimer's disease: a systematic review of pre-clinical studies. BMC Complementary and Alternative Medicine. 2019;19(1):109-.

[156].Kukula-Koch WA, Widelski J. Chapter 9 - Alkaloids. In: Badal S, Delgoda R, editors. Pharmacognosy. Boston: Academic Press; 2017. p. 163-98.

[157].Melzig MF, Putscher I, Henklein P, Haber H. In vitro pharmacological activity of the tetrahydroisoquinoline salsolinol present in products from Theobroma cacao L. like cocoa and chocolate. Journal of Ethnopharmacology. 2000 2000/11/01/;73(1):153-9.

[158].Maramai S, Gemma S, Brogi S, Campiani G, Butini S, Stark H, et al. Dopamine D3 Receptor Antagonists as Potential Therapeutics for the Treatment of Neurological Diseases. Frontiers in Neuroscience. 2016;10:451-.

[159].Gerrard J. The Maillard Reaction: Chemistry, Biochemistry and Implications by Harry Nursten. Australian Journal of Chemistry. 2005;58:756-.

[160].Wrodnigg TM, Eder B. The Amadori and Heyns Rearrangements: Landmarks in the History of Carbohydrate Chemistry or Unrecognized Synthetic Opportunities? In: Stütz AE, editor. Glycoscience: Epimerisation, Isomerisation and Rearrangement Reactions of Carbohydrates. Berlin, Heidelberg: Springer Berlin Heidelberg; 2001. p. 115-52.

[161].Tareke E, Rydberg P, Karlsson P, Eriksson S, Törnqvist M. Analysis of Acrylamide, a Carcinogen Formed in Heated Foodstuffs. Journal of Agricultural and Food Chemistry. 2002 2002/08/01;50(17):4998-5006.

[162].Lee K-G, Shibamoto T. TOXICOLOGY AND ANTIOXIDANT ACTIVITIES OF NON-ENZYMATIC BROWNING REACTION PRODUCTS: REVIEW. Food Reviews International. 2002 2002/01/10;18(2-3):151-75.

[163].Wijaya C, Wijaya W, Mehta B. General Properties of Major Food Components. 2015.

[164].Bringmann G, Feineis D, Friedrich H, Hille A. Endogenous Alkaloids in Man - Synthesis, Analytics, in vivo Identification, and Medicinal Importance*,1. Planta Med. 1991;57(7 Suppl):2006-960233.

[165].Aniszewski T. Chapter 1 - Definition, typology, and occurrence of alkaloids. In: Aniszewski T, editor. Alkaloids (Second Edition). Boston: Elsevier; 2015. p. 1-97.

[166].Melchior C, Collins MA. The route and significance of endogenous synthesis of alkaloids in animals. Critical Reviews in Toxicology. 1982;9(4):313-56.

[167].Davis VE, Walsh MJ. Alcohol, amines, and alkaloids: a possible biochemical basis for alcohol addiction. Science. 1970;167(3920):1005-7.

[168].Mattei G, Giusti S, Ahluwalia A. Design Criteria for Generating Physiologically Relevant In Vitro Models in Bioreactors. Processes. 2014;2:548-69.

[169].Langhans SA. Three-Dimensional in Vitro Cell Culture Models in Drug Discovery and Drug Repositioning. Front Pharmacol. 2018;9:6-.

[170].Mohs RC, Greig NH. Drug discovery and development: Role of basic biological research. Alzheimers Dement (N Y). 2017;3(4):651-7.

[171].Gribkoff VK, Kaczmarek LK. The need for new approaches in CNS drug discovery: Why drugs have failed, and what can be done to improve outcomes. Neuropharmacology. 2017;120:11-9.

[172].Cummings J, Feldman HH, Scheltens P. The "rights" of precision drug development for Alzheimer's disease. Alzheimer's Research & Therapy. 2019 2019/08/31;11(1):76.

[173].Duval K, Grover H, Han L-H, Mou Y, Pegoraro AF, Fredberg J, et al. Modeling Physiological Events in 2D vs. 3D Cell Culture. Physiology. 2017;32(4):266-77.

[174].Bonnier F, Keating ME, Wrobel TP, Majzner K, Baranska M, Garcia-Munoz A, et al. Cell viability assessment using the Alamar blue assay: a comparison of 2D and 3D cell culture models. Toxicology In Vitro. 2015;29(1):124-31.

[175].Baker BM, Chen CS. Deconstructing the third dimension – how 3D culture microenvironments alter cellular cues. Journal of Cell Science. 2012;125(13):3015-24.

[176].Lee J, Cuddihy MJ, Kotov NA. Three-dimensional cell culture matrices: state of the art. Tissue Engineering Part B Reviews. 2008;14(1):61-86.

[177].Huang G, Li F, Zhao X, Ma Y, Li Y, Lin M, et al. Functional and Biomimetic Materials for Engineering of the Three-Dimensional Cell Microenvironment. Chem Rev. 2017;117(20):12764-850.

[178].Thatikonda N, Högskolan K. Functionalization of spider silk with affinity and bioactive domains via genetic engineering for in vitro disease diagnosis and tissue engineering 2018.

[179].Birgersdotter A, Sandberg R, Ernberg I. Gene expression perturbation in vitro--a growing case for three-dimensional (3D) culture systems. Seminars in Cancer Biology. 2005;15(5):405-12.

[180].Bhadriraju K, Chen CS. Engineering cellular microenvironments to improve cell-based drug testing. Drug Discovery Today. 2002;7(11):612-20.

[181].Zietarska M, Maugard CM, Filali-Mouhim A, Alam-Fahmy M, Tonin PN, Provencher DM, et al. Molecular description of a 3D in vitro model for the study of epithelial ovarian cancer (EOC). Mol Carcinog. 2007;46(10):872-85.

[182].Benton JA, Fairbanks BD, Anseth KS. Characterization of valvular interstitial cell function in three dimensional matrix metalloproteinase degradable PEG hydrogels. Biomaterials. 2009;30(34):6593-603.

[183].Bi YA, Kazolias D, Duignan DB. Use of cryopreserved human hepatocytes in sandwich culture to measure hepatobiliary transport. Drug Metabolism & Disposition. 2006;34(9):1658-65.

[184].Lancaster MA, Renner M, Martin CA, Wenzel D, Bicknell LS, Hurles ME, et al. Cerebral organoids model human brain development and microcephaly. Nature. 2013;501(7467):373-9.

[185].Beauchamp P, Moritz W, Kelm JM, Ullrich ND, Agarkova I, Anson BD, et al. Development and Characterization of a Scaffold-Free 3D Spheroid Model of Induced Pluripotent Stem Cell-Derived Human Cardiomyocytes. Tissue Engineering Part C Methods. 2015;21(8):852-61.

[186].Suga H, Kadoshima T, Minaguchi M, Ohgushi M, Soen M, Nakano T, et al. Self-formation of functional adenohypophysis in three-dimensional culture. Nature. 2011;480(7375):57-62.

[187].Nakano T, Ando S, Takata N, Kawada M, Muguruma K, Sekiguchi K, et al. Self-formation of optic cups and storable stratified neural retina from human ESCs. Cell Stem Cell. 2012;10(6):771-85.

[188].Sato T, Vries RG, Snippert HJ, van de Wetering M, Barker N, Stange DE, et al. Single Lgr5 stem cells build crypt-villus structures in vitro without a mesenchymal niche. Nature. 2009;459(7244):262-5.

[189].Zanoni M PF, Arienti C, Zamagni A, Santi S, Polico R et al. . 3D tumor spheroid models for in vitro therapeutic screening: A systematic approach to enhance the biological relevance of data obtained. Scientific Reports. 2016 11 January;6(19103).

[190].Lee J, Lilly GD, Doty RC, Podsiadlo P, Kotov NA. In vitro toxicity testing of nanoparticles in 3D cell culture. Small. 2009;5(10):1213-21.

[191].Otieno MA, Gan J, Proctor W. Status and Future of 3D Cell Culture in Toxicity Testing. In: Chen M, Will Y, editors. Drug-Induced Liver Toxicity. New York, NY: Springer New York; 2018. p. 249-61.

[192].Jitcy Saji Joseph STM, Monde Ntwasa. Two-Dimensional (2D) and Three-Dimensional (3D) Cell Culturing in Drug Discovery: IntechOpen; 2019.

[193].Antoni D, Burckel H, Josset E, Noel G. Three-dimensional cell culture: a breakthrough in vivo. International Journal of Molecular Sciences (IJMS). 2015;16(3):5517-27.

[194].Kim JB. Three-dimensional tissue culture models in cancer biology. Seminars in Cancer Biology. 2005;15(5):365-77.

[195].Yip D, Cho CH. A multicellular 3D herospheroid model of liver tumor and stromal cells in collagen gel for anti-cancer drug testing. Biochemical and Biophysical Research Communications. 2013;433(3):327-32.

[196].Pontes Soares C, Midlej V, de Oliveira ME, Benchimol M, Costa ML, Mermelstein C. 2D and 3D-organized cardiac cells shows differences in cellular morphology, adhesion junctions, presence of myofibrils and protein expression. PLOS One. 2012;7(5):25.

[197].Chitcholtan K, Asselin E, Parent S, Sykes PH, Evans JJ. Differences in growth properties of endometrial cancer in three dimensional (3D) culture and 2D cell monolayer. Experimental Cell Research. 2013;319(1):75-87.

[198].Schyschka L, Sánchez JJ, Wang Z, Burkhardt B, Müller-Vieira U, Zeilinger K, et al. Hepatic 3D cultures but not 2D cultures preserve specific transporter activity for acetaminophen-induced hepatotoxicity. Archives of Toxicology. 2013;87(8):1581-93.

[199].Elkayam T, Amitay-Shaprut S, Dvir-Ginzberg M, Harel T, Cohen S. Enhancing the drug metabolism activities of C3A--a human hepatocyte cell line--by tissue engineering within alginate scaffolds. Tissue Engineering. 2006;12(5):1357-68.

[200].Bokhari M, Carnachan RJ, Cameron NR, Przyborski SA. Culture of HepG2 liver cells on three dimensional polystyrene scaffolds enhances cell structure and function during toxicological challenge. Journal of Anatomy. 2007;211(4):567-76.

[201].Chopra V, Dinh TV, Hannigan EV. Three-dimensional endothelial-tumor epithelial cell interactions in human cervical cancers. In Vitro Cellular & Developmental Biology – Animal. 1997;33(6):432-42.

[202].Torisawa YS, Shiku H, Yasukawa T, Nishizawa M, Matsue T. Multi-channel 3-D cell culture device integrated on a silicon chip for anticancer drug sensitivity test. Biomaterials. 2005;26(14):2165-72.

[203].Li Y, Huang G, Li M, Wang L, Elson EL, Lu TJ, et al. An approach to quantifying 3D responses of cells to extreme strain. Scientific Reports. 2016;6(19550).

[204].Li CL, Tian T, Nan KJ, Zhao N, Guo YH, Cui J, et al. Survival advantages of multicellular spheroids vs. monolayers of HepG2 cells in vitro. Oncology Reports. 2008;20(6):1465-71.

[205].Shamir E, Ewald A. Three-dimensional organotypic culture: Experimental models of mammalian biology and disease. Nature reviews Molecular cell biology. 2014;15.

[206].Guerrero RR, Rounds DE, Booher J. An improved organ culture method for adult mammalian lung. In Vitro. 1977;13(8):517-24.

[207].Browning TH, Trier JS. Organ culture of mucosal biopsies of human small intestine. Journal of Clinical Investigation. 1969;48(8):1423-32.

[208].Randall KJ, Turton J, Foster JR. Explant culture of gastrointestinal tissue: a review of methods and applications. Cell Biology Toxicology. 2011;27(4):267-84.

[209].Stoppini L, Buchs PA, Muller D. A simple method for organotypic cultures of nervous tissue. Journal of Neuroscience Methods. 1991;37(2):173-82.

[210].Aplin AC, Fogel E, Zorzi P, Nicosia RF. The aortic ring model of angiogenesis. Methods in Enzymology 2008;443:119-36.

[211].Using Perfecta3D™H anging Drop Plates to Assess Chemosensitivity White Paper 3D Biomatrix; Available from: http://www.volttecnologia.com.br/pdfs/3D/Hanging%20Drop%20Plates.pdf.

[212].Hydrogels for 3D cell culture. Merck; Available from: https://www.sigmaaldrich.com/technical-documents/articles/biology/3d-hydrogels.html.

[213].Haigh J. 3D Cell Culture for Biological-Relevant, Neuroscientific, In Vitro Environments2017: Available from: https://www.advancedsciencenews.com/3d-cell-culture-towards-realistic-biological-environments-cell-culture/.

[214].Kuo C-T, Wang J-Y, Lin Y-F, Wo AM, Chen BPC, Lee H. Three-dimensional spheroid culture targeting versatile tissue bioassays using a PDMS-based hanging drop array. Scientific Reports. 2017 2017/06/29;7(1):4363.

[215].Gunness P, Mueller D, Shevchenko V, Heinzle E, Ingelman-Sundberg M, Noor F. 3D organotypic cultures of human HepaRG cells: a tool for in vitro toxicity studies. Toxicology Sciences. 2013;133(1):67-78.

[216].Nzou G, Wicks RT, Wicks EE, Seale SA, Sane CH, Chen A, et al. Human Cortex Spheroid with a Functional Blood Brain Barrier for High-Throughput Neurotoxicity Screening and Disease Modeling. Scientific Reports. 2018 2018/05/09;8(1):7413.

[217].Larson B. 3D Cell Culture: A Review of Current Techniques. Biotek; 2015; Available from: https://www.biotek.pt/pt/resources/white-papers/3d-cell-culture-a-review-of-current-techniques/.

[218].Amaral RLF, Miranda M, Marcato PD, Swiech K. Comparative Analysis of 3D Bladder Tumor Spheroids Obtained by Forced Floating and Hanging Drop Methods for Drug Screening. Front Physiol. 2017;8:605-.

[219].Ivanov DP, Parker TL, Walker DA, Alexander C, Ashford MB, Gellert PR, et al. Multiplexing spheroid volume, resazurin and acid phosphatase viability assays for high-throughput screening of tumour spheroids and stem cell neurospheres. PLOS One. 2014;9(8).

[220].Vinci M, Gowan S, Boxall F, Patterson L, Zimmermann M, Court W, et al. Advances in establishment and analysis of three-dimensional tumor spheroid-based functional assays for target validation and drug evaluation. BMC Biology. 2012;10(29):1741-7007.

[221].Iskandar AR, Xiang Y, Frentzel S, Talikka M, Leroy P, Kuehn D, et al. Impact Assessment of Cigarette Smoke Exposure on Organotypic Bronchial Epithelial Tissue Cultures: A Comparison of Mono-Culture and Coculture Model Containing Fibroblasts. Toxicological Sciences. 2015;147(1):207-21.

[222].Liao W, Wang J, Xu J, You F, Pan M, Xu X, et al. High-throughput three-dimensional spheroid tumor model using a novel stamp-like tool. J Tissue Eng. 2019;10:2041731419889184-.

[223].Norotte C, Marga FS, Niklason LE, Forgacs G. Scaffold-free vascular tissue engineering using bioprinting. Biomaterials. 2009;30(30):5910-7.

[224].Thomsen AR, Aldrian C, Bronsert P, Thomann Y, Nanko N, Melin N, et al. A deep conical agarose microwell array for adhesion independent three-dimensional cell culture and dynamic volume measurement. Lab on a Chip. 2017;18(1):179-89.

[225].Dingle Y-TL, Boutin ME, Chirila AM, Livi LL, Labriola NR, Jakubek LM, et al. Three-Dimensional Neural Spheroid Culture: An In Vitro Model for Cortical Studies. Tissue Engineering Part C, Methods. 2015;21(12):1274-83.

[226].Barros AS, Costa EC, Nunes AS, de Melo-Diogo D, Correia IJ. Comparative study of the therapeutic effect of Doxorubicin and Resveratrol combination on 2D and 3D (spheroids) cell culture models. International Journal of Pharmaceutics. 2018 2018/11/15/;551(1):76-83.

[227].Balmaña M, Diniz F, Feijão T, Barrias CC, Mereiter S, Reis CA. Analysis of the Effect of Increased α2,3-Sialylation on RTK Activation in MKN45 Gastric Cancer Spheroids Treated with Crizotinib. International journal of molecular sciences. 2020;21(3):722.

[228].The 3D Petri Dish The ® 3D Petri Dish®. A New Cutting-Edge Culture Format. Available from: https://www.sigmaaldrich.com/content/dam/sigma-aldrich/docs/Sigma-Aldrich/General_Information/1/3d-petri-dish-of-microtissues.pdf.

[229].van Duinen V, Trietsch SJ, Joore J, Vulto P, Hankemeier T. Microfluidic 3D cell culture: from tools to tissue models. Current Opinion in Biotechnology. 2015 2015/12/01/;35:118-26.

[230].Castiaux AD, Spence DM, Martin RS. Review of 3D cell culture with analysis in microfluidic systems. Analytical Methods. [10.1039/C9AY01328H]. 2019;11(33):4220-32.

[231].Li XJ, Valadez AV, Zuo P, Nie Z. Microfluidic 3D cell culture: potential application for tissue-based bioassays. Bioanalysis. 2012;4(12):1509-25.

[232].Ong SM, Zhang C, Toh YC, Kim SH, Foo HL, Tan CH, et al. A gel-free 3D microfluidic cell culture system. Biomaterials. 2008;29(22):3237-44.

[233].Jang K, Sato K, Igawa K, Chung UI, Kitamori T. Development of an osteoblast-based 3D continuous-perfusion microfluidic system for drug screening. Analytical and Bioanalytical Chemistry 2008;390(3):825-32.

[234].Musick K, Khatami D, Wheeler BC. Three-dimensional micro-electrode array for recording dissociated neuronal cultures. Lab Chip. 2009;9(14):2036-42.

[235].Hattersley SM, Greenman J, Haswell SJ. Study of ethanol induced toxicity in liver explants using microfluidic devices. Biomedical Microdevices. 2011;13(6):1005-14.

[236].Derda R, Laromaine A, Mammoto A, Tang SK, Mammoto T, Ingber DE, et al. Paper-supported 3D cell culture for tissue-based bioassays. Proceedings of the National Academy of Sciences of the United States of America. 2009;106(44):18457-62.

[237].Toh YC, Lim TC, Tai D, Xiao G, van Noort D, Yu H. A microfluidic 3D hepatocyte chip for drug toxicity testing. Lab Chip. 2009;9(14):2026-35.

[238].Cushing MC, Anseth KS. Materials science. Hydrogel cell cultures. Science. 2007;316(5828):1133-4.

[239].Salinas CN, Anseth KS. The enhancement of chondrogenic differentiation of human mesenchymal stem cells by enzymatically regulated RGD functionalities. Biomaterials. 2008;29(15):2370-7.

[240].Mann BK, West JL. Cell adhesion peptides alter smooth muscle cell adhesion, proliferation, migration, and matrix protein synthesis on modified surfaces and in polymer scaffolds. Journal of Biomedical Materials Research. 2002;60(1):86-93.

[241].West JL, Hubbell JA. Polymeric Biomaterials with Degradation Sites for Proteases Involved in Cell Migration. Macromolecules. 1999 1999/01/01;32(1):241-4.

[242].MERCK. How to use the TrueGel3D™ system. Available from: https://www.sigmaaldrich.com/technical-documents/articles/biology/truegel3d.html.

[243].Li L, LaBarbera DV. 3D High-Content Screening of Organoids for Drug Discovery. Comprehensive Medicinal Chemistry III2017. p. 388-415.

[244].Astashkina A, Grainger DW. Critical analysis of 3-D organoid in vitro cell culture models for high-throughput drug candidate toxicity assessments. Advanced Drug Delivery Reviews. 2014 2014/04/20/;69-70:1-18.

[245].Pereira S, Coutinho D, Flávia de Oliveira Gonçalves de Matos A, Silva W, Fabrino D. Three-dimensional cell culture, opportunities and challenges for bioprocess engineers2016.

[246].Sharma R, Barakzai SZ, Taylor SE, Donadeu FX. Epidermal-like architecture obtained from equine keratinocytes in three-dimensional cultures. Journal of Tissue Engineering and Regenerative Medicine. 2016;10(8):627-36.

[247].Blan NR, Birla RK. Design and fabrication of heart muscle using scaffold-based tissue engineering. The Journal of Biomedical Materials Research. 2008;86(1):195-208.

[248].Chen X, Ergun A, Gevgilili H, Ozkan S, Kalyon DM, Wang H. Shell-core bi-layered scaffolds for engineering of vascularized osteon-like structures. Biomaterials. 2013;34(33):8203-12.

[249].Fischbach C, Chen R, Matsumoto T, Schmelzle T, Brugge JS, Polverini PJ, et al. Engineering tumors with 3D scaffolds. Nature Methods. 2007;4(10):855-60.

[250].In vivo, In vitro. NanoSurface Biomedical, Inc.; Available from: https://www.vitascientific.com/NANOSURFACE-BIOMEDICAL.

[251].Raghavan S, Ward MR, Rowley KR, Wold RM, Takayama S, Buckanovich RJ, et al. Formation of stable small cell number three-dimensional ovarian cancer spheroids using hanging drop arrays for preclinical drug sensitivity assays. Gynecologic Oncology. 2015;138(1):181-9.

[252].Tung Y-C, Hsiao AY, Allen SG, Torisawa Y-s, Ho M, Takayama S. High-throughput 3D spheroid culture and drug testing using a 384 hanging drop array. Analyst. 2011;136(3):473-8.

[253].Vinci M, Gowan S, Boxall F, Patterson L, Zimmermann M, Court W, et al. Advances in establishment and analysis of three-dimensional tumor spheroid-based functional assays for target validation and drug evaluation. BMC Biology. 2012 2012/03/22;10(1):29.

[254].Sridhar A, de Boer HL, van den Berg A, Le Gac S. Microstamped Petri dishes for scanning electrochemical microscopy analysis of arrays of microtissues. PLOS One. 2014;9(4).

[255].Dissanayaka W, Zhu L, Hargreaves K, Jin L, Zhang C. Scaffold-free Prevascularized Microtissue Spheroids for Pulp Regeneration. Journal of Dental Research. 2014.

[256].Patel BB, McNamara MC, Pesquera-Colom LS, Kozik EM, Okuzonu J, Hashemi NN, et al. Recovery of Encapsulated Adult Neural Progenitor Cells from Microfluidic-Spun Hydrogel Fibers Enhances Proliferation and Neuronal Differentiation. ACS Omega. 2020;5(14):7910-8.

[257].Huang G, Wang S, He X, Zhang X, Lu TJ, Xu F. Helical spring template fabrication of cell-laden microfluidic hydrogels for tissue engineering. Biotechnology Bioengineering. 2013;110(3):980-9.

[258].Stock K, Estrada MF, Vidic S, Gjerde K, Rudisch A, Santo VE, et al. Capturing tumor complexity in vitro: Comparative analysis of 2D and 3D tumor models for drug discovery. Scientific Reports. 2016;6:28951-.

[259].Guzman A, Ziperstein MJ, Kaufman LJ. The effect of fibrillar matrix architecture on tumor cell invasion of physically challenging environments. Biomaterials. 2014 2014/08/01/;35(25):6954-63.

[260].Dhiman HK, Ray AR, Panda AK. Three-dimensional chitosan scaffold-based MCF-7 cell culture for the determination of the cytotoxicity of tamoxifen. Biomaterials. 2005;26(9):979-86.

[261].Elias Volkmer ID, Sven Otto, Achim Stangelmayer, Michael Stengele, Bobby Cherian Kallukalam, Wolf Mutschler, and Matthias Schieker. Hypoxia in Static and Dynamic 3D Culture Systems for Tissue Engineering of Bone. Tissue Engineering Part A. 2008 August 4;14(8).

[262].Barbosa DJ, Capela JP, de Lourdes Bastos M, Carvalho F. In vitro models for neurotoxicology research. Toxicology Research. 2015;4(4):801-42.

[263].Gozes I, Levine J. Introduction. In: Gozes I, Levine J, editors. Neuroprotection in Autism, Schizophrenia and Alzheimer's Disease: Academic Press; 2020. p. xiii-xviii.

[264].Costa LG. Neurotoxicity testing: a discussion of in vitro alternatives. Environ Health Perspect. 1998;2:505-10.

[265].Pereira CV, Moreira AC, Pereira SP, Machado NG, Carvalho FS, Sardao VA, et al. Investigating drug-induced mitochondrial toxicity: a biosensor to increase drug safety? Current Drug Safety. 2009;4(1):34-54.

[266].Bai F, Witzmann FA. Synaptosome proteomics. Subcellular Biochemistry. 2007;43:77-98.

[267].Chinopoulos C, Adam-Vizi V. Mitochondria deficient in complex I activity are depolarized by hydrogen peroxide in nerve terminals: relevance to Parkinson's disease. Journal of Neurochemistry. 2001;76(1):302-6.

[268].Banker G, Goslin K. Culturing nerve cells. 2nd ed. Massachusetts, USA: MIT press; 1998.

[269].Ehret F, Vogler S, Kempermann G. A co-culture model of the hippocampal neurogenic niche reveals differential effects of astrocytes, endothelial cells and pericytes on proliferation and differentiation of adult murine precursor cells. Stem Cell Research. 2015;15(3):514-21.

[270].Radio NM, Mundy WR. Developmental neurotoxicity testing in vitro: models for assessing chemical effects on neurite outgrowth. Neurotoxicology. 2008;29(3):361-76.

[271].Gradinaru D, Minn AL, Artur Y, Minn A, Heydel JM. Effect of oxidative stress on UDP-glucuronosyltransferases in rat astrocytes. Toxicology Letters. 2012;213(3):316-24.

[272].Bajpai P, Sangar MC, Singh S, Tang W, Bansal S, Chowdhury G, et al. Metabolism of 1-methyl-4-phenyl-1,2,3,6-tetrahydropyridine by mitochondrion-targeted cytochrome P450 2D6: implications in Parkinson disease. J Biol Chem. 2013;288(6):4436-51.

[273].Roqué PJ, Dao K, Costa LG. Microglia mediate diesel exhaust particle-induced cerebellar neuronal toxicity through neuroinflammatory mechanisms. Neurotoxicology. 2016;56:204-14.

[274].Boraso M, Viviani B. Glia-neuron sandwich cocultures: an in vitro approach to evaluate cell-to-cell communication in neuroinflammation and neurotoxicity. Methods in Molecular Biology. 2011;758:135-52.

[275].Viviani B, Corsini E, Galli CL, Marinovich M. Glia increase degeneration of hippocampal neurons through release of tumor necrosis factor-alpha. Toxicology and Applied Pharmacology 1998;150(2):271-6.

[276].Barbosa D, Capela J, Bastos M, Carvalho F. In vitro models for neurotoxicology research. Toxicology Research. 2015;4.

[277].Gähwiler BH. Organotypic cultures of neural tissue. Trends in Neurosciences. 1988 1988/01/01/;11(11):484-9.

[278].Garthwaite G, Garthwaite J. AMPA Neurotoxicity in Rat Cerebellar and Hippocampal Slices: Histological Evidence for Three Mechanisms. Eur J Neurosci. 1991;3(8):715-28.

[279].Humpel C. Organotypic brain slice cultures: A review. Neuroscience. 2015;305:86-98.

[280].Spencer PS, Crain SM, Bornstein MB, Peterson ER, Van de Water T. Chemical neurotoxicity: detection and analysis in organotypic cultures of sensory and motor systems. Food and Chemical Toxicology. 1986;24(6-7):539-44.

[281].Ryan KR, Sirenko O, Parham F, Hsieh JH, Cromwell EF, Tice RR, et al. Neurite outgrowth in human induced pluripotent stem cell-derived neurons as a high-throughput screen for developmental neurotoxicity or neurotoxicity. Neurotoxicology. 2016;53:271-81.

[282].Buzanska L, Sypecka J, Nerini-Molteni S, Compagnoni A, Hogberg HT, del Torchio R, et al. A human stem cell-based model for identifying adverse effects of organic and inorganic chemicals on the developing nervous system. Stem Cells. 2009;27(10):2591-601.

[283].Leite PEC, Pereira MR, Harris G, Pamies D, dos Santos LMG, Granjeiro JM, et al. Suitability of 3D human brain spheroid models to distinguish toxic effects of gold and poly-lactic acid nanoparticles to assess biocompatibility for brain drug delivery. Particle and Fibre Toxicology. 2019 2019/06/03;16(1):22.

[284].Tofighi R, Moors M, Bose R, Ibrahim WN, Ceccatelli S. Neural stem cells for developmental neurotoxicity studies. Methods in Molecular Biology. 2011;758:67-80.

[285].Schmidt BZ, Lehmann M, Gutbier S, Nembo E, Noel S, Smirnova L, et al. In vitro acute and developmental neurotoxicity screening: an overview of cellular platforms and high-throughput technical possibilities. Archives of Toxicology. 2017;91(1):1-33.

[286].Kelava I, Lancaster Madeline A. Stem Cell Models of Human Brain Development. Cell Stem Cell. 2016 2016/06/02/;18(6):736-48.

[287].Venstrom KA, Reichardt LF. Extracellular matrix. 2: Role of extracellular matrix molecules and their receptors in the nervous system. FASEB Journal. 1993;7(11):996-1003.

[288].Honegger P, Defaux A, Monnet-Tschudi F, Zurich MG. Preparation, maintenance, and use of serum-free aggregating brain cell cultures. Methods in Molecular Biology. 2011;758:81-97.

[289].Roach P, Parker T, Gadegaard N, Alexander MR. Surface strategies for control of neuronal cell adhesion: A review. Surface Science Reports. 2010 2010/06/15/;65(6):145-73.

[290].Choi YJ, Park J, Lee SH. Size-controllable networked neurospheres as a 3D neuronal tissue model for Alzheimer's disease studies. Biomaterials. 2013;34(12):2938-46.

[291].Innala M, Riebe I, Kuzmenko V, Sundberg J, Gatenholm P, Hanse E, et al. 3D Culturing and differentiation of SH-SY5Y neuroblastoma cells on bacterial nanocellulose scaffolds. Artificial Cells, Nanomedicine, and Biotechnology. 2014 2014/10/01;42(5):302-8.

[292].Peretz H, Talpalar AE, Vago R, Baranes D. Superior survival and durability of neurons and astrocytes on 3-dimensional aragonite biomatrices. Tissue Engineering. 2007;13(3):461-72.

[293].Zurich M-G, Stanzel S, Kopp-Schneider A, Prieto P, Honegger P. Evaluation of aggregating brain cell cultures for the detection of acute organ-specific toxicity. Toxicology in Vitro. 2013 2013/06/01/;27(4):1416-24.

[294].Hill EJ, Woehrling EK, Prince M, Coleman MD. Differentiating human NT2/D1 neurospheres as a versatile in vitro 3D model system for developmental neurotoxicity testing. Toxicology. 2008;249(2-3):243-50.

[295].Salama M, Lotfy A, Fathy K, Makar M, El-Emam M, El-Gamal A, et al. Developmental neurotoxic effects of Malathion on 3D neurosphere system. Applied & Translational Genomics. 2015;7:13-8.

[296].Zhang SC, Wernig M, Duncan ID, Brüstle O, Thomson JA. In vitro differentiation of transplantable neural precursors from human embryonic stem cells. Nature Biotechnology. 2001;19(12):1129-33.

[297].Ying Q-L, Stavridis M, Griffiths D, Li M, Smith A. Conversion of embryonic stem cells into neuroectodermal precursors in adherent monoculture. Nature Biotechnology. 2003 2003/02/01;21(2):183-6.

[298].Watanabe K, Kamiya D, Nishiyama A, Katayama T, Nozaki S, Kawasaki H, et al. Directed differentiation of telencephalic precursors from embryonic stem cells. Nature Neuroscience. 2005 2005/03/01;8(3):288-96.

[299].Elkabetz Y, Panagiotakos G, Al Shamy G, Socci ND, Tabar V, Studer L. Human ES cell-derived neural rosettes reveal a functionally distinct early neural stem cell stage. Genes and Development. 2008;22(2):152-65.

[300].Gaspard N, Bouschet T, Hourez R, Dimidschstein J, Naeije G, van den Ameele J, et al. An intrinsic mechanism of corticogenesis from embryonic stem cells. Nature. 2008 2008/09/01;455(7211):351-7.

[301].Eiraku M, Watanabe K, Matsuo-Takasaki M, Kawada M, Yonemura S, Matsumura M, et al. Self-organized formation of polarized cortical tissues from ESCs and its active manipulation by extrinsic signals. Cell Stem Cell. 2008;3(5):519-32.

[302].Chambers SM, Fasano CA, Papapetrou EP, Tomishima M, Sadelain M, Studer L. Highly efficient neural conversion of human ES and iPS cells by dual inhibition of SMAD signaling. Nature Biotechnology 2009;27(3):275-80.

[303].Koch P, Opitz T, Steinbeck JA, Ladewig J, Brüstle O. A rosette-type, self-renewing human ES cell-derived neural stem cell with potential for in vitro instruction and synaptic integration. Proceedings of the National Academy of Sciences. 2009;106(9):3225-30.

[304].Eiraku M, Takata N, Ishibashi H, Kawada M, Sakakura E, Okuda S, et al. Self-organizing optic-cup morphogenesis in three-dimensional culture. Nature. 2011 2011/04/01;472(7341):51-6.

[305].Shi Y, Kirwan P, Smith J, Robinson HPC, Livesey FJ. Human cerebral cortex development from pluripotent stem cells to functional excitatory synapses. Nature Neuroscience. 2012 2012/03/01;15(3):477-86.

[306].Mariani J, Simonini MV, Palejev D, Tomasini L, Coppola G, Szekely AM, et al. Modeling human cortical development in vitro using induced pluripotent stem cells. Proceedings of the National Academy of Sciences. 2012;109(31):12770-5.

[307].Zhu Y, Carido M, Meinhardt A, Kurth T, Karl MO, Ader M, et al. Three-dimensional neuroepithelial culture from human embryonic stem cells and its use for quantitative conversion to retinal pigment epithelium. PLOS One. 2013;8(1):24.

[308].Meinhardt A, Eberle D, Tazaki A, Ranga A, Niesche M, Wilsch-Bräuninger M, et al. 3D reconstitution of the patterned neural tube from embryonic stem cells. Stem Cell Reports. 2014;3(6):987-99.

[309].Lancaster MA, Renner M, Martin C-A, Wenzel D, Bicknell LS, Hurles ME, et al. Cerebral organoids model human brain development and microcephaly. Nature. 2013 2013/09/01;501(7467):373-9.

[310].Kadoshima T, Sakaguchi H, Nakano T, Soen M, Ando S, Eiraku M, et al. Self-organization of axial polarity, inside-out layer pattern, and species-specific progenitor dynamics in human ES cell–derived neocortex. Proceedings of the National Academy of Sciences. 2013;110(50):20284-9.

[311].Muguruma K, Nishiyama A, Kawakami H, Hashimoto K, Sasai Y. Self-Organization of Polarized Cerebellar Tissue in 3D Culture of Human Pluripotent Stem Cells. Cell Reports. 2015;10(4):537-50.

[312].Paşca AM, Sloan SA, Clarke LE, Tian Y, Makinson CD, Huber N, et al. Functional cortical neurons and astrocytes from human pluripotent stem cells in 3D culture. Nature Methods. 2015 2015/07/01;12(7):671-8.

[313].Mariani J, Coppola G, Zhang P, Abyzov A, Provini L, Tomasini L, et al. FOXG1-Dependent Dysregulation of GABA/Glutamate Neuron Differentiation in Autism Spectrum Disorders. Cell. 2015;162(2):375-90.

[314].Sakaguchi H, Kadoshima T, Soen M, Narii N, Ishida Y, Ohgushi M, et al. Generation of functional hippocampal neurons from self-organizing human embryonic stem cell-derived dorsomedial telencephalic tissue. Nature Communications. 2015 2015/11/17;6(1):8896.

[315].Qian X, Nguyen Ha N, Song Mingxi M, Hadiono C, Ogden Sarah C, Hammack C, et al. Brain-Region-Specific Organoids Using Mini-bioreactors for Modeling ZIKV Exposure. Cell. 2016;165(5):1238-54.

[316].Laviță SI, Aro R, Kiss B, Manto M, Duez P. The Role of β-Carboline Alkaloids in the Pathogenesis of Essential Tremor. Cerebellum. 2016;15(3):276-84.

[317].Piechowska P, Zawirska-Wojtasiak R, Mildner-Szkudlarz S. Bioactive β-Carbolines in Food: A Review. Nutrients. 2019;11(4):814.

[318].Seidl SE, Santiago JA, Bilyk H, Potashkin JA. The emerging role of nutrition in Parkinson's disease. Front Aging Neurosci. 2014;6:36-.

[319].ALjahdali N CF. Impact of Maillard reaction products on nutrition and health: Current knowledge and need to understand their fate in the human digestive system. Critical Reviews in Food Science and Nutrition 2019;59(3):474-87.

[320].Cobos Á, Díaz O. Chemical Composition of Meat and Meat Products. In: Cheung PCK, editor. Handbook of Food Chemistry. Berlin, Heidelberg: Springer Berlin Heidelberg; 2015. p. 1-32.

[321].Raynie DE. Looking at the Past to Understand the Future: Soxhlet Extraction. LCGC North America; 2019; Available from: https://www.chromatographyonline.com/view/looking-past-understand-future-soxhlet-extraction.

[322].Engel W, Bahr W, Schieberle P. Solvent assisted flavour evaporation – a new and versatile technique for the careful and direct isolation of aroma compounds from complex food matrices. European Food Research and Technology. 1999 1999/08/01;209(3):237-41.

[323].Louis ED, Zheng W, Jiang W, Bogen KT, Keating GA. Quantification of the neurotoxic beta-carboline harmane in barbecued/grilled meat samples and correlation with level of doneness. Journal of Toxicology and Environmental Health. 2007;70(12):1014-9.

[324].Zheng W, Wang S, Barnes LF, Guan Y, Louis ED. Determination of harmane and harmine in human blood using reversed-phased high-performance liquid chromatography and fluorescence detection. Analytical Biochemistry. 2000;279(2):125-9.

[325].Tsuchiya H, Yamada K, Ohtani S, Takagi N, Todoriki H, Hayashi T. Determination of tetrahydro-β-carbolines in rat brain by gas chromatography-negative-ion chemical ionization mass spectrometry

without interference from artifactual formation. Journal of Neuroscience Methods. 1995 1995/11/01/;62(1):37-41.

[326].Jeannot MA, Cantwell FF. Solvent Microextraction into a Single Drop. Analytical Chemistry. 1996 1996/07/01;68(13):2236-40.

[327].Li N, Deng C, Yin X, Yao N, Shen X, Zhang X. Gas chromatography–mass spectrometric analysis of hexanal and heptanal in human blood by headspace single-drop microextraction with droplet derivatization. Analytical Biochemistry. 2005 2005/07/15/;342(2):318-26.

[328].Singh RP, Subbarao HN, Dev S. Organic reactions in a solid matrix-vi11Part V, Tetrahedron 35, 1789 (1979).: Silica-gel supported reagents for the isolation of aldehydes and ketones. Tetrahedron. 1981 1981/01/01/;37(4):843-6.

[329].Bensalem S, Soubhye J, Aldib I, Bournine L, Nguyen AT, Vanhaeverbeek M, et al. Inhibition of myeloperoxidase activity by the alkaloids of Peganum harmala L. (Zygophyllaceae). Journal of Ethnopharmacology. 2014 2014/06/11/;154(2):361-9.

[330].Dator RP, Solivio MJ, Villalta PW, Balbo S. Bioanalytical and Mass Spectrometric Methods for Aldehyde Profiling in Biological Fluids. Toxics. 2019;7(2).

[331].Johnson DW. A modified Girard derivatizing reagent for universal profiling and trace analysis of aldehydes and ketones by electrospray ionization tandem mass spectrometry. Rapid Communications in Mass Spectrometry. 2007;21(18):2926-32.

[332].Jayasena DD, Ahn DU, Nam KC, Jo C. Flavour chemistry of chicken meat: a review. Asian-Australas J Anim Sci. 2013;26(5):732-42.

[333].Suyama K, Arakawa T, Adachi S. Free fatty aldehydes and their aldol condensation products in heated meat. Journal of Agricultural and Food Chemistry. 1981 1981/07/01/;29(4):875-8.

[334].Bunel V, Hamel M, Duez P, Caroline S. Artifactual generation of an alkaloid in the course of Mondia whitei (Hook.f.) Skeels roots extraction: A clue to endogenous-formed bioactive compounds? Phytochemistry Letters. 2014;10:101-6.

[335].Choma I, Jesionek W. TLC-Direct Bioautography as a High Throughput Method for Detection of Antimicrobials in Plants. Chromatography. 2015;2:225-38.

[336].Ji C, Svensson F, Zoufir A, Bender A. eMolTox: prediction of molecular toxicity with confidence. Bioinformatics. 2018;34(14):2508-9.

[337].Pires DEV, Blundell TL, Ascher DB. pkCSM: Predicting Small-Molecule Pharmacokinetic and Toxicity Properties Using Graph-Based Signatures. J Med Chem. 2015;58(9):4066-72.

[338].Kim S, Thiessen PA, Bolton EE, Chen J, Fu G, Gindulyte A, et al. PubChem Substance and Compound databases. Nucleic Acids Res. 2016;44(D1):D1202-D13.

[339].Dingle YT, Boutin ME, Chirila AM, Livi LL, Labriola NR, Jakubek LM, et al. Three-Dimensional Neural Spheroid Culture: An In Vitro Model for Cortical Studies. Tissue Engineering Methods (Part C). 2015;21(12):1274-83.

[340].Casting, Equilibrating and Seeding the 3D Petri Dish®. MicroTissues Inc.; Available from: https://www.microtissues.com/protocols.

[341].ImageJ. Available from: https://imagej.net/Fiji/Downloads.

[342].Cuijpers V, Walboomers X, Jansen J. Scanning Electron Microscopy Stereoimaging for Three-Dimensional Visualization and Analysis of Cells in Tissue-Engineered Constructs: Technical Note. Tissue Engineering Part C, Methods. 2011;17:663-8.

[343].Pamies D, Block K, Lau P, Gribaldo L, Pardo CA, Barreras P, et al. Rotenone exerts developmental neurotoxicity in a human brain spheroid model. Toxicology and Applied Pharmacology. 2018;354:101-14.

[344].Bunel V, Ouedraogo M, Nguyen AT, Stévigny C, Duez P. Methods applied to the in vitro primary toxicology testing of natural products: state of the art, strengths, and limits. Planta Medica. 2014;80(14):1210-26.

[345].Silveira LR, Pereira-Da-Silva L, Juel C, Hellsten Y. Formation of hydrogen peroxide and nitric oxide in rat skeletal muscle cells during contractions. Free Radical Biology and Medicine. 2003;35(5):455-64.

[346].Cathcart R, Schwiers E, Ames BN. Detection of picomole levels of hydroperoxides using a fluorescent dichlorofluorescein assay. Analytical Biochemistry. 1983;134(1):111-6.

[347].Kyrylkova K, Kyryachenko S, Leid M, Kioussi C. Detection of apoptosis by TUNEL assay. Methods in Molecular Biology. 2012;887:41-7.

[348].Duan WR, Garner DS, Williams SD, Funckes-Shippy CL, Spath IS, Blomme EA. Comparison of immunohistochemistry for activated caspase-3 and cleaved cytokeratin 18 with the TUNEL method for quantification of apoptosis in histological sections of PC-3 subcutaneous xenografts. Journal of Pathology. 2003;199(2):221-8.

[349].Lawrenson CL, Watson TC, Apps R. Transmission of Predictable Sensory Signals to the Cerebellum via Climbing Fiber Pathways Is Gated during Exploratory Behavior. The Journal of Neuroscience. 2016;36(30):7841.

[350].Lawrenson CL, Watson TC, Apps R. Transmission of Predictable Sensory Signals to the Cerebellum via Climbing Fiber Pathways Is Gated during Exploratory Behavior. Journal of Neuroscience. 2016;36(30):7841-51.

[351].Kathryn Bennett NC, Marc Goodfellow, Alan Whone, Richard Apps. The effect of harmaline on coherent oscillations across the cerebellar-thalamo-cortical network Poster "Federation of European Neuroscience Societies" ed. Berlin2018.

[352].Murebwayire S. Etudes des propriétés antiplasmodiales, antitrypanosomales et inhibitrices d'acétylcholinestérase de triclisia sacleuxii (Pierre) Diels "Menispermaceae". Bruxelles: Université Libre de Bruxelles; 2008.

[353].Habib A-AM. False-Positive Alkaloid Reactions. Journal of Pharmaceutical Sciences. 1980 1980/01/01/;69(1):37-43.

[354].National Center for Biotechnology Information PubChem. Compound Summary for CID 5281404, Harman. National Center for Biotechnology Information; 2021 [cited 2021 February 22]; Available from: https://pubchem.ncbi.nlm.nih.gov/compound/Harman.

[355].National Center for Biotechnology Information PubChem. Compound Summary for CID 177511. 2021; Available from: https://pubchem.ncbi.nlm.nih.gov/compound/1-benzyl-1_2_3_4-tetrahydroisoquinoline-6_7-diol. .

[356].Kawai H, Kotake Y, Ohta S. Inhibition of dopamine receptors by endogenous amines: binding to striatal receptors and pharmacological effects on locomotor activity. Bioorganic & Medicinal Chemistry Letters. 2000;10(15):1669-71.

[357].Choi WY, Morvan C, Balsam PD, Horvitz JC. Dopamine D1 and D2 antagonist effects on response likelihood and duration. Behav Neurosci. 2009;123(6):1279-87.

[358].Gilbert DL. 96 - Drug-Induced Movement Disorders in Children. In: Swaiman KF, Ashwal S, Ferriero DM, Schor NF, Finkel RS, Gropman AL, et al., editors. Swaiman's Pediatric Neurology (Sixth Edition): Elsevier; 2017. p. 728-33.

[359].National Center for Biotechnology Information PubChem. Compound Summary for CID 487622, 1-Pentyl-1,2,3,4-tetrahydroisoquinoline-6,7-diol, . PubChem; 2021; Available from: https://pubchem.ncbi.nlm.nih.gov/compound/1-Pentyl-1_2_3_4-tetrahydroisoquinoline-6_7-diol. .

[360].National Center for Biotechnology Information PubChem. Compound Summary for CID 4410331, 1-Phenyl-4,9-dihydro-3H-pyrido[3,4-b]indole. 2021; Available from: https://pubchem.ncbi.nlm.nih.gov/compound/1-Phenyl-4_9-dihydro-3H-pyrido_3_4-b_indole. .

[361].Shill HA, Adler CH, Sabbagh MN, Connor DJ, Caviness JN, Hentz JG, et al. Pathologic findings in prospectively ascertained essential tremor subjects. Neurology. 2008;70(16 Pt 2):1452-5.

[362].O'Brien J, Morrissey PA. Nutritional and toxicological aspects of the Maillard browning reaction in foods. Critical Reviews in Food Science and Nutrition 1989;28(3):211-48.

[363].Reddy VP, Obrenovich ME, Atwood CS, Perry G, Smith MA. Involvement of Maillard Reactions in Alzheimer Disease. Neurotoxicity Research. 2002 2002/01/01;4(3):191-209.

[364].Takeuchi M, Bucala R, Suzuki T, Ohkubo T, Yamazaki M, Koike T, et al. Neurotoxicity of advanced glycation end-products for cultured cortical neurons. Journal of Neuropathology & Experimental Neurology. 2000;59(12):1094-105.

[365].Lavita SI, Aro R, Kiss B, Manto M, Duez P. The Role of beta-Carboline Alkaloids in the Pathogenesis of Essential Tremor. Cerebellum. 2016;15(3):276-84.

[366].Aro R., Duez P., Nachtergael A., Manto M. Hampering the neurodegenerative process in essential tremor: present and future directions. In: Atta-ur-Rahman ZA, editor. Frontiers in Clinical Drug Research - CNS and Neurological Disorders: Bentham science; 2020. p. 40-71.

[367].Wood PL. Neurodegeneration and aldehyde load: from concept to therapeutics. J Psychiatry Neurosci. 2006;31(5):296-7.

[368].Resconi VC, Escudero A, Campo MM. The development of aromas in ruminant meat. Molecules. 2013;18(6):6748-81.

[369].Wieczorek MN, Majcher M, Jeleń H. Comparison of Three Extraction Techniques for the Determination of Volatile Flavor Components in Broccoli. Foods. 2020;9(4):398.

[370].Arsad A, Danlami J, Ahmad Zaini MA, Sulaiman H. A comparative study of various oil extraction techniques from plants. Reviews in Chemical Engineering. 2014;30:605-26.

[371].Medeiros M. DNA Damage by Endogenous and Exogenous Aldehydes. Journal of the Brazilian Chemical Society. 2019;30.

[372].O'Donnell JP. The reaction of amines with carbonyls: its significance in the nonenzymatic metabolism of xenobiotics. drug metabolism reviews. 1982;13(1):123-59.

[373].Rao X, Kobayashi R, White-Morris R, Spaulding R, Frazey P, Charles MJ. GC/ITMS measurement of carbonyls and multifunctional carbonyls in PM2.5 particles emitted from motor vehicles. Journal of AOAC INTERNATIONAL. 2001;84(3):699-705.

[374].Tessini C, Müller N, Mardones C, Meier D, Berg A, von Baer D. Chromatographic approaches for determination of low-molecular mass aldehydes in bio-oil. Journal of Chromatography A. 2012 2012/01/06/;1219:154-60.

[375].Mayr CM, Capone DL, Pardon KH, Black CA, Pomeroy D, Francis IL. Quantitative analysis by GC-MS/MS of 18 aroma compounds related to oxidative off-flavor in wines. Journal of Agricultural and Food Chemistry. 2015;63(13):3394-401.

[376].Cancho-Grande B, Ventura F, Galceran M. Determination of aldehydes in drinking water using pentafluorbenzylhydroxylamine derivatization and solid phase microextarction. Journal of chromatography A. 2002;943:1-13.

[377].Richardson SD, Caughran TV, Poiger T, Guo Y, Crumley FG. Application of DNPH Derivatization with LC/MS to the Identification of Polar Carbonyl Disinfection Byproducts in Drinking Water. Ozone: Science & Engineering. 2000 2000/12/01;22(6):653-75.

[378].Bao M, Joza P, Masters A, Rickert W. Analysis of Selected Carbonyl Compounds in Tobacco Samples by Using Pentafluorobenzylhydroxylamine Derivatization and Gas Chromatography-Mass Spectrometry. Beiträge zur Tabakforschung / Contributions to Tobacco Research. 2014;26.

[379].J.W. Munch, D.J. Munch, Winslow SD. EPA Method 556. Determination of Carbonyl Compounds in Drinking Water by Pentafluorobenzylhydroxylamine Derivatization and Capillary Gas Chromatography With Electron Capture Detection. In: National Exposure Research Laboratory (NERL), Office of Research and Development (ORD), U.S. Environmental Protection Agency, editors. June 1998 ed. CINCINNATI, OHIO 452681998.

[380].Li M, Li Q, Nantz MH, Fu X-A. Analysis of Carbonyl Compounds in Ambient Air by a Microreactor Approach. ACS Omega. 2018;3(6):6764-9.

[381].Dabrowska A, Borcz A, Nawrocki J. Aldehyde contamination of mineral water stored in PET bottles. Food additives and contaminants. 2004;20:1170-7.

[382].Herraiz T, Galisteo J, Chamorro C. l -Tryptophan Reacts with Naturally Occurring and Food-Occurring Phenolic Aldehydes To Give Phenolic Tetrahydro-??-carboline Alkaloids: Activity as Antioxidants and Free Radical Scavengers. Journal of Agricultural and Food Chemistry. 2003;51:2168-73.

[383].Rönner B, Lerche H, Bergmüller W, Freilinger C, Severin T, Pischetsrieder M. Formation of Tetrahydro-β-carbolines and β-Carbolines during the Reaction of l -Tryptophan with d -Glucose. Journal of Agricultural and Food Chemistry. 2000;48:2111-6.

[384].González-Arancibia C, Urrutia-Piñones J, Illanes-González J, Martinez-Pinto J, Sotomayor-Zárate R, Julio-Pieper M, et al. Do your gut microbes affect your brain dopamine? Psychopharmacology. 2019;236(5):1611-22.

[385].Raies AB, Bajic VB. In silico toxicology: computational methods for the prediction of chemical toxicity. Wiley Interdiscip Rev Comput Mol Sci. 2016;6(2):147-72.

[386].Hemmerich J, Ecker GF. In silico toxicology: From structure–activity relationships towards deep learning and adverse outcome pathways. WIREs Computational Molecular Science. [https://doi.org/10.1002/wcms.1475]. 2020 2020/07/01;10(4):e1475.

[387].Doniger S, Hofmann T, Yeh J. Predicting CNS permeability of drug molecules: comparison of neural network and support vector machine algorithms. Journal of Computational Biology. 2002;9(6):849-64.

[388].Combes RD. In Silico Methods for Toxicity Prediction. In: Balls M, Combes RD, Bhogal N, editors. New Technologies for Toxicity Testing. New York, NY: Springer US; 2012. p. 96-116.

[389].Nagatsu T. Isoquinoline neurotoxins in the brain and Parkinson's disease. Neurosci Res. 1997;29(2):99-111.

[390].Edmondson R, Broglie JJ, Adcock AF, Yang L. Three-dimensional cell culture systems and their applications in drug discovery and cell-based biosensors. Assay and Drug Development Technologies. 2014;12(4):207-18.

[391].Ravi M, Paramesh V, Kaviya SR, Anuradha E, Solomon FDP. 3D Cell Culture Systems: Advantages and Applications. Journal of Cellular Physiology. 2015;230(1):16-26.

[392].Elliott NT, Yuan F. A Review of Three-Dimensional In Vitro Tissue Models for Drug Discovery and Transport Studies. Journal of Pharmaceutical Sciences. 2011 2011/01/01/;100(1):59-74.

[393].Barisam M, Saidi M, Kashaninejad N, Nguyen N-T. Prediction of Necrotic Core and Hypoxic Zone of Multicellular Spheroids in a Microbioreactor with a U-Shaped Barrier. Micromachines. 2018;9(3):94.

[394].Osaki T, Sivathanu V, Kamm RD. Engineered 3D vascular and neuronal networks in a microfluidic platform. Scientific Reports. 2018 2018/03/26;8(1):5168.

[395].Kriston-Vizi J, Flotow H. Getting the whole picture: High content screening using three-dimensional cellular model systems and whole animal assays. Cytometry Part A. 2017;91(2):152-9.

[396].Leary E, Rhee C, Wilks B, Morgan JR. Accurate quantitative wide-field fluorescence microscopy of 3-D spheroids. Biotechniques. 2016;61(5):237-47.

[397].Boutin ME, Voss TC, Titus SA, Cruz-Gutierrez K, Michael S, Ferrer M. A high-throughput imaging and nuclear segmentation analysis protocol for cleared 3D culture models. Scientific Reports. 2018 2018/07/24;8(1):11135.

[398].Graf BW, Boppart SA. Imaging and analysis of three-dimensional cell culture models. Methods in molecular biology (Clifton, NJ). 2010;591:211-27.

250

[399].Gabriel J, Brennan D, Elisseeff JH, Beachley V. Microarray Embedding/Sectioning for Parallel Analysis of 3D Cell Spheroids. Scientific Reports. 2019 2019/11/08;9(1):16287.

[400].Aricioglu F, Arkan G, Kandemir C, Sirvanci S, Ozkartal C, Utkan T. Harmane suppresses microglial neuroinflammatory response and induce antidepressant-like effect in rats. European Psychiatry. 2017 2017/04/01/;41:S366.

[401].Herraiz T, Chaparro C. Human monoamine oxidase enzyme inhibition by coffee and ??-carbolines norharman and harman isolated from coffee. Life Sciences. 2006;78:795-802.

[402].Khan H, Patel S, Kamal M. Pharmacological and Toxicological Profile of Harmane-β-Carboline Alkaloid: Friend or Foe. Current Drug Metabolism. 2017;18.

[403].Sammi SR, Agim ZS, Cannon JR. From the Cover: Harmane-Induced Selective Dopaminergic Neurotoxicity in Caenorhabditis elegans. Toxicological Sciences. 2018;161(2):335-48.

[404].Kotake Y, Ohta S, Kanazawa I, Sakurai M. Neurotoxicity of an endogenous brain amine, 1-benzyl-1,2,3,4-tetrahydroisoquinoline, in organotypic slice co-culture of mesencephalon and striatum. Neuroscience. 2003;117(1):63-70.

[405].Abe K, Saitoh T, Horiguchi Y, Utsunomiya I, Taguchi K. Synthesis and Neurotoxicity of Tetrahydroisoquinoline Derivatives for Studying Parkinson's Disease. Biological & pharmaceutical bulletin. 2005;28:1355-62.

[406].Shavali S, Ebadi M. 1-Benzyl-1,2,3,4-tetrahydroisoquinoline (1BnTIQ), an endogenous neurotoxin, induces dopaminergic cell death through apoptosis. Neurotoxicology. 2003;24(3):417-24.

[407].Wąsik A, Kajta M, Lenda T, Antkiewicz-Michaluk L. Concentration-Dependent Opposite Effects of 1-Benzyl-1,2,3,4-tetrahydroisoquinoline on Markers of Apoptosis: In Vitro and Ex Vivo Studies. Neurotoxicity Research. 2014 2014/01/01;25(1):90-9.

[408].Goto K, Mochizuki H, Hattori T, Nakamura N, Mizuno Y. Neurotoxic effects of papaverine, tetrahydropapaverine and dimethoxyphenylethylamine on dopaminergic neurons in ventral mesencephalic-striatal co-culture. Brain research. 1997;754(1):260-8.

[409].Surh Y-J, Kim H-J. Neurotoxic Effects of Tetrahydroisoquinolines and Underlying Mechanisms. Experimental neurobiology. 2010;19:63-70.

[410].O'Brien J, Wilson I, Orton T, Pognan F. Investigation of the Alamar Blue (resazurin) fluorescent dye for the assessment of mammalian cell cytotoxicity. European journal of molecular biology and biochemistry. 2000;267(17):5421-6.

[411].Walzl A, Unger C, Kramer N, Unterleuthner D, Scherzer M, Hengstschläger M, et al. The Resazurin Reduction Assay Can Distinguish Cytotoxic from Cytostatic Compounds in Spheroid Screening Assays. Journal of Biomolecular Screening. 2014;19(7):1047-59.

[412].Wolf SA, Boddeke HW, Kettenmann H. Microglia in Physiology and Disease. Annual Review of Physiology 2017;79:619-43.

[413].Dheen ST, Kaur C, Ling EA. Microglial activation and its implications in the brain diseases. Current Medicinal Chemistry. 2007;14(11):1189-97.

[414].Reznikov K, Kolesnikova L, Pramanik A, Tan-No K, Gileva I, Yakovleva T, et al. Clustering of apoptotic cells via bystander killing by peroxides. FASEB journal : official publication of the Federation of American Societies for Experimental Biology. 2000;14:1754-64.

[415].Fink SL, Cookson BT. Apoptosis, pyroptosis, and necrosis: mechanistic description of dead and dying eukaryotic cells. Infect Immun. 2005;73(4):1907-16.

[416].Gülden M, Jess A, Kammann J, Maser E, Seibert H. Cytotoxic potency of H2O2 in cell cultures: impact of cell concentration and exposure time. Free radical biology & medicine. 2010;49(8):1298-305.

[417].Mischel RE, Kim YS, Sheldon RA, Ferriero DM. Hydrogen peroxide is selectively toxic to immature murine neurons in vitro. Neuroscience letters. 1997;231(1):17-20.

[418].Guan Y, Louis ED, Zheng W. Toxicokinetics of tremorogenic natural products, harmane and harmine, in male Sprague-Dawley rats. Journal of toxicology and environmental health Part A. 2001;64(8):645-60.

[419].LeDoux M. CHAPTER E3 - Harmaline Tremor. In: LeDoux M, editor. Animal Models of Movement Disorders. Burlington: Academic Press; 2005. p. 361-8.

[420].Wakabayashi K, Totsuka Y, Fukutome K, Oguri A, Ushiyama H, Sugimura T. Human exposure to mutagenic/carcinogenic heterocyclic amines and comutagenic beta-carbolines. Mutation research. 1997;376(1-2):253-9.

[421].Gross GA, Turesky RJ, Fay LB, Stillwell WG, Skipper PL, Tannenbaum SR. Heterocyclic aromatic amine formation in grilled bacon, beef and fish and in grill scrapings. Carcinogenesis. 1993;14(11):2313-8.

[422].Snook ME, Chortyk OT. Capillary gas chromatography of carbolines: Application to cigarette smoke. Journal of Chromatography A. 1982 1982/08/27/;245(3):331-8.

[423].Collins MA. Acetaldehyde and Its Condensation Products as Markers in Alcoholism. In: Galanter M, Begleiter H, Deitrich R, Goodwin D, Gottheil E, Paredes A, et al., editors. Recent Developments in Alcoholism: Volume 6. Boston, MA: Springer US; 1988. p. 387-403.

[424].Kurnik-Łucka M, Panula P, Bugajski A, Gil K. Salsolinol: an Unintelligible and Double-Faced Molecule—Lessons Learned from In Vivo and In Vitro Experiments. Neurotoxicity Research. 2018;33(2):485-514.

8. Annexes

8.1 Annex 1: Mass spectra of reference aldehydes derivatized with HTMOB
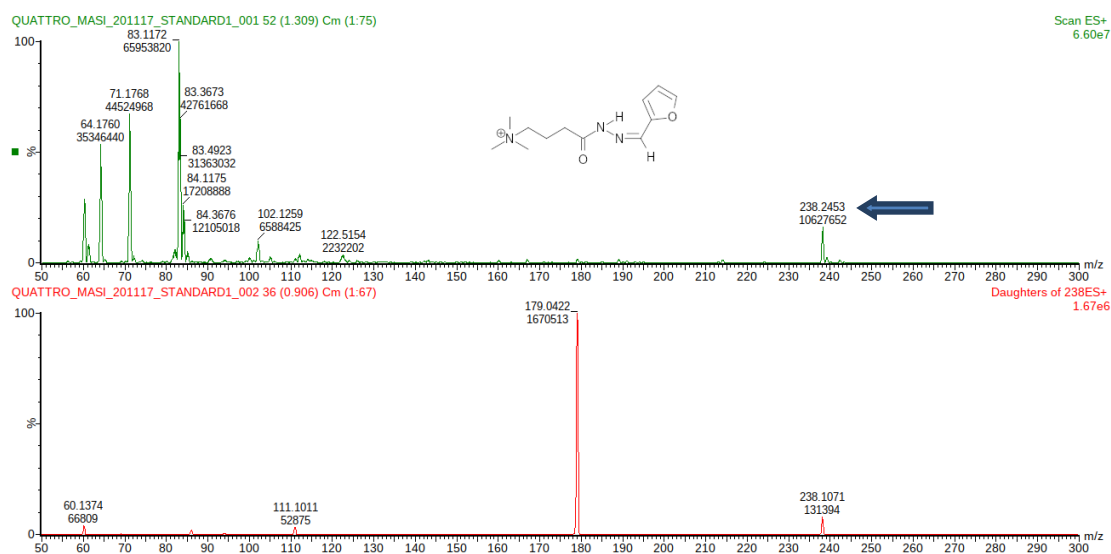
Figure 8.1: Structure and mass spectra (Full scan and daughter of neutral loss 59 (M$^+$) of the HTMOB derivatives of furfuraldehyde. The arrow indicates the parent ions (m/z 238.24 M$^+$)
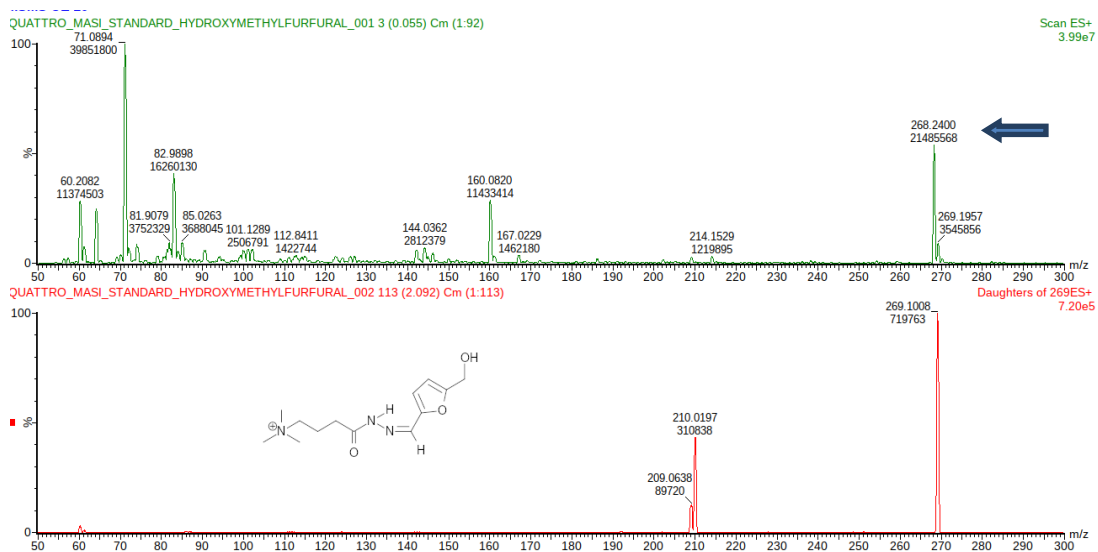
Figure 8.2 : Structure and mass spectra (Full scan and daughter of neutral loss 59 (M$^+$) of the HTMOB derivatives of 5-hydroxymethylfurfural. The arrow indicates the parent ions (m/z 268.24 M$^+$).
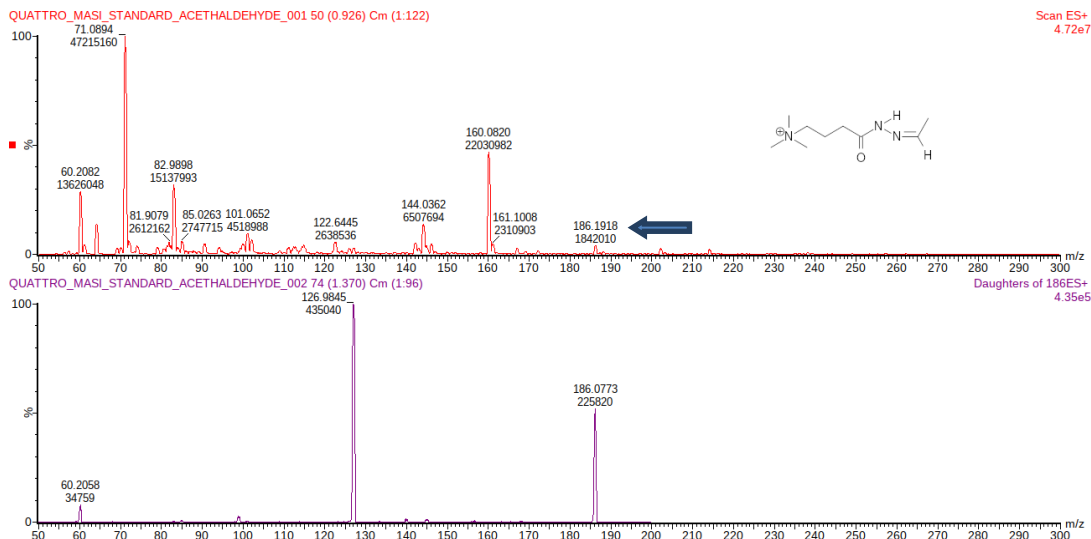
Figure 8.3: Structure and mass spectra (Full scan and daughter of neutral loss 59 (M$^+$)) of the HTMOB derivatives of acetaldehyde. The arrow indicates the parent ions (m/z 186.19 M$^+$).
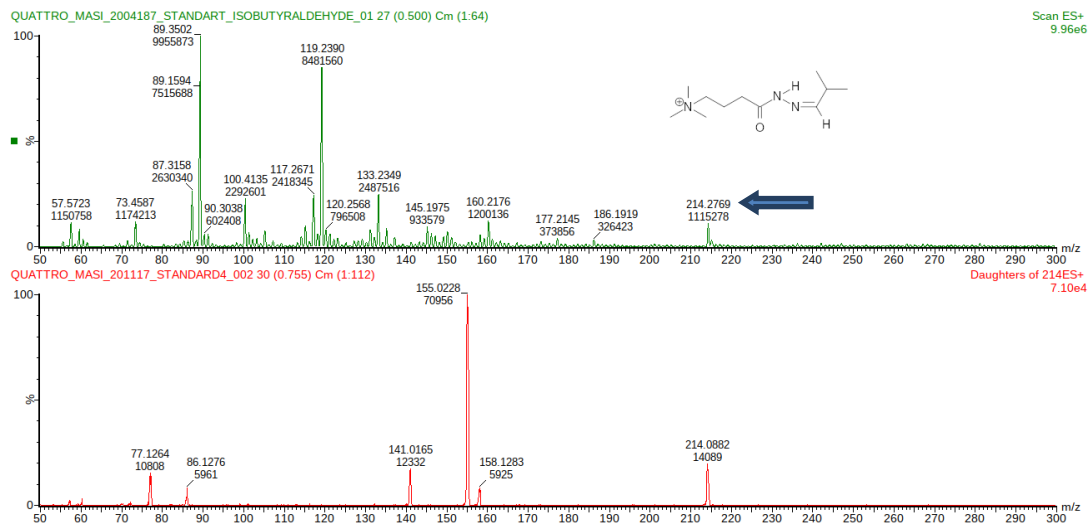
Figure 8.4: Structure and mass spectra (Full scan and daughter of neutral loss 59 M$^+$) of the HTMOB derivatives of isobutyraldehyde. The arrow indicates the parent ions (m/z 214.27 M$^+$).
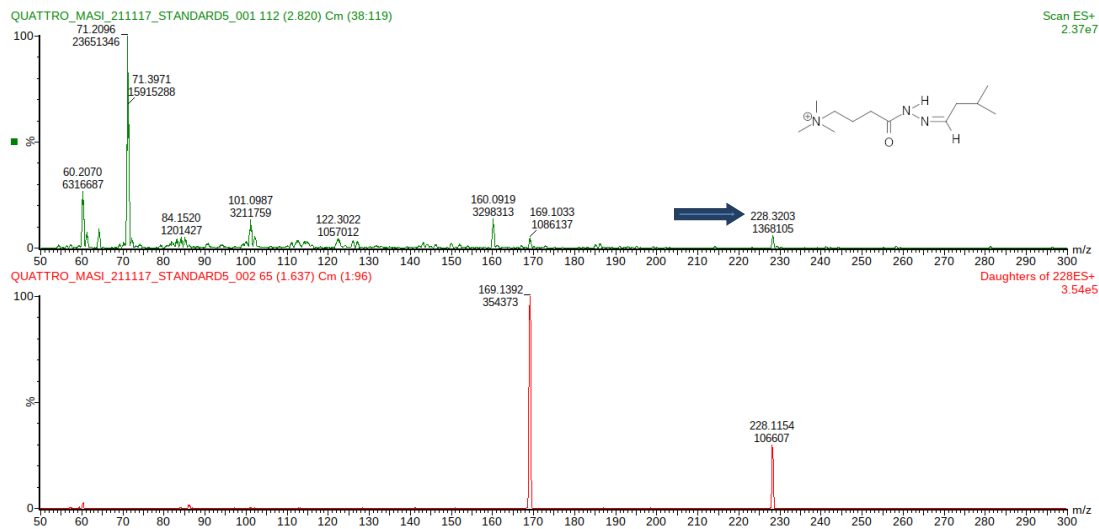
Figure 8.5: Structure and mass spectra (Full scan and daughter of neutral loss 59 M$^+$) of the HTMOB derivatives of isovaleraldehyde. The arrow indicates the parent ions (m/z 228.32 M$^+$)
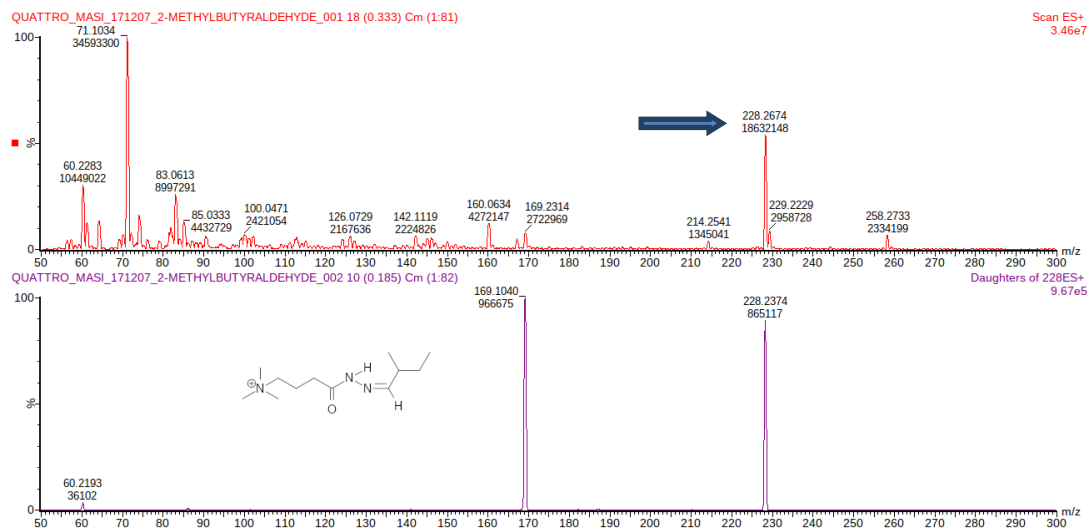
Figure 8.6: Structure and mass spectra (Full scan and daughter of neutral loss 59 M$^+$) of the HTMOB derivatives of 2-methylbutyraldehyde. The arrows indicate the parent ions (m/z 228.26 M$^+$).
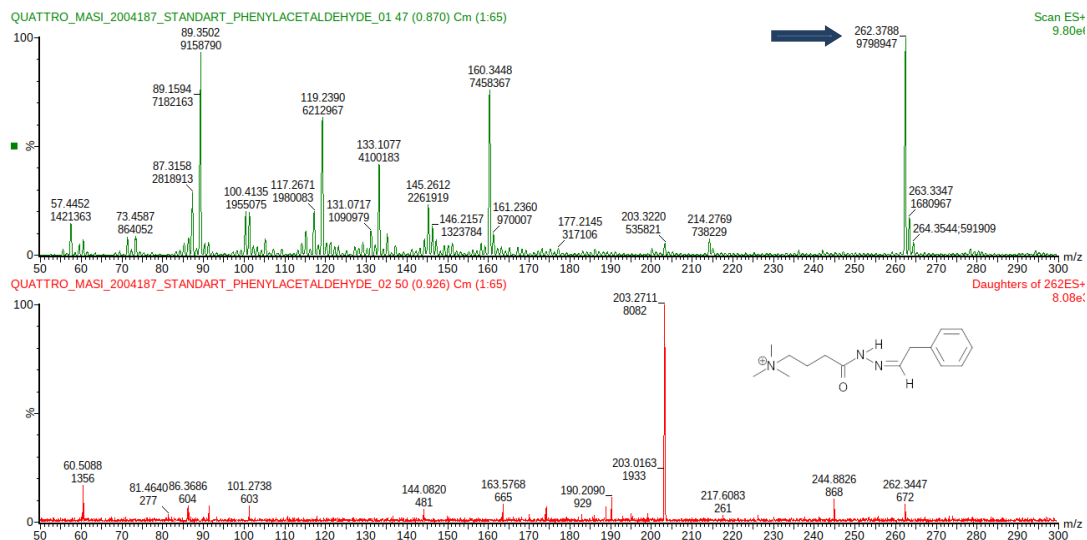
Figure 8.7: Structure and mass spectra (Full scan and daughter of neutral loss 59 M+) of the HTMOB derivatives of phenylacetaldehyde. The arrow indicates the parent ions(m/z 262.37 M$^+$)
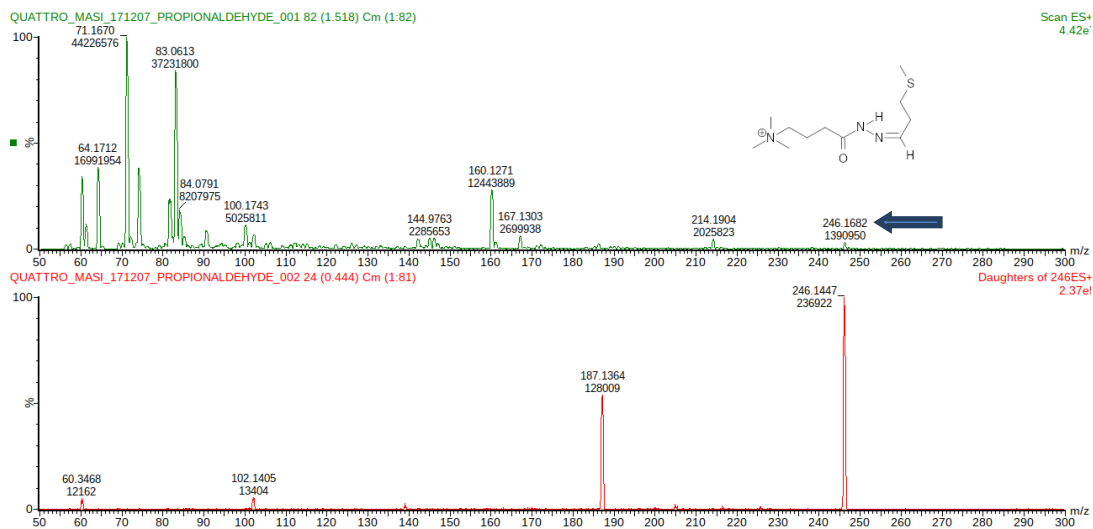
Figure 8.8: Structure and mass spectra (Full scan and daughter of neutral loss 59 M+) of the HTMOB derivatives of 3-methylthiopropionaldehyde. The arrow indicates the parent ions (m/z 247.16 M$^+$)
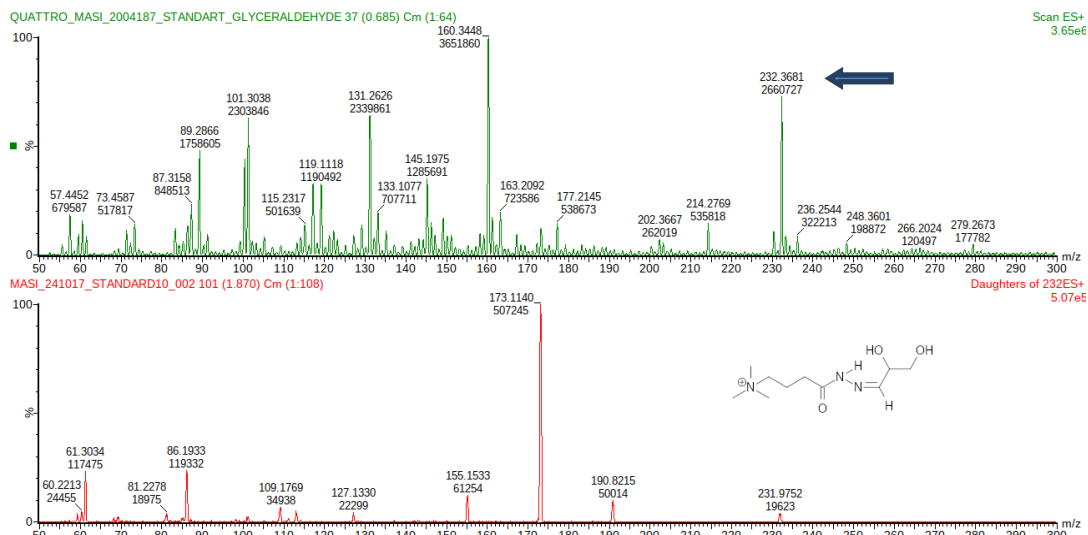
Figure 8.9: Structure and mass spectra (Full scan and daughter of neutral loss 59 M+) of the HTMOB derivatives of glyceraldehyde. The arrows indicate the parent ions (m/z 232.36 M$^+$)
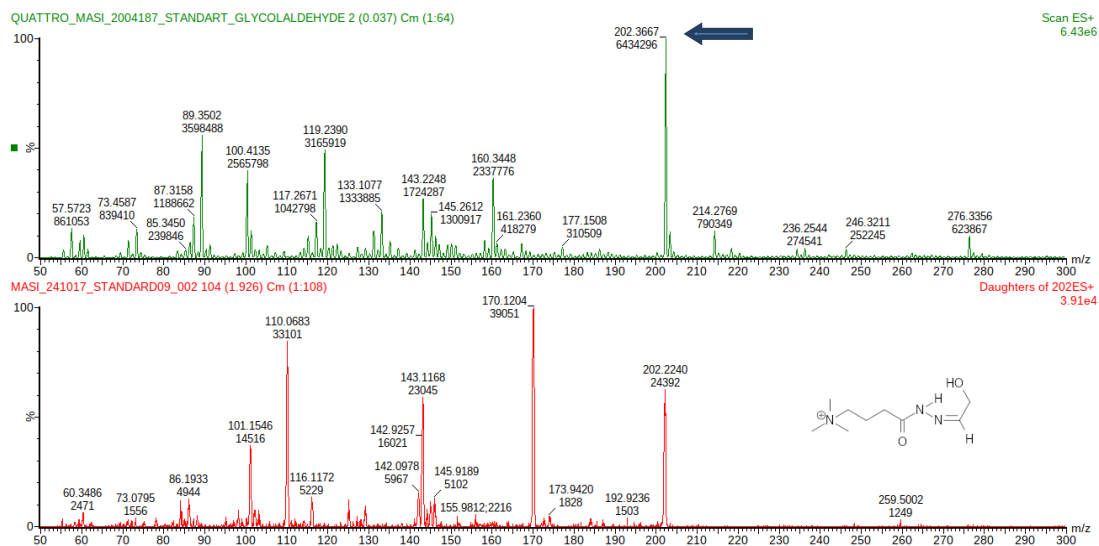
Figure 8.10: Structure and mass spectra (Full scan and daughter of neutral loss 59 M+) of the HTMOB derivatives of glycolaldehyde. The arrows indicate the parent ions (m/z 202.37 M$^+$)
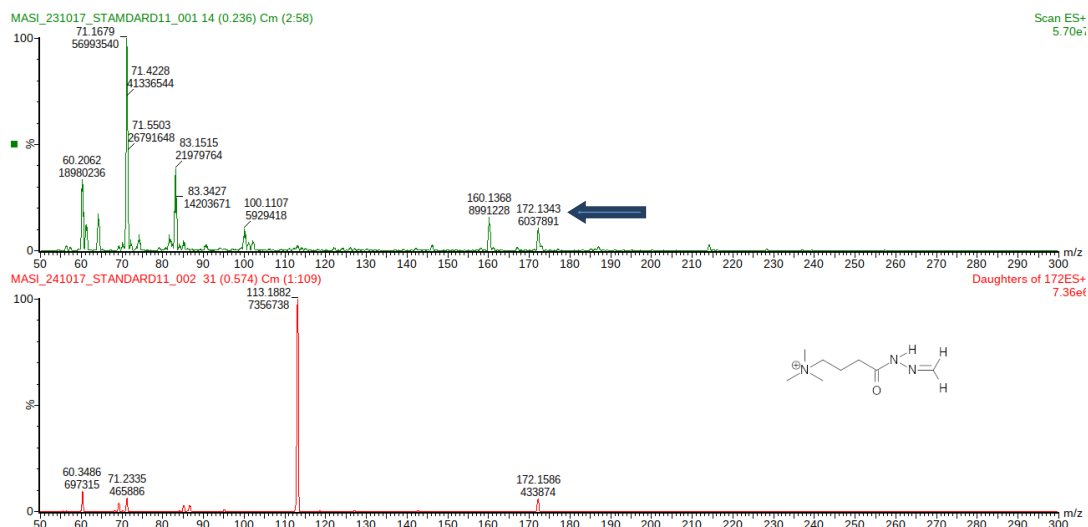
Figure 8.11: Structure and mass spectra (Full scan and daughter of neutral loss 59 M⁺) of the HTMOB derivatives of) formaldehyde. The arrows indicate the parent ions (m/z 172.13 M⁺).
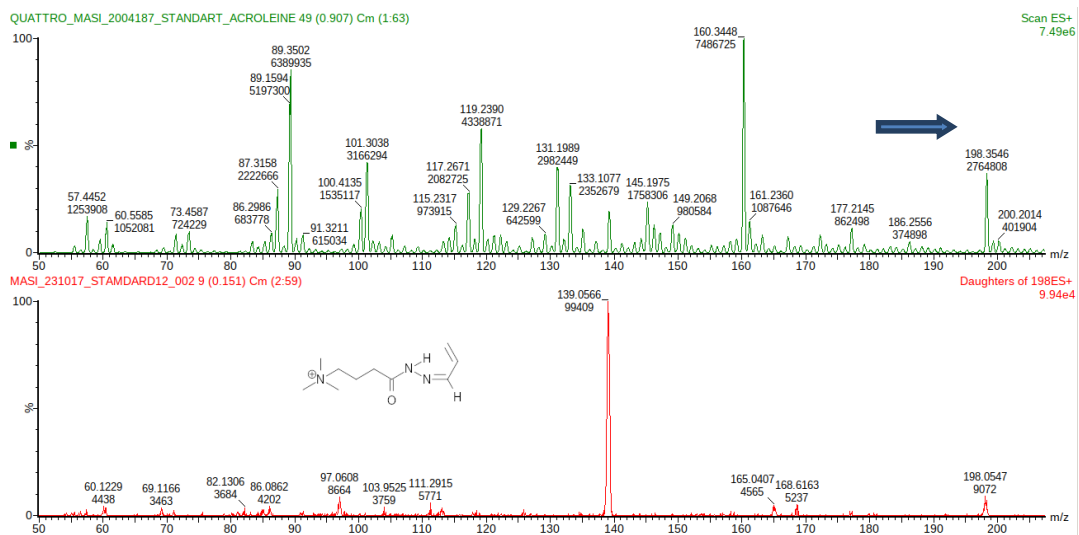
Figure 8.12Structure and mass spectra (Full scan and daughter of neutral loss 59 M+) of the HTMOB derivatives of the derivative of acrolein. The arrows indicate the parent ions (m/z 189.35 M⁺).

8.2 Annex 2: SAFE distillate derivatized with PFBHA followed by GC/MS

8.2.1 Blank procedure of SAFE extraction derivatized with PFBHA followed by Gas Chromatography-Mass Spectrometry
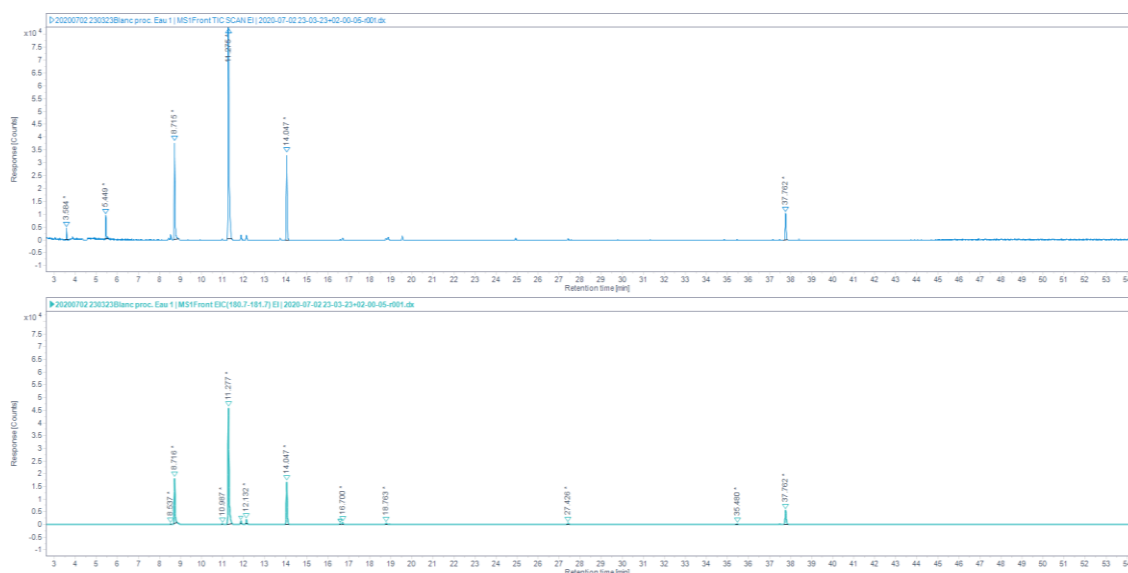
Figure 8.13: Total ion chromatogram (TIC) for deionized water (procedural blank) extracted by SAFE and derivatized with PFBHA (up) and the extracted-ion chromatogram (EIC) 180.7-181.7 EI.

Table 8.1: Identification of carbonyl compounds in deionized water extracted by SAFE and derivatized with PFBHA based on RT, KRI and fragmentation

Retention time T(min)	Analytes	KRI	% Probability (NIST)
5.45	Pentafluorobenzaldehyde		95.3 %
8.72	Formaldehyde oxime	1007.060	41.5 %
11.28	Formaldehyde oxime	1087.833	72.0 %
11.87	Acetaldehyde oxime	1004.974	11.2 %
12.13	not identified	1013.375	
13.73	Cyclopentasiloxane	1062.290	61.5 %
14.05	Acetone oxime	1071.277	70.0 %
16.59	not identified	1046.752	
16.70	not identified	1050.058	
18.76	not identified	1010.325	
27.43	not identified	1091.470	
37.76	Glycoldial, bis-oxime	1088.105	8.5 %

8.2.2 Reference standards extracted by SAFE method and derivatized with PFBHA followed by Gas Chromatography-Mass Spectrometry
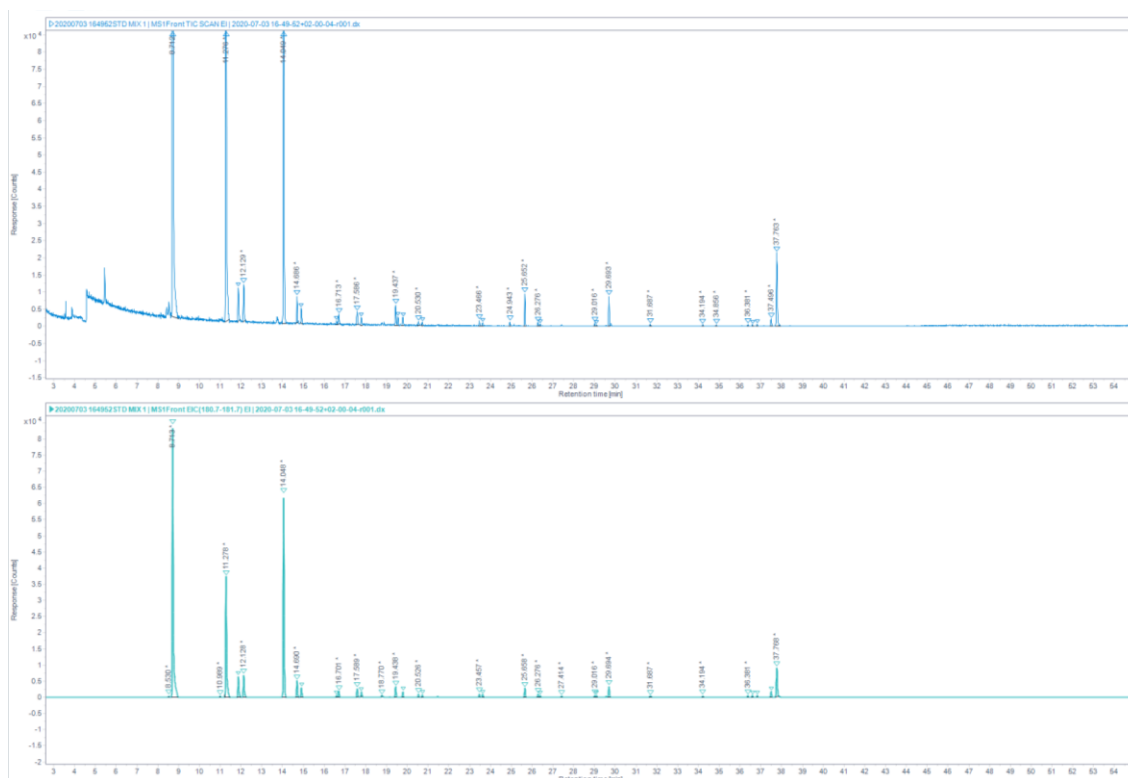
Figure 8.14Total ion chromatogram (TIC) of aldehyde mix standards extracted by the SAFE method and derivatized with PFBHA (up) and the extracted-ion chromatogram (EIC) 180.7-181.7 *m/z* (down).

Table 8.2: Retention data for aldehyde mix standards extracted by the SAFE method and derivatized with PFBHA, identified based on EPA 556 method

Retention time T(min)	Analytes	KRI	% Probability (NIST)
8.530	Succenic acid	1100.278	47.0 %
8.712	PFB hydroxylamine	1106.952	30.8 %
10.989	Hexane	1079.775	50.4 %
11.276	Formaldehyde oxime	1087.861	76.5 %
11.876	Acetaldehyde oxime (E)	1005.173	35.6 %
12.129	Acetaldehyde oxime (Z)	1013.473	36.2 %
14.049	Acetone oxime	1071.334	52.4 %
14.686	Propionaldehyde oxime (E)	1088.793	57.2 %
14.900	Propionaldehyde oxime (Z)	1094.489	58.3 %
16.592	Methyl ethyl ketone oxime (E)	1046.812	57.2 %
16.713	Methyl ethyl ketone oxime (Z)	1050.448	57.2 %
17.586	Butyraldehyde oxime (E)	1075.922	48.3 %
17.791	Butyraldehyde oxime (Z)	1081.721	12.8 %

Retention time T(min)	Analytes	KRI	% Probability (NIST)
19.437	Crotonaldehyde oxime (E)	1032.198	71.4 %
19.793	Crotonaldehyde oxime (Z)	1043.447	48.6 %
20.530	Valeraldehyde oxime (E)	1066.106	/
20.730	Valeraldehyde oxime (Z)	1072.114	/
23.457	Hexanal oxime (E)	1059.283	64.6 %
23.629	Hexanal oxime (Z)	1064.794	1.4 %
25.658	Cyclohexanone oxime	1031.913	21.4 %
26.276	Heptanal oxime (E)	1053.185	0.8 %
26.373	Heptanal oxime (Z)	1056.479	/
29.016	Octanal oxime (E)	1048.895	< 0.01 %
29.097	Octanal oxime (Z)	1051.807	< 0.01 %
29.694	Benzaldehyde oxime	1073.02	67.0 %
31.687	Nonanal oxime	1047.026	< 0.01 %
34.194	Decanal oxime	1043.668	/
36.381	Glyoxal oxime (E)	1031.432	/
36.591	Glyoxal oxime (Z)	1040.2	/
36.623	Methyl glyoxal oxime (E)	1041.532	/
37.496	Methylglyoxal bis-oxime	1077.418	0.4 %
37.763	Methyl glyoxal oxime (2)	1088.226	3.8 %

8.3 Annex 3: HS-SDME with PFBHA droplet derivatization followed by GC/MS

8.3.1 Distilled water extracted by HS-SDME followed by Gas Chromatography-Mass Spectrometry
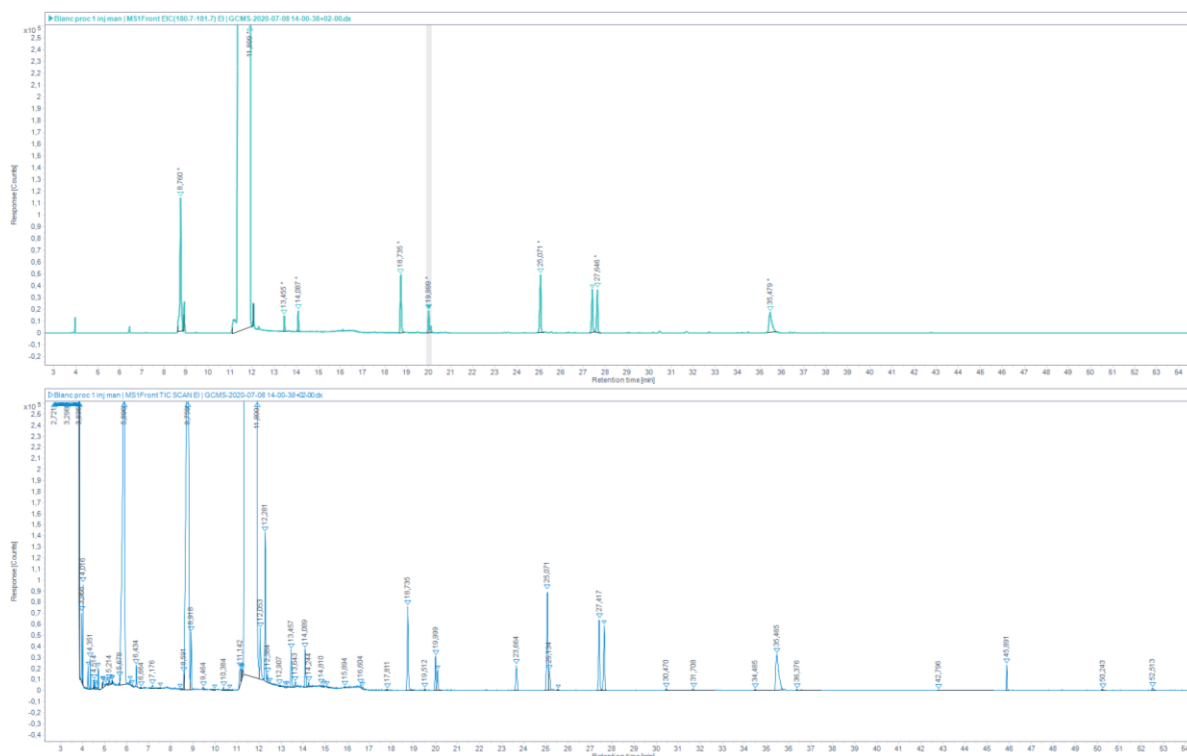
Figure 8.15: Total ion chromatogram (TIC) for procedural blank extracted by HS-SDME on PFBHA droplet (up) and the extracted-ion chromatogram (EIC) 180.7-181.7 EI (down).

Table 8.3: Identification of carbonyl compounds in deionized water extracted by HS-SDME on PFBHA droplet, based on RT, KRI and fragmentation

Retention time T(min)	Analytes	KRI	%Probability (NIST)
12.275	/	1018.180	
13.455	o-(Pfb) hydroxylamine	1054.320	29.60 %
14.09	Acetone oxime	1072.480	73.00 %
16.61	Carbonic acid, allyl PFB ester	1047.350	40.40 %
18.74	Dihydroxypropanone oxime	1009.570	23.50 %
20.00	Pentafluorobenzyl ester	1049.830	19.70 %
20.94	Dihydroxypropanone oxime	1078.360	24.70 %
25.08	PFB aldehyde PFB oxime	1011.410	54.10 %
27.00	PFB aldehyde PFB oxime	1077.480	68.70 %
27.65	Dihydroxypropanone oxime	1098.740	31.50 %
35.48	Dihydroxypropanone oxime	1093.910	18.00 %

8.3.2 Reference standards extracted by HS-SDME followed by Gas Chromatography-Mass Spectrometry
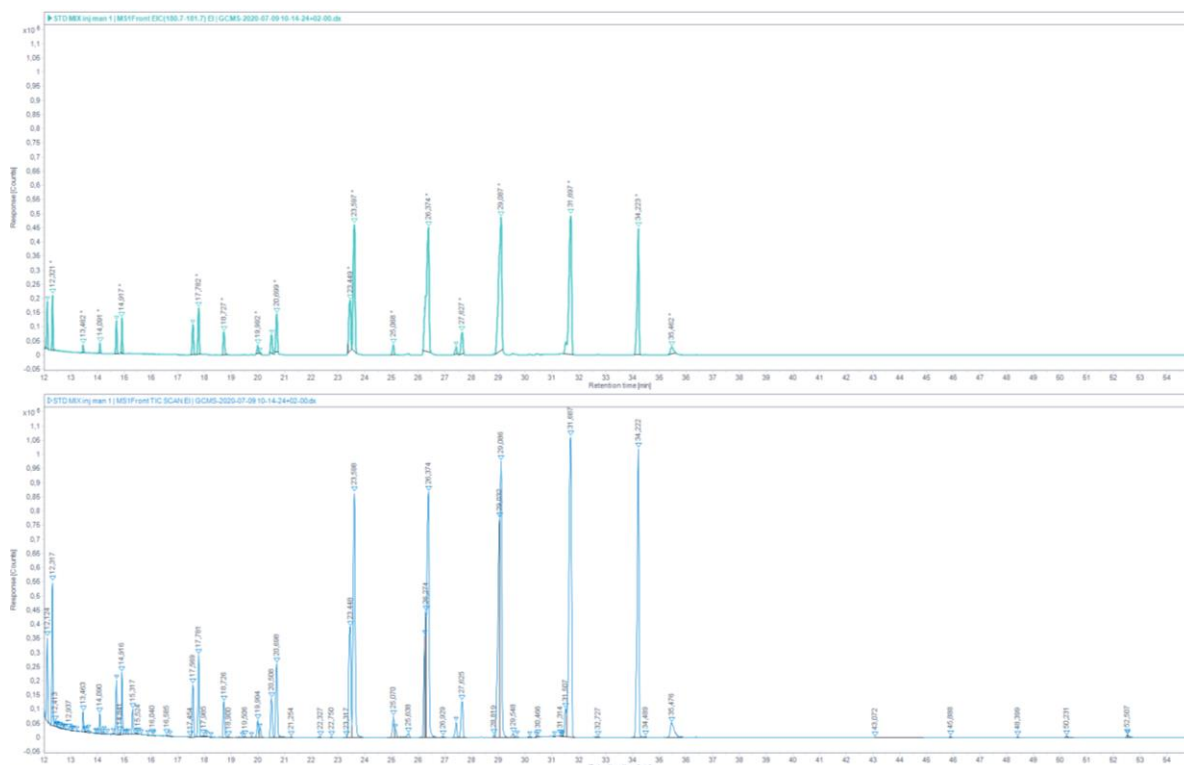
Figure 8.16: Total ion chromatogram (TIC) for the "Aldehydes mixtures-556" extracted by HS-SDME on PFBHA droplet (up) and the extracted-ion chromatogram (EIC) 180.7-181.7 EI (down).

Table 8.4: Retention data for aldehyde mix standards extracted by HS-SDME on PFBHA droplet (HS-SDME), identified based on EPA 556 method

Retention time T(min)	Analytes	KRI	%Probability (NIST)
12.120	Acetaldehyde (E)	1013.180	48.20 %
12.320	Acetaldehyde (Z)	1019.625	31.20 %
13.462	PFB hydroxylamine	1054.529	35.50 %
14.049	Acetone oxime	1071.334	69.90 %
14.710	Propionaldehyde oxime (E)	1089.436	60.80 %
14.900	Propionaldehyde oxime (Z)	1094.489	72.40 %
17.569	Butyraldehyde oxime (E)	1075.439	52.40 %
17.720	Butyraldehyde oxime (Z)	1079.720	58.90 %
18.770	Not identified	1010.557	
19.760	Crotonaldehyde oxime (E)	1042.413	48.00 %
19.998	Crotonaldehyde oxime (Z)	1049.834	0.40 %
20.530	Pentanal oxime (E)	1066.106	30.50 %
20.699	Pentanal oxime (Z)	1071.187	64.30 %
Retention time T(min)	Analytes	KRI	% Probability (NIST)

264

23.457	Hexanal oxime (E)	1059.283	37.60 %
23.629	Hexanal oxime (Z)	1064.794	36.90 %
25.070	Cyclohexanone oxime	1011.193	/
25.658	Cyclohexanone oxime	1031.913	70.80 %
26.276	Heptanal oxime (E)	1053.185	40.90 %
26.373	Heptanal oxime (Z)	1056.479	29.20 %
29.016	Octanal oxime (E)	1048.895	6.50 %
29.097	Octanal oxime (Z)	1051.807	1.77 %
29.547	Benzaldehyde oxime	1067.837	91.70 %
31.507	Nonanal oxime (E)	1040.180	20.70 %
31.687	Nonanal oxime (Z)	1047.026	22.60 %
34.194	Decanal oxime	1043.668	48.70 %
35.462	Methylglyoxal bis-oxime	1093.257	0.47 %

8.4 Annex 4: Tables of complete results of eMolTox prediction

		Harmane			1-Benz THIQ diol			1-Isobutyl - DHβCa		
		Cc2nccc3c1ccccc1[nH]c23			Oc3cc2CCNC(Cc1ccccc1)c2cc3O			CCC(C)/C1=N/CCc2c1[nH]c3ccccc23		
Action	Injury	Outcome	Confidence	Similar_Positive_Mol	Outcome	Confidence	Similar_Positive_Mol	Outcome	Confidence	Similar_Positive_Mol
Antagonist of the androgen receptor (AR) signaling pathway	Endocrine, Central nervous system	Inconclusive	0	-	Inconclusive	0	-	Inconclusive	0	-
Modulator of Dopamine D1 receptor	Central nervous system, Kidney, Heart	Negative	0.986	-	Positive	1	Oc1cc2c(cc1O)C1c3ccccc3CCC1NCC2	Inconclusive	0	-
Modulator of Glutamate receptor ionotropic, AMPA	Central nervous system	Negative	0.985	-	Negative	0.988	-	Negative	0.982	-
Modulator of Calcitonin gene-related peptide type 1 receptor	Heart, Nervous system, Gastrointestinal, blood	Negative	0.996	-	Negative	0.992	-	Negative	0.993	-
Modulator of Cannabinoid CB1 receptor	Nervous system, Heart	Negative	1	-	Negative	0.999	-	Negative	0.999	-
Modulator of Histamine H1 receptor	Immune, Nervous system, Heart, Gastrointestinal	Negative	0.994	-	Negative	0.999	-	Negative	0.989	-
Modulator of Glucocorticoid receptor	Endocrine, immune, Nervous system	Negative	0.998	-	Negative	0.998	-	Negative	0.998	-
Modulator of GABA-A receptor; alpha-1/beta-3/gamma-2	Central nervous system	Inconclusive	0	-	Negative	0.994	-	Inconclusive	0	-
Modulator of Adenosine A2a receptor	Heart, blood, Central nervous system	Negative	0.998	-	Negative	0.999	-	Negative	0.999	-
Modulator of Serotonin 7 (5-HT7) receptor	Nervous system, immune	Negative	0.993	-	Negative	0.994	-	Negative	0.983	-
Modulator of Neuronal acetylcholine receptor protein alpha-7 subunit	Central nervous system	Inconclusive	0	-	Inconclusive	0	-	Inconclusive	0	-
Modulator of Neuronal acetylcholine receptor; alpha3/beta4	Central nervous system	Negative	0.987	-	Negative	0.996	-	Inconclusive	0	-
Modulator of Dopamine D2 receptor	Central nervous system, Gastrointestinal, Heart, Kidney	Negative	1	-	Negative	0.993	-	Negative	0.996	-
Modulator of Alpha-2a adrenergic receptor	Heart, Nervous system, Gastrointestinal, pancreas	Inconclusive	0	-	Inconclusive	0	-	Positive	0.998	CCc1ccccc1OC(C)C1=NCCN1
Modulator of Serotonin 2b (5-HT2b) receptor	Heart, Nervous system, Gastrointestinal	Inconclusive	0	-	Inconclusive	0	-	Positive	0.996	CC(CN)c1c[nH]c2ccccc12
Modulator of Glutamate NMDA receptor	Central nervous system	Negative	0.983	-	Negative	0.986	-	Inconclusive	0	-
Modulator of Muscarinic acetylcholine receptor M5	Nervous system	Negative	0.994	-	Negative	0.989	-	Inconclusive	0	-
Modulator of Androgen Receptor	Endocrine, Central nervous system	Negative	0.998	-	Negative	0.998	-	Negative	1	-
Modulator of Mu opioid receptor	Nervous system, respiratory, Gastrointestinal, Heart, pancreas, Kidney	Negative	0.999	-	Negative	1	-	Negative	0.998	-
Antagonist of the glucocorticoid receptor (GR) signaling pathway	Endocrine, immune, Nervous system	Inconclusive	0	-	Inconclusive	0	-	Inconclusive	0	-
Modulator of Serotonin 3a (5-HT3a) receptor	Gastrointestinal, Heart, Central nervous system	Inconclusive	0	-	Negative	0.989	-	Inconclusive	0	-

		Harmane			1-Benz THIQ diol (Pheylacetaldehyde+dopamine)			1-Isobutyl - DHβCa (methylbutyraldehyde + tryptamine)		
		Cc2nccc3c1ccccc1[nH]c23			Oc3cc2CCNC(Cc1ccccc1)c2cc3O			CCC(C)/C1=N/CCc2c1[nH]c3ccccc23		
Action	Injury	Outcome	Confidence	Similar_Positive_Mol	Outcome	Confidence	Similar_Positive_Mol	Outcome	Confidence	Similar_Positive_Mol
Agonist of the androgen receptor (AR) signaling pathway	Endocrine, Central nervous system	Inconclusive	0	-	Inconclusive	0	-	Negative	0.992	-
Modulator of Endothelin receptor ET-A	Heart, Kidney, Nervous system, Gastrointestinal	Negative	0.997	-	Negative	0.997	-	Negative	1	-
Modulator of Neuropeptide Y receptor type 1	Gastrointestinal, immune, Nervous system	Negative	0.999	-	Negative	0.988	-	Negative	0.995	-
Modulator of Serotonin 2c (5-HT2c) receptor	Nervous system	Negative	0.986	-	Negative	0.992	-	Positive	0.98	COc1ccc2[nH]c3c(c2c1)CCN=C3C
Modulator of Dopamine transporter	Nervous system	Negative	0.998	-	Negative	0.984	-	Inconclusive	0	-
Modulator of Alpha-1b adrenergic receptor	Heart, Nervous system, Kidney	Negative	0.998	-	Negative	0.998	-	Negative	0.993	-
Modulator of Melatonin receptor 1B	Central nervous system	Negative	0.995	-	Negative	0.998	-	Negative	0.997	-
Modulator of Neuronal acetylcholine receptor protein alpha-4 subunit	Central nervous system	Inconclusive	0	-	Inconclusive	0	-	Negative	0.995	-
Modulator of Adenosine A2b receptor	Immune, Peripheral nervous system	Negative	0.998	-	Negative	0.997	-	Negative	0.998	-
Modulator of GABA-A receptor; anion channel	Central nervous system	Negative	0.99	-	Inconclusive	0	-	Negative	0.993	-
Activator Alzheimer's amyloid precursor	Central nervous system	Inconclusive	0	-	Inconclusive	0	-	Inconclusive	0	-
Modulator of GABA-A receptor; alpha-5/beta-3/gamma-2	Central nervous system	Negative	0.987	-	Negative	0.994	-	Negative	0.995	-
Modulator of Kappa opioid receptor	Nervous system, Heart, Gastrointestinal	Negative	0.999	-	Negative	0.999	-	Negative	1	-
Modulator of Serotonin 4 (5-HT4) receptor	Gastrointestinal, Heart, Central nervous system	Negative	0.992	-	Negative	0.999	-	Negative	0.991	-
Modulator of Alpha-2b adrenergic receptor	Heart, Nervous system	Inconclusive	0	-	Inconclusive	0	-	Positive	0.996	CCc1ccccc1OC(C)C1=NCCN1
Modulator of GABA-A receptor; alpha-2/beta-3/gamma-2	Central nervous system	Negative	0.984	-	Negative	0.993	-	Negative	0.998	-
Modulator of GABA-A receptor; alpha-3/beta-3/gamma-2	Central nervous system	Negative	1	-	Negative	0.996	-	Inconclusive	0	-
Modulator of Muscarinic acetylcholine receptor M4	Nervous system, Heart	Negative	0.994	-	Negative	0.991	-	Negative	0.987	-
Modulator of Cholecystokinin A receptor	Gastrointestinal, gallbladder, Nervous system	Negative	0.984	-	Negative	0.985	-	Negative	0.984	-
Modulator of Serotonin 1b (5-HT1b) receptor	Nervous system, Heart	Negative	0.981	-	Negative	0.997	-	Inconclusive	0	-
Modulator of Neuronal acetylcholine receptor, alpha4/beta2	Central nervous system	Negative	0.994	-	Negative	0.997	-	Negative	0.987	-

Action	Injury	Harmane			1-Benz THIQ diol			1-Isobutyl - DHβCa		
		Outcome	Confidence	Similar_Positive_Mol	Outcome	Confidence	Similar_Positive_Mol	Outcome	Confidence	Similar_Positive_Mol
Modulator of Muscarinic acetylcholine receptor M2	Heart, respiratory, Nervous system	Negative	0.999	-	Negative	0.998	-	Negative	0.999	-
Modulator of Bradykinin B2 receptor	Heart, respiratory, Kidney, Central nervous system	Negative	0.991	-	Negative	0.988	-	Negative	0.993	-
Modulator of Sigma opioid receptor	Nervous system	Negative	0.997	-	Inconclusive	0	-	Negative	0.995	-
Modulator of Adenosine A3 receptor	Nervous system, respiratory	Negative	0.996	-	Negative	0.996	-	Negative	0.995	-
Modulator of Muscarinic acetylcholine receptor M3	Gastrointestinal, Nervous system, respiratory, Heart, liver	Negative	0.998	-	Negative	0.998	-	Negative	0.997	-
Modulator of Serotonin 1a (5-HT1a) receptor	Nervous system, Heart, endocrine	Negative	0.998	-	Negative	0.999	-	Negative	0.99	-
Modulator of Cannabinoid CB2 receptor	Immune, Nervous system	Negative	0.999	-	Negative	0.999	-	Negative	0.999	-
Modulator of Neurokinin 1 receptor	Nervous system, immune, Gastrointestinal, gonad	Negative	0.999	-	Negative	1	-	Negative	0.998	-
Modulator of Delta opioid receptor	Central nervous system	Negative	0.999	-	Negative	0.999	-	Negative	0.999	-
Modulator of Serotonin 2a (5-HT2a) receptor	Nervous system, blood, Heart	Inconclusive	0	-	Negative	0.996	-	Inconclusive	0	-
Modulator of Norepinephrine transporter	Heart, Nervous system	Negative	0.998	-	Negative	0.986	-	Inconclusive	0	-
Modulator of Muscarinic acetylcholine receptor M1	Nervous system, respiratory, Gastrointestinal, Heart, liver	Negative	0.996	-	Negative	0.999	-	Negative	0.997	-
Modulator of Monoamine oxidase A	Pharmaco-kinetics, Central nervous system	Inconclusive	0	-	Inconclusive	0	-	Inconclusive	0	-
Antagonist of the androgen receptor (AR) signaling pathway	Endocrine, Central nervous system	Inconclusive	0	-	Inconclusive	0	-	Inconclusive	0	-
Modulator of P2X purinoceptor 7	Nervous system, immune, Kidney	Negative	0.997	-	Negative	0.999	-	Negative	0.998	-
Modulator of Vasopressin V1a receptor	Heart, Kidney, Central nervous system	Negative	0.998	-	Negative	0.992	-	Negative	0.999	-
Modulator of P2X purinoceptor 3	Nervous system, immune, Kidney	Negative	0.999	-	Negative	0.998	-	Negative	1	-
Modulator of Acetylcholinesterase	Central nervous system	Negative	0.99	-	Negative	0.998	-	Negative	0.996	-
Modulator of Adenosine A1 receptor	Nervous system, Kidney, Heart	Negative	0.992	-	Negative	1	-	Negative	0.999	-
Modulator of Serotonin transporter	Central nervous system, blood, Heart, Gastrointestinal	Negative	0.997	-	Negative	0.996	-	Inconclusive	0	-
Modulator of GABA-A receptor; anion channel	Central nervous system	Negative	0.981	-	Negative	0.994	-	Inconclusive	0	-
Agonist of the glucocorticoid receptor (GR) signaling pathway	Endocrine, immune, Nervous system	Inconclusive	0	-	Inconclusive	0	-	Inconclusive	0	-

		Dopamine + hexanal			Serotonin + hexanal			Tryptamine + hexanal			Benzaldehyde + tryptamine		
		1-Pentyl-THIQ			1-Pentyl-THβCa-ol			1-Pentyl-DHβCa			1-Phenyl-DHβCa		
		CCCCCC2NCCc1cc(O)c(O)cc12			CCCCCC1NCCc2c1[nH]c3ccc(O)cc23			CCCCC/C1=N/CCc2c1[nH]c3cccc23			c4ccc(/C1=N/CCc2c1[nH]c3ccccc23)cc4		
Action	Injury	Outcome	Confidence	Similar_Positive_Mol	Outcome	Confidence	Similar_Positive_Mol	Outcome	Confidence	Similar_Positive_Mol	Outcome	Confidence	Similar_Positive_Mol
Antagonist of the androgen receptor (AR) signaling pathway	Endocrine, Central nervous system	Inconclu.	0	-	Inconclu.	0	-	Inconclu.	0	-	Inconclusive	0	-
Modulator of Dopamine D1 receptor	Central nervous system, Kidney, Heart	Positive	0.998	Oc1cc2c(cc1O)C1c3ccccc3CCC1NCC2	Positive	0.995	c2Cc2[nH]c3ccc(O)cc3c2CC1	Inconclu.	0	-	Inconclusive	0	-
Modulator of Glutamate receptor ionotropic, AMPA	Central nervous system	Negative	0.981	-	Negative	0.998	-	Negative	0.983	-	Negative	0.993	-
Modulator of Calcitonin gene-related peptide type 1 receptor	Heart, Nervous system, Gastrointestinal, blood	Negative	0.993	-	Negative	0.994	-	Negative	0.997	-	Negative	0.999	-
Modulator of Cannabinoid CB1 receptor	Nervous system, Heart	Negative	0.999	-	Negative	0.999	-	Negative	0.999	-	Negative	0.999	-
Modulator of Histamine H1 receptor	Immune, Nervous system, Heart, Gastrointestinal	Negative	0.996	-	Negative	0.999	-	Inconclu.	0	-	Inconclusive	0	-
Modulator of Glucocorticoid receptor	Endocrine, immune, Nervous system	Negative	0.999	-	Negative	0.996	-	Negative	0.998	-	Negative	0.998	-
Modulator of GABA-A receptor; alpha-1/beta-3/gamma-2	Central nervous system	Negative	0.996	-	Inconclu.	0	-	Inconclu.	0	-	Inconclusive	0	-
Modulator of Adenosine A2a receptor	Heart, blood, Central nervous system	Negative	0.999	-	Negative	0.998	-	Negative	0.999	-	Negative	0.997	-
Modulator of Serotonin 7 (5-HT7) receptor	Nervous system, immune	Negative	0.997	-	Inconclu.	0	-	Inconclu.	0	-	Inconclusive	0	-
Modulator of Neuronal acetylcholine receptor protein alpha-7 subunit	Central nervous system	Inconclu.	0	-	Inconclu.	0	-	Inconclu.	0	-	Inconclusive	0	-
Modulator of Neuronal acetylcholine receptor; alpha3/beta4	Central nervous system	Inconclu.	0	-	Negative	0.983	-	Inconclu.	0	-	Negative	0.987	-
Modulator of Dopamine D2 receptor	Central nervous system, Gastrointestinal, Heart, Kidney	Negative	0.994	-	Negative	0.989	-	Negative	0.993	-	Negative	0.996	-
Modulator of Alpha-2a adrenergic receptor	Heart, Nervous system, Gastrointestinal, pancreas	Inconclu.	0	-	Inconclu.	0	-	Positive	0.988	c1ccc2c(NC3=NCCN3)n[nH]c2c1	Inconclusive	0	-
Modulator of Serotonin 2b (5-HT2b) receptor	Heart, Nervous system, Gastrointestinal	Inconclu.	0	-	Inconclu.	0	-	Inconclu.	0	-	Inconclusive	0	-
Modulator of Glutamate NMDA receptor	Central nervous system	Inconclu.	0	-	Inconclu.	0	-	Negative	0.984	-	Inconclusive	0	-
Modulator of Muscarinic acetylcholine receptor M5	Nervous system	Negative	0.986	-	Inconclu.	0	-	Inconclu.	0	-	Inconclusive	0	-
Modulator of Androgen Receptor	Endocrine, Central nervous system	Negative	0.996	-	Negative	0.991	-	Negative	0.986	-	Negative	0.992	-

269

Action	Injury	1-Pentyl-THIQ			1-Pentyl-THβCa-ol			1-Pentyl-DHβCa			1-Phenyl-DHβCa		
		Outcome	Confidence	Similar_Positive_Mol	Outcome	Confidence	Similar_Positive_Mol	Outcome	Confidence	Similar_Positive_Mol	Outcome	Confidence	Similar_Positive_Mol
Modulator of Mu opioid receptor	Nervous system, respiratory, Gastrointestinal, Heart, pancreas, Kidney	Negative	1	-	Inconclu.	0	-	Negative	0.999	-	Negative	1	-
Antagonist of the glucocorticoid receptor (GR) signaling pathway	Endocrine, immune, Nervous system	Inconclu.	0	-	Inconclu.	0	-	Inconclu.	0	-	Inconclusive	0	-
Modulator of Serotonin 3a (5-HT3a) receptor	Gastrointestinal, Heart, Central nervous system	Negative	0.988	-	Inconclu.	0	-	Inconclu.	0	-	Inconclusive	0	-
Agonist of the androgen receptor (AR) signaling pathway	Endocrine, Central nervous system	Inconclu.	0	-	Inconclu.	0	-	Negative	0.998	-	Inconclusive	0	-
Modulator of Endothelin receptor ET-A	Heart, Kidney, Nervous system, Gastrointestinal	Negative	0.996	-	Negative	0.998	-	Negative	0.999	-	Negative	0.998	-
Modulator of Neuropeptide Y receptor type 1	Gastrointestinal, immune, Nervous system	Negative	0.991	-	Negative	0.991	-	Negative	0.994	-	Negative	0.991	-
Modulator of Serotonin 2c (5-HT2c) receptor	Nervous system	Negative	0.993	-	Inconclu.	0	-	Inconclu.	0	-	Inconclusive	0	-
Modulator of Dopamine transporter	Nervous system	Negative	0.983	-	Inconclu.	0	-	Inconclu.	0	-	Inconclusive	0	-
Modulator of Alpha-1b adrenergic receptor	Heart, Nervous system, Kidney	Negative	0.999	-	Negative	0.996	-	Negative	0.987	-	Negative	0.991	-
Modulator of Melatonin receptor 1B	Central nervous system	Negative	0.994	-	Negative	0.995	-	Negative	0.998	-	Negative	0.997	-
Modulator of Neuronal acetylcholine receptor protein alpha-4 subunit	Central nervous system	Inconclu.	0	-	Inconclu.	0	-	Negative	0.991	-	Inconclusive	0	-
Modulator of Adenosine A2b receptor	Immune, Peripheral nervous system	Negative	0.998	-	Negative	0.999	-	Negative	0.998	-	Negative	0.999	-
Modulator of GABA-A receptor; anion channel	Central nervous system	Inconclu.	0	-	Negative	0.996	-	Negative	0.984	-	Inconclusive	0	-
Activator Alzheimer's amyloid precursor	Central nervous system	Inconclu.	0	-	Inconclu.	0	-	Inconclu.	0	-	Positive	0.984	O=C1c2[nH]c3ccccc3c2CCC1=Cc1ccccc1
Modulator of GABA-A receptor; alpha-5/beta-3/gamma-2	Central nervous system	Negative	0.995	-	Negative	0.994	-	Negative	0.998	-	Negative	0.985	-
Modulator of Kappa opioid receptor	Nervous system, Heart, Gastrointestinal	Negative	1	-	Negative	0.993	-	Negative	0.999	-	Negative	0.999	-
Modulator of Serotonin 4 (5-HT4) receptor	Gastrointestinal, Heart, Central nervous system	Negative	0.993	-	Negative	0.999	-	Negative	0.995	-	Negative	0.997	-
Modulator of Alpha-2b adrenergic receptor	Heart, Nervous system	Inconclu.	0	-	Inconclu.	0	-	Positive	0.987	CCCc1ccccc1COC1=NCCN1	Positive	0.984	COC(=O)C1C(O)CCC2CN3CCc4c([nH]c5ccccc45)C3CC21
Modulator of GABA-A receptor; alpha-2/beta-3/gamma-2	Central nervous system	Negative	0.994	-	Negative	0.992	-	Negative	0.997	-	Negative	0.986	-
Modulator of GABA-A receptor; alpha-3/beta-3/gamma-2	Central nervous system	Negative	0.995	-	Negative	0.993	-	Negative	0.98	-	Negative	0.981	-
Modulator of Muscarinic acetylcholine receptor M4	Nervous system, Heart	Negative	0.989	-	Negative	0.992	-	Negative	0.981	-	Negative	0.986	-

270

Action	Injury	1-Pentyl-THIQ			1-Pentyl-THβCa-ol			1-Pentyl-DHβCa			1-Phenyl-DHβCa		
		Outcome	Confidence	Similar_Positive_Mol	Outcome	Confidence	Similar_Positive_Mol	Outcome	Confidence	Similar_Positive_Mol	Outcome	Confidence	Similar_Positive_Mol
Modulator of Cholecystokinin A receptor	Gastrointestinal, gallbladder, Nervous system	Negative	0.999	-	Negative	0.994	-	Negative	0.989	-	Negative	0.995	-
Modulator of Serotonin 1b (5-HT1b) receptor	Nervous system, Heart	Negative	0.983	-	Positive	0.989	CCCCCCOc1cc2[nH]c3c(c2c1)CC(N)CC3	Inconclu.	0	-	Inconclusive	0	-
Modulator of Neuronal acetylcholine receptor; alpha4/beta2	Central nervous system	Negative	0.994	-	Negative	0.99	-	Negative	0.987	-	Negative	0.998	-
Modulator of Muscarinic acetylcholine receptor M2	Heart, respiratory, Nervous system	Negative	0.996	-	Negative	0.996	-	Negative	0.998	-	Negative	0.996	-
Modulator of Bradykinin B2 receptor	Heart, respiratory, Kidney, Central nervous system	Negative	0.99	-	Negative	0.998	-	Negative	0.996	-	Negative	0.997	-
Modulator of Sigma opioid receptor	Nervous system	Negative	0.994	-	Inconclu.	0	-	Inconclu.	0	-	Negative	0.984	-
Modulator of Adenosine A3 receptor	Nervous system, respiratory	Negative	0.996	-	Negative	0.99	-	Negative	0.991	-	Negative	0.986	-
Modulator of Muscarinic acetylcholine receptor M3	Gastrointestinal, Nervous system, respiratory, Heart, liver	Negative	0.997	-	Negative	0.994	-	Negative	1	-	Negative	0.996	-
Modulator of Serotonin 1a (5-HT1a) receptor	Nervous system, Heart, endocrine	Negative	0.996	-	Inconclu.	0	-	Negative	0.99	-	Negative	0.991	-
Modulator of Cannabinoid CB2 receptor	Immune, Nervous system	Negative	0.998	-	Negative	0.993	-	Negative	0.999	-	Negative	0.999	-
Modulator of Neurokinin 1 receptor	Nervous system, immune, Gastrointestinal, gonad	Negative	1	-	Negative	0.999	-	Negative	0.998	-	Negative	1	-
Modulator of Delta opioid receptor	Central nervous system	Negative	0.998	-	Negative	0.987	-	Negative	0.999	-	Negative	0.999	-
Modulator of Serotonin 2a (5-HT2a) receptor	Nervous system, blood, Heart	Negative	0.987	-	Inconclu.	0	-	Inconclu.	0	-	Inconclusive	0	-
Modulator of Norepinephrine transporter	Heart, Nervous system	Negative	0.989	-	Inconclu.	0	-	Inconclu.	0	-	Negative	0.983	-
Modulator of Muscarinic acetylcholine receptor M1	Nervous system, respiratory, Gastrointestinal, Heart, liver	Negative	0.998	-	Negative	0.998	-	Negative	0.998	-	Negative	1	-
Modulator of Monoamine oxidase A	Pharmaco-kinetics, Central nervous system	Inconclu.	0	-	Inconclu.	0	-	Inconclu.	0	-	Inconclusive	0	-
Antagonist of the androgen receptor (AR) signaling pathway	Endocrine, Central nervous system	Inconclu.	0	-	Inconclu.	0	-	Inconclu.	0	-	Inconclusive	0	-
Modulator of P2X purinoceptor 7	Nervous system, immune, Kidney	Negative	0.999	-	Negative	0.998	-	Negative	1	-	Negative	0.998	-
Modulator of Vasopressin V1a receptor	Heart, Kidney, Central nervous system	Negative	0.997	-	Negative	0.999	-	Negative	1	-	Negative	0.996	-

Action	Injury	1-Pentyl-THIQ			1-Pentyl-THβCa-ol			1-Pentyl-DHβCa			1-Phenyl-DHβCa		
		Outcome	Confidence	Similar_Positive_Mol	Outcome	Confidence	Similar_Positive_Mol	Outcome	Confidence	Similar_Positive_Mol	Outcome	Confidence	Similar_Positive_Mol
Modulator of P2X purinoceptor 3	Nervous system, immune, Kidney	Negative	0.997	-	Negative	0.998	-	Negative	0.997	-	Negative	0.994	-
Modulator of Acetylcholinesterase	Central nervous system	Negative	0.997	-	Negative	0.986	-	Negative	0.993	-	Negative	0.996	-
Modulator of Adenosine A1 receptor	Nervous system, Kidney, Heart	Negative	0.998	-	Negative	0.999	-	Negative	0.999	-	Negative	1	-
Modulator of Serotonin transporter	Central nervous system, blood, Heart, Gastrointestinal	Negative	0.996	-	Negative	0.988	-	Inconclu.	0	-	Inconclusive	0	-
Modulator of GABA-A receptor; anion channel	Central nervous system	Negative	0.992	-	Negative	0.989	-	Inconclu.	0	-	Inconclusive	0	-
Agonist of the glucocorticoid receptor (GR) signaling pathway	Endocrine, immune, Nervous system	Inconclu.	0	-	Inconclu.	0	-	Inconclu.	0	-	Inconclusive	0	-

Action	Injury	1-Pentyl-THIQ			1-Pentyl-THβCa-ol			1-Pentyl-DHβCa			1-Phenyl-DHβCa		
		Outcome	Confidence	Similar_Positive_Mol	Outcome	Confidence	Similar_Positive_Mol	Outcome	Confidence	Similar_Positive_Mol	Outcome	Confidence	Similar_Positive_Mol
Modulator of Mu opioid receptor	Nervous system, respiratory, Gastrointestinal, Heart, pancreas, Kidney	Negative	1	-	Inconclu.	0	-	Negative	0.999	-	Negative	1	-
Antagonist of the glucocorticoid receptor (GR) signaling pathway	Endocrine, immune, Nervous system	Inconclu.	0	-	Inconclu.	0	-	Inconclu.	0	-	Inconclusive	0	-
Modulator of Serotonin 3a (5-HT3a) receptor	Gastrointestinal, Heart, Central nervous system	Negative	0.988	-	Inconclu.	0	-	Inconclu.	0	-	Inconclusive	0	-
Agonist of the androgen receptor (AR) signaling pathway	Endocrine, Central nervous system	Inconclu.	0	-	Inconclu.	0	-	Negative	0.998	-	Inconclusive	0	-
Modulator of Endothelin receptor ET-A	Heart, Kidney, Nervous system, Gastrointestinal	Negative	0.996	-	Negative	0.998	-	Negative	0.999	-	Negative	0.998	-
Modulator of Neuropeptide Y receptor type 1	Gastrointestinal, immune, Nervous system	Negative	0.991	-	Negative	0.991	-	Negative	0.994	-	Negative	0.991	-
Modulator of Serotonin 2c (5-HT2c)	Nervous system	Negative	0.993	-	Inconclu.	0	-	Inconclu.	0	-	Inconclusive	0	-
Modulator of Dopamine transporter	Nervous system	Negative	0.983	-	Inconclu.	0	-	Inconclu.	0	-	Inconclusive	0	-
Modulator of Alpha-1b adrenergic receptor	Heart, Nervous system, Kidney	Negative	0.999	-	Negative	0.996	-	Negative	0.987	-	Negative	0.991	-
Modulator of Melatonin receptor 1B	Central nervous system	Negative	0.994	-	Negative	0.995	-	Negative	0.998	-	Negative	0.997	-
Modulator of Neuronal acetylcholine receptor protein alpha-4 subunit	Central nervous system	Inconclu.	0	-	Inconclu.	0	-	Negative	0.991	-	Inconclusive	0	-
Modulator of Adenosine A2b receptor	Immune, Peripheral nervous system	Negative	0.998	-	Negative	0.999	-	Negative	0.998	-	Negative	0.999	-
Modulator of GABA-A receptor; anion channel	Central nervous system	Inconclu.	0	-	Negative	0.996	-	Negative	0.984	-	Inconclusive	0	-
Activator Alzheimer's amyloid precursor	Central nervous system	Inconclu.	0	-	Inconclu.	0	-	Inconclu.	0	-	Positive	0.984	O=C1c2[nH]c3ccccc3c2CCC1=Cc1ccccc1
Modulator of GABA-A receptor; alpha-5/beta-3/gamma-2	Central nervous system	Negative	0.995	-	Negative	0.994	-	Negative	0.998	-	Negative	0.985	-
Modulator of Kappa opioid receptor	Nervous system, Heart, Gastrointestinal	Negative	1	-	Negative	0.993	-	Negative	0.999	-	Negative	0.999	-
Modulator of Serotonin 4 (5-HT4) receptor	Gastrointestinal, Heart, Central nervous system	Negative	0.993	-	Negative	0.999	-	Negative	0.995	-	Negative	0.997	-
Modulator of Alpha-2b adrenergic receptor	Heart, Nervous system	Inconclu.	0	-	Inconclu.	0	-	Positive	0.987	CCCc1ccccc1COC1=NCCN1	Positive	0.984	COC(=O)C1C(O)CCC2CN3CCc4c([nH]c5ccccc45)C3CC21
Modulator of GABA-A receptor; alpha-2/beta-3/gamma-2	Central nervous system	Negative	0.994	-	Negative	0.992	-	Negative	0.997	-	Negative	0.986	-
Modulator of GABA-A receptor; alpha-3/beta-3/gamma-2	Central nervous system	Negative	0.995	-	Negative	0.993	-	Negative	0.98	-	Negative	0.981	-
Modulator of Muscarinic acetylcholine receptor M4	Nervous system, Heart	Negative	0.989	-	Negative	0.992	-	Negative	0.981	-	Negative	0.986	-

273

Action	Injury	1-Pentyl-THIQ			1-Pentyl-THβCa-ol			1-Pentyl-DHβCa			1-Phenyl-DHβCa		
		Outcome	Confidence	Similar_Positive_Mol	Outcome	Confidence	Similar_Positive_Mol	Outcome	Confidence	Similar_Positive_Mol	Outcome	Confidence	Similar_Positive_Mol
Modulator of Cholecystokinin A receptor	Gastrointestinal, gallbladder, Nervous system	Negative	0.999	-	Negative	0.994	-	Negative	0.989	-	Negative	0.995	-
Modulator of Serotonin 1b (5-HT1b) receptor	Nervous system, Heart	Negative	0.983	-	Positive	0.989	CCCCCCOc1cc c2[nH]c3c(c2c 1)CC(N)CC3	Inconclu.	0	-	Inconclusive	0	-
Modulator of Neuronal acetylcholine receptor; alpha4/beta2	Central nervous system	Negative	0.994	-	Negative	0.99	-	Negative	0.987	-	Negative	0.998	-
Modulator of Muscarinic acetylcholine receptor M2	Heart, respiratory, Nervous system	Negative	0.996	-	Negative	0.996	-	Negative	0.998	-	Negative	0.996	-
Modulator of Bradykinin B2 receptor	Heart, respiratory, Kidney, Central nervous system	Negative	0.99	-	Negative	0.998	-	Negative	0.996	-	Negative	0.997	-
Modulator of Sigma opioid receptor	Nervous system	Negative	0.994	-	Inconclu.	0	-	Inconclu.	0	-	Negative	0.984	-
Modulator of Adenosine A3 receptor	Nervous system, respiratory	Negative	0.996	-	Negative	0.99	-	Negative	0.991	-	Negative	0.986	-
Modulator of Muscarinic acetylcholine receptor M3	Gastrointestinal, Nervous system, respiratory, Heart, liver	Negative	0.997	-	Negative	0.994	-	Negative	1	-	Negative	0.996	-
Modulator of Serotonin 1a (5-HT1a) receptor	Nervous system, Heart, endocrine	Negative	0.996	-	Inconclu.	0	-	Negative	0.99	-	Negative	0.991	-
Modulator of Cannabinoid CB2 receptor	Immune, Nervous system	Negative	0.998	-	Negative	0.993	-	Negative	0.999	-	Negative	0.999	-
Modulator of Neurokinin 1 receptor	Nervous system, immune, Gastrointestinal, gonad	Negative	1	-	Negative	0.999	-	Negative	0.998	-	Negative	1	-
Modulator of Delta opioid receptor	Central nervous system	Negative	0.998	-	Negative	0.987	-	Negative	0.999	-	Negative	0.999	-
Modulator of Serotonin 2a (5-HT2a) receptor	Nervous system, blood, Heart	Negative	0.987	-	Inconclu.	0	-	Inconclu.	0	-	Inconclusive	0	-
Modulator of Norepinephrine transporter	Heart, Nervous system	Negative	0.989	-	Inconclu.	0	-	Inconclu.	0	-	Negative	0.983	-
Modulator of Muscarinic acetylcholine receptor M1	Nervous system, respiratory, Gastrointestinal, Heart, liver	Negative	0.998	-	Negative	0.998	-	Negative	0.998	-	Negative	1	-
Modulator of Monoamine oxidase A	Pharmaco-kinetics, Central nervous system	Inconclu.	0	-	Inconclu.	0	-	Inconclu.	0	-	Inconclusive	0	-
Antagonist of the androgen receptor (AR) signaling pathway	Endocrine, Central nervous system	Inconclu.	0	-	Inconclu.	0	-	Inconclu.	0	-	Inconclusive	0	-
Modulator of P2X purinoceptor 7	Nervous system, immune, Kidney	Negative	0.999	-	Negative	0.998	-	Negative	1	-	Negative	0.998	-
Modulator of Vasopressin V1a receptor	Heart, Kidney, Central nervous system	Negative	0.997	-	Negative	0.999	-	Negative	1	-	Negative	0.996	-

274

Action	Injury	1-Pentyl-THIQ			1-Pentyl-THβCa-ol			1-Pentyl-DHβCa			1-Phenyl-DHβCa		
		Outcome	Confidence	Similar_Positive_Mol	Outcome	Confidence	Similar_Positive_Mol	Outcome	Confidence	Similar_Positive_Mol	Outcome	Confidence	Similar_Positive_Mol
Modulator of P2X purinoceptor 3	Nervous system, immune, Kidney	Negative	0.997	-	Negative	0.998	-	Negative	0.997	-	Negative	0.994	-
Modulator of Acetylcholinesterase	Central nervous system	Negative	0.997	-	Negative	0.986	-	Negative	0.993	-	Negative	0.996	-
Modulator of Adenosine A1 receptor	Nervous system, Kidney, Heart	Negative	0.998	-	Negative	0.999	-	Negative	0.999	-	Negative	1	-
Modulator of Serotonin transporter	Central nervous system, blood, Heart, Gastrointestinal	Negative	0.996	-	Negative	0.988	-	Inconclu.	0	-	Inconclusive	0	-
Modulator of GABA-A receptor; anion channel	Central nervous system	Negative	0.992	-	Negative	0.989	-	Inconclu.	0	-	Inconclusive	0	-
Agonist of the glucocorticoid receptor (GR) signaling pathway	Endocrine, immune, Nervous system	Inconclu.	0	-	Inconclu.	0	-	Inconclu.	0	-	Inconclusive	0	-